Anonymous Referee #1

General comments

1. With this manuscript, the authors are delivering a new version of the POMINO product. This product is based on slant columns retrievals from DOMINO, uses nested GEOS-Chem simulation, and applies MODIS and CALIOP/CALIPSO data for AMF calculation, with each item presenting concerns for reporting it as a new version of the POMINO product. NO2 slant column retrievals used here is version 2 product, which is reported to be erroneous. NO2 profiles and other model dependent parameters are taken from two versions of nested model that switch from one resolution to another in 2013. They apply CALIOP/CALIPSO data over 2007-2015 to OMI data taken over 2004-present. MODIS AOD data are taken from two versions (collection 5.1 and collection 6 with a switch in 2013). There is enough ground to suggest that the product is erroneous, is not consistent over time, and should not be distributed to users as an updated version.

The latest study by Zara et al. (2018) shows that the uncertainty of SCD is ~1.32 x 10^{15} molec/cm^2 in DOMINO v2, which is reduced to ~0.84 x 10^{15} molec/cm^2 in the newly released QA4ECV product (used for comparison here). The SCD errors are thus much smaller than the errors introduced from AMF calculation over polluted regions like China (Boersma et al., 2011; Lin et al., 2015; Lorente et al., 2017). Also, any bias in the total SCD is mostly absorbed by the stratospheric separation step, and may not propagate into the tropospheric SCD (van Geffen et al., 2015). In other words, the tropospheric SCDs used in POMINO (from DOMINO v2) are well-established. We are considering moving to using tropospheric SCDs from QA4ECV, once these have been evaluated more thoroughly (something that this paper contributes to).

We had to choose two model versions according to the availability of meteorological data – GEOS-5 data on the 0.5 x 0.667 grid were replaced by GEOS-FP on the 0.25 x 0.3125 grid after May 2013). Despite the differences in horizontal resolution and driving meteorology, the two model versions have the same vertical coordinate and use the same schemes for advection, PBL mixing and convection, which is important for vertical distribution of NO2 and aerosols. We consider the discontinuity in GEOS-Chem model resolution as a minor limitation for our NO_2 product for long-term trend studies.

We used the CALIOP/CALIPSO data over 2007-2015 according to data availability. Our correction of vertical profiles is on the basis of monthly climatology, thus applying the correction to other years is appropriate. Analogous approaches have been used in previous studies, for example, applying the 3-year average or 5-year average OMI surface albedo data to all years in DOMINO (Boersma et al., 2007; 2011), and applying 4-year average (2004-2007) monthly mean NO_2 profile shapes derived from GMI CTM simulation to retrieve tropospheric NO_2 in NASA's SPv2 (Bucsela et al., 2013).

MODIS AOD data were taken from two versions in our POMINO product. We agree that using the same version of MODIS AOD data would be better. However, the difference in C5.1 and C6 is relatively small (C6 is smaller by 13.7% averaged over East China in 2012), compared to the difference between GEOS-Chem and C5.1 or between CEOS-Chem and C6. Our one-year test by using C5.1 versus C6 AOD (to correct model AOD) leads to 3.8% decrease in the retrieved NO_2 averaged over East China in 2012.

As suggested by the second reviewer, we have included the newest QA4ECV NO2 product in the revised manuscript. Figure 9, Table 2 and Table 3 have been updated accordingly. QA4ECV is biased low in cases with high aerosol loading, but its R^2 with respect to MAX-DOAS is better than DOMINO v2. This additional comparison further strengthens the importance of aerosol correction in NO_2 retrieval over East Asia. Despite its various limitations discussed here, POMINO v1.1 is closer to MAX-DOAS than QA4ECV is, especially in hazy days, highlighting the capability of POMINO v1.1.

Given these above discussions, we have decided to not release POMINO v1.1 to users. Rather, we will eventually release POMINO v2, which will include MODIS C6 merged AOD and MCD43C2 C6 daily BRDF. The POMINO v1.1 will be used as an intermediate (and the most important) step between POMINO and POMINO v2. And this paper documents how improvement in aerosol vertical distribution affects the POMINO NO_2 product, such that all other factors are consistent between POMINO and POMINO v1.1. We have clarified this point in the revised abstract and conclusion.

2. To justify the improvement in the retrieved product, authors have used a small set of MAX-DOAS measurements. Improvements are justified based on improved correlation coefficient with the POMINO product. It appears from Figure 10 that the enhanced correlation might, in fact, be driven by changes in ~6 data points only with very large (>100 x 10^15 molec cm-2) values. In many instances (for columns < 100 x 10^15 molec cm2), the agreement between OMI and MAX-DOAS appears to be better for DOMINO. Author should use different means of validation, larger set of validation datasets, and various statistical methods to assess the products.

The high values represent very polluted cases that our algorithm intends to capture. Excluding these polluted cases would lead to a substantial sampling bias over polluted regions. We have made the distinction between hazy cases and less hazy situations. The latter are more representative for retrievals over the US and Europe. In those cases, QA4ECV may perform better and POMINO is more likely to be biased high (Table 3).

We would definitely prefer to have a larger set of MAX-DOAS NO_2 data. Unfortunately, very few high-quality MAX-DOAS measurements are available over China. We have made efforts to get data from multiple sites to enhance the spatial representativeness. Our criteria to select MAX-DOAS data and OMI data mainly follow Wang et al., (2017b) and Lin et al., (2014), who have already discussed the influence from various statistical methods.

We have included a statement in the end of Sect. 6 that "Further research may use additional MAX-DOAS datasets to evaluate the satellite products more systematically."

3. The whole discussion about processing (filtering, regridding) and comparison of CALIPSO data is distracting and unnecessary. These could be completely removed, shortened, or moved to the Appendix/Supplementary section. Also, data processing is largely subjective. Why not use more mature data assimilation technique instead?

We have revised the manuscript accordingly. The discussion on the treatment of CALIOP data has been moved to Appendix B.

Data assimilation is subject to the very limited availability of CALIOP data. It is also computationally prohibitive for our application here (multiple years over a large domain on a high-resolution grid).

Specific comments

1. Page 9, line 225: This statement may not be true. Please, replace "will not" to "may not".

Changed.

2. Page 9, line 227-231: Please be more specific on AMF calculation. What wavelength range is used for AMF for POMINO/DOMINO? I assume this is more important than the difference between online and look-up table approach.

Changed. The wavelength is 438 nm in both DOMINO and POMINO. The dependence of AMF on the wavelength is weak (actually 0.25%/nm, Boersma et al. (2018)). Other details of AMF calculations can be found in Lin et al. (2014b, 2015).

3. Page 9, line 228: This paper is all about POMINO and DOMINO. Please, say "DOMINO" instead of "in most retrieval algorithms".

As far as we know, most algorithms use look-up tables, including but not limited to NASA's SP product, DOMINO, and others participating the QA4ECV project.

4. Page 10, line 237: What are those "Other aspects"? Please, list them.

Changed.

5. Page 10, lines 237-239: This statement is likely misleading as look-up table may have been used in certain aspect of your calculation. Please, remove “without use of look-up tables”.

Changed.

6. Page 10, lines 239-244, 257-259: See my general comment. The same product cannot use simulated fields from two different models. The retrievals should be based on single model.

See response to general comment.

7. Page 13, lines 314-316: How does the se of CALIPSO constraints affect cloud pressure, cloud fraction, and radiative cloud fraction? Please include relevant results and discussions.

The detailed results can be found in Sect. 4.

8. Page 13, lines 321-325: Please, clarify this statement.

Clarified.

9. Page 14, line 360: What is the justification of 2-hour averaging of MAX-DOAS? Why do you expect instantaneous OMI measurements compare well with MAX-DOAS averaged over 2-hours? Is this exercise described in the following sentences motivated to show only good results?

As already clarified in manuscript, we used the criteria based on several previous studies (Lin et al., 2014; Wang et al., 2015, 2017b). These previous papers have already discussed the most appropriate criteria to balance data coverage, passing time, spatial domain around the pixel center, etc.

10. Page 15, lines 366-367: “to some degree” is redundant.

Changed.

11. Page 15, lines 374-375: Why is this necessary? How do cloud and haze differ for their impact on measurement sensitivity of OMI?

As emphasized in the manuscript, we wanted to separate the hazy days from cloudy days. Some days are cloud-free but hazy (with heavy NO2 pollution as well). These days were filtered out in DOMINO and QA4ECV through the criteria on cloud radiance fraction. By comparison, our algorithm was able to retain these days and avoid sampling bias (by missing polluted days) while preserving the overall accuracy of NO2 product.

As explained in the manuscript, neither the OMI cloud product nor the MODIS cloud product is able to provide the true cloud fraction, so we used the meteorological monitoring stations and the MODIS RGB product to manually check whether a day is cloudy or hazy.

12. Page 16, line 395: Please, add citations for this statement.

Changed.

13. Page 17, line 418: How does the emission strength affect the height of peak extinction?

The effect of emission strength on aerosol vertical profiles is season and location dependent. For the case here (Figure 4), emissions over Eastern China are higher in winter, in which season the atmosphere is more stagnant vertically. This means that more aerosols are concentrated near the surface, thus decreasing the height of peak extinction.

14. Page 19, lines 470-472: The spatial correlations suggest that GEOS-Chem performs very poorly in simulating aerosol fields. Why do you still use GEOS-Chem? Could not you just use CALIPSO-based aerosol information?

GEOS-Chem provides daily and spatially resolved information, which is what is needed by the satellite retrieval. CALIOP, in contrast, has poor temporal and spatial coverage, preventing fully CALIOP-based aerosol profile information to be used to retrieve the NO_2 product. The spatial correlation between GEOS-Chem and CALIOP is not as good as their temporal correlation. We thus used CALIOP for monthly climatological corrections, while retaining the GEOS-Chem simulated day-to-day variability.

Anonymous Referee #2

The paper "Improved aerosol correction for OMI tropospheric NO2 retrieval over East Asia: constraint from CALIOP aerosol vertical profile" by Liu et al. describes an improved OMI tropospheric NO2 retrieval for East China using CALIOP aerosol vertical profile information. This study updates the POMINO retrieval algorithm described in Lin et al., 2014 and 2015. Comparisons have been made between the NO2 satellite data and ground-based MAX-DOAS measurements at three sites in East-China.

The topic of the manuscript is within the scope of AMT and it is of interest to the scientific community. It can be recommended for publication, if the authors make an effort to address the comments listed below, and improve the manuscript accordingly.

Specific comments:

Section 2.2

P9-10 The improved POMINO NO2 algorithm for China builds on the Dutch OMI NO2 v2 algorithm from 2011. The DOMINO v2 algorithm is now about 7 years old, and the authors shortly discuss some recent improvements in the satellite retrieval (e.g. improvements in the slant column retrieval). Please include the recently released "Dutch/European" OMI NO2 product provided in the framework of the QA4ECV project (v1.1) in this discussion as well (e.g. including the latest developments in the STS and the trop. AMF algorithms).

Thank you for this valuable suggestion. We have now included an evaluation of QA4ECV in the revised manuscript. Figure 9, Table 2 and Table 3 have been updated accordingly. QA4ECV is still bias low in highly polluted cases, although its R^2 with respect to MAX-DOAS is better than DOMINO v2. This additional comparison further strengthens the importance of aerosol correction in NO_2 retrieval over East Asia. POMINO v1.1 is closer to MAX-DOAS than QA4ECV is, especially in hazy days, highlighting the capability of POMINO v1.1.

P11 The authors mention that the climatological adjustments in the aerosol information is based on the assumption that systematic model limitations are month-dependent and persist over the years and days. On the other hand, the daily variations in the aerosol extinction profile are coming from the model only (Eq. 3). How good are the daily variations in the aerosol parameters modeled by GEOS-Chem?

The extent to which model aerosol information can be corrected depends on the availability of aerosol observations. MODIS and especially CALIOP suffer from low coverage on the day-to-day scale, preventing their direct use in satellite NO2 retrieval product and in daily correction of model aerosols.

Previous studies have shown that GEOS-Chem is able to simulate day-to-day variation of AOD from AERONET (Li et al., 2013, 2015) and satellite (Johnson et al., 2012), surface $PM_{2.5}$ (Liu et al., 2018), and aerosol vertical profile (Ford and Heald, 2012).

P11 From Eq. (2) and (3), I would expect a "jump" in the aerosol extinction profile from the last day of the month to the first day of the next month (because of the change in R). Is this 'jump' also noticeable in the trop. AMF and VCD?

Here we test this "jump" issue over Northern East China. For every first day in each month of year 2012, we use the monthly correction from the last month (ie. For 1st, Feb, we will use the ratio of January to adjust aerosol extinction profile of GEOS-Chem on this day). Figure R1 shows the test results. In particular, the difference in NO_2 VCD between this sensitivity test and our actual retrieval is below 3.8% for most cases. Besides, the distribution of VCD difference seems to be random. Thus the "jump" issue does not influence our results systematically.

We have added in the revised Sect. 2.2 that "Although this monthly adjustment means discontinuity on the day-to-day basis (e.g., from the last day of a month to the first day of the next month), such discontinuity does not affect the NO_2 retrieval significantly, based on our sensitivity test."

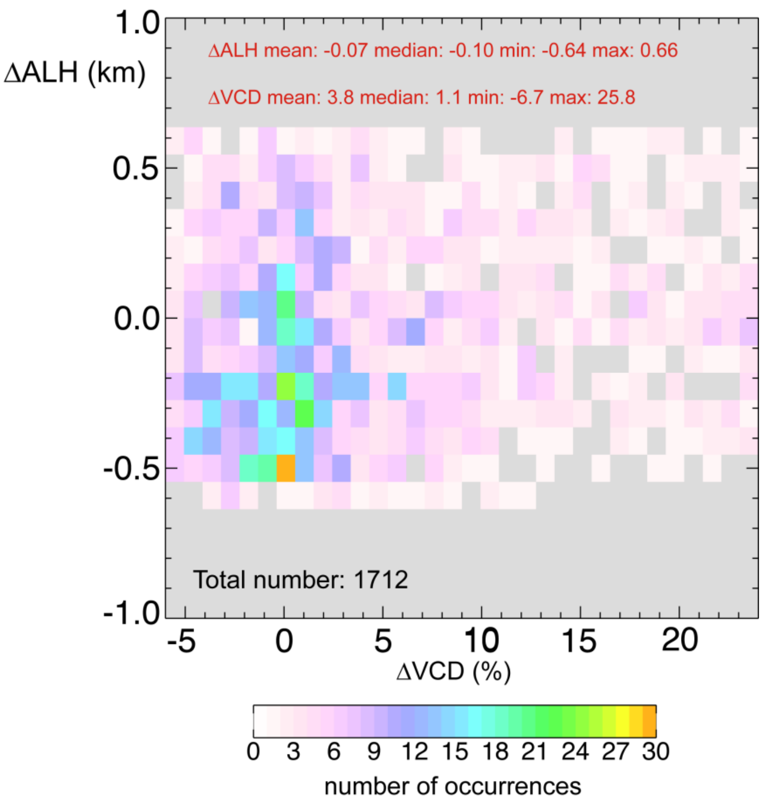

Figure R1. Percentage change in retrieved NO_2 VCD when using the CALIOP aerosol extinction profile in a formal month (POMINO_change) to adjust modeled profile on the first day of each month ([POMINO_change-POMINO v1.1]/[POMINO v1.1]), for each bin of ΔALH (bin size = 0.1 km) and ΔVCD (bin size = 1%) across pixels in 2012 over Northern East China. Here we only choose the pixels with WCLD < 0.5, surface albedo < 0.3 and SZA < 70°.

P12 How large is the effect of neglecting polarization in the RTM (LIDORT) on the trop. AMF calculation?

The impact of polarization is small, affecting stratospheric retrievals by 0.1% and reducing tropospheric AMF by < 0.5% (Boersma et al., 2011). According on Lorente et al., (2017), top-of-atmosphere reflectance simulated by four RTMs (DAK with polarization, McArtim, SCIATRAN and VLIDORT with polarization) agree within 1.5%.

Section 3.1

Fig.3 For some specific areas there seem to be large differences between the two CALIOP ALH datasets, e.g. for Shandong in summer. Is this only caused by the differences in resolution/sampling/regridding, or are there other factors?

The large difference over Shandong is persistent across the seasons. It is mainly caused by resolution/sampling/regridding process. Our climatological dataset uses the same criteria as the NASA Level-3 product does, but we aim at compiling a climatology to adjust GEOS-Chem outputs in a temporally and spatially consistent manner.

Section 4

A difficult/confusing concept of the POMINO NO2 algorithm is that for the trop. AMF, (thin) clouds are treated as reflecting boundaries in the RTM calculations (using effective cloud parameters retrieved from the O2-O2 band), while Mie parameters are used in the RTM for the layers with aerosols. It is clear that the aerosols are included in the POMINO O2-O2 cloud retrieval, but the different treatment of scattering by clouds and aerosols in the trop. AMF calculation could be addressed in more detail.

As in all other cloud products used for NO_2 retrieval, we treat clouds as "effective" Lambertian reflector with a fixed albedo (80%). Assuming Mie scattering for clouds implies an explicit treatment of vertical cloud structure, cloud droplet sizes, etc., which is actually a new direction we could explore for NO_2 retrieval.

We have added a statement in the revised Sect. 2.2: "Note that the treatment of cloud scattering (as "effective" Lambertian reflector, as in other NO_2 algorithms) is different from the treatment of aerosol scattering/absorption (vertically resolved based on the Mie scheme)."

Section 6

The evaluating of the improved OMI NO2 product with MAX-DOAS data is an important part of this study. However, the number of measurements/points in Fig. 10 seems low (e.g. compared to other satellite validation studies using the BIRA-IASB MAXDOAS data at these sites). Can the number of points be increased, e.g. by increasing the time period, relaxing the cloud screening, collocation criteria etc? Then the statistics can be improved and also time series could be added.

We would definitely prefer to have a larger set of MAX-DOAS NO_2 data. Unfortunately, very few high-quality MAX-DOAS measurements are available over China. We have made efforts to get data from multiple sites to enhance the spatial representativeness. Our criteria to select MAX-DOAS data and OMI data mainly follow Wang et al., (2017b) and Lin et al., (2014b), who have already discussed the influence from various statistical methods.

We have included a statement in the end of Sect. 6 that "Further research may use additional MAX-DOAS datasets to evaluate the satellite products more systematically."

In addition to the comparisons in Fig. 10, the MAXDOAS retrieved NO2 profiles could also be exploited with the Averaging Kernel (AK) of the OMI NO2 columns. Comparisons of the satellite NO2 columns with these "smoothed" MAXDOAS NO2 columns could provide useful additional information (e.g. to isolate the impact of the satellite a priori NO2 profile).

We only have the vertical profiles at Xianghe, with lack of spatial representativeness. Our previous study (Lin et al., 2014b) shows that using the MAX-DOAS vertical profiles have a minor impact on the retrieved NO_2.

References:

Ford, B. and Heald, C. L.: An A-train and model perspective on the vertical distribution of aerosols and CO in the Northern Hemisphere, J. Geophys. Res. Atmos., 117(D6), n/a-n/a, doi:10.1029/2011JD016977, 2012.

Johnson, M. S., Meskhidze, N. and Praju Kiliyanpilakkil, V.: A global comparison of GEOS-Chem-predicted and remotely-sensed mineral dust aerosol optical depth and extinction profiles, J. Adv. Model. Earth Syst., 4(3), M07001, doi:10.1029/2011MS000109, 2012.

Li, S., Garay, M. J., Chen, L., Rees, E. and Liu, Y.: Comparison of GEOS-Chem aerosol optical depth with AERONET and MISR data over the contiguous United States, , 118(April), 228–241, doi:10.1002/jgrd.50867, 2013.

Li, S., Chen, L., Fan, M., Tao, J., Wang, Z., Yu, C., Si, Y., Letu, H. and Liu, Y.: Estimation of GEOS-Chem and GOCART Simulated Aerosol Profiles Using CALIPSO Observations over the Contiguous United States, , (2008), 3256–3265, doi:10.4209/aaqr.2015.03.0173, 2015.

Liu, M., Lin, J., Wang, Y., Sun, Y., Zheng, B., Shao, J., Chen, L., Zheng, Y., Chen, J., Fu, M., Yan, Y., Zhang, Q. and Wu, Z.: Spatiotemporal variability of NO_2 and $PM_{2.5}$ over Eastern China: observational and model analyses with a novel statistical method, Atmos. Chem. Phys. Discuss., 2018, 1–34, doi:10.5194/acp-2017-1180, 2018.

This is my second review of this manuscript. The authors have addressed some of the concerns I had in my previous review. Re-organization of some sections has been helpful for clarity. Inclusion of the QA4ECV data is commendable. However, the authors have not addressed many of my earlier comments. Therefore, I would not recommend accepting the manuscript in the current form.

Major concerns:

1) Data/results discussed in this manuscript are based on biased slant column data and inconsistent inputs as I have discussed in detail in my previous review. Instead of revisiting the work, the authors chose to modify the version number and suggested that they will not release the data. This may be a conflict to AMT's data policy. Moreover, I could not locate how each of the comments is addressed in the revised manuscript.

As we have replied to the previous review (general comment 1), the bias in DOMINO v2 SCD should have a very small effect on our VCD results. To address this issue more clearly, here we use the SCDs of QA4ECV (to replace DOMINO v2 SCD) and re-do the VCD retrieval. As shown in Fig. S1, using QA4ECV SCD instead of DOMINO v2 SCD only improves the comparison with MAX-DOAS VCD data slightly – for example, the underestimate is reduced from 3.7% to 0.2%. Other statistics (intercept, slope, and R^2) are very similar. This test justifies our previous reasoning. We have added in the revised Appendix A (Line 623-624) that "Our test suggests that using the QA4ECV SCD data instead of DOMINO SCD data would reduce the underestimate against MAX-DOAS VCD data from 3.7% to 0.2%, a relative minor improvement."

The main purpose of this paper is to present the substantial effect of aerosol vertical profile correction on the NO_2 retrieval. As we continuously improve the NO_2 product, we have added updates for other retrieval aspects as well. We have decided to name the intermediate product shown in this paper as v1.1, because it does not include all updates we have so far. To comply with the AMT requirement, we will provide the reader v1.1 data for the time period studied in this paper (i.e., 2012). However, for a general user of our product, we will recommend to use POMINO v2 that is available since October 2004.

We will provide a Microsoft WORD document with changes tracked.

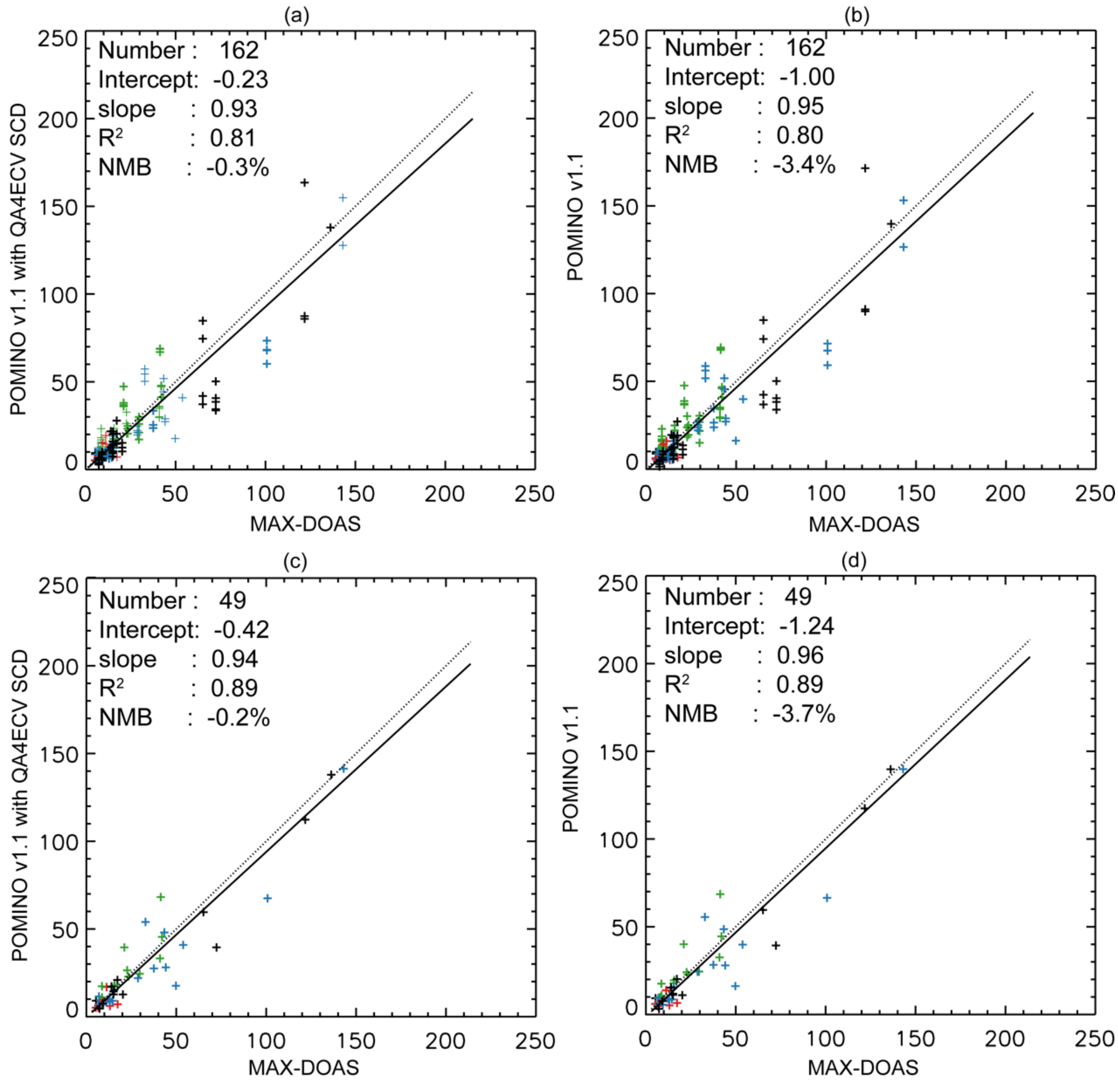

Figure S1. (a-b) Scatter plot for NO_2 VCD (10^{15} molec. cm^{-2}) between MAX-DOAS and POMINO v1.1 data with (a) QA4ECV or (b) DOMINO SCD. Each "+" corresponds to an OMI pixel, as several pixels may be available in a day. (c-d) Similar to (a-b) but after averaging over all OMI pixels in the same day, such that each "+" represents a day.

2) Their explanation for the limited number of MAX-DOAS data is well taken. But, they could still use various statistical methods and maybe other data sources to assess the improvements. Small increase in correlation alone, which may not be statistically significant, cannot be a measure of retrieval improvements (main message of this manuscript). One can raise many questions for results presented in Tables 2 and 3: What explains more than 20% difference between POMINO v1.1 and POMINO?, how is the 30% high bias of v1.1 versus MAX-DOAS an improvement?, what explains a factor of 2 difference in slope between DOMINO and QA4ECV if it is not related to slant column?, why is the comparison so poor for the improved QA4ECV OMI product?, are MAX-DOAS data accurate/reliable?, etc. From Figure 9, the relationship between DOMINO and MAX-DOAS looks much tighter as compared to POMINO and MAX-

DOAS (except for few data points) and POMINO does not show an improvement if MAX-DOAS is the ground truth.

The only difference between POMINO v1.1 and POMINO comes from the different shapes of aerosol vertical profile. Our manuscript, together with several previous studies cited in our manuscript, has clearly shown a systematic error in GEOS-Chem simulated vertical profile. Correcting for this error means an improvement of in the retrieval algorithm from POMINO to POMINO v1.1, regardless of how many MAX-DOAS (or other independent) data are available to demonstrate the algorithm improvement.

In general, the higher NO_2 VCD values in POMINO v1.1 than POMINO are because of the increased shielding effect of aerosols, which leads to smaller NO_2 AMFs. The magnitude of this increase depends on many conditions such as the fraction of clouds. In the revised manuscript, Table 2 shows a 6% increase (NMB of -9.6% versus -3.4%), Table 3 shows a 14% increase (NMB of -9.4% versus 4.4%), and Table 4 shows a 9% increase (NMB of 20.8% versus 29.4%) – these values are specific to their conditions.

Table 3 (Table 4 in our revised manuscript) basically shows that under cloud free conditions (POMINO CF = 0), the aerosol loading is much smaller than under haze days (AOD = 0.60 versus 1.13 in Table 3). In this case, POMINO v1.1, POMINO, and DOMINO v2 have similar bias (20.8%–29.4%) and R^2 (0.53–0.56) against MAX-DOAS NO_2 data, and the performance of QA4ECV is better. QA4ECV is essentially an ensemble of several European retrieval algorithms, all of which treat aerosols as "effective" clouds, thus its better performance (when aerosol loadings are relatively small) is not surprising. In Sect. 6, we have clarified this point that "Here, POMINO v1.1, POMINO and DONIMO v2 do not show large differences in R^2 (0.53–0.56) and NMB (20.8–29.4%) with respect to MAX-DOAS. QA4ECV has a higher R^2 (0.63) and a lower NMB (-5.8%), presumably reflecting the improvements in this (EU-) consortium approach, at least in mostly cloud-free situations. However, the R^2 values for POMINO and POMINO v1.1 are much smaller than the R^2 values in haze days, whereas the opposite changes are true for DOMINO v2 and QA4ECV. Thus, for this limited set of data, the changes from DOMINO v2 and QA4ECV to POMINO and POMINO v1.1 mainly reflect the improved aerosol treatment in hazy scenes."

As for "what explains a factor of 2 difference in slope between DOMINO and QA4ECV if it is not related to slant column?, why is the comparison so poor for the improved QA4ECV OMI product?", both our study and previous studies (van Geffen et al., 2015; Zara et al., 2018) show SCDs contribute insignificantly to the VCD differences. We suspect that the VCD differences come from the fact that QA4ECV is essentially an ensemble of several European retrieval algorithms. However, specific analysis of the difference between DOMINO v2 and QA4ECV is not the main topic of this study.

The reliability of MAX-DOAS data have been analyzed in many papers, including those cited in our paper (Hendrick et al., 2014; Lin et al., 2014b; Wang et al., 2017a).

In our reply to comment 3 of the previous review, we wrote that "We would definitely prefer to have a larger set of MAX-DOAS NO_2 data. Unfortunately, very few high-quality MAX-DOAS measurements are available over China. We have made efforts to get data from multiple sites to enhance the spatial representativeness." Although we have tried very hard to get all data available, the amount of MAX-DOAS data points here do not allow to fully evaluating each satellite product. Based on this limited set of MAX-DOAS data, it is not expected that any product shows superiority in all aspects of comparison with MAX-DOAS – for example, although DOMINO v2 is a relatively older product, it may compare with (this limited set of) MAX-DOAS data better than other products under some special conditions, as pointed out by the reviewer.

Given the limited amount of available MAX-DOAS data, here we test the effect of sampling criteria (i.e., time and distance) on the comparison; the criteria chosen in the main text are described in Line 314-317, and are highlighted in bold in Tables S1 and S2. Table S1 selects OMI pixels within 25 km of MAX-DOAS sites and MAX-DOAS measurements within different hours (1 h, 1.5h, and 2 h) of OMI overpass time. For each product, the comparison results (slope, intercept, R^2, NMB) do not change significantly.

Table S2 selects MAX-DOAS data within 1 h of OMI overpass time and OMI pixels within various distances to MAX-DOAS sites (40 km, 35 km, 30 km, 25 km, and 20 km). For POMINO, POMINO v1.1, and POMINO v1.1 with QA4ECV SCDs, the R^2 value changes slightly when the distance increases from 20 km to 30 km, and starts to decline at longer distances. This reflects that as the distance increases, the satellite data tend to represent regional NO_2, in contrast to the MAX-DOAS data which are "line" measurements. Other statistics (slope, intercept, and NMB) do not change significantly with distance. Similar changes with distance are shown in DOMINO v2 and QA4ECV data.

3) The "Author's Response" does not seem to include a marked-up manuscript version. Therefore, it is not clear if the authors have sufficiently addressed the reviewers' comments and how they are addressed.

We will provide a Microsoft WORD document with changes tracked.

Minor comment:

4) It is difficult to relate the reported contents (numbers) in abstract/conclusions/discussions to tables as the tables provide results for a subset of samples but not for the entire samples. Including statistics of Figure 9 in table would be helpful.

We have added a table (Table 2) to summarize the statistics in Fig. 9, and have changed numbering of other tables accordingly.

Table S1 Evaluation of OMI products against MAX-DOAS under different temporal criteria.

	Slope			Intercept			R^2			NMB (%)		
Hours within OMI overpass time	**1h**	1.5h	2h	**1h**	1.5h	2h	**1h**	1.5h	2h	**1h**	1.5h	2h
Number of pixels	**162**	175	184	**162**	175	184	**162**	175	184	**162**	175	184
POMINO v1.1	**0.95**	0.96	0.97	**-1.00**	-2.24	-2.42	**0.80**	0.77	0.76	**-3.4**	-5.5	-5.5
POMINO	**0.78**	0.80	0.80	**0.96**	-0.04	-0.35	**0.80**	0.78	0.77	**-9.6**	-11.3	-11.3
POMINO v1.1 (with QA4ECV SCD)	**0.93**	0.94	0.94	**0.23**	-1.57	-1.73	**0.81**	0.78	0.76	**-0.3**	-3.1	-2.5
DOMINO v2	**1.06**	1.10	1.10	**-3.86**	-5.08	-5.00	**0.68**	0.68	0.67	**-2.1**	-3.7	-2.2
QA4ECV	**0.66**	0.65	0.67	**1.09**	0.47	0.43	**0.75**	0.72	0.74	**-22.0**	-24.3	-22.7

Table S2 Evaluation of OMI products against MAX-DOAS under different spatial criteria.

Distance from MAX-DOAS site	40km	35km	30km	**25km**	20km	40km	35km	30km	**25km**	20km
Number of pixels	510	383	272	**163**	98	510	383	272	**163**	98
	slope					intercept				
POMINO v1.1	1.03	1.07	0.95	**0.95**	0.98	-4.87	-5.22	-1.67	**-1.00**	-1.57
POMINO	0.80	0.82	0.79	**0.78**	0.71	-0.90	-0.77	0.36	**0.96**	2.12
POMINO v1.1 (with QA4ECV SCD)	1.02	1.05	0.93	**0.93**	0.94	-3.97	-4.37	-0.70	**0.23**	-0.50
DOMINO v2	1.03	1.05	1.05	**1.06**	0.70	-3.91	-4.10	-3.49	**-3.86**	3.37
QA4ECV	0.64	0.64	0.65	**0.66**	0.65	0.15	0.45	0.86	**1.09**	1.34
	R^2					NMB (%)				
POMINO v1.1	0.63	0.64	0.75	**0.80**	0.78	-6.5	-4.9	-4.4	**-3.4**	-5.7
POMINO	0.69	0.71	0.75	**0.80**	0.80	-12.3	-11.0	-10.2	**-9.6**	-12.2
POMINO v1.1 (with QA4ECV SCD)	0.63	0.64	0.75	**0.81**	0.78	-2.1	-0.8	-0.1	**-0.3**	-2.4
DOMINO v2	0.60	0.63	0.66	**0.68**	0.63	1.5	1.2	0.6	**-2.1**	-5.0
QA4ECV	0.64	0.67	0.72	**0.75**	0.68	-22.0	-21.4	-22.0	**-22.0**	-23.4

Improved aerosol correction for OMI tropospheric NO_2 retrieval over East Asia: constraint from CALIOP aerosol vertical profile

Mengyao Liu[1,2], Jintai Lin[1], K. Folkert Boersma[2,3], Gaia Pinardi[4], Yang Wang[5], Julien Chimot[6], Thomas Wagner[5], Pinghua Xie[7,8,9], Henk Eskes[2], Michel Van Roozendael[4], François Hendrick[4], Pucai Wang[10], Ting Wang[10], Yingying Yan[1]

1, Laboratory for Climate and Ocean-Atmosphere Studies, Department of Atmospheric and Oceanic Sciences, School of Physics, Peking University, Beijing, China

2, Royal Netherlands Meteorological Institute, De Bilt, the Netherlands

3, Meteorology and Air Quality department, Wageningen University, Wageningen, the Netherlands

4, Royal Belgian Institute for Space Aeronomy (BIRA-IASB), Brussels, Belgium

5, Max Planck Institute for Chemistry, Mainz, Germany

6, Department of Geoscience and Remote Sensing (GRS), Civil Engineering and Geosciences, TU Delft, the Netherlands

7, Anhui Institute of Optics and Fine Mechanics, Key laboratory of Environmental Optics and Technology, Chinese Academy of Sciences, Hefei, China

8, CAS Center for Excellence in Urban Atmospheric Environment, Institute of Urban Environment, Chinese Academy of Sciences, Xiamen, China

9, School of Environmental Science and Optoelectronic Technology, University of Science and Technology of China, Hefei, China

样式定义：标题 1：与下段不同页
样式定义：标题 2：段落间距段后：1 行，与下段不同页
带格式的：上标

10, IAP/CAS, Institute of Atmospheric Physics, Chinese Academy of Sciences, Beijing, China

Correspondence to: Jintai Lin (linjt@pku.edu.cn); K. Folkert Boersma (folkert.boersma@knmi.nl)

Abstract

Satellite retrieval of vertical column densities (VCDs) of tropospheric nitrogen dioxide (NO_2) is critical for NO_x pollution and impact evaluation. For regions with high aerosol loadings, the retrieval accuracy is greatly affected by whether aerosol optical effects are treated implicitly (as additional "effective" clouds) or explicitly, among other factors. Our previous POMINO algorithm explicitly accounts for aerosol effects to improve the retrieval especially in polluted situations over China, by using aerosol information from GEOS-Chem simulations with further monthly constraints by MODIS/Aqua aerosol optical depth (AOD) data. Here we present a major algorithm update, POMINO v1.1, by constructing a monthly climatological data set of aerosol extinction profiles, based on Level-2 CALIOP/CALIPSO data over 2007–2015, to better constrain the modeled aerosol vertical profiles.

We find that GEOS-Chem captures the month-to-month variation of CALIOP aerosol layer height but with a systematic underestimate by about 300–600 m (season and location dependent), due to a too strong negative vertical gradient of extinction above 1 km. Correcting the model aerosol extinction profiles results in small changes in retrieved cloud fraction, increases in cloud top pressure (within 2–6% in most cases), and increases in tropospheric NO_2 VCD by 4–16% over China on a monthly basis in 2012. The improved NO_2 VCDs (in POMINO v1.1) are more consistent with independent ground-based MAX-DOAS observations (R^2 = 0.80, NMB = -3.4%, for 162 pixels in 49 days) than POMINO (R^2 = 0.80, NMB = -9.6%), DOMINO v2 (R^2 =

删除的内容: t

删除的内容: AOD

删除的内容: This study is the kernel updates of our newthe retrieval algorithm, to POMINO v21.1,

删除的内容:

删除的内容: and

0.68, NMB = -2.1%) and QA4ECV (R^2 = 0.75, NMB = -22.0%) are. Especially on haze days, R^2 reaches 0.76 for POMINO v1.1, much higher than that for POMINO (0.68), DOMINO v2 (0.38) and QA4ECV (0.34). Furthermore, the increase in cloud pressure likely reveals a more realistic vertical relationship between cloud and aerosol layers, with aerosols situated above the clouds in certain months instead of always below the clouds. The POMINO v1.1 algorithm is a core step towards our next public release of data product (POMINO v2), and it will also be applied to the recently launched S5P-TropOMI sensor.

1. Introduction

Air pollution is a major environmental problem in China. In particular, China has become the world's largest emitting country of nitrogen oxides (NO_X=NO+NO_2) due to its rapid economic growth, heavy industries, coal-dominated energy sources, and relatively weak emission control (Cui et al., 2016; Lin et al., 2014a; Stavrakou et al., 2016; Zhang et al., 2009). Tropospheric vertical column densities (VCDs) of nitrogen dioxide (NO_2) retrieved from the Ozone Monitoring Instrument (OMI) onboard the Earth Observing System (EOS) Aura satellite have been widely used to monitor and analyze NO_X pollution over China because of its high spatiotemporal coverage (e.g. (Lin et al., 2010; Miyazaki and Eskes, 2013; Verstraeten et al., 2015; Zhao and Wang, 2009). However, NO_2 retrieved from OMI and other space-borne instruments are subject to errors in the conversion process from radiance to VCD, particularly with respect to the calculation of tropospheric air mass factor (AMF) that is used to convert tropospheric slant column density to VCD (e.g. Boersma et al., 2011; Bucsela et al., 2013; Lin et al., 2015; Lorente et al., 2017).

Most current-generation NO_2 algorithms do not explicitly account for the effects of aerosols on NO_2 AMFs and on prerequisite cloud parameter retrievals. These retrievals often adopt an implicit approach wherein cloud algorithms retrieve

- 带格式的: 上标
- 删除的内容: 82
- 删除的内容: 7
- 删除的内容:
- 删除的内容: and
- 删除的内容: This
- 删除的内容: improvement in ourOur POMINO v1.1 algorithm
- 删除的内容: ↵

"effective cloud" parameters that include the optical effects of aerosols. This implicit method is based on aerosols exerting an effect on the top-of-atmosphere radiance level, whereas the assumed cloud model does not account for the presence of aerosols in the atmosphere (Stammes et al., 2008; Veefkind et al., 2016; Wang et al., 2008b; Wang and Stammes, 2014). In the absence of clouds, an aerosol optical thickness of 1 is then interpreted as an effective cloud fraction of ±0.10, and the value also depends on the aerosol properties (scattering or absorbing), true surface albedo and geometry angles (Chimot et al., 2016) with an effective cloud pressure closely related to the aerosol layer, at least for aerosols of predominantly scattering nature (e.g. Boersma et al., 2004, 2011, Castellanos et al., 2014, 2015). However, in polluted situations with high aerosol loadings and more absorbing aerosol types, which often occur over China and many other developing regions, the implicit method can result in considerable biases (Castellanos et al., 2014, 2015; Chimot et al., 2016; Kanaya et al., 2014; Lin et al., 2014b).

Lin et al. (2014b, 2015) established the POMINO NO_2 algorithm, which builds on the DOMINO v2 algorithm (for OMI NO_2 slant columns and stratospheric correction), but improves upon it through a more sophisticated AMF calculation over China. In POMINO, the effects of aerosols on cloud retrievals and NO_2 AMFs are explicitly accounted for. In particular, daily information on aerosol optical properties such as aerosol optical depth (AOD), single scattering albedo (SSA), phase function and vertical extinction profiles are taken from nested Asian GEOS-Chem v9-02 simulations. The modeled AOD at 550 nm is further constrained by MODIS/Aqua monthly AOD, with the correction applied to other wavelengths based on modeled aerosol refractive indices (Lin et al., 2014b). However, the POMINO algorithm does not include an observation-based constraint on the vertical profile of aerosols, whose altitude relative to NO_2 has strong and complex influences on NO_2 retrieval (Castellanos et al., 2015; Leitão et al., 2010; Lin et al., 2014b). This study improves

upon the POMINO algorithm by incorporating CALIOP monthly climatology of aerosol vertical extinction profiles to correct for model biases.

The CALIOP lidar, carried on the sun-synchronous CALIPSO satellite, has been acquiring global aerosol extinction profiles since June 2006 (Winker et al., 2010). CALIPSO and Aura are both parts of the National Aeronautics and Space Administration (NASA) A-train constellation of satellites. The overpass time of CALIOP/CALIPSO is only 15 minutes later than OMI/Aura. In spite of issues with the detection limit, radar ratio selection and cloud contamination that cause some biases in CALIOP aerosol extinction vertical profiles (Amiridis et al., 2015; Koffi et al., 2012; Winker et al., 2013), comparisons of aerosol extinction profiles between ground-based lidar and CALIOP show good agreements (Kacenelenbogen et al., 2014; Kim et al., 2009; Misra et al., 2012). However, CALIOP is a nadir-viewing instrument that measures the atmosphere along the satellite ground-track with a narrow field-of-view. This means that the daily geographical coverage of CALIOP is much smaller than that of OMI. Thus previous studies often used monthly/seasonal regional mean CALIOP data to study aerosol vertical distributions or to evaluate model simulations (Chazette et al., 2010; Johnson et al., 2012; Koffi et al., 2012; Ma and Yu, 2014; Sareen et al., 2010).

There exist a few CALIOP Level-3 gridded datasets, such as LIVAS (Amiridis et al. 2015) and NASA official Level-3 monthly dataset (Winker et al., 2013). However, LIVAS is an annual average day-night combined product, not suitable to be applied to OMI NO_2 retrievals (around early afternoon, and in need of a higher temporal resolution than annual). The horizontal resolution (2° long. × 5° lat.) of NASA official product is much coarser than OMI footprints and the GEOS-Chem model resolution.

删除的内容: are some mature data of

删除的内容:

删除的内容: yearly

删除的内容: but

带格式的: 下标

删除的内容: measurement is only available in the daytime, besides, the temporal resolution (yearly) is not very suitable for daily aerosol extinction profiles usage

删除的内容: s

Here we construct a custom monthly climatology of aerosol vertical extinction profiles based on 9-years (2007–2015) worth of CALIOP Version 3 Level-2 532 nm data. On a climatological basis, we use the CALIOP monthly data to adjust GEOS-Chem profiles in each grid cell for each day of the same month in any year. We then use the corrected GEOS-Chem vertical extinction profiles in the retrievals of cloud parameters and NO_2. Finally, we evaluate our updated POMINO retrieval (hereafter referred to as POMINO v1.1), our previous POMINO product, DOMINO v2 and the newly released Quality Assurance for Essential Climate Variables product (QA4ECV, see Appendix A), using ground-based MAX-DOAS NO_2 column measurements at three urban/suburban sites in East China for the year of 2012 and several months in 2008/2009.

Section 2 describes the construction of CALIOP aerosol extinction vertical profile monthly climatology, the POMINO v1.1 retrieval approach, and the MAX-DOAS data. It also presents the criteria for comparing different NO_2 retrieval products and for selecting coincident OMI and MAX-DOAS data. Section 3 compares our CALIOP climatology with NASA's official Level-3 CALIOP dataset and GEOS-Chem simulation results. Sections 4 and 5 compare POMINO v1.1 to POMINO to analyze the influence of improved aerosol vertical profiles on retrievals of cloud parameters and NO_2 VCDs, respectively. Section 6 evaluates POMINO, POMINO v1.1, DOMNO v2 and QA4ECV NO_2 VCD products using the MAX-DOAS data. Section 7 concludes our study.

2. Data and methods

2.1 CALIOP monthly mean extinction profile climatology

CALIOP is a dual-wavelength polarization lidar measuring attenuated backscatter radiation at 532 and 1064 nm since June 2006. The vertical resolution of aerosol

删除的内容: In order to constrain daily aerosol extinction profiles simulated by GEOS-Chem.However, the major monthly/seasonal CALIOP data are too coarse in spatial resolution (i.e. NASA's official monthly Level-3 CALIOP dataset with spatial resolution 2° long. × 5° lat.) or in temporal resolution (i.e. LIVAS 5-year based 1° × 1° CALIOP dataset).
H

删除的内容: and the existing

删除的内容: and

删除的内容: retrievals

删除的内容:

删除的内容: and

删除的内容: new released Quality Assurance for Essential Cliamte Variables (QA4ECV, see detailed introduction in Appedix B)

删除的内容: s

删除的内容: *Constructing a*

extinction profiles is 30 m below 8.2 km and 60 m up to 20.2 km (Winker et al., 2013), with a total of 399 sampled altitudes. The horizontal resolution of CALIOP scenes is 335 m along the orbital track and is given over a 5 km horizontal resolution in Level-2 data.

As detailed in Appendix B, we use the daily all-sky Version 3 CALIOP Level-2 aerosol profile product at 532 nm from 2007 to 2015 to construct a monthly Level-3 climatological dataset of aerosol extinction profiles over China and nearby regions. This dataset is constructed on the GEOS-Chem model grid (0.667° long. x 0.5° lat.) and vertical resolution (47 layers, with 36 layers or so in the troposphere).

The ratio of climatological monthly CALIOP to monthly GEOS-Chem profiles represents the scaling profile to adjust the daily GEOS-Chem profiles in the same month (see Sect. 2.2).

2.2 POMINO v1.1 retrieval approach

The NO_2 retrieval consists of three steps. First, the total NO_2 slant columns density (SCD) is retrieved using the Differential Optical Absorption Spectroscopy (DOAS) technique (for the 405-465 nm spectral window in the case of OMI). The uncertainty of the SCD is determined by the appropriateness of the fitting technique, the instrument noise, the choice of fitting window, and the orthogonality of the absorbers' cross sections (Bucsela et al., 2006; van Geffen et al., 2015; Lerot et al., 2010; Richter et al., 2011; Zara et al., 2018). The NO_2 SCD in DOMINO v2 has a bias at about 0.5~1.3 × 10^{15} molec. cm^{-2} (Belmonte Rivas et al., 2014; Dirksen et al., 2011; Marchenko et al., 2015; van Geffen et al., 2015; Zara et al., 2018), which can be reduced by improving wavelength calibration and including O_2–O_2 and liquid water absorption in the fitting model (van Geffen et al., 2015). The tropospheric SCD is then obtained by subtracting the stratospheric SCD from the total SCD. The bias in

删除的内容: Here

已下移 [5]: We choose the all-sky product instead of clear-sky data, since previous studies indicate that the climatological aerosol extinction profiles are affected insignificantly by the presence of clouds (Koffi et al. 2012; Winker et al. 2013). As we use this climatological data to adjust GEOS-Chem results, choosing all-sky data improves consistency with the model simulation when doing the daily correction.

已下移 [1]: In brief, only the pixels with Cloud Aerosol Discrimination (CAD) scores between -20 and -100 with extinction Quality Control (QC) flag valued at 0, 1, 18, and 16 are selected. We further discard samples with an extinction uncertainty of 99.9 km^{-1}, which is indicative of unreliable retrieval. We only accept extinction values falling in the range from 0.0 to 1.25, according to CALIOP observation thresholds. Previous studies showed that weakly scattering edges of icy clouds are sometimes misclassified as aerosols (Winker et al. 2013). To eliminate contamination from icy clouds we exclude the aerosol layers above the cloud layer (with layer-top temperature below 0 ℃) when both of them are above 4km (Winker et al. 2013).

已下移 [2]: CALIOP Level-2 data are always presented at the fixed 399 altitudes above sea level. To account for the difference in surface elevation between a CALIOP pixel and the respective model grid cell,

删除的内容: We apply a number of criteria to ensure data quality of each pixel, mainly following Winker et al. (2013) and Amiridis et al. ... [1]

带格式的: 非突出显示

删除的内容:

删除的内容: After the pixel-based screening, we aggregate the CALIOP data at the model grid (0.667° long. x 0.5° lat.) and vertical ... [2]

删除的内容:

已下移 [3]: Figure 1 shows the number of aerosol extinction profiles in each grid cell and 12 x 9 = 108 months that are used to compile the

删除的内容: .

删除的内容: As discussed above, we choose the CALIOP pixels within 1.5° of a grid cell center. We test this choice by examining the ... [3]

已下移 [4]: For each grid cell in each month, we further correct singular values in the vertical profile. In a month, if a grid cell *i* has

批注 [JL1]: Add Zara et al. (2018)

the total SCD is mostly absorbed by this stratospheric separation step, which may not propagate into the tropospheric SCD (van Geffen et al., 2015). The last step converts the tropospheric SCD to VCD by using the tropospheric AMF (VCD = SCD / AMF). The tropospheric AMF is calculated at 438 nm by using look-up tables (in most retrieval algorithms) or online radiative transfer modeling (in POMINO) driven by ancillary parameters, which act as the dominant source of errors in retrieved NO_2 VCD data over polluted areas (Boersma et al., 2007; Lin et al., 2014b, 2015; Lorente et al., 2017).

Our POMINO algorithm focuses on the tropospheric AMF calculation over China and nearby regions, taking the tropospheric SCD (Dirksen et al., 2011) from DOMINO v2 (Boersma et al., 2011). POMINO improves upon the DOMINO v2 algorithm in the treatment of aerosols, surface reflectance, online radiative transfer calculations, spatial resolution of NO_2, temperature and pressure vertical profiles, and consistency between cloud and NO_2 retrievals (Lin et al., 2014b, 2015). In brief, we use the parallelized LIDORT-driven AMFv6 package to derive both cloud parameters and tropospheric NO_2 AMFs for individual OMI pixels online. NO_2 vertical profiles, aerosol optical properties and aerosol vertical profiles are taken from the nested GEOS-Chem model over Asia (0.667 ° long. × 0.5° lat. before May 2013 and 0.3125 ° long. × 0.25 ° lat. afterwards), and pressure and temperature profiles are taken from the GEOS-5 and GEOS-FP assimilated meteorological fields that drive GEOS-Chem simulations. Model aerosols are further adjusted by satellite data (see below). We adjust the pressure profiles based on the difference in elevation between the pixel center and the matching model grid cell (Zhou et al., 2010). We also account for the effects of surface bidirectional reflectance distribution function (BRDF) (Lin et al., 2014b; Zhou et al., 2010) by taking three kernel parameters (isotropic, volumetric and geometric) from the MODIS MCD43C2 data set at 440 nm (Lucht et al., 2000).

删除的内容:
删除的内容: will
删除的内容: at 439 nm
删除的内容: nearly
删除的内容: , improved surface elevation
删除的内容: and other aspects
删除的内容:
删除的内容: without use of look-up tables
删除的内容:
删除的内容:

As a prerequisite to the POMINO NO_2 retrieval, clouds are retrieved through the O_2-O_2 algorithm (Acarreta et al., 2004; Stammes et al., 2008) with O_2-O_2 SCDs from OMCLDO2, and with pressure, temperature, surface reflectance, aerosols and other ancillary information consistent with the NO_2 retrieval. Note that the treatment of cloud scattering (as "effective" Lambertian reflector, as in other NO_2 algorithms) is different from the treatment of aerosol scattering/absorption (vertically resolved based on the Mie scheme).

POMINO uses the temporally and spatially varying aerosol information, including AOD, single scattering albedo (SSA), phase function and vertical profiles from GEOS-Chem simulations. POMINO v1.1 (this work) further uses CALIOP data to constrain the shape of aerosol vertical extinction profile. We run the model at a resolution of 0.3125° long. × 0.25° lat. before May 2013 and 0.667° long. × 0.5° lat. afterwards, as determined by the resolution of the driving meteorological fields. We then regrid the finer resolution model results to 0.667° long. × 0.5° lat., to be consistent with the CALIOP data grid. We then sample the model data at times and locations with valid CALIOP data at 532 nm to establish the model monthly climatology.

For any month in a grid cell, we divide the CALIOP monthly climatology of aerosol extinction profile shape by model climatological profile shape to obtain a unitless scaling profile (Eq. 1), and apply this scaling profile to all days of that month in all years (Eq. 2). Such a climatological adjustment is based on the assumption that systematic model limitations are month-dependent and persist over the years and days (e.g., a too strong vertical gradient, see Sect. 3.3). Although this monthly adjustment means discontinuity on the day-to-day basis (e.g., from the last day of a month to the first day of the next month), such discontinuity does not significantly affect the NO_2 retrieval, based on our sensitivity test.

删除的内容: the
删除的内容: al is done
带格式的: 下标
删除的内容: It should be noticed
删除的内容: s
带格式的: 下标
删除的内容: scattering by clouds and
删除的内容: s in tropospheric AMF calculation are different. The cloud are treated as lambert reflector while Mie scattering scheme is used for aerosols in RTM calculations
删除的内容:
删除的内容:
删除的内容:
删除的内容: 2
删除的内容: 3
带格式的: 下标
删除的内容: significantly

In Eqs. 1 and 2, E^C represents the CALIOP climatological aerosol extinction coefficient, E^G the GEOS-Chem extinction, E^{Gr} the post-scaling model extinction, and R the scaling profile. The subscript *i* denotes a grid cell, *k* a vertical layer, *d* a day, *m* a month, and *y* a year. Note that in Eq. 1, the extinction coefficient at each layer is normalized relative to the maximum value of that profile. This procedure ensures that the scaling is based on the relative shape of the extinction profile and is thus independent of the accuracies of CALIOP and GEOS-Chem AOD. We keep the absolute AOD value of GEOS-Chem unchanged in this step.

$$R_{i,k,m} = \frac{E^C_{i,k,m}/\max(E^C_{i,k,m})}{E^G_{i,k,m}/\max(E^G_{i,k,m})} \quad (1)$$

$$E^{Gr}_{i,k,d,m,y} = E^G_{i,k,d,m,y} \times R_{i,k,m} \quad (2)$$

In POMINO, the GEOS-Chem AOD are further constrained by a MODIS/Aqua Collection 5.1 monthly AOD dataset compiled on the model grid (Lin et al., 2014b, 2015). POMINO v1.1 uses the Collection 5.1 AOD data before May 2013 and Collection 6 data afterwards. For adjustment, model AOD are projected to a 0.667° long. × 0.5° lat. grid and then sampled at times and locations with valid MODIS data (Lin et al., 2015). As shown in Eq. 3, τ^M denotes MODIS AOD, τ^G GEOS-Chem AOD, and τ^{Mr} post-adjustment model AOD. The subscript *i* denotes a grid cell, *d* a day, *m* a month, and *y* a year. This AOD adjustment ensures that in any month, monthly mean GEOS-Chem AOD is the same as MODIS AOD while the modeled day-to-day variability is kept.

$$\tau^{Gr}_{i,d,m,y} = \frac{\tau^M_{i,m,y}}{\tau^G_{i,m,y}} \times \tau^G_{i,d,m,y} \quad (3)$$

Equations 4–5 show the complex effects of aerosols in calculating the AMF for any pixel. The AMF is the linear sum of tropospheric layer contributions to the slant

删除的内容: Actually, the correction to model simulated aerosol extinction profiles are main restricted by observation. CALIOP observation are only one highly spatialtemporal coverage data we can find.
删除的内容: 2
删除的内容: 3
删除的内容:
删除的内容: 2
删除的内容: 2
删除的内容: 3
删除的内容:
删除的内容: 4
删除的内容: 4
删除的内容: 5
删除的内容: 6

column weighted by the vertical subcolumns (Eq. 4). The box AMF, amf_k, describes the sensitivity of NO_2 SCD to layer k, and $x_{a,k}$ represent the subcolumn of layer k from a priori NO_2 profile. The l represent the first integrated layer, which is the layer above the ground for clear sky, or the layer above cloud top for cloudy sky. The t represent the tropopause layer. POMINO assumes the independent pixel approximation (IPA) (Martin et al., 2002; Boersma et al., 2002). This means that the calculated AMF for any pixel consists of a fully cloudy-sky portion (AMF_{clr}) and a fully clear-sky portion (AMF_{cld}), with weights based on the cloud radiance fraction ($\mathrm{CRF} = (1 - \mathrm{CF}) \cdot \mathrm{A}_{\mathrm{clr}} + \mathrm{CF} \cdot \mathrm{A}_{\mathrm{cld}}$, $\mathrm{A}_{\mathrm{clr}}$, $\mathrm{A}_{\mathrm{cld}}$ are radiance from the clear-sky part and cloudy part of the pixel, respectively.) (Eq. 5). AMF_{cld} is affected by above-cloud aerosols, and AMF_{clr} is affected by aerosols in the entire column. Also, aerosols affect the retrieval of CRF. Thus, the improvement of aerosol vertical profile in POMINO v1.1 affects all the three quantities in Eq. 5 and thus leads to complex impacts on retrieved NO_2 VCD.

$$\mathrm{AMF} = \frac{\sum_l^t amf_k x_{a,k}}{\sum_l^t x_{a,k}} \quad (4)$$

$$\mathrm{AMF} = \mathrm{AMF}_{cld} \cdot \mathrm{CRF} + \mathrm{AMF}_{clr} \cdot (1 - \mathrm{CRF}) \quad (5)$$

2.3 OMI pixel selection to evaluate POMINO v1.1, POMINO, DOMINO v2 and QA4ECV

We exclude OMI pixels affected by row anomaly (Schenkeveld et al., 2017) or with high albedo caused by icy/snowy ground. To screen out cloudy scenes, we choose pixels with CRF below 50% (effective cloud fraction is typically below 20%) in POMINO.

The selection of CRF threshold influences the validity of pixels. The “effective” CRF in DOMINO implicitly includes the influence of aerosols. In POMINO, the aerosol

删除的内容: 5

删除的内容: CRF

删除的内容: 6

删除的内容: whole

删除的内容: 6

删除的内容: 5

删除的内容: 6

删除的内容: *and*

contribution is separated from that of the clouds, resulting in a lower CRF than for DOMINO. The CRF differs insignificantly between POMINO and POMINO v1.1, because the same AOD and other non-aerosol ancillary parameters are used in the retrieval process. Using the CRF from POMINO instead of DOMINO or QA4ECV for cloud screening means that the number of "valid" pixels in DOMINO increases by about 25%, particularly because much more pixels with high pollutant (aerosol and NO_2) loadings are now included. This potentially reduces the sampling bias (Lin et al., 2014b, 2015), and the ensemble of pixels now includes scenes with high "aerosol radiative fractions". Further research is needed to fully understand how much these high-aerosol scenes may be subject to the same screening issues as the cloudy scenes. Nevertheless, the limited evidence here and in Lin et al. (2014b, 2015) suggests that including these high-aerosol scenes does not affect the accuracy of NO_2 retrieval.

删除的内容: but

删除的内容: the drawback is that

删除的内容: ing

删除的内容: although

2.4 MAX-DOAS data

We use MAX-DOAS measurements at three suburban or urban sites in East China, including one urban site at the Institute of Atmospheric Physics (IAP) in Beijing (116.38° E, 39.38 ° N), one suburban site in Xianghe County (116.96° E, 39.75 ° N) to the south of Beijing, and one urban site in the Wuxi City (120.31° E, 31.57 ° N) in the Yangzi River delta (YRD). Figure 1 shows the locations of these sites overlaid with POMINO v1.1 NO_2 VCDs in August 2012. Table 1 summarizes the information of MAX-DOAS measurements.

删除的内容: 2

删除的内容: 2

The instruments in IAP and in Xianghe were designed at BIRA-IASB (Clémer et al., 2010). Such an instrument is a dual-channel system composed of two thermally regulated grating spectrometers, covering the ultraviolet (300–390 nm) and visible (400–720 nm) wavelengths. It measures scattered sunlight every 15 minutes at nine elevation angles: 2° , 4° , 6° , 8° , 10° , 12° , 15° , 30° , and 90° . The telescope of the instrument is pointed to the north. The data are analyzed following

Hendrick et al. (2014). The Xianghe suburban site is influenced by pollution from the surrounding major cities like Beijing and Tianjin. At Xianghe, MAX-DOAS data are data are continuously available since early 2011, and data in 2012 are used here for comparison with OMI products. At IAP, MAX-DOAS data are available in 2008 and 2009 (Table 1), thus for comparison purposes we process OMI products to match the MAX-DOAS times.

删除的内容: 2

Located on the roof of an 11-story building, the instrument at Wuxi was developed by Anhui Institute of Optics and Fine Mechanics (AIOFM) (Wang et al., 2015, 2017a). Its telescope is pointed to the north and records at five elevation angles (5°, 10°, 20°, 30° and 90°). Wuxi is a typical urban site affected by heavy NO_x and aerosol pollution. The measurements used here are analyzed in Wang et al. (2017a). Data are available in 2012 for comparison with OMI products.

When comparing the four OMI products against MAX-DOAS observations, temporal and spatial inconsistency in sampling is inevitable. The spatial inconsistency, together with the substantial horizontal inhomogeneity in NO_2, might be more important than the influence of temporal inconsistency (Wang et al., 2017b). The influence of the horizontal inhomogeneity was suggested to be about 10–30% for MAX-DOAS measurements in Beijing (Lin et al., 2014b; Ma et al., 2013) and 10–15% for less polluted locations like Tai'an, Mangshan and Rudong (Irie et al., 2012). Following previous studies (Lin et al., 2014b; Wang et al., 2015, 2017b), we average MAX-DOAS data within 2 h of the OMI overpass time, and we select OMI pixels within 25 km of a MAX-DOAS site whose viewing zenith angle is below 30°. To exclude local pollution events near the MAX-DOAS site (such as the abrupt increase of NO_2 caused by the pass of consequent vehicles during a very short period), the standard deviation of MAX-DOAS data within 2 h should not exceed 20% of their

删除的内容: three

mean value (Lin et al., 2014b). We elect not to spatially average the OMI pixels because they can, to some degree, reflect the spatial variability in NO_2 and aerosols.

删除的内容: to some degree

We further exclude MAX-DOAS data in cloudy conditions, as clouds can cause large uncertainties in MAX-DOAS and OMI data. To find the actual cloudy days, we use MODIS/Aqua cloud fraction data, MODIS/Aqua Level-3 corrected reflectance (true color) data at the 1^0 x 1^0 resolution, and current weather data observed from the nearest ground meteorological station (indicated by the black triangles in Fig. 1b). Since there is only one meteorological station available near the Beijing area, it is used for both IAP and Xianghe MAX-DOAS sites. We first use MODIS/Aqua corrected reflectance (true color) to distinguish clouds from haze. For cloudy days determined by the reflectance checking, we examine both the MODIS/Aqua cloud fraction data and the meteorological station cloud records, considering that MODIS/Aqua cloud fraction data may be missing or have a too coarse horizontal resolution to accurately interpret the cloud conditions at the MAX-DOAS site. We exclude MAX-DOAS NO_2 data if the MODIS/Aqua cloud fraction is larger than 60% and the meteorological station reports a “BROKEN” (cloud fraction ranges from 5/8 to 7/8) or “OVERCAST” (full cloud cover) sky. For the three MAX-DOAS sites together, this leads to 49 days with valid data out of 64 days with pre-screening data.

删除的内容: 2

We note here that using cloud fraction data from MODIS/Aqua or MAX-DOAS (for Xianghe only, see Gielen et al., 2014) alone to screen cloudy scenes may not be appropriate on heavy-haze days. For example, on 8th January, 2012, MODIS/Aqua cloud fraction is about 70–80% over the North China Plain and MAX-DOAS at Xianghe suggests the presence of “thick clouds”. However, both the meteorological station and MODIS/Aqua corrected reflectance (true color) product suggest that the North China Plain was covered by a thick layer of haze. Consequently, this day was excluded from the analysis.

3. Monthly climatology of aerosol extinction profiles from CALIOP and GEOS-Chem

3.1 CALIOP monthly climatology

The aerosol layer height (ALH) is a good indicator to what extent aerosols are mixed vertically (Castellanos et al., 2015). As defined in Eq. A1 in Appendix B, the ALH is the average height of aerosols weighted by vertically resolved aerosol extinction. Figure 2a shows the spatial distribution of our CALIOP ALH climatology in each season. At most places, the ALH reaches a maximum in spring or summer and a minimum in fall or winter. The lowest ALH in fall and winter can be attributed to heavy near-surface pollution and weak vertical transport. The high values in summer are related to strong convective activities. Over the north, the high values in spring are partly associated with Asian dust events, due to high surface winds and dry soil in this season (Huang et al., 2010; Proestakis et al., 2017; Wang et al., 2010), which also affects the oceanic regions via atmospheric transport. The springtime high ALH over the south may be related to the transport of carbonaceous aerosols from Southeast Asian biomass burning (Jethva et al., 2016). Averaged over the domain, the seasonal mean ALHs are 1.48 km, 1.43 km, 1.27km, 1.18 km in spring, summer, fall and winter.

删除的内容: 3

Figure 3a,b further shows the climatological monthly variations of ALH averaged over Northern East China (the anthropogenic source region shown in orange in Fig. 1a) and Northwest China (the dust source region shown in yellow in Fig. 1a). The two regions exhibit distinctive temporal variations. Over Northern East China, the ALH reaches a maximum in April (~1.53 km) and a minimum in December (~1.14 km). Over Northwest China, the ALH peaks in August (~1.59km) because of strongest convection (Zhu et al., 2013), although the springtime ALH is also high.

删除的内容: 4

删除的内容: 2

删除的内容: 2

Figure 4a shows the climatological seasonal regional average vertical profiles of aerosol extinction over Northern East China. Here, the aerosol extinction increases from the ground level to a peak at about 300–600 m (season dependent), above which it decreases gradually. The height of peak extinction is lowest in winter, consistent with a stagnant atmosphere, thin mixing layer, and increased emissions (from residential and industrial sectors). The large error bars (horizontal lines in different layers, standing for 1 standard deviation) indicate strong spatiotemporal variability of aerosol extinction.

Over Northwest China (Fig. 5a), the column total aerosol extinction is much smaller than that over Northern East China (Fig. 4a), due to lower anthropogenic sources and dominant natural dust emissions. Vertically, the decline of extinction from the peak-extinction height to 2 km is also much more gradual than the decline over Northern East China, indicating stronger lifting of surface emitted aerosols. In winter, the column total aerosol extinction is close to the high value in dusty spring, whereas the vertical gradient of extinction is strongest among the seasons. This reflects the high anthropogenic emissions in parts of Northwest China, which have been rapidly increasing in the 2000s due to relatively weak emission control supplemented by growing activities of relocation of polluted industries from the eastern coastal regions (Cui et al., 2016; Zhao et al., 2015).

Overall, the spatial and seasonal variations of CALIOP aerosol vertical profiles are consistent with changes in meteorological conditions, anthropogenic sources, and natural emissions. The data will be used to evaluate and adjust GEOS-Chem simulation results in Sect. 3.2. A comparison of our CALIOP dataset with NASA's official Level-3 data is presented in Appendix C.

3.2 Evaluation of GEOS-Chem aerosol extinction profiles

删除的内容: 5

删除的内容: 6

删除的内容: 5

删除的内容: 3

删除的内容: C

删除的内容: *3.2 Comparison to NASA CALIOP monthly climatology*

We compare our gridded climatological profiles to NASA CALIOP Version 3 Level-3 all-sky monthly profiles at 532 nm (Winker et al. 2013). The NASA Level-3 data has a horizontal resolution of 2° lat. × 5° lon. and a vertical resolution of 60 m (from -0.5 to 12 km above sea level). We combine NASA monthly data over 2007–2015 to construct a monthly climatology for comparison with our own compilation. We only choose aerosol extinction data in the troposphere with error less than 0.15 (the valid range given in the CALIOP dataset). If the number of valid monthly profiles in a grid cell is less than five (i.e., for the same month in five out of the nine years), then we exclude data in that grid cell; see the dark gray grid cells in Fig. 23c.

Several methodological differences exist between generating our and NASA CALIOP datasets. First, the two datasets have different horizontal resolutions. Also, we sample all valid CALIOP pixels within 1.5° of a grid cell center, whereas the NASA dataset samples all valid pixels within a grid cell. Besides, our CALIOP dataset involves several steps of horizontal interpolation, for purposes of subsequent cloud and NO_2 retrievals, which is not done in the NASA dataset. In addition, we match CALIOP data vertically to the GEOS-Chem vertical resolution, whereas the NASA dataset maintains the original resolution.

... [4]

删除的内容: *3*

Figure 2b shows the spatial distribution of seasonal ALHs simulated by GEOS-Chem. The model captures the spatial and seasonal variations of CALIOP ALH (Fig. 2a) to some degree, with an underestimate by about 0.3 km on average. The spatial correlation between CALIOP (Fig. 2a) and GEOS-Chem (Fig. 2b) ALH is 0.37 in spring, 0.57 in summer, 0.40 in fall, and 0.44 in winter. The spatiotemporal consistency and underestimate is also clear from the regional mean monthly ALH data in Fig. 3 – the temporal correlation between GEOS-Chem and CALIOP ALH is 0.90 in Northern East China and 0.97 in Northwest China.

Figures 4a and 5a show the GEOS-Chem simulated 2007–2015 monthly climatological vertical profiles of aerosol extinction coefficient over Northern East China and Northwest China, respectively. Over Northern East China (Fig. 4a), the model (red line) captures the vertical distribution of CALIOP extinction (black line) below the height of 1 km, despite a slight underestimate in the magnitude of extinction and an overestimate in the peak-extinction height. From 1 to 5 km above the ground, the model substantially overestimates the rate of decline in extinction coefficient with increasing altitude. Across the seasons, GEOS-Chem underestimates the magnitude of aerosol extinction by up to 37% (depending on the height). Over Northwest China (Fig. 5a), GEOS-Chem has an underestimate in all seasons, with the largest bias by about 80% in winter likely due to underestimated water-soluble aerosols and dust emissions (Li et al., 2016; Wang et al., 2008a).

Since the POMINO v1.1 algorithm uses MODIS AOD to adjust model AOD, it only uses the CALIOP aerosol extinction profile shape to adjust the modeled shape (Eqs. 1 and 2). Figures 4b and 4b show the vertical shapes of aerosol extinction, averaged across all profiles in each season over Northern East China and Northwest China, respectively. Over Northern East China (Fig. 4b), GEOS-Chem underestimates the CALIOP values above 1 km by 52–71%. This underestimate leads to a lower ALH,

删除的内容: 3
删除的内容: 3
删除的内容: 3
删除的内容: 3
删除的内容: 4
删除的内容: 5
删除的内容: 6
删除的内容: 5
删除的内容: 6
删除的内容: 2
删除的内容: 3
删除的内容: 5
删除的内容: 6
删除的内容: 5

consistent with the finding by van Donkelaar et al. (2013) and Lin et al. (2014b). Over Northwest China (Fig. 5b), the model also underestimates the CALIOP values above 1 km by 50–62%. These results imply the importance of correcting the modeled aerosol vertical shape prior to cloud and NO_2 retrievals.

删除的内容: 6

4. Effects of aerosol vertical profile improvement on cloud retrieval in 2012

Figure 6a, b shows the monthly average ALH and cloud top height (CTH, corresponding to cloud pressure, CP) over Northern East China and Northwest China in 2012. In order to discuss the CTH, only cloudy days are analyzed here, by excluding days with zero cloud fraction (CF = 0, clear-sky cases) in POMINO. Although “clear sky” is used sometimes in the literature to represent low cloud coverage (e.g., CF < 0.2 or CRF < 0.5, Boersma et al., 2011; Chimot et al., 2016), here it strictly means CF = 0 while “cloudy sky” means CF > 0. About 62.7% of days contain non-zero fractions of clouds over Northern East China, and the number is 59.1% for Northwest China. The CF changes from POMINO to POMINO v1.1 (i.e., after aerosol vertical profile adjustment) are negligible (within ±0.5%, not shown) due to the same values of AOD and SSA used in both products. This is because overall CF is mostly driven by the continuum reflectance at 475 nm (mainly determined by AOD and surface reflectance, which remain unchanged), which is independent of aerosol profile but CTH is driven by the O_2-O_2 SCD, which is itself impacted by ALH.

删除的内容: 7

Figure 6a, b shows that over the two regions, the CTH varies notably from one month to another, whereas the ALH is much more stable across the months. Over Northern East China, the ALH increases by 0.52 km from POMINO (orange dashed line) to POMINO v1.1 (orange solid line) due to the CALIOP-based monthly climatological adjustment. The increase in ALH means a stronger “shielding” effect of aerosols on the O_2-O_2 absorbing dimer, which, in turn, results in a reduced CTH by 0.69 km on average. For POMINO over Northern East China (Fig. 6a), the retrieved clouds

删除的内容: 7

删除的内容: 7

usually extend above the aerosol layer, i.e., the CTH (grey dashed line) is much larger than the ALH (orange dashed line). Using the CALIOP climatology in POMINO v1.1 results in the ALH higher than the CTH in fall and winter. The more elevated ALH is consistent with the finding of Jethva et al. (2016) that a significant amount of absorbing aerosols resides above clouds over Northern East China based on 11-year (2004–2015) OMI near-UV observations.

The CTH in Northwest China is much lower than in Northern East China (Fig. 6a versus 7b). This is because the dominant type of actual clouds is (optically thin) cirrus over western China (Wang et al., 2014), which is interpreted by the O_2-O_2 cloud retrieval algorithm as reduced CTH (with cloud base from the ground). The reduction in CTH from POMINO to POMINO v1.1 over Northwest China is also smaller than the reduction over Northern East China, albeit with a similar enhancement in ALH, due to lower aerosol loadings (Fig. 6c versus 6d).

Figure 7g,h presents the relative change in CP from POMINO to POMINO v1.1 as a function of AOD (binned at an interval of 0.1) and changes in ALH from POMINO to POMINO v1.1 (ΔALH, binned every 0.2 km) across all pixels in 2012 over Northern East China. Results are separated for low cloud fraction (CF < 0.05 in POMINO, Fig. 7g) and modest cloud fraction (0.2 < CF < 0.3, Fig. 7h). The median of the CP changes for pixels within each AOD and ΔALH bin is shown. Figure 7e,f presents the corresponding numbers of occurrence under the two cloud conditions.

Figure 7 shows that over Northern East China, the increase in ALH is typically within 0.6 km for the case of CF < 0.05 (Fig. 7e), and the corresponding increase in CP is within 6% (Fig. 7g). In this case, the average CTH (2.95 km in POMINO versus 1.58 km in POMINO v1.1) becomes much lower than the average ALH (1.06 km in POMINO versus 1.98 km in POMINO v1.1). For the case with CF between 0.2 and 0.3, the increase in ALH is within 1.2 km for most scenes (Fig. 7f), which leads to a

CP change of 2% (Fig. 7h), much smaller than the CP change for CF < 0.05 (Fig. 7g). This is partly because the larger the CF is, the smaller a change in CF is required to compensate for the ΔALH in the O_2-O_2 cloud retrieval algorithm. Furthermore, with 0.2 < CF < 0.3, the mean value of CTH is much higher than ALH in both POMINO (2.76 km for CTH versus 1.13km for ALH) and POMINO v1.1 (2.60km for CTH versus 2.09 km for ALH), thus a large portion of clouds are above aerosols so that the change in CP is less sensitive to ΔALH. We find that the summertime data contribute the highest portion (36.5%) to the occurrences for 0.2 < CF < 0.3.

删除的内容: 8

删除的内容: 8

For Northwest China (not shown), the dependence of CP changes to AOD and ΔALH is similar to that for Northern East China. In particular, the CP change is within 10% on average for the case of CF < 0.05 and 1.5% for the case of 0.2 < CF < 0.3.

5. Effects of aerosol vertical profile improvement on NO_2 retrieval in 2012

Figure 7a presents the percentage changes in clear-sky NO_2 VCD from POMINO to POMINO v1.1 as a function of binned AOD and ΔALH over Northern East China. Here, clear-sky pixels are chosen based on CF = 0 in POMINO. In any AOD bin, an increase in ΔALH leads to an enhancement in NO_2. And for any ΔALH, the change in VCD is greater (smaller) when AOD becomes larger (smaller), which indicates that the NO_2 retrieval is more sensitive to ALH in high aerosol loading cases. Clearly, the change in NO_2 is not a linear function of AOD and ΔALH.

删除的内容: 8

For cloudy scenes (Fig. 7b,c, cloud data are based on POMINO), the change in NO_2 VCD is less sensitive to AOD and ΔALH. This is because the existence of clouds limits the optical effect of aerosols on tropospheric NO_2. Figure 6a presents the nitrogen layer height (NLH, defined as the average height of model simulated NO_2 weighted by its volume mixing ratio in each layer) in comparison to the ALH and CLH over Northern East China. The figure shows that the POMINO v1.1 CTH is

删除的内容: 8

删除的内容: 7

higher than the NLH in all months and higher than the ALH in warm months, which means a "shielding" effect on both NO_2 and aerosols.

Over Northwest China (not shown), the changes in clear-sky NO_2 VCD are within 9% for most cases, which are much smaller than over Eastern China (within 18%). This is because the NLH is much higher than the CLH and ALH (Fig. 6b) in absence of surface anthropogenic emissions.

删除的内容: 7

We convert the valid pixels into monthly mean Level-3 values datasets on a 0.25° long. × 0.25° lat. grid. Figure 8a,b compares the seasonal spatial variations of NO_2 VCD in POMINO v1.1 and POMINO in 2012. In both products, NO_2 peaks in winter due to the longest lifetime and highest anthropogenic emissions (Lin, 2012). NO_2 also reaches a maximum over Northern East China as a result of substantial anthropogenic sources. From POMINO to POMINO v1.1, the NO_2 VCD increases by 3.4% (-67.5–41.7%) in spring for the domain average (range), 3.0% (-59.5–34.4%) in summer, 4.6% (-15.3–39.6%) in fall and 5.3% (-68.4–49.3%) in winter. The NO_2 change is highly dependent on the location and season. The increase over Northern East China is largest in winter, wherein the positive value for ΔALH implies that elevated aerosol layers "shield" the NO_2 absorption.

删除的内容: 9

删除的内容: mean

删除的内容: that better

6. Evaluating satellite products using MAX-DOAS data

We use MAX-DOAS data, after cloud screening (Sect. 2.4), to evaluate DOMNO v2, QA4ECV, POMINO and POMINO v1.1. The scatterplots in Fig. 9a-d compare the NO_2 VCDs from 162 OMI pixels on 49 days with their MAX-DOAS counterparts. Different colors differentiate the seasons. The high values of NO_2 VCD (> 30 × 10^{15} molec. cm^{-2}) occur mainly in fall (blue) and winter (black). POMINO v1.1 and POMINO capture the day-to-day variability of MAX-DOAS data, i.e., R^2 = 0.804 and 0.799, respectively. The normalized mean bias (NMB) of POMINO v1.1 relative to

删除的内容: 10a-c

MAX-DOAS data (-3.4%) is smaller than the NMB of POMINO (-9.6%). Also, the reduced major axis (RMA) regression shows that the slope for POMINO v1.1 (0.95) is closer to unity than the slope for POMINO (0.78). When all OMI pixels in a day are averaged (Fig. 9e,f), the correlation across the total of 49 days further increase for both POMINO v1.1 (R^2 = 0.89) and POMINO (R^2 = 0.86), whereas POMINO v1.1 still has a lower NMB (-3.7%) and better slope (0.96) than POMINO (-10.4% and 0.82, respectively). These results suggest that correcting aerosol vertical profiles, at least on a climatology basis, already leads to a significant improved NO_2 retrieval from OMI.

Figure 9 shows that DOMINO v2 is correlated with MAX-DOAS (R^2 = 0.68 in Fig. 9c and 0.75 in Fig. 9g) but not as strong as POMINO and POMINO v1.1 for all days. The discrepancy between DOMINO v2 and MAX-DOAS is particularly large for very high NO_2 values (> 70 × 10^{15} molec. cm^{-2}). The R^2 for QA4ECV (0.75 in Fig. 9d and 0.82 in Fig. 9h) is slightly better than DOMINO, but the NMB is higher (-22.0% and -22.7%) and the slope drops to 0.66. These results are consistent with the finding of Lin et al. (2014b, 2015) that explicitly including aerosol optical effects improves the NO_2 retrieval.

Table 2 further shows the comparison statistics for 27 haze days. The haze days are determined when both the ground meteorological station data and MODIS/Aqua corrected reflectance (true color) data indicate a haze day. The table also lists AOD, SSA, CF and MAX-DOAS NO_2 VCD, as averaged over all haze days. A large amount of absorbing aerosols occurs on these haze days (AOD = 1.13, SSA = 0.90). The average MAX-DOAS NO_2 VCD reaches 51.92 × 10^{15} molec. cm^{-2}. Among the four satellite products, POMINO v1.1 has the highest R^2 (0.76) and the lowest bias (4.4%) with respect to MAX-DOAS, whereas DOMINO v2 and QA4ECV reproduce the variability to a limited extent (R^2 = 0.38 and 0.34, respectively). This is consistent

删除的内容: 11d,e

删除的内容:

批注 [FB3]: Please clarify if this is now for haze days, or all days.

删除的内容: 10c,f

删除的内容: 10

删除的内容: 45

删除的内容: 10

删除的内容: f

删除的内容: well

带格式的: 上标

删除的内容: much

删除的内容: 4

删除的内容: three

删除的内容: s

with the previous finding that the accuracy of DOMINO v2 is reduced for polluted, aerosol-loaded scenes (Boersma et al., 2011; Chimot et al., 2016; Kanaya et al., 2014; Lin et al., 2014b).

Table 3 shows the comparison statistics for 36 cloud-free days (CF = 0 in POMINO and AOD = 0.60 on average). Here, POMINO v1.1, POMINO and DONIMO v2 do not show large differences in R^2 (0.53–0.56) and NMB (20.8–29.4%) with respect to MAX-DOAS. QA4ECV has a higher R^2 (0.63) and a lower NMB (-5.83%), presumably reflecting the improvements in this community best practices approach, at least in mostly cloud-free situations. However, the R^2 values for POMINO and POMINO v1.1 are much smaller than the R^2 values in haze days, whereas the opposite changes are true for DOMINO v2 and QA4ECV. Thus, for this limited set of data, the changes from DOMINO v2 and QA4ECV to POMINO and POMINO v1.1 mainly reflect the improved aerosol treatment in hazy scenes. Further research may use additional MAX-DOAS datasets to evaluate the satellite products more systematically.

7. Conclusions

This paper improves upon our previous POMINO algorithm (Lin et al., 2015) to retrieve the tropospheric NO_2 VCDs from OMI, by compiling a 9-year (2007–2015) CALIOP monthly climatology of aerosol vertical extinction profiles to adjust GEOS-Chem aerosol profiles used in the NO_2 retrieval process. The improved algorithm is referred to as POMINO v1.1. Compared to monthly climatological CALIOP data over China, GEOS-Chem simulations tend to underestimate the aerosol extinction above 1 km, as characterized by an underestimate in ALH by 300–600 m (seasonal and location dependent). Such a bias is corrected in POMINO v1.1 by dividing, for any month and grid cell, the CALIOP monthly climatological profile by

删除的内容: c

带格式的: 段落间距段后: 10 磅, 图案: 清除

删除的内容: 5

删除的内容: the three OMI products

删除的内容: and NMB (20.8–29.4%)

带格式的: 字体: (中文) +中文正文 (宋体), 上标

删除的内容: that in the cloud-free cases the ensemble of algorithms improves the retrieval results

删除的内容: is

删除的内容: ↵

删除的内容: product

the model climatological profile to obtain a scaling profile and then applying the scaling profile to model data in all days of that month in all years.

The aerosol extinction profile correction leads to an insignificant change in CF from POMINO to POMINO v1.1, since the AOD and surface reflectance are unchanged. In contrast, the correction results in a notably increase in CP (i.e., a decrease in CTH), due to lifting of aerosol layers. The CP changes are generally within 6% for scenes with low cloud fraction (CF < 0.05 in POMINO), and within 2% for scenes with modest cloud fraction (0.2 < CF < 0.3 in POMINO).

The NO_2 VCDs increase from POMINO to POMINO v1.1 in most cases due to lifting of aerosol layers that enhances the "shielding" of NO_2 absorption. The NO_2 VCD increases by 3.4% (-67.5–41.7%) in spring for the domain average (range), 3.0% (-59.5–34.4%) in summer, 4.6% (-15.3–39.6%) in fall and 5.3% (-68.4–49.3%) in winter. The NO_2 changes highly season and location dependent, and are most significant for wintertime Northern East China.

Further comparisons with independent MAX-DOAS NO_2 VCD data for 162 OMI pixels in 49 days show good performance of both POMINO v1.1 and POMINO in capturing the day-to-day variation of NO_2 (R^2=0.80, n=162), compared to DOMINO v2 (R^2=0.67) and the new QA4ECV product (R^2=0.75). The NMB is smaller in POMINO v1.1 (-3.4%) than in POMINO (-9.6%), with a slightly better slope (0.804 versus 0.784). On hazy days with high aerosol loadings (AOD = 1.13 on average), POMINO v1.1 has the highest R^2 (0.76) and the lowest bias (4.4%) whereas DOMINO and QA4ECV have difficulty in reproducing the day-to-day variability in MAX-DOAS NO_2 measurements (R^2 = 0.38 and 0.34, respectively). The four products show small differences in R^2 on clear-sky days (CF = 0 in POMINO, AOD = 0.60 on average). Thus the explicit aerosol treatment (in POMINO and POMINO v1.1)

删除的内容: or
删除的内容: has
删除的内容: ,
删除的内容: three
删除的内容: and NMB

and the aerosol vertical profile correction (in POMINO v1.1) improves the NO_2 retrieval especially in hazy cases.

The POMINO v1.1 algorithm is a core step towards our next public release of data product, POMINO v2. This new release will contain a few additional updates, including but not limited to using MODIS Collection 6 Merged 10-km Level-2 AOD data that combine the Dark Target (Levy et al., 2013) and Deep Blue (Sayer et al., 2014) products, as well as MODIS MCD43C2 Collection 6 daily BRDF data. Meanwhile, the POMINO algorithm framework is being applied to the recently launched TropOMI instrument that provides NO_2 information at a much higher spatial resolution (3.5 x 7 km^2). A modified algorithm can also be used to retrieve sulfur dioxide, formaldehyde and other trace gases from TropOMI, for which purposes our algorithm will be available to the community on a collaborative basis. Future research can correct the SSA and NO_2 vertical profile to further improve the retrieval algorithm, and can use more comprehensive independent data to evaluate the resulting satellite products.

Acknowledgements

This research is supported by the National Natural Science Foundation of China (41775115), the 973 program (2014CB441303), the Chinese Scholarship Council, and the EU FP7 QA4ECV project (grant no. 607405).

Appendix A: Introduction to the QA4ECV product

The QA4ECV NO_2 product (http://www.qa4ecv.eu/) builds on a (EU-) consortium best practices approach to retrieve NO_2 from GOME, SCIAMACHY, GOME-2, and OMI. The main contributions are provided by BIRA-IASB, the University of Bremen (IUP), MPIC, KNMI, and Wageningen University. Uncertainties in spectral fitting for NO_2 SCDs and in AMF calculations were evaluated by Zara et al. (2018) and Lorente

删除的内容:

删除的内容: KFB: I think a sentence on the relatively good performance of QA4ECV in non-hazy days would be useful. Your paper adds value to the literature by being one of the first to do a systematic validation of the QA4ECV product! You have already some good indications when the algorithm does fine, and under which circumstances it is biased. This should be highlighted.

删除的内容: (Levy et al., 2013)

批注 [JL4]: citation

删除的内容: (Sayer et al., 2013)

删除的内容: Our POMINO v1.1

删除的内容:

带格式的

带格式的: 标题 1, 左, 段落间距段后: 0 磅, 图案: 清除

删除的内容: The

删除的内容: i

带格式的

带格式的

带格式的: 字体: 非加粗

删除的内容: EU FP7-project Quality Assurance for Essential ... [5]

删除的内容:)

删除的内容: is aim at making rapid judgments on validitiy and ... [6]

删除的内容: is

带格式的: 字体: 非加粗

带格式的: 下标

删除的内容: a kind of

删除的内容: essentially an ensemble data sets of satellite products ... [7]

删除的内容: and

删除的内容: , with a fully traceable quality assurance on all aspects ... [8]

带格式的: 下标

删除的内容: The u

删除的内容: of

删除的内容: algorithms

删除的内容: the

带格式的: 下标

删除的内容: ,

et al. (2017), respectively. QA4ECV contains improved SCD NO_2 data (Zara et al., 2018). Lorente et al., (2017) showed that across the above algorithms, there a structural uncertainty by 42% in the NO_2 AMF calculation over polluted areas. By comparing to our POMINO product, Lorente et al. also showed that the choice of aerosol correction may introduce an additional uncertainty by up to 50% for situations with high polluted cases, consistent with Lin et al. (2014b, 2015) and the findings here. For a complete description of the QA4ECV algorithm improvements, and quality assurance, please see Boersma et al. (2018).

Appendix B: Constructing the CALIOP monthly climatology of aerosol extinction vertical profile

Our use the all-sky Level-2 CALIOP data to construct the Level-3 monthly climatology. We choose the all-sky product instead of clear-sky data, since previous studies indicate that the climatological aerosol extinction profiles are affected insignificantly by the presence of clouds (Koffi et al., 2012; Winker et al., 2013). As we use this climatological data to adjust GEOS-Chem results, choosing all-sky data improves consistency with the model simulation when doing the daily correction.

To select valid pixels, we follow the data quality criteria by Winker et al., (2013) and Amiridis et al., (2015). Only the pixels with Cloud Aerosol Discrimination (CAD) scores between -20 and -100 with extinction Quality Control (QC) flag valued at 0, 1, 18, and 16 are selected. We further discard samples with an extinction uncertainty of 99.9 km^{-1}, which is indicative of unreliable retrieval. We only accept extinction values falling in the range from 0.0 to 1.25, according to CALIOP observation thresholds. Previous studies showed that weakly scattering edges of icy clouds are sometimes misclassified as aerosols (Winker et al., 2013). To eliminate contamination from icy clouds we exclude the aerosol layers above the cloud layer (with layer-top temperature below 0 ℃) when both of them are above 4km (Winker et al., 2013).

删除的内容: ,
删除的内容: The improved
删除的内容: NO_2
带格式的: 下标
删除的内容: shows better performance in
删除的内容: but do not altogether eliminated systematic errors in ththee fitting approach
删除的内容: 42%
删除的内容: of
带格式的: 下标
删除的内容: s
删除的内容: aereas
删除的内容: , and
删除的内容: s
删除的内容: average
删除的内容: of
批注 [JL5]: Revise the format of the reference list
带格式的: 荷兰语
删除的内容:
带格式的
删除的内容: **The way to c**
带格式的
带格式的
删除的内容: **mean**
带格式的
带格式的
带格式的
删除的内容: **climatology**
带格式的: 字体: 非加粗
已移动(插入) [5]
删除的内容: The way to select the good quality profile mainly
删除的内容: s
已移动(插入) [1]

After the pixel-based screening, we aggregate the CALIOP data at the model grid (0.667° long. x 0.5° lat.) and vertical resolution (47 layers, with 36 layers or so in the troposphere). For each grid cell, we choose the CALIOP pixels within 1.5° of the grid cell center. CALIOP Level-2 data are always presented at the fixed 399 altitudes above sea level. To account for the difference in surface elevation between a CALIOP pixel and the respective model grid cell, we convert the altitude of the pixel to a height above the ground, by using the surface elevation data provided in CALIOP. We then average horizontally and vertically the profiles of all pixels within one model grid cell and layer. We do the regridding day-by-day for all grid cells to ensure that GEOS-Chem and CALIOP extinction profiles are coincident spatially and temporally. Finally, we compile a monthly climatological dataset by averaging over 2007–2015.

Figure A1 shows the number of aerosol extinction profiles in each grid cell and 12 x 9 = 108 months that are used to compile the CALIOP climatology, both before and after data screening. Table A1 presents additional information on monthly and yearly bases. On average, there are 165 and 47 aerosol extinction profiles per month per grid cell before and after screening, respectively. In the final 9-year monthly climatology, each grid cell has about 420 aerosol extinction profiles on average, about 28% of the prior-screening profiles. Figure A1 shows that the number of valid profiles decreases sharply over the Tibet Plateau and at higher latitudes (> 43° N) due to complex terrain and icy/snowy ground.

As discussed above, we choose the CALIOP pixels within 1.5° of a grid cell center. We test this choice by examining the aerosol layer height (ALH) produced for that grid cell. The ALH is defined as the extinction-weighted height of aerosols (see Eq. A1, where n denotes the number of tropospheric layers, ε_i the aerosol extinction at layer i, and H_i the layer center height above the ground). We find that choosing pixels within 1.0° of a grid cell center leads to a nosier horizontal distribution of

已移动(插入) [2]

删除的内容: ↵

已移动(插入) [3]

ALH, owing to the small footprint of CALIOP. On the other hand, choosing 2.0° leads to a too smooth spatial gradient of ALH with local characteristics of aerosol vertical distributions are largely lost. We thus decide that 1.5° is a good balance between noise and smoothness.

$$\mathrm{ALH} = \frac{\sum_{i=1}^{i=n} \varepsilon_i \mathrm{H}_i}{\sum_{i=1}^{i=n} \varepsilon_i} \qquad \text{(A1)}$$

Certain grid cells do not contain sufficient valid observations for some months of the climatological dataset. We fill in missing monthly values of a grid cell using valid data in the surrounding 5 x 5 = 25 grid cells (within ~ 100 km). If the 25 grid cells do not have enough valid data, we use those in the surrounding 7 x 7 = 49 grid cells (within ~ 150 km). A similar procedure is used by Lin et al. (2014b, 2015) to fill in missing values in the gridded MODIS AOD dataset.

For each grid cell in each month, we further correct singular values in the vertical profile. In a month, if a grid cell *i* has an ALH outside mean±1σ of its surrounding 25 or 49 grid cells, we select *i*'s surrounding grid cell *j* whose ALH is the median of *i*'s surrounding grid cells, and use *j*'s profile to replace *i*'s. Whether 25 or 49 surrounding grid cells are chosen depends on the number of valid pixels shown in Fig. A1b. If the number of valid pixels in *i* is below mean–1σ of all grid cells in the whole domain, which is often the case for Tibetan grid cells, we use *i*'s surrounding 49 grid cells; otherwise we use *i*'s surrounding 25 grid cells.

删除的内容: Certain grid cells do not contain sufficient valid observations for some months of the climatological data set. We fill in missing monthly values of a grid cell using valid data in the surrounding 25 or 49 grid cells.

已移动(插入) [4]

带格式的: 字体: 非加粗

带格式的: 字体: 非加粗

Appendix C. Comparing our and NASA's CALIOP monthly climatology

带格式的: 标题 1

We compare our gridded climatological profiles to NASA CALIOP Version 3 Level-3 all-sky monthly profiles at 532 nm (Winker et al., 2013). The NASA Level-3 data has a horizontal resolution of 2° lat. × 5° lon. and a vertical resolution of 60 m (from -0.5 to 12 km above sea level). We combine NASA monthly data over 2007–

2015 to construct a monthly climatology for comparison with our own compilation. We only choose aerosol extinction data in the troposphere with error less than 0.15 (the valid range given in the CALIOP dataset). If the number of valid monthly profiles in a grid cell is less than five (i.e., for the same month in five out of the nine years), then we exclude data in that grid cell; see the dark gray grid cells in Fig. 2c.

Several methodological differences exist between generating our and NASA CALIOP datasets. First, the two datasets have different horizontal resolutions. Also, we sample all valid CALIOP pixels within 1.5^0 of a grid cell center, whereas the NASA dataset samples all valid pixels within a grid cell. Besides, our CALIOP dataset involves several steps of horizontal interpolation, for purposes of subsequent cloud and NO_2 retrievals, which is not done in the NASA dataset. In addition, we match CALIOP data vertically to the GEOS-Chem vertical resolution, whereas the NASA dataset maintains the original resolution.

Figure 2c shows the spatial distribution of ALH in all seasons based on NASA CALIOP Level-3 all-sky monthly climatology. The horizontal resolution of NASA data is much coarser than ours; and NASA data are largely missing over the southwest with complex terrains. We choose to focus on the comparison over East China (the black box in Fig. 1a). Over East China, the two climatology datasets generally exhibit similar spatial patterns of ALH in all seasons (Fig. 2a, c). The NASA dataset suggests higher ALHs than ours over Eastern China, especially in summer, due mainly to differences in the sampling and regridding processes. Figure 3c further compares the monthly variation of ALH between our (black line with error bars) and NASA (blue filled triangles) datasets averaged over East China. The two datasets are consistent in almost all months, indicating that their regional differences are largely smoothed out by spatial averaging.

References

带格式的: 图案：清除

带格式的: 字体：非加粗

删除的内容: **Appendix C: The introduction to new version of POMINO product**

In our new relased version, several aspect will be update:

1) Use 9-year CALIOP climatology aerosol extinction profile to adjust GEOS-Chem daily aerosol extinction profiles. This is the main update in our new released version, which will also be applied to the retrieval algorithm of newly laughed TropOMI sensor.

2) MODIS Collection 6 Merged 10-km Level-2 AOD product will be used to replace the MODIS Collection 5 Dark Target (DT) product to adjust model simulation. Previous studies has shown various contextual biases exist in C5 version (Levy et al., 2010; Bréon et al., 2011). The C6 product update**s the widely used DT (Levy et al., 2013) and Deep Blue (DB) product (Sayer et al., 2013). It also relased the merged AOD product to provide a more gap-filled data set based on DT, DB and MODIS-derived climatologies of NDVI (Huete et al., 2011).**

3) MODIS MCD43C2 Collection 6 daily BRDF/Albedo Snow-free Model Parameters Daily L3 Global 0.05Deg data set is used to replace C5 8-day averaged data set to account for the daily BRDF effect of surface. There is improved quality and more retrieval at high latitudes and use current day snow status when retrieval in C6.

带格式的

Acarreta, J. R., De Haan, J. F. and Stammes, P.: Cloud pressure retrieval using the O_2-O_2 absorption band at 477 nm, J. Geophys. Res., 109(D5), D05204, doi:10.1029/2003JD003915, 2004.

Amiridis, V., Marinou, E., Tsekeri, A., Wandinger, U., Schwarz, A., Giannakaki, E., Mamouri, R., Kokkalis, P., Binietoglou, I., Solomos, S., Herekakis, T., Kazadzis, S., Gerasopoulos, E., Proestakis, E., Kottas, M., Balis, D., Papayannis, A., Kontoes, C., Kourtidis, K., Papagiannopoulos, N., Mona, L., Pappalardo, G., Le Rille, O. and Ansmann, A.: LIVAS: a 3-D multi-wavelength aerosol/cloud database based on CALIPSO and EARLINET, Atmos. Chem. Phys., 15(13), 7127–7153, doi:10.5194/acp-15-7127-2015, 2015.

Belmonte Rivas, M., Veefkind, P., Boersma, F., Levelt, P., Eskes, H. and Gille, J.: Intercomparison of daytime stratospheric NO_2 satellite retrievals and model simulations, Atmos. Meas. Tech., 7(7), 2203–2225, doi:10.5194/amt-7-2203-2014, 2014.

Boersma, K. F., Eskes, H. J. and Brinksma, E. J.: Error analysis for tropospheric NO_2 retrieval from space, J. Geophys. Res. Atmos., 109(D4), n/a-n/a, doi:10.1029/2003JD003962, 2004.

Boersma, K. F., Eskes, H. J., Veefkind, J. P., Brinksma, E. J., van der A, R. J., Sneep, M., van den Oord, G. H. J., Levelt, P. F., Stammes, P., Gleason, J. F. and Bucsela, E. J.: Near-real time retrieval of tropospheric NO_2 from OMI, Atmos. Chem. Phys., 7(8), 2103–2118, doi:10.5194/acp-7-2103-2007, 2007.

Boersma, K. F., Eskes, H. J., Dirksen, R. J., van der A, R. J., Veefkind, J. P., Stammes, P., Huijnen, V., Kleipool, Q. L., Sneep, M., Claas, J., Leitão, J., Richter, A., Zhou, Y. and Brunner, D.: An improved tropospheric NO_2 column retrieval algorithm for the

带格式的: 两端对齐

删除的内容: <sub>

删除的内容: </sub&gt

删除的内容: <sub>

删除的内容: </sub&gt

删除的内容: <sub>

删除的内容: </sub&gt

Ozone Monitoring Instrument, Atmos. Meas. Tech., 4(9), 1905–1928, doi:10.5194/amt-4-1905-2011, 2011a.

Boersma, K.F., Eskes, H. J., Richter, A., De Smedt, I., Lorente, A., Beirle, S., van Geffen, J. H. G. M., Zara, M., Peters, E., Van Roozendael, M., Wagner, T., Maasakkers, J. D., van der A, R. J., Nightingale, J., De Rudder, A., Irie, H., and Pinardi, G.: Improving algorithms and uncertainty estimates for satellite NO_2 retrievals: Results from the Quality Assurance for Essential Climate Variables (QA4ECV) project, amt-2018-200, submitted, 2018.

Bucsela, E. J., Celarier, E. A., Wenig, M. O., Gleason, J. F., Veefkind, J. P., Boersma, K. F. and Brinksma, E. J.: Algorithm for NO2 vertical column retrieval from the ozone monitoring instrument, IEEE Trans. Geosci. Remote Sens., 44(5), 1245–1258, doi:10.1109/TGRS.2005.863715, 2006.

Bucsela, E. J., Krotkov, N. A., Celarier, E. A., Lamsal, L. N., Swartz, W. H., Bhartia, P. K., Boersma, K. F., Veefkind, J. P., Gleason, J. F. and Pickering, K. E.: A new stratospheric and tropospheric NO2 retrieval algorithm for nadir-viewing satellite instruments: applications to OMI, Atmos. Meas. Tech., 6(10), 2607–2626, doi:10.5194/amt-6-2607-2013, 2013.

Castellanos, P., Boersma, K. F. and van der Werf, G. R.: Satellite observations indicate substantial spatiotemporal variability in biomass burning NOx emission factors for South America, Atmos. Chem. Phys., 14(8), 3929–3943, doi:10.5194/acp-14-3929-2014, 2014.

Castellanos, P., Boersma, K. F., Torres, O. and de Haan, J. F.: OMI tropospheric NO2 air mass factors over South America: effects of biomass burning aerosols, Atmos. Meas. Tech., 8(9), 3831–3849, doi:10.5194/amt-8-3831-2015, 2015.

删除的内容: Boersma, K. F., Eskes, H. J., Dirksen, R. J., van der A, R. J., Veefkind, J. P., Stammes, P., Huijnen, V., Kleipool, Q. L., Sneep, M., Claas, J., Leitão, J., Richter, A., Zhou, Y. and Brunner, D.: An improved tropospheric NO₂ column retrieval algorithm for the Ozone Monitoring Instrument, Atmos. Meas. Tech., 4(9), 1905–1928, doi:10.5194/amt-4-1905-2011, 2011b. KFB: cited twice.
Boersma, K. F., Eskes, H. J., Dirksen, R. J., van der A, R. J., Veefkind, J. P., Stammes, P., Huijnen, V., Kleipool, Q. L., Sneep, M., Claas, J., Leitão, J., Richter, A., Zhou, Y. and Brunner, D.: An improved tropospheric NO₂ column retrieval algorithm for the Ozone Monitoring Instrument, Atmos. Meas. Tech., 4(9), 1905–1928, doi:10.5194/amt-4-1905-2011, 2011c. Cited thrice.

删除的内容: /sub

删除的内容: /

删除的内容: <sub>

删除的内容: </sub&gt

删除的内容: <sub>

删除的内容: </sub&gt

删除的内容: <sub>

删除的内容: </sub&gt

Chazette, P., Raut, J.-C., Dulac, F., Berthier, S., Kim, S.-W., Royer, P., Sanak, J., Loaëc, S. and Grigaut-Desbrosses, H.: Simultaneous observations of lower tropospheric continental aerosols with a ground-based, an airborne, and the spaceborne CALIOP lidar system, J. Geophys. Res., 115(D4), D00H31, doi:10.1029/2009JD012341, 2010.

Chimot, J., Vlemmix, T., Veefkind, J. P., de Haan, J. F. and Levelt, P. F.: Impact of aerosols on the OMI tropospheric NO_2 retrievals over industrialized regions: how accurate is the aerosol correction of cloud-free scenes via a simple cloud model?, Atmos. Meas. Tech., 9(2), 359–382, doi:10.5194/amt-9-359-2016, 2016.

Clémer, K., Van Roozendael, M., Fayt, C., Hendrick, F., Hermans, C., Pinardi, G., Spurr, R., Wang, P. and De Mazière, M.: Multiple wavelength retrieval of tropospheric aerosol optical properties from MAXDOAS measurements in Beijing, Atmos. Meas. Tech., 3(4), 863–878, doi:10.5194/amt-3-863-2010, 2010.

Cui, Y., Lin, J., Song, C., Liu, M., Yan, Y., Xu, Y. and Huang, B.: Rapid growth in nitrogen dioxide pollution over Western China, 2005–2013, Atmos. Chem. Phys., 16(10), 6207–6221, doi:10.5194/acp-16-6207-2016, 2016.

Dirksen, R. J., Boersma, K. F., Eskes, H. J., Ionov, D. V., Bucsela, E. J., Levelt, P. F. and Kelder, H. M.: Evaluation of stratospheric NO_2 retrieved from the Ozone Monitoring Instrument: Intercomparison, diurnal cycle, and trending, J. Geophys. Res., 116(D8), D08305, doi:10.1029/2010JD014943, 2011.

van Geffen, J. H. G. M., Boersma, K. F., Van Roozendael, M., Hendrick, F., Mahieu, E., De Smedt, I., Sneep, M. and Veefkind, J. P.: Improved spectral fitting of nitrogen dioxide from OMI in the 405–465 nm window, Atmos. Meas. Tech., 8(4), 1685–1699, doi:10.5194/amt-8-1685-2015, 2015.

删除的内容: <sub>

删除的内容: </sub>

Gielen, C., Van Roozendael, M., Hendrick, F., Pinardi, G., Vlemmix, T., De Bock, V., De Backer, H., Fayt, C., Hermans, C., Gillotay, D. and Wang, P.: A simple and versatile cloud-screening method for MAX-DOAS retrievals, Atmos. Meas. Tech., 7(10), 3509–3527, doi:10.5194/amt-7-3509-2014, 2014.

Huang, Z., Huang, J., Bi, J., Wang, G., Wang, W., Fu, Q., Li, Z., Tsay, S.-C. and Shi, J.: Dust aerosol vertical structure measurements using three MPL lidars during 2008 China-U.S. joint dust field experiment, J. Geophys. Res. Atmos., 115(D7), n/a-n/a, doi:10.1029/2009JD013273, 2010.

Irie, H., Boersma, K. F., Kanaya, Y., Takashima, H., Pan, X. and Wang, Z. F.: Quantitative bias estimates for tropospheric NO_2 columns retrieved from SCIAMACHY, OMI, and GOME-2 using a common standard for East Asia, Atmos. Meas. Tech., 5(10), 2403–2411, doi:10.5194/amt-5-2403-2012, 2012.

删除的内容: <sub>

删除的内容: </sub&gt

Johnson, M. S., Meskhidze, N. and Praju Kiliyanpilakkil, V.: A global comparison of GEOS-Chem-predicted and remotely-sensed mineral dust aerosol optical depth and extinction profiles, J. Adv. Model. Earth Syst., 4(3), M07001, doi:10.1029/2011MS000109, 2012.

Kacenelenbogen, M., Redemann, J., Vaughan, M. A., Omar, A. H., Russell, P. B., Burton, S., Rogers, R. R., Ferrare, R. A. and Hostetler, C. A.: An evaluation of CALIOP/CALIPSO's aerosol-above-cloud detection and retrieval capability over North America, J. Geophys. Res. Atmos., 119(1), 230–244, doi:10.1002/2013JD020178, 2014.

Kanaya, Y., Irie, H., Takashima, H., Iwabuchi, H., Akimoto, H., Sudo, K., Gu, M., Chong, J., Kim, Y. J., Lee, H., Li, A., Si, F., Xu, J., Xie, P.-H., Liu, W.-Q., Dzhola, A., Postylyakov, O., Ivanov, V., Grechko, E., Terpugova, S. and Panchenko, M.: Long-term MAX-DOAS network observations of NO_2 in Russia and Asia (MADRAS)

删除的内容: <sub>

删除的内容: </sub>

during the period 2007-2012: instrumentation, elucidation of climatology, and comparisons with OMI satellite observations and global model simulations, Atmos. Chem. Phys., 14(15), 7909–7927, doi:10.5194/acp-14-7909-2014, 2014.

Kim, S.-W., Heckel, A., Frost, G. J., Richter, A., Gleason, J., Burrows, J. P., McKeen, S., Hsie, E.-Y., Granier, C. and Trainer, M.: NO_2 columns in the western United States observed from space and simulated by a regional chemistry model and their implications for NO_x emissions, J. Geophys. Res., 114(D11), D11301, doi:10.1029/2008JD011343, 2009.

Koffi, B., Schulz, M., Bréon, F.-M., Griesfeller, J., Winker, D., Balkanski, Y., Bauer, S., Berntsen, T., Chin, M., Collins, W. D., Dentener, F., Diehl, T., Easter, R., Ghan, S., Ginoux, P., Gong, S., Horowitz, L. W., Iversen, T., Kirkevåg, A., Koch, D., Krol, M., Myhre, G., Stier, P. and Takemura, T.: Application of the CALIOP layer product to evaluate the vertical distribution of aerosols estimated by global models: AeroCom phase I results, J. Geophys. Res. Atmos., 117(D10), n/a-n/a, doi:10.1029/2011JD016858, 2012.

Leitão, J., Richter, A., Vrekoussis, M., Kokhanovsky, A., Zhang, Q. J., Beekmann, M. and Burrows, J. P.: On the improvement of NO2 satellite retrievals – aerosol impact on the airmass factors, Atmos. Meas. Tech., 3(2), 475–493, doi:10.5194/amt-3-475-2010, 2010.

Lerot, C., Stavrakou, T., De Smedt, I., Müller, J.-F. and Van Roozendael, M.: Glyoxal vertical columns from GOME-2 backscattered light measurements and comparisons with a global model, Atmos. Chem. Phys., 10(24), 12059–12072, doi:10.5194/acp-10-12059-2010, 2010.

删除的内容: –

删除的内容: <sub>

删除的内容: </sub>

Levy, R. C., Mattoo, S., Munchak, L. A., Remer, L. A., Sayer, A. M., Patadia, F. and Hsu, N. C.: The Collection 6 MODIS aerosol products over land and ocean, Atmos. Meas. Tech., 6(11), 2989–3034, doi:10.5194/amt-6-2989-2013, 2013.

Li, S., Yu, C., Chen, L., Tao, J., Letu, H., Ge, W., Si, Y. and Liu, Y.: Inter-comparison of model-simulated and satellite-retrieved componential aerosol optical depths in China, Atmos. Environ., 141, 320–332, doi:https://doi.org/10.1016/j.atmosenv.2016.06.075, 2016.

Lin, J., Pan, D., Davis, S. J., Zhang, Q., He, K., Wang, C., Streets, D. G., Wuebbles, D. J. and Guan, D.: China's international trade and air pollution in the United States, Proc. Natl. Acad. Sci., 111(5), 1736–1741, doi:10.1073/pnas.1312860111, 2014a.

Lin, J.-T.: Satellite constraint for emissions of nitrogen oxides from anthropogenic, lightning and soil sources over East China on a high-resolution grid, Atmos. Chem. Phys., 12(6), 2881–2898, doi:10.5194/acp-12-2881-2012, 2012.

Lin, J.-T., McElroy, M. B. and Boersma, K. F.: Constraint of anthropogenic NOx emissions in China from different sectors: a new methodology using multiple satellite retrievals, Atmos. Chem. Phys., 10(1), 63–78, doi:10.5194/acp-10-63-2010, 2010.

Lin, J.-T., Martin, R. V., Boersma, K. F., Sneep, M., Stammes, P., Spurr, R., Wang, P., Van Roozendael, M., Clémer, K. and Irie, H.: Retrieving tropospheric nitrogen dioxide from the Ozone Monitoring Instrument: effects of aerosols, surface reflectance anisotropy, and vertical profile of nitrogen dioxide, Atmos. Chem. Phys., 14(3), 1441–1461, doi:10.5194/acp-14-1441-2014, 2014b.

Lin, J.-T., Liu, M.-Y., Xin, J.-Y., Boersma, K. F., Spurr, R., Martin, R. and Zhang, Q.: Influence of aerosols and surface reflectance on satellite NO_2 retrieval: seasonal and spatial characteristics and implications for NO_x emission constraints, Atmos. Chem. Phys., 15(19), 11217–11241, doi:10.5194/acp-15-11217-2015, 2015.

删除的内容: <sub>

删除的内容: </sub>

Lorente, A., Folkert Boersma, K., Yu, H., Dörner, S., Hilboll, A., Richter, A., Liu, M., Lamsal, L. N., Barkley, M., De Smedt, I., Van Roozendael, M., Wang, Y., Wagner, T., Beirle, S., Lin, J.-T., Krotkov, N., Stammes, P., Wang, P., Eskes, H. J. and Krol, M.: Structural uncertainty in air mass factor calculation for and HCHO satellite retrievals, Atmos. Meas. Tech., 10(3), 759–782, doi:10.5194/amt-10-759-2017, 2017.

Lucht, W., Schaaf, C. B. and Strahler, A. H.: An algorithm for the retrieval of albedo from space using semiempirical BRDF models, IEEE Trans. Geosci. Remote Sens., 38(2), 977–998, doi:10.1109/36.841980, 2000.

Ma, J. Z., Beirle, S., Jin, J. L., Shaiganfar, R., Yan, P. and Wagner, T.: Tropospheric NO_2 vertical column densities over Beijing: results of the first three years of ground-based MAX-DOAS measurements (2008–2011) and satellite validation, Atmos. Chem. Phys., 13(3), 1547–1567, doi:10.5194/acp-13-1547-2013, 2013.

Ma, X. and Yu, F.: Seasonal variability of aerosol vertical profiles over east US and west Europe: GEOS-Chem/APM simulation and comparison with CALIPSO observations, Atmos. Res., 140–141, 28–37, doi:https://doi.org/10.1016/j.atmosres.2014.01.001, 2014.

Martin, R. V.: An improved retrieval of tropospheric nitrogen dioxide from GOME, J. Geophys. Res., 107(D20), 4437, doi:10.1029/2001JD001027, 2002.

Misra, A., Tripathi, S. N., Kaul, D. S. and Welton, E. J.: Study of MPLNET-Derived Aerosol Climatology over Kanpur, India, and Validation of CALIPSO Level 2 Version 3 Backscatter and Extinction Products, J. Atmos. Ocean. Technol., 29(9), 1285–1294, doi:10.1175/JTECH-D-11-00162.1, 2012.

删除的内容: NO₂

删除的内容: <sub>

删除的内容: </sub>

Miyazaki, K. and Eskes, H.: Constraints on surface NO_x emissions by assimilating satellite observations of multiple species, Geophys. Res. Lett., 40(17), 4745–4750, doi:10.1002/grl.50894, 2013.

Proestakis, E., Amiridis, V., Marinou, E., Georgoulias, A. K., Solomos, S., Kazadzis, S., Chimot, J., Che, H., Alexandri, G., Binietoglou, I., Kourtidis, K. A., de Leeuw, G. and van der A, R. J.: 9-year spatial and temporal evolution of desert dust aerosols over South-East Asia as revealed by CALIOP, Atmos. Chem. Phys. Discuss., 1–35, doi:10.5194/acp-2017-797, 2017.

Richter, A., Begoin, M., Hilboll, A. and Burrows, J. P.: An improved NO2 retrieval for the GOME-2 satellite instrument, Atmos. Meas. Tech., 4(6), 1147–1159, doi:10.5194/amt-4-1147-2011, 2011.

Sareen, N., Schwier, A. N., Shapiro, E. L., Mitroo, D. and McNeill, V. F.: Secondary organic material formed by methylglyoxal in aqueous aerosol mimics, Atmos. Chem. Phys., 10(3), 997–1016, doi:10.5194/acp-10-997-2010, 2010.

Sayer, A. M., Munchak, L. A., Hsu, N. C., Levy, R. C., Bettenhausen, C. and Jeong, M.-J.: MODIS Collection 6 aerosol products: Comparison between Aqua's e-Deep Blue, Dark Target, and "merged" data sets, and usage recommendations, J. Geophys. Res. Atmos., 119(24), 13,965-13,989, doi:10.1002/2014JD022453, 2014.

Stammes, P., Sneep, M., de Haan, J. F., Veefkind, J. P., Wang, P. and Levelt, P. F.: Effective cloud fractions from the Ozone Monitoring Instrument: Theoretical framework and validation, J. Geophys. Res., 113(D16), D16S38, doi:10.1029/2007JD008820, 2008.

Stavrakou, T., Müller, J.-F., Bauwens, M., De Smedt, I., Lerot, C., Van Roozendael, M., Coheur, P.-F., Clerbaux, C., Boersma, K. F., van der A, R. and Song, Y.: Substantial Underestimation of Post-Harvest Burning Emissions in the North China

删除的内容: x

删除的内容: <sub>

删除的内容: </sub>

Plain Revealed by Multi-Species Space Observations, Sci. Rep., 6, 32307, doi:10.1038/srep32307, 2016.

Veefkind, J. P., de Haan, J. F., Sneep, M. and Levelt, P. F.: Improvements to the OMI O2–O2 operational cloud algorithm and comparisons with ground-based radar–lidar observations, Atmos. Meas. Tech., 9(12), 6035–6049, doi:10.5194/amt-9-6035-2016, 2016.

Verstraeten, W. W., Neu, J. L., Williams, J. E., Bowman, K. W., Worden, J. R. and Boersma, K. F.: Rapid increases in tropospheric ozone production and export from China, Nat. Geosci., 8, 690 [online] Available from: http://dx.doi.org/10.1038/ngeo2493, 2015.

Wang, J., Jacob, D. J. and Martin, S. T.: Sensitivity of sulfate direct climate forcing to the hysteresis of particle phase transitions, J. Geophys. Res. Atmos., 113(D11), n/a-n/a, doi:10.1029/2007JD009368, 2008a.

Wang, M., Gu, J., Yang, R., Zeng, L. and Wang, S.: Comparison of cloud type and frequency over China from surface, FY-2E, and CloudSat observations, vol. 9259, pp. 925913–925914. [online] Available from: http://dx.doi.org/10.1117/12.2069110, 2014.

Wang, P. and Stammes, P.: Evaluation of SCIAMACHY Oxygen A band cloud heights using Cloudnet measurements, Atmos. Meas. Tech., 7(5), 1331–1350, doi:10.5194/amt-7-1331-2014, 2014.

Wang, P., Stammes, P., van der A, R., Pinardi, G. and van Roozendael, M.: FRESCO+: an improved O2 A-band cloud retrieval algorithm for tropospheric trace gas retrievals, Atmos. Chem. Phys., 8(21), 6565–6576, doi:10.5194/acp-8-6565-2008, 2008b.

删除的内容: <sub>

删除的内容: </sub>

删除的内容: <sub>

删除的内容: </sub>

删除的内容: <sub>

删除的内容: </sub>

Wang, X., Huang, J., Zhang, R., Chen, B. and Bi, J.: Surface measurements of aerosol properties over northwest China during ARM China 2008 deployment, J. Geophys. Res. Atmos., 115(D7), n/a-n/a, doi:10.1029/2009JD013467, 2010.

Wang, Y., Penning de Vries, M., Xie, P. H., Beirle, S., Dörner, S., Remmers, J., Li, A. and Wagner, T.: Cloud and aerosol classification for 2.5 years of MAX-DOAS observations in Wuxi (China) and comparison to independent data sets, Atmos. Meas. Tech., 8(12), 5133–5156, doi:10.5194/amt-8-5133-2015, 2015.

Wang, Y., Lampel, J., Xie, P., Beirle, S., Li, A., Wu, D. and Wagner, T.: Ground-based MAX-DOAS observations of tropospheric aerosols, NO2, SO2 and HCHO in Wuxi, China, from 2011 to 2014, Atmos. Chem. Phys., 17(3), 2189–2215, doi:10.5194/acp-17-2189-2017, 2017a.

Wang, Y., Beirle, S., Lampel, J., Koukouli, M., De Smedt, I., Theys, N., Li, A., Wu, D., Xie, P., Liu, C., Van Roozendael, M., Stavrakou, T., Müller, J.-F. and Wagner, T.: Validation of OMI, GOME-2A and GOME-2B tropospheric NO2, SO2 and HCHO products using MAX-DOAS observations from 2011 to 2014 in Wuxi, China: investigation of the effects of priori profiles and aerosols on the satellite products, Atmos. Chem. Phys., 17(8), 5007–5033, doi:10.5194/acp-17-5007-2017, 2017b.

Winker, D. M., Pelon, J., Coakley, J. A., Ackerman, S. A., Charlson, R. J., Colarco, P. R., Flamant, P., Fu, Q., Hoff, R. M., Kittaka, C., Kubar, T. L., Le Treut, H., Mccormick, M. P., Mégie, G., Poole, L., Powell, K., Trepte, C., Vaughan, M. A. and Wielicki, B. A.: The CALIPSO Mission, Bull. Am. Meteorol. Soc., 91(9), 1211–1230, doi:10.1175/2010BAMS3009.1, 2010.

Winker, D. M., Tackett, J. L., Getzewich, B. J., Liu, Z., Vaughan, M. A. and Rogers, R. R.: The global 3-D distribution of tropospheric aerosols as characterized by

删除的内容: <sub>

删除的内容: </sub>

删除的内容: <sub>

删除的内容: </sub>

CALIOP, Atmos. Chem. Phys., 13(6), 3345–3361, doi:10.5194/acp-13-3345-2013, 2013.

Zara, M., Boersma, K. F., De Smedt, I., Richter, A., Peters, E., Van Geffen, J. H. G. M., Beirle, S., Wagner, T., Van Roozendael, M., Marchenko, S., Lamsal, L. N. and Eskes, H. J.: Improved slant column density retrieval of nitrogen dioxide and formaldehyde for OMI and GOME-2A from QA4ECV: intercomparison, uncertainty characterization, and trends, Atmos. Meas. Tech. Discuss., 1–47, doi:10.5194/amt-2017-453, 2018.

Zhang, Q., Streets, D. G., Carmichael, G. R., He, K. B., Huo, H., Kannari, A., Klimont, Z., Park, I. S., Reddy, S., Fu, J. S., Chen, D., Duan, L., Lei, Y., Wang, L. T. and Yao, Z. L.: Asian emissions in 2006 for the NASA INTEX-B mission, Atmos. Chem. Phys., 9(14), 5131–5153, doi:10.5194/acp-9-5131-2009, 2009.

Zhao, C. and Wang, Y.: Assimilated inversion of NO_x emissions over east Asia using OMI NO_2 column measurements, Geophys. Res. Lett., 36(6), L06805, doi:10.1029/2008GL037123, 2009.

Zhao, H. Y., Zhang, Q., Guan, D. B., Davis, S. J., Liu, Z., Huo, H., Lin, J. T., Liu, W. D. and He, K. B.: Assessment of China's virtual air pollution transport embodied in trade by using a consumption-based emission inventory, Atmos. Chem. Phys., 15(10), 5443–5456, doi:10.5194/acp-15-5443-2015, 2015.

Zhou, Y., Brunner, D., Spurr, R. J. D., Boersma, K. F., Sneep, M., Popp, C. and Buchmann, B.: Accounting for surface reflectance anisotropy in satellite retrievals of tropospheric NO2, Atmos. Meas. Tech., 3(5), 1185–1203, doi:10.5194/amt-3-1185-2010, 2010.

删除的内容:

删除的内容: <sub>

删除的内容: </sub>

Zhu, W., Xu, C., Qian, X. and Wei, H.: Statistical analysis of the spatial-temporal distribution of aerosol extinction retrieved by micro-pulse lidar in Kashgar, China, Opt. Express, 21(3), 2531–2537, doi:10.1364/OE.21.002531, 2013.

Hendrick, F., Muller, J. F., Clemer, K., Wang, P., De Maziere, M., Fayt, C., Gielen, C., Hermans, C., Ma, J. Z., Pinardi, G., Stavrakou, T., Vlemmix, T., and Van Roozendael, M.: Four years of ground-based MAX-DOAS observations of HONO and NO2 in the Beijing area, Atmospheric Chemistry and Physics, 14, 765-781, 10.5194/acp-14-765-2014, 2014.

Jethva, H., Torres, O., and Ahn, C.: A ten-year global record of absorbing aerosols above clouds from OMI's near-UV observations, in: Remote Sensing of the Atmosphere, Clouds, and Precipitation Vi, edited by: Im, E., Kumar, R., and Yang, S., Proceedings of SPIE, 2016.

Schenkeveld, V. M. E., Jaross, G., Marchenko, S., Haffner, D., Kleipool, Q. L., Rozemeijer, N. C., Veefkind, J. P., and Levelt, P. F.: In-flight performance of the Ozone Monitoring Instrument, Atmospheric Measurement Techniques, 10, 1957-1986, 10.5194/amt-10-1957-2017, 2017.

van Donkelaar, A., Martin, R. V., Spurr, R. J. D., Drury, E., Remer, L. A., Levy, R. C., and Wang, J.: Optimal estimation for global ground-level fine particulate matter concentrations, Journal of Geophysical Research-Atmospheres, 118, 5621-5636, 10.1002/jgrd.50479, 2013.

删除的内容: Wang, Y., Lampel, J., Xie, P., Beirle, S., Li, A., Wu, D., and Wagner, T.: Ground-based MAX-DOAS observations of tropospheric aerosols, NO2, SO2 and HCHO in Wuxi, China, from 2011 to 2014, Atmospheric Chemistry and Physics, 17, 2189-2215, 10.5194/acp-17-2189-2017, 2017.

第 7 页: [1] 删除的内容　Jintai Lin　2018/6/21 PM5:19:00

We apply a number of criteria to ensure data quality of each pixel, mainly following Winker et al. (2013) and Amiridis et al. (2015). More detailed inoframtion about criteria to select the Level-2 are referred to Appendix A.

第 7 页: [2] 删除的内容　Jintai Lin　2018/6/21 PM5:20:00

After the pixel-based screening, we aggregate the CALIOP data at the model grid (0.667° long. x 0.5° lat.) and vertical resolution (47 layers, with 36 layers or so in the troposphere). For each grid cell, we choose the CALIOP pixels within 1.5° of the grid cell center. The way to compile gridded CALIOP climatology aerosol extinction profiles is referred to Appendix B. CALIOP Level-2 data are always presented at the fixed 399 altitudes above sea level. To account for the difference in surface elevation between a CALIOP pixel and the respective model grid cell, we convert the altitude of the pixel to a height above the ground, by using the surface elevation data provided in CALIOP. We then average horizontally and vertically the profiles of all pixels within one model grid cell and layer. We do the regridding day-by-day for all grid cells to ensure that GEOS-Chem and CALIOP extinction profiles are coincident spatially and temporally. Finally, we compile a monthly climatological dataset by averaging over 2007–2015.

第 7 页: [3] 删除的内容　Jintai Lin　2018/6/21 PM5:33:00

As discussed above, we choose the CALIOP pixels within 1.5° of a grid cell center. We test this choice by examining the aerosol layer height (ALH) produced for that grid cell. The ALH is defined as the extinction-weighted height of aerosols (see Eq. 1, where n denotes the number of tropospheric layers, ε_i the aerosol extinction at

layer i, and H_i the layer center height above the ground). We find that choosing pixels within 1.0° of a grid cell center leads to a nosier horizontal distribution of ALH, owing to the small footprint of CALIOP. On the other hand, choosing 2.0° leads to a too smooth spatial gradient of ALH with local characteristics of aerosol vertical distributions are largely lost. We thus decide that 1.5° is a good balance between noise and smoothness.

$$\mathrm{ALH} = \frac{\sum_{i=1}^{i=n} \varepsilon_i H_i}{\sum_{i=1}^{i=n} \varepsilon_i} \qquad (1)$$

Certain grid cells do not contain sufficient valid observations for some months of the climatological dataset. We fill in missing monthly values of a grid cell using valid data in the surrounding 5 x 5 = 25 grid cells (within ~ 100 km). If the 25 grid cells do not have enough valid data (see Appedix B for details next paragraph for details), we use those in the surrounding 7 x 7 = 49 grid cells (within ~ 150 km). A similar procedure is used by Lin et al. (2014b, 2015) to fill in missing values in the gridded MODIS AOD dataset.

第 16 页: [4] 删除的内容 Jintai Lin 2018/6/21 PM5:38:00

3.2 Comparison to NASA CALIOP monthly climatology

We compare our gridded climatological profiles to NASA CALIOP Version 3 Level-3 all-sky monthly profiles at 532 nm (Winker et al. 2013). The NASA Level-3 data has a horizontal resolution of 2° lat. × 5° lon. and a vertical resolution of 60 m (from -0.5 to 12 km above sea level). We combine NASA monthly data over 2007–2015 to construct a monthly climatology for comparison with our own compilation. We only choose aerosol extinction data in the troposphere with error less than 0.15 (the valid range given in the CALIOP dataset). If the number of valid monthly profiles in a grid cell is less than five (i.e., for the same month in five out of the nine years), then we exclude data in that grid cell; see the dark gray grid cells in Fig. 23c.

Several methodological differences exist between generating our and NASA CALIOP datasets. First, the two datasets have different horizontal resolutions. Also, we sample all valid CALIOP pixels within 1.5 ^{0} of a grid cell center, whereas the NASA dataset samples all valid pixels within a grid cell. Besides, our CALIOP dataset involves several steps of horizontal interpolation, for purposes of subsequent cloud and NO_2 retrievals, which is not done in the NASA dataset. In addition, we match CALIOP data vertically to the GEOS-Chem vertical resolution, whereas the NASA dataset maintains the original resolution.

Figure 23c shows the spatial distribution of ALH in all seasons based on NASA CALIOP Level-3 all-sky monthly climatology. The horizontal resolution of NASA data is much coarser than ours; and NASA data are largely missing over the southwest with complex terrains. We choose to focus on the comparison over East China (the black box in Fig. 12a). Over East China, the two climatology datasets generally exhibit similar spatial patterns of ALH in all seasons (Fig. 23a, c). The NASA dataset suggests higher ALHs than ours over Eastern China, especially in summer, due mainly to differences in the sampling and regridding processes. Figure 34c further compares the monthly variation of ALH between our (black line with error bars) and NASA (blue filled triangles) datasets averaged over East China. The two datasets are consistent in almost all months, indicating that their regional differences are largely smoothed out by spatial averaging.

第 25 页: [5] 删除的内容	Jintai Lin	2018/6/21 PM5:44:00

EU FP7-project Quality Assurance for Essential Climate Variables (

第 25 页: [6] 删除的内容	Jintai Lin	2018/6/21 PM5:44:00

is aim at making rapid judgments on validitiy and trustworthiness of Earth Observation data and the derived climate data sets. It

第 25 页: [7] 删除的内容　　Folkert Boersma　　2018/6/28 AM10:51:00

essentially an ensemble data sets of satellite products provide

第 25 页: [8] 删除的内容　　Jintai Lin　　2018/6/21 PM5:46:00

, with a fully traceable quality assurance on all aspects of the NO_2, HCHO and carbon monoxide (CO) (Zara et al., 2018)

Improved aerosol correction for OMI tropospheric NO_2 retrieval over East Asia: constraint from CALIOP aerosol vertical profile

Mengyao Liu[1,2], Jintai Lin[1], K. Folkert Boersma[2,3], Gaia Pinardi[4], Yang Wang[5], Julien Chimot[6], Thomas Wagner[5], Pinghua Xie[7,8,9], Henk Eskes[2], Michel Van Roozendael[4], François Hendrick[4], Pucai Wang[10], Ting Wang[10], Yingying Yan[1]

1, Laboratory for Climate and Ocean-Atmosphere Studies, Department of Atmospheric and Oceanic Sciences, School of Physics, Peking University, Beijing, China

2, Royal Netherlands Meteorological Institute, De Bilt, the Netherlands

3, Meteorology and Air Quality department, Wageningen University, Wageningen, the Netherlands

4, Royal Belgian Institute for Space Aeronomy (BIRA-IASB), Brussels, Belgium

5, Max Planck Institute for Chemistry, Mainz, Germany

6, Department of Geoscience and Remote Sensing (GRS), Civil Engineering and Geosciences, TU Delft, the Netherlands

7, Anhui Institute of Optics and Fine Mechanics, Key laboratory of Environmental Optics and Technology, Chinese Academy of Sciences, Hefei, China

8, CAS Center for Excellence in Urban Atmospheric Environment, Institute of Urban Environment, Chinese Academy of Sciences, Xiamen, China

9, School of Environmental Science and Optoelectronic Technology, University of Science and Technology of China, Hefei, China

Improved aerosol correction for OMI tropospheric NO_2 retrieval over East Asia: constraint from CALIOP aerosol vertical profile

Mengyao Liu[1,2], Jintai Lin[1], K. Folkert Boersma[2,3], Gaia Pinardi[4], Yang Wang[5], Julien Chimot[6], Thomas Wagner[5], Pinghua Xie[7,8,9], Henk Eskes[2], Michel Van Roozendael[4], François Hendrick[4], Pucai Wang[10], Ting Wang[10], Yingying Yan[1], Lulu Chen[1], Ruijing Ni[1]

1, Laboratory for Climate and Ocean-Atmosphere Studies, Department of Atmospheric and Oceanic Sciences, School of Physics, Peking University, Beijing, China

2, Royal Netherlands Meteorological Institute, De Bilt, the Netherlands

3, Meteorology and Air Quality department, Wageningen University, Wageningen, the Netherlands

4, Royal Belgian Institute for Space Aeronomy (BIRA-IASB), Brussels, Belgium

5, Max Planck Institute for Chemistry, Mainz, Germany

6, Department of Geoscience and Remote Sensing (GRS), Civil Engineering and Geosciences, TU Delft, the Netherlands

7, Anhui Institute of Optics and Fine Mechanics, Key laboratory of Environmental Optics and Technology, Chinese Academy of Sciences, Hefei, China

8, CAS Center for Excellence in Urban Atmospheric Environment, Institute of Urban Environment, Chinese Academy of Sciences, Xiamen, China

9, School of Environmental Science and Optoelectronic Technology, University of Science and Technology of China, Hefei, China

批注 **[Microsof1]:** Add new co-authors

10, IAP/CAS, Institute of Atmospheric Physics, Chinese Academy of Sciences, Beijing, China

Correspondence to: Jintai Lin (linjt@pku.edu.cn); K. Folkert Boersma (folkert.boersma@knmi.nl)

Abstract

Satellite retrieval of vertical column densities (VCDs) of tropospheric nitrogen dioxide (NO_2) is critical for NO_x pollution and impact evaluation. For regions with high aerosol loadings, the retrieval accuracy is greatly affected by whether aerosol optical effects are treated implicitly (as additional "effective" clouds) or explicitly, among other factors. Our previous POMINO algorithm explicitly accounts for aerosol effects to improve the retrieval especially in polluted situations over China, by using aerosol information from GEOS-Chem simulations with further monthly constraints by MODIS/Aqua aerosol optical depth (AOD) data. Here we present a major algorithm update, POMINO v1.1, by constructing a monthly climatological data set of aerosol extinction profiles, based on Level-2 CALIOP/CALIPSO data over 2007–2015, to better constrain the modeled aerosol vertical profiles.

We find that GEOS-Chem captures the month-to-month variation of CALIOP aerosol layer height but with a systematic underestimate by about 300–600 m (season and location dependent), due to a too strong negative vertical gradient of extinction above 1 km. Correcting the model aerosol extinction profiles results in small changes in retrieved cloud fraction, increases in cloud top pressure (within 2–6% in most cases), and increases in tropospheric NO_2 VCD by 4–16% over China on a monthly basis in 2012. The improved NO_2 VCDs (in POMINO v1.1) are more consistent with independent ground-based MAX-DOAS observations (R^2 = 0.80, NMB = -3.4%, for 162 pixels in 49 days) than POMINO (R^2 = 0.80, NMB = -9.6%), DOMINO v2 (R^2 =

0.68, NMB = -2.1%) and QA4ECV (R^2 = 0.75, NMB = -22.0%) are. Especially on haze days, R^2 reaches 0.76 for POMINO v1.1, much higher than that for POMINO (0.68), DOMINO v2 (0.38) and QA4ECV (0.34). Furthermore, the increase in cloud pressure likely reveals a more realistic vertical relationship between cloud and aerosol layers, with aerosols situated above the clouds in certain months instead of always below the clouds. The POMINO v1.1 algorithm is a core step towards our next public release of data product (POMINO v2), and it will also be applied to the recently launched S5P-TropOMI sensor.

批注 [Microsof2]: Add QA4ECV results.

批注 [Microsof3]: Clarify POMINO v1.1 won't be our new released product.

1. Introduction

Air pollution is a major environmental problem in China. In particular, China has become the world's largest emitting country of nitrogen oxides (NO_X=NO+NO_2) due to its rapid economic growth, heavy industries, coal-dominated energy sources, and relatively weak emission control (Cui et al., 2016; Lin et al., 2014a; Stavrakou et al., 2016; Zhang et al., 2009). Tropospheric vertical column densities (VCDs) of nitrogen dioxide (NO_2) retrieved from the Ozone Monitoring Instrument (OMI) onboard the Earth Observing System (EOS) Aura satellite have been widely used to monitor and analyze NO_X pollution over China because of its high spatiotemporal coverage (e.g. (Lin et al., 2010; Miyazaki and Eskes, 2013; Verstraeten et al., 2015; Zhao and Wang, 2009). However, NO_2 retrieved from OMI and other space-borne instruments are subject to errors in the conversion process from radiance to VCD, particularly with respect to the calculation of tropospheric air mass factor (AMF) that is used to convert tropospheric slant column density to VCD (e.g. Boersma et al., 2011; Bucsela et al., 2013; Lin et al., 2015; Lorente et al., 2017).

Most current-generation NO_2 algorithms do not explicitly account for the effects of aerosols on NO_2 AMFs and on prerequisite cloud parameter retrievals. These retrievals often adopt an implicit approach wherein cloud algorithms retrieve "effective cloud" parameters that include the optical effects of aerosols. This implicit method is based on aerosols exerting an effect on the top-of-atmosphere radiance level, whereas the assumed cloud model does not account for the presence of aerosols in the atmosphere (Stammes et al., 2008; Veefkind et al., 2016; Wang et al., 2008b; Wang and Stammes, 2014). In the absence of clouds, an aerosol optical thickness of 1 is then interpreted as an effective cloud fraction of ± 0.10, and the value also depends on the aerosol properties (scattering or absorbing), true surface albedo and geometry angles (Chimot et al., 2016) with an effective cloud pressure closely related to the aerosol layer, at least for aerosols of predominantly scattering nature (e.g. Boersma et al., 2004, 2011, Castellanos et al., 2014, 2015). However, in polluted situations with high aerosol loadings and more absorbing aerosol types, which often occur over China and many other developing regions, the implicit method can result in considerable biases (Castellanos et al., 2014, 2015; Chimot et al., 2016; Kanaya et al., 2014; Lin et al., 2014b).

Lin et al. (2014b, 2015) established the POMINO NO_2 algorithm, which builds on the DOMINO v2 algorithm (for OMI NO_2 slant columns and stratospheric correction), but improves upon it through a more sophisticated AMF calculation over China. In POMINO, the effects of aerosols on cloud retrievals and NO_2 AMFs are explicitly accounted for. In particular, daily information on aerosol optical properties such as aerosol optical depth (AOD), single scattering albedo (SSA), phase function and vertical extinction profiles are taken from nested Asian GEOS-Chem v9-02 simulations. The modeled AOD at 550 nm is further constrained by MODIS/Aqua monthly AOD, with the correction applied to other wavelengths based on modeled aerosol refractive indices (Lin et al., 2014b). However, the POMINO algorithm does not include an observation-based constraint on the vertical profile of aerosols, whose altitude relative to NO_2 has strong and complex influences on NO_2 retrieval (Castellanos et al., 2015; Leitão et al., 2010; Lin et al., 2014b). This study improves upon the POMINO algorithm by incorporating CALIOP monthly climatology of aerosol vertical extinction profiles to correct for model biases.

The CALIOP lidar, carried on the sun-synchronous CALIPSO satellite, has been acquiring global aerosol extinction profiles since June 2006 (Winker et al., 2010). CALIPSO and Aura are both parts of the National Aeronautics and Space Administration (NASA) A-train constellation of satellites. The overpass time of CALIOP/CALIPSO is only 15 minutes later than OMI/Aura. In spite of issues with the detection limit, radar ratio selection and cloud contamination that cause some biases in CALIOP aerosol extinction vertical profiles (Amiridis et al., 2015; Koffi et al., 2012; Winker et al., 2013), comparisons of aerosol extinction profiles between ground-based lidar and CALIOP show good agreements (Kacenelenbogen et al., 2014; Kim et al., 2009; Misra et al., 2012). However, CALIOP is a nadir-viewing instrument that measures the atmosphere along the satellite ground-track with a narrow field-of-view. This means that the daily geographical coverage of CALIOP is much smaller than that of OMI. Thus previous studies often used monthly/seasonal regional mean CALIOP data to study aerosol vertical distributions or to evaluate model simulations (Chazette et al., 2010; Johnson et al., 2012; Koffi et al., 2012; Ma and Yu, 2014; Sareen et al., 2010).

There exist a few CALIOP Level-3 gridded datasets, such as LIVAS (Amiridis et al. 2015) and NASA official Level-3 monthly dataset (Winker et al., 2013). However, LIVAS is an annual average day-night combined product, not suitable to be applied to OMI NO_2 retrievals (around early afternoon, and in need of a higher temporal resolution than annual). The horizontal resolution (2° long. × 5° lat.) of NASA official product is much coarser than OMI footprints and the GEOS-Chem model resolution.

批注 [Microsof4]: Clarify our statements

Here we construct a custom monthly climatology of aerosol vertical extinction profiles based on 9-years (2007–2015) worth of CALIOP Version 3 Level-2 532 nm data. On a climatological basis, we use the CALIOP monthly data to adjust GEOS-Chem profiles in each grid cell for each day of the same month in any year. We then use the corrected GEOS-Chem vertical extinction profiles in the retrievals of cloud parameters and NO_2. Finally, we evaluate our updated POMINO retrieval (hereafter referred to as POMINO v1.1), our previous POMINO product, DOMINO v2 and the newly released Quality Assurance for Essential Climate Variables product (QA4ECV, see Appendix A), using ground-based MAX-DOAS NO_2 column measurements at three urban/suburban sites in East China for the year of 2012 and several months in 2008/2009.

Section 2 describes the construction of CALIOP aerosol extinction vertical profile monthly climatology, the POMINO v1.1 retrieval approach, and the MAX-DOAS data. It also presents the criteria for comparing different NO_2 retrieval products and for selecting coincident OMI and MAX-DOAS data. Section 3 compares our CALIOP climatology with NASA's official Level-3 CALIOP dataset and GEOS-Chem simulation results. Sections 4 and 5 compare POMINO v1.1 to POMINO to analyze the influence of improved aerosol vertical profiles on retrievals of cloud parameters and NO_2 VCDs, respectively. Section 6 evaluates POMINO, POMINO v1.1, DOMNO v2 and QA4ECV NO_2 VCD products using the MAX-DOAS data. Section 7 concludes our study.

2. Data and methods

2.1 CALIOP monthly mean extinction profile climatology

CALIOP is a dual-wavelength polarization lidar measuring attenuated backscatter radiation at 532 and 1064 nm since June 2006. The vertical resolution of aerosol extinction profiles is 30 m below 8.2 km and 60 m up to 20.2 km (Winker et al., 2013), with a total of 399 sampled altitudes. The horizontal resolution of CALIOP scenes is

335 m along the orbital track and is given over a 5 km horizontal resolution in Level-2 data.

As detailed in Appendix B, we use the daily all-sky Version 3 CALIOP Level-2 aerosol profile product at 532 nm from 2007 to 2015 to construct a monthly Level-3 climatological dataset of aerosol extinction profiles over China and nearby regions. This dataset is constructed on the GEOS-Chem model grid (0.667° long. x 0.5° lat.) and vertical resolution (47 layers, with 36 layers or so in the troposphere). The ratio of climatological monthly CALIOP to monthly GEOS-Chem profiles represents the scaling profile to adjust the daily GEOS-Chem profiles in the same month (see Sect. 2.2)

2.2 POMINO v1.1 retrieval approach

The NO_2 retrieval consists of three steps. First, the total NO_2 slant columns density (SCD) is retrieved using the Differential Optical Absorption Spectroscopy (DOAS) technique (for the 405-465 nm spectral window in the case of OMI). The uncertainty of the SCD is determined by the appropriateness of the fitting technique, the instrument noise, the choice of fitting window, and the orthogonality of the absorbers' cross sections (Bucsela et al., 2006; van Geffen et al., 2015; Lerot et al., 2010; Richter et al., 2011; Zara et al., 2018). The NO_2 SCD in DOMINO v2 has a bias at about 0.5~1.3 × 10^{15} molec. cm^{-2} (Belmonte Rivas et al., 2014; Dirksen et al., 2011; van Geffen et al., 2015; Marchenko et al., 2015; Zara et al., 2018), which can be reduced by improving wavelength calibration and including O_2-O_2 and liquid water absorption in the fitting model (van Geffen et al., 2015; Zara et al., 2018). The tropospheric SCD is then obtained by subtracting the stratospheric SCD from the total SCD. The bias in the total SCD is mostly absorbed by this stratospheric separation step, which may not propagate into the tropospheric SCD (van Geffen et al., 2015). The last step converts the tropospheric SCD to VCD by using the tropospheric AMF (VCD = SCD / AMF). The tropospheric AMF is calculated at 438 nm by using look-up tables (in most retrieval algorithms) or online radiative transfer modeling (in POMINO) driven by ancillary parameters, which act as the dominant source of errors in retrieved NO_2 VCD data over polluted areas (Boersma et al., 2007; Lin et al., 2014b, 2015; Lorente et al., 2017).

Our POMINO algorithm focuses on the tropospheric AMF calculation over China and nearby regions, taking the tropospheric SCD (Dirksen et al., 2011) from DOMINO v2 (Boersma et al., 2011). POMINO improves upon the DOMINO v2 algorithm in the treatment of aerosols, surface reflectance, online radiative transfer calculations, spatial resolution of NO_2, temperature and pressure vertical profiles, and consistency between cloud and NO_2 retrievals (Lin et al., 2014b, 2015). In brief, we use the parallelized LIDORT-driven AMFv6 package to derive both cloud parameters and tropospheric NO_2 AMFs for individual OMI pixels online. NO_2 vertical profiles, aerosol optical properties and aerosol vertical profiles are taken from the nested GEOS-Chem model over Asia (0.667 ° long.×0.5° lat. before May 2013 and 0.3125 ° long.×0.25 ° lat. afterwards), and pressure and temperature profiles are taken from the GEOS-5 and GEOS-FP assimilated meteorological fields that drive GEOS-Chem simulations. Model aerosols are further adjusted by satellite data (see below). We adjust the pressure profiles based on the difference in elevation between the pixel center and the matching model grid cell (Zhou et al., 2010). We also account for the effects of surface bidirectional reflectance distribution function (BRDF) (Lin et al., 2014b; Zhou et al., 2010) by taking three kernel parameters (isotropic, volumetric and geometric) from the MODIS MCD43C2 data set at 440 nm (Lucht et al., 2000).

As a prerequisite to the POMINO NO_2 retrieval, clouds are retrieved through the O_2-O_2 algorithm (Acarreta et al., 2004; Stammes et al., 2008) with O_2-O_2 SCDs from OMCLDO2, and with pressure, temperature, surface reflectance, aerosols and other ancillary information consistent with the NO_2 retrieval. Note that the treatment of cloud scattering (as "effective" Lambertian reflector, as in other NO_2 algorithms) is different from the treatment of aerosol scattering/absorption (vertically resolved based on the Mie scheme).

批注 [Microsof5]: Add specific explanations.

POMINO uses the temporally and spatially varying aerosol information, including AOD, single scattering albedo (SSA), phase function and vertical profiles from GEOS-Chem simulations. POMINO v1.1 (this work) further uses CALIOP data to constrain the shape of aerosol vertical extinction profile. We run the model at a resolution of 0.3125° long.×0.25° lat. before May 2013 and 0.667° long.×0.5° lat. afterwards, as determined by the resolution of the driving meteorological fields. We then regrid the finer resolution model results to 0.667° long.×0.5° lat., to be consistent with the CALIOP data grid. We then sample the model data at times and locations with valid CALIOP data at 532 nm to establish the model monthly climatology.

For any month in a grid cell, we divide the CALIOP monthly climatology of aerosol extinction profile shape by model climatological profile shape to obtain a unitless scaling profile (Eq. 1), and apply this scaling profile to all days of that month in all years (Eq. 2). Such a climatological adjustment is based on the assumption that systematic model limitations are month-dependent and persist over the years and days (e.g., a too strong vertical gradient, see Sect. 3.3). Although this monthly adjustment means discontinuity on the day-to-day basis (e.g., from the last day of a month to the first day of the next month), such discontinuity does not significantly affect the NO_2 retrieval, based on our sensitivity test.

In Eqs. 1 and 2, E^C represents the CALIOP climatological aerosol extinction coefficient, E^G the GEOS-Chem extinction, E^{Gr} the post-scaling model extinction, and R the scaling profile. The subscript *i* denotes a grid cell, *k* a vertical layer, *d* a day, *m* a month, and *y* a year. Note that in Eq. 1, the extinction coefficient at each layer is normalized relative to the maximum value of that profile. This procedure ensures that the scaling is based on the relative shape of the extinction profile and is thus independent of the accuracies of CALIOP and GEOS-Chem AOD. We keep the absolute AOD value of GEOS-Chem unchanged in this step.

$$\mathrm{R}_{i,k,m} = \frac{\mathrm{E}^{C}_{i,k,m}/\max\,(\mathrm{E}^{C}_{i,k,m})}{\mathrm{E}^{G}_{i,k,m}/max\,(\mathrm{E}^{G}_{i,k,m})} \quad (1)$$

$$\mathrm{E}^{Gr}_{i,k,d,m,y} = \mathrm{E}^{G}_{i,k,d,m,y} \times \mathrm{R}_{i,k,m} \quad (2)$$

In POMINO, the GEOS-Chem AOD are further constrained by a MODIS/Aqua Collection 5.1 monthly AOD dataset compiled on the model grid (Lin et al., 2014b, 2015). POMINO v1.1 uses the Collection 5.1 AOD data before May 2013 and Collection 6 data afterwards. For adjustment, model AOD are projected to a 0.667° long.×0.5° lat. grid and then sampled at times and locations with valid MODIS data (Lin et al., 2015). As shown in Eq. 3, τ^{M} denotes MODIS AOD, τ^{G} GEOS-Chem AOD, and τ^{Mr} post-adjustment model AOD. The subscript *i* denotes a grid cell, *d* a day, *m* a month, and *y* a year. This AOD adjustment ensures that in any month, monthly mean GEOS-Chem AOD is the same as MODIS AOD while the modeled day-to-day variability is kept.

$$\tau^{Gr}_{i,d,m,y} = \frac{\tau^{M}_{i,m,y}}{\tau^{G}_{i,m,y}} \times \tau^{G}_{i,d,m,y} \quad (3)$$

Equations 4–5 show the complex effects of aerosols in calculating the AMF for any pixel. The AMF is the linear sum of tropospheric layer contributions to the slant column weighted by the vertical sub columns (Eq. 4). The box AMF, amf_k, describes the sensitivity of NO_2 SCD to layer k, and $x_{a,k}$ represent the subcolumn of layer k from a priori NO_2 profile. The l represent the first integrated layer, which is the layer above the ground for clear sky, or the layer above cloud top for cloudy sky. The t represent the tropopause layer. POMINO assumes the independent pixel approximation (IPA)

(Martin et al., 2002; Boersma et al., 2002). This means that the calculated AMF for any pixel consists of a fully cloudy-sky portion (AMF_{clr}) and a fully clear-sky portion (AMF_{cld}), with weights based on the cloud radiance fraction (CRF = $(1 - CF) \cdot A_{clr} + CF \cdot A_{cld}$, where A_{clr}, A_{cld} are radiance from the clear-sky part and fully cloudy part of the pixel, respectively.) (Eq. 5). AMF_{cld} is affected by above-cloud aerosols, and AMF_{clr} is affected by aerosols in the entire column. Also, aerosols affect the retrieval of CRF. Thus, the improvement of aerosol vertical profile in POMINO v1.1 affects all the three quantities in Eq. 5 and thus leads to complex impacts on retrieved NO_2 VCD.

$$AMF = \frac{\sum_l^t amf_k x_{a,k}}{\sum_l^t x_{a,k}} \quad (4)$$

$$AMF = AMF_{cld} \cdot CRF + AMF_{clr} \cdot (1 - CRF) \quad (5)$$

2.3 OMI pixel selection to evaluate POMINO v1.1, POMINO, DOMINO v2 and QA4ECV

We exclude OMI pixels affected by row anomaly (Schenkeveld et al., 2017) or with high albedo caused by icy/snowy ground. To screen out cloudy scenes, we choose pixels with CRF below 50% (effective cloud fraction is typically below 20%) in POMINO.

The selection of CRF threshold influences the validity of pixels. The "effective" CRF in DOMINO implicitly includes the influence of aerosols. In POMINO, the aerosol contribution is separated from that of the clouds, resulting in a lower CRF than for DOMINO. The CRF differs insignificantly between POMINO and POMINO v1.1, because the same AOD and other non-aerosol ancillary parameters are used in the retrieval process. Using the CRF from POMINO instead of DOMINO or QA4ECV for cloud screening means that the number of "valid" pixels in DOMINO increases by about 25%, particularly because much more pixels with high pollutant (aerosol and NO_2)

批注 [Microsof6]: Add explanation for CRF.

loadings are now included. This potentially reduces the sampling bias (Lin et al., 2014b, 2015), and the ensemble of pixels now includes scenes with high "aerosol radiative fractions". Further research is needed to fully understand how much these high-aerosol scenes may be subject to the same screening issues as the cloudy scenes. Nevertheless, the limited evidence here and in Lin et al. (2014b, 2015) suggests that including these high-aerosol scenes does not affect the accuracy of NO_2 retrieval.

2.4 MAX-DOAS data

We use MAX-DOAS measurements at three suburban or urban sites in East China, including one urban site at the Institute of Atmospheric Physics (IAP) in Beijing (116.38° E, 39.38 ° N), one suburban site in Xianghe County (116.96° E, 39.75 ° N) to the south of Beijing, and one urban site in the Wuxi City (120.31° E, 31.57 ° N) in the Yangzi River delta (YRD). Figure 1 shows the locations of these sites overlaid with POMINO v1.1 NO_2 VCDs in August 2012. Table 1 summarizes the information of MAX-DOAS measurements.

The instruments in IAP and in Xianghe were designed at BIRA-IASB (Clémer et al., 2010). Such an instrument is a dual-channel system composed of two thermally regulated grating spectrometers, covering the ultraviolet (300–390 nm) and visible (400–720 nm) wavelengths. It measures scattered sunlight every 15 minutes at nine elevation angles: 2°, 4°, 6°, 8°, 10°, 12°, 15°, 30°, and 90°. The telescope of the instrument is pointed to the north. The data are analyzed following Hendrick et al. (2014). The Xianghe suburban site is influenced by pollution from the surrounding major cities like Beijing and Tianjin. At Xianghe, MAX-DOAS data are data are continuously available since early 2011, and data in 2012 are used here for comparison with OMI products. At IAP, MAX-DOAS data are available in 2008 and 2009 (Table 1), thus for comparison purposes we process OMI products to match the MAX-DOAS times.

Located on the roof of an 11-story building, the instrument at Wuxi was developed by Anhui Institute of Optics and Fine Mechanics (AIOFM) (Wang et al., 2015, 2017a). Its telescope is pointed to the north and records at five elevation angles (5°, 10°, 20°, 30° and 90°). Wuxi is a typical urban site affected by heavy NO_x and aerosol pollution. The measurements used here are analyzed in Wang et al. (2017a). Data are available in 2012 for comparison with OMI products.

When comparing the four OMI products against MAX-DOAS observations, temporal and spatial inconsistency in sampling is inevitable. The spatial inconsistency, together with the substantial horizontal inhomogeneity in NO_2, might be more important than the influence of temporal inconsistency (Wang et al., 2017b). The influence of the horizontal inhomogeneity was suggested to be about 10–30% for MAX-DOAS measurements in Beijing (Lin et al., 2014b; Ma et al., 2013) and 10–15% for less polluted locations like Tai'an, Mangshan and Rudong (Irie et al., 2012). Following previous studies (Lin et al., 2014b; Wang et al., 2015, 2017b), we average MAX-DOAS data within 2 h of the OMI overpass time, and we select OMI pixels within 25 km of a MAX-DOAS site whose viewing zenith angle is below 30°. To exclude local pollution events near the MAX-DOAS site (such as the abrupt increase of NO_2 caused by the pass of consequent vehicles during a very short period), the standard deviation of MAX-DOAS data within 2 h should not exceed 20% of their mean value (Lin et al., 2014b). We elect not to spatially average the OMI pixels because they can, to some degree, reflect the spatial variability in NO_2 and aerosols.

We further exclude MAX-DOAS data in cloudy conditions, as clouds can cause large uncertainties in MAX-DOAS and OMI data. To find the actual cloudy days, we use MODIS/Aqua cloud fraction data, MODIS/Aqua Level-3 corrected reflectance (true color) data at the $1° \times 1°$ resolution, and current weather data observed from the nearest ground meteorological station (indicated by the black triangles in Fig. 1b).

Since there is only one meteorological station available near the Beijing area, it is used for both IAP and Xianghe MAX-DOAS sites. We first use MODIS/Aqua corrected reflectance (true color) to distinguish clouds from haze. For cloudy days determined by the reflectance checking, we examine both the MODIS/Aqua cloud fraction data and the meteorological station cloud records, considering that MODIS/Aqua cloud fraction data may be missing or have a too coarse horizontal resolution to accurately interpret the cloud conditions at the MAX-DOAS site. We exclude MAX-DOAS NO_2 data if the MODIS/Aqua cloud fraction is larger than 60% and the meteorological station reports a "BROKEN" (cloud fraction ranges from 5/8 to 7/8) or "OVERCAST" (full cloud cover) sky. For the three MAX-DOAS sites together, this leads to 49 days with valid data out of 64 days with pre-screening data.

We note here that using cloud fraction data from MODIS/Aqua or MAX-DOAS (for Xianghe only, see Gielen et al., 2014) alone to screen cloudy scenes may not be appropriate on heavy-haze days. For example, on 8th January, 2012, MODIS/Aqua cloud fraction is about 70–80% over the North China Plain and MAX-DOAS at Xianghe suggests the presence of "thick clouds". However, both the meteorological station and MODIS/Aqua corrected reflectance (true color) product suggest that the North China Plain was covered by a thick layer of haze. Consequently, this day was excluded from the analysis.

3. Monthly climatology of aerosol extinction profiles from CALIOP and GEOS-Chem

3.1 CALIOP monthly climatology

The aerosol layer height (ALH) is a good indicator to what extent aerosols are mixed vertically (Castellanos et al., 2015). As defined in Eq. A1 in Appendix B, the ALH is the average height of aerosols weighted by vertically resolved aerosol extinction. Figure

2a shows the spatial distribution of our CALIOP ALH climatology in each season. At most places, the ALH reaches a maximum in spring or summer and a minimum in fall or winter. The lowest ALH in fall and winter can be attributed to heavy near-surface pollution and weak vertical transport. The high values in summer are related to strong convective activities. Over the north, the high values in spring are partly associated with Asian dust events, due to high surface winds and dry soil in this season (Huang et al., 2010; Proestakis et al., 2017; Wang et al., 2010), which also affects the oceanic regions via atmospheric transport. The springtime high ALH over the south may be related to the transport of carbonaceous aerosols from Southeast Asian biomass burning (Jethva et al., 2016). Averaged over the domain, the seasonal mean ALHs are 1.48 km, 1.43 km, 1.27km, 1.18 km in spring, summer, fall and winter.

Figure 3a,b further shows the climatological monthly variations of ALH averaged over Northern East China (the anthropogenic source region shown in orange in Fig. 1a) and Northwest China (the dust source region shown in yellow in Fig. 1a). The two regions exhibit distinctive temporal variations. Over Northern East China, the ALH reaches a maximum in April (~1.53 km) and a minimum in December (~1.14 km). Over Northwest China, the ALH peaks in August (~1.59km) because of strongest convection (Zhu et al., 2013), although the springtime ALH is also high.

Figure 4a shows the climatological seasonal regional average vertical profiles of aerosol extinction over Northern East China. Here, the aerosol extinction increases from the ground level to a peak at about 300–600 m (season dependent), above which it decreases gradually. The height of peak extinction is lowest in winter, consistent with a stagnant atmosphere, thin mixing layer, and increased emissions (from residential and industrial sectors). The large error bars (horizontal lines in different layers, standing for 1 standard deviation) indicate strong spatiotemporal variability of aerosol extinction.

Over Northwest China (Fig. 5a), the column total aerosol extinction is much smaller than that over Northern East China (Fig. 4a), due to lower anthropogenic sources and dominant natural dust emissions. Vertically, the decline of extinction from the peak-extinction height to 2 km is also much more gradual than the decline over Northern East China, indicating stronger lifting of surface emitted aerosols. In winter, the column total aerosol extinction is close to the high value in dusty spring, whereas the vertical gradient of extinction is strongest among the seasons. This reflects the high anthropogenic emissions in parts of Northwest China, which have been rapidly increasing in the 2000s due to relatively weak emission control supplemented by growing activities of relocation of polluted industries from the eastern coastal regions (Cui et al., 2016; Zhao et al., 2015).

Overall, the spatial and seasonal variations of CALIOP aerosol vertical profiles are consistent with changes in meteorological conditions, anthropogenic sources, and natural emissions. The data will be used to evaluate and adjust GEOS-Chem simulation results in Sect. 3.2. A comparison of our CALIOP dataset with NASA’s official Level-3 data is presented in Appendix C.

3.2 Evaluation of GEOS-Chem aerosol extinction profiles

Figure 2b shows the spatial distribution of seasonal ALHs simulated by GEOS-Chem. The model captures the spatial and seasonal variations of CALIOP ALH (Fig. 2a) to some degree, with an underestimate by about 0.3 km on average. The spatial correlation between CALIOP (Fig. 2a) and GEOS-Chem (Fig. 2b) ALH is 0.37 in spring, 0.57 in summer, 0.40 in fall, and 0.44 in winter. The spatiotemporal consistency and underestimate is also clear from the regional mean monthly ALH data in Fig. 3 – the temporal correlation between GEOS-Chem and CALIOP ALH is 0.90 in Northern East China and 0.97 in Northwest China.

Figures 4a and 5a show the GEOS-Chem simulated 2007–2015 monthly climatological vertical profiles of aerosol extinction coefficient over Northern East China and Northwest China, respectively. Over Northern East China (Fig. 4a), the model (red line) captures the vertical distribution of CALIOP extinction (black line) below the height of 1 km, despite a slight underestimate in the magnitude of extinction and an overestimate in the peak-extinction height. From 1 to 5 km above the ground, the model substantially overestimates the rate of decline in extinction coefficient with increasing altitude. Across the seasons, GEOS-Chem underestimates the magnitude of aerosol extinction by up to 37% (depending on the height). Over Northwest China (Fig. 5a), GEOS-Chem has an underestimate in all seasons, with the largest bias by about 80% in winter likely due to underestimated water-soluble aerosols and dust emissions (Li et al., 2016; Wang et al., 2008a).

Since the POMINO v1.1 algorithm uses MODIS AOD to adjust model AOD, it only uses the CALIOP aerosol extinction profile shape to adjust the modeled shape (Eqs. 1 and 2). Figures 4b and 4b show the vertical shapes of aerosol extinction, averaged across all profiles in each season over Northern East China and Northwest China, respectively. Over Northern East China (Fig. 4b), GEOS-Chem underestimates the CALIOP values above 1 km by 52–71%. This underestimate leads to a lower ALH, consistent with the finding by van Donkelaar et al. (2013) and Lin et al. (2014b). Over Northwest China (Fig. 5b), the model also underestimates the CALIOP values above 1 km by 50–62%. These results imply the importance of correcting the modeled aerosol vertical shape prior to cloud and NO_2 retrievals.

4. Effects of aerosol vertical profile improvement on cloud retrieval in 2012

Figure 6a, b shows the monthly average ALH and cloud top height (CTH, corresponding to cloud pressure, CP) over Northern East China and Northwest China in 2012. In order to discuss the CTH, only cloudy days are analyzed here, by excluding days with zero cloud fraction (CF = 0, clear-sky cases) in POMINO. Although "clear sky" is used sometimes in the literature to represent low cloud coverage (e.g., CF < 0.2 or CRF < 0.5, Boersma et al., 2011; Chimot et al., 2016), here it strictly means CF = 0 while "cloudy sky" means CF > 0. About 62.7% of days contain non-zero fractions of clouds over Northern East China, and the number is 59.1% for Northwest China. The CF changes from POMINO to POMINO v1.1 (i.e., after aerosol vertical profile adjustment) are negligible (within ±0.5%, not shown) due to the same values of AOD and SSA used in both products. This is because overall CF is mostly driven by the continuum reflectance at 475 nm (mainly determined by AOD and surface reflectance, which remain unchanged), which is independent of aerosol profile but CTH is driven by the O_2-O_2 SCD, which is itself impacted by ALH.

Figure 6a, b shows that over the two regions, the CTH varies notably from one month to another, whereas the ALH is much more stable across the months. Over Northern East China, the ALH increases by 0.52 km from POMINO (orange dashed line) to POMINO v1.1 (orange solid line) due to the CALIOP-based monthly climatological adjustment. The increase in ALH means a stronger "shielding" effect of aerosols on the O_2-O_2 absorbing dimer, which, in turn, results in a reduced CTH by 0.69 km on average. For POMINO over Northern East China (Fig. 6a), the retrieved clouds usually extend above the aerosol layer, i.e., the CTH (grey dashed line) is much larger than the ALH (orange dashed line). Using the CALIOP climatology in POMINO v1.1 results in the ALH higher than the CTH in fall and winter. The more elevated ALH is consistent with the finding of Jethva et al. (2016) that a significant amount of absorbing aerosols resides above clouds over Northern East China based on 11-year (2004–2015) OMI near-UV observations.

The CTH in Northwest China is much lower than in Northern East China (Fig. 6a versus 7b). This is because the dominant type of actual clouds is (optically thin) cirrus over western China (Wang et al., 2014), which is interpreted by the O_2-O_2 cloud retrieval algorithm as reduced CTH (with cloud base from the ground). The reduction in CTH from POMINO to POMINO v1.1 over Northwest China is also smaller than the reduction over Northern East China, albeit with a similar enhancement in ALH, due to lower aerosol loadings (Fig. 6c versus 6d).

Figure 7g,h presents the relative change in CP from POMINO to POMINO v1.1 as a function of AOD (binned at an interval of 0.1) and changes in ALH from POMINO to POMINO v1.1 (ΔALH, binned every 0.2 km) across all pixels in 2012 over Northern East China. Results are separated for low cloud fraction (CF < 0.05 in POMINO, Fig. 7g) and modest cloud fraction (0.2 < CF < 0.3, Fig. 7h). The median of the CP changes for pixels within each AOD and ΔALH bin is shown. Figure 7e,f presents the corresponding numbers of occurrence under the two cloud conditions.

Figure 7 shows that over Northern East China, the increase in ALH is typically within 0.6 km for the case of CF < 0.05 (Fig. 7e), and the corresponding increase in CP is within 6% (Fig. 7g). In this case, the average CTH (2.95 km in POMINO versus 1.58 km in POMINO v1.1) becomes much lower than the average ALH (1.06 km in POMINO versus 1.98 km in POMINO v1.1). For the case with CF between 0.2 and 0.3, the increase in ALH is within 1.2 km for most scenes (Fig. 7f), which leads to a CP change of 2% (Fig. 7h), much smaller than the CP change for CF < 0.05 (Fig. 7g). This is partly because the larger the CF is, the smaller a change in CF is required to compensate for the ΔALH in the O_2-O_2 cloud retrieval algorithm. Furthermore, with 0.2 < CF < 0.3, the mean value of CTH is much higher than ALH in both POMINO (2.76 km for CTH versus 1.13km for ALH) and POMINO v1.1 (2.60km for CTH versus 2.09 km for ALH), thus a large portion of clouds are above aerosols so that the change in CP is less sensitive to ΔALH. We find that the summertime data contribute the highest portion (36.5%) to the occurrences for 0.2 < CF < 0.3.

For Northwest China (not shown), the dependence of CP changes to AOD and ΔALH is similar to that for Northern East China. In particular, the CP change is within 10% on average for the case of CF < 0.05 and 1.5% for the case of 0.2 < CF < 0.3.

5. Effects of aerosol vertical profile improvement on NO_2 retrieval in 2012

Figure 7a presents the percentage changes in clear-sky NO_2 VCD from POMINO to POMINO v1.1 as a function of binned AOD and ΔALH over Northern East China. Here, clear-sky pixels are chosen based on CF = 0 in POMINO. In any AOD bin, an increase in ΔALH leads to an enhancement in NO_2. And for any ΔALH, the change in VCD is greater (smaller) when AOD becomes larger (smaller), which indicates that the NO_2 retrieval is more sensitive to ALH in high aerosol loading cases. Clearly, the change in NO_2 is not a linear function of AOD and ΔALH.

For cloudy scenes (Fig. 7b,c, cloud data are based on POMINO), the change in NO_2 VCD is less sensitive to AOD and ΔALH. This is because the existence of clouds limits the optical effect of aerosols on tropospheric NO_2. Figure 6a presents the nitrogen layer height (NLH, defined as the average height of model simulated NO_2 weighted by its volume mixing ratio in each layer) in comparison to the ALH and CLH over Northern East China. The figure shows that the POMINO v1.1 CTH is higher than the NLH in all months and higher than the ALH in warm months, which means a “shielding” effect on both NO_2 and aerosols.

Over Northwest China (not shown), the changes in clear-sky NO_2 VCD are within 9% for most cases, which are much smaller than over Eastern China (within 18%). This is because the NLH is much higher than the CLH and ALH (Fig. 6b) in absence of surface anthropogenic emissions.

We convert the valid pixels into monthly mean Level-3 values datasets on a 0.25° long. × 0.25° lat. grid. Figure 8a,b compares the seasonal spatial variations of NO_2 VCD in POMINO v1.1 and POMINO in 2012. In both products, NO_2 peaks in winter due to the longest lifetime and highest anthropogenic emissions (Lin, 2012). NO_2 also reaches a maximum over Northern East China as a result of substantial anthropogenic sources. From POMINO to POMINO v1.1, the NO_2 VCD increases by 3.4% (-67.5–41.7%) in spring for the domain average (range), 3.0% (-59.5–34.4%) in summer, 4.6% (-15.3–39.6%) in fall and 5.3% (-68.4–49.3%) in winter. The NO_2 change is highly dependent on the location and season. The increase over Northern East China is largest in winter, wherein the positive value for ΔALH implies that elevated aerosol layers "shield" the NO_2 absorption.

6. Evaluating satellite products using MAX-DOAS data

We use MAX-DOAS data, after cloud screening (Sect. 2.4), to evaluate DOMNO v2, QA4ECV, POMINO and POMINO v1.1. The scatterplots in Fig. 9a-d compare the NO_2 VCDs from 162 OMI pixels on 49 days with their MAX-DOAS counterparts. Different colors differentiate the seasons. The high values of NO_2 VCD (> 30 × 10^{15} molec. cm^{-2}) occur mainly in fall (blue) and winter (black). POMINO v1.1 and POMINO capture the day-to-day variability of MAX-DOAS data, i.e., R^2 = 0.804 and 0.799, respectively. The normalized mean bias (NMB) of POMINO v1.1 relative to MAX-DOAS data (-3.4%) is smaller than the NMB of POMINO (-9.6%). Also, the reduced major axis (RMA) regression shows that the slope for POMINO v1.1 (0.95) is closer to unity than the slope for POMINO (0.78). When all OMI pixels in a day are averaged (Fig. 9e,f), the correlation across the total of 49 days further increase for both POMINO v1.1 (R^2 = 0.89) and POMINO (R^2 = 0.86), whereas POMINO v1.1 still has a lower NMB (-3.7%) and better slope (0.96) than POMINO (-10.4% and 0.82, respectively). These results suggest that correcting aerosol vertical profiles, at least on a climatology basis, already leads to a significant improved NO_2 retrieval from OMI.

Figure 9 shows that DOMINO v2 is correlated with MAX-DOAS ($R^2 = 0.68$ in Fig. 9c and 0.75 in Fig. 9g) but not as strong as POMINO and POMINO v1.1 for all days. The discrepancy between DOMINO v2 and MAX-DOAS is particularly large for very high NO_2 values (> 70 × 10^{15} molec. cm^{-2}). The R^2 for QA4ECV (0.75 in Fig. 9d and 0.82 in Fig. 9h) is slightly better than DOMINO, but the NMB is higher (-22.0% and -22.7%) and the slope drops to 0.66. These results are consistent with the finding of Lin et al. (2014b, 2015) that explicitly including aerosol optical effects improves the NO_2 retrieval.

Table 2 further shows the comparison statistics for 27 haze days. The haze days are determined when both the ground meteorological station data and MODIS/Aqua corrected reflectance (true color) data indicate a haze day. The table also lists AOD, SSA, CF and MAX-DOAS NO_2 VCD, as averaged over all haze days. A large amount of absorbing aerosols occurs on these haze days (AOD = 1.13, SSA = 0.90). The average MAX-DOAS NO_2 VCD reaches 51.92 × 10^{15} molec. cm^{-2}. Among the four satellite products, POMINO v1.1 has the highest R^2 (0.76) and the lowest bias (4.4%) with respect to MAX-DOAS, whereas DOMINO v2 and QA4ECV reproduce the variability to a limited extent ($R^2 = 0.38$ and 0.34, respectively). This is consistent with the previous finding that the accuracy of DOMINO v2 is reduced for polluted, aerosol-loaded scenes (Boersma et al., 2011; Chimot et al., 2016; Kanaya et al., 2014; Lin et al., 2014b).

Table 3 shows the comparison statistics for 36 cloud-free days (CF = 0 in POMINO, and AOD = 0.60 on average). Here, POMINO v1.1, POMINO and DONIMO v2 do not show large differences in R^2 (0.53–0.56) and NMB (20.8–29.4%) with respect to MAX-DOAS. QA4ECV has a higher R^2 (0.63) and a lower NMB (-5.83%), presumably

批注 [Microsof7]: Add discussion about QA4ECV product.

reflecting the improvements in this (EU-) consortium approach, at least in mostly cloud-free situations. However, the R^2 values for POMINO and POMINO v1.1 are much smaller than the R^2 values in haze days, whereas the opposite changes are true for DOMINO v2 and QA4ECV. Thus, for this limited set of data, the changes from DOMINO v2 and QA4ECV to POMINO and POMINO v1.1 mainly reflect the improved aerosol treatment in hazy scenes. Further research may use additional MAX-DOAS datasets to evaluate the satellite products more systematically.

7. Conclusions

This paper improves upon our previous POMINO algorithm (Lin et al., 2015) to retrieve the tropospheric NO_2 VCDs from OMI, by compiling a 9-year (2007–2015) CALIOP monthly climatology of aerosol vertical extinction profiles to adjust GEOS-Chem aerosol profiles used in the NO_2 retrieval process. The improved algorithm is referred to as POMINO v1.1. Compared to monthly climatological CALIOP data over China, GEOS-Chem simulations tend to underestimate the aerosol extinction above 1 km, as characterized by an underestimate in ALH by 300–600 m (seasonal and location dependent). Such a bias is corrected in POMINO v1.1 by dividing, for any month and grid cell, the CALIOP monthly climatological profile by the model climatological profile to obtain a scaling profile and then applying the scaling profile to model data in all days of that month in all years.

The aerosol extinction profile correction leads to an insignificant change in CF from POMINO to POMINO v1.1, since the AOD and surface reflectance are unchanged. In contrast, the correction results in a notably increase in CP (i.e., a decrease in CTH), due to lifting of aerosol layers. The CP changes are generally within 6% for scenes with low cloud fraction (CF < 0.05 in POMINO), and within 2% for scenes with modest cloud fraction (0.2 < CF < 0.3 in POMINO).

The NO_2 VCDs increase from POMINO to POMINO v1.1 in most cases due to lifting of aerosol layers that enhances the "shielding" of NO_2 absorption. The NO_2 VCD increases by 3.4% (-67.5–41.7%) in spring for the domain average (range), 3.0% (-59.5–34.4%) in summer, 4.6% (-15.3–39.6%) in fall and 5.3% (-68.4–49.3%) in winter. The NO_2 changes highly season and location dependent, and are most significant for wintertime Northern East China.

Further comparisons with independent MAX-DOAS NO_2 VCD data for 162 OMI pixels in 49 days show good performance of both POMINO v1.1 and POMINO in capturing the day-to-day variation of NO_2 (R^2=0.80, n=162), compared to DOMINO v2 (R^2=0.67) and the new QA4ECV product (R^2=0.75). The NMB is smaller in POMINO v1.1 (-3.4%) than in POMINO (-9.6%), with a slightly better slope (0.804 versus 0.784). On hazy days with high aerosol loadings (AOD = 1.13 on average), POMINO v1.1 has the highest R^2 (0.76) and the lowest bias (4.4%) whereas DOMINO and QA4ECV have difficulty in reproducing the day-to-day variability in MAX-DOAS NO_2 measurements (R^2 = 0.38 and 0.34, respectively). The four products show small differences in R^2 on clear-sky days (CF = 0 in POMINO, AOD = 0.60 on average), among which QA4ECV shows a highest R^2 (0.63) and lowest NMB (-5.83%), presumably reflecting the improvements in less polluted place such as Europe and the US. Thus the explicit aerosol treatment (in POMINO and POMINO v1.1) and the aerosol vertical profile correction (in POMINO v1.1) improves the NO_2 retrieval especially in hazy cases.

The POMINO v1.1 algorithm is a core step towards our next public release of data product, POMINO v2. This new release will contain a few additional updates, including but not limited to using MODIS Collection 6 Merged 10-km Level-2 AOD data that combine the Dark Target (Levy et al., 2013) and Deep Blue (Sayer et al., 2014) products, as well as MODIS MCD43C2 Collection 6 daily BRDF data. Meanwhile, the POMINO

批注 **[Microsof8]:** Clarify POMINO v1.1 won't be our released version.

algorithm framework is being applied to the recently launched TropOMI instrument that provides NO_2 information at a much higher spatial resolution (3.5 x 7 km^2). A modified algorithm can also be used to retrieve sulfur dioxide, formaldehyde and other trace gases from TropOMI, for which purposes our algorithm will be available to the community on a collaborative basis. Future research can correct the SSA and NO_2 vertical profile to further improve the retrieval algorithm, and can use more comprehensive independent data to evaluate the resulting satellite products.

Acknowledgements

This research is supported by the National Natural Science Foundation of China (41775115), the 973 program (2014CB441303), the Chinese Scholarship Council, and the EU FP7 QA4ECV project (grant no. 607405).

Appendix A: Introduction to the QA4ECV product

The QA4ECV NO_2 product (http://www.qa4ecv.eu/) builds on a (EU-) consortium approach to retrieve NO_2 from GOME, SCIAMACHY, GOME-2, and OMI. The main contributions are provided by BIRA-IASB, the University of Bremen (IUP), MPIC, KNMI, and Wageningen University. Uncertainties in spectral fitting for NO_2 SCDs and in AMF calculations were evaluated by Zara et al. (2018) and Lorente et al. (2017), respectively. QA4ECV contains improved SCD NO_2 data (Zara et al., 2018). Lorente et al., (2017) showed that across the above algorithms, there a structural uncertainty by 42% in the NO_2 AMF calculation over polluted areas. By comparing to our POMINO product, Lorente et al. also showed that the choice of aerosol correction may introduce an additional uncertainty by up to 50% for situations with high polluted cases, consistent with Lin et al. (2014b, 2015) and the findings here. For a complete description of the QA4ECV algorithm improvements, and quality assurance, please see Boersma et al. (2018).

Appendix B: Constructing the CALIOP monthly climatology of aerosol extinction vertical profile

Our use the all-sky Level-2 CALIOP data to construct the Level-3 monthly climatology. We choose the all-sky product instead of clear-sky data, since previous studies indicate that the climatological aerosol extinction profiles are affected insignificantly by the presence of clouds (Koffi et al., 2012; Winker et al., 2013). As we use this climatological data to adjust GEOS-Chem results, choosing all-sky data improves consistency with the model simulation when doing the daily correction.

To select valid pixels, we follow the data quality criteria by Winker et al., (2013) and Amiridis et al., (2015). Only the pixels with Cloud Aerosol Discrimination (CAD) scores between -20 and -100 with extinction Quality Control (QC) flag valued at 0, 1, 18, and 16 are selected. We further discard samples with an extinction uncertainty of 99.9 km^{-1}, which is indicative of unreliable retrieval. We only accept extinction values falling in the range from 0.0 to 1.25, according to CALIOP observation thresholds. Previous studies showed that weakly scattering edges of icy clouds are sometimes misclassified as aerosols (Winker et al., 2013). To eliminate contamination from icy clouds we exclude the aerosol layers above the cloud layer (with layer-top temperature below 0 ℃) when both of them are above 4km (Winker et al., 2013).

After the pixel-based screening, we aggregate the CALIOP data at the model grid (0.667° long. x 0.5° lat.) and vertical resolution (47 layers, with 36 layers or so in the troposphere). For each grid cell, we choose the CALIOP pixels within 1.5° of the grid cell center. CALIOP Level-2 data are always presented at the fixed 399 altitudes above sea level. To account for the difference in surface elevation between a CALIOP pixel and the respective model grid cell, we convert the altitude of the pixel to a height above the ground, by using the surface elevation data provided in CALIOP. We then average horizontally and vertically the profiles of all pixels within one model grid cell and layer.

We do the regridding day-by-day for all grid cells to ensure that GEOS-Chem and CALIOP extinction profiles are coincident spatially and temporally. Finally, we compile a monthly climatological dataset by averaging over 2007–2015.

Figure A1 shows the number of aerosol extinction profiles in each grid cell and 12 x 9 = 108 months that are used to compile the CALIOP climatology, both before and after data screening. Table A1 presents additional information on monthly and yearly bases. On average, there are 165 and 47 aerosol extinction profiles per month per grid cell before and after screening, respectively. In the final 9-year monthly climatology, each grid cell has about 420 aerosol extinction profiles on average, about 28% of the prior-screening profiles. Figure A1 shows that the number of valid profiles decreases sharply over the Tibet Plateau and at higher latitudes (> 43 ° N) due to complex terrain and icy/snowy ground.

As discussed above, we choose the CALIOP pixels within 1.5° of a grid cell center. We test this choice by examining the aerosol layer height (ALH) produced for that grid cell. The ALH is defined as the extinction-weighted height of aerosols (see Eq. A1, where *n* denotes the number of tropospheric layers, ε_i the aerosol extinction at layer i, and H_i the layer center height above the ground). We find that choosing pixels within 1.0° of a grid cell center leads to a nosier horizontal distribution of ALH, owing to the small footprint of CALIOP. On the other hand, choosing 2.0° leads to a too smooth spatial gradient of ALH with local characteristics of aerosol vertical distributions are largely lost. We thus decide that 1.5 ° is a good balance between noise and smoothness.

$$\mathrm{ALH} = \frac{\sum_{i=1}^{i=n} \varepsilon_i \mathrm{H}_i}{\sum_{i=1}^{i=n} \varepsilon_i} \qquad \text{(A1)}$$

Certain grid cells do not contain sufficient valid observations for some months of the climatological dataset. We fill in missing monthly values of a grid cell using valid data in the surrounding 5 x 5 = 25 grid cells (within ~ 100 km). If the 25 grid cells do not have enough valid data, we use those in the surrounding 7 x 7 = 49 grid cells (within ~ 150 km). A similar procedure is used by Lin et al. (2014b, 2015) to fill in missing values in the gridded MODIS AOD dataset.

For each grid cell in each month, we further correct singular values in the vertical profile. In a month, if a grid cell *i* has an ALH outside mean $\pm 1\sigma$ of its surrounding 25 or 49 grid cells, we select *i*'s surrounding grid cell *j* whose ALH is the median of *i*'s surrounding grid cells, and use *j*'s profile to replace *i*'s. Whether 25 or 49 surrounding grid cells are chosen depends on the number of valid pixels shown in Fig. A1b. If the number of valid pixels in *i* is below mean–1σ of all grid cells in the whole domain, which is often the case for Tibetan grid cells, we use *i*'s surrounding 49 grid cells; otherwise we use *i*'s surrounding 25 grid cells.

Appendix C. Comparing our and NASA's CALIOP monthly climatology

We compare our gridded climatological profiles to NASA CALIOP Version 3 Level-3 all-sky monthly profiles at 532 nm (Winker et al., 2013). The NASA Level-3 data has a horizontal resolution of 2° lat. × 5° lon. and a vertical resolution of 60 m (from -0.5 to 12 km above sea level). We combine NASA monthly data over 2007–2015 to construct a monthly climatology for comparison with our own compilation. We only choose aerosol extinction data in the troposphere with error less than 0.15 (the valid range given in the CALIOP dataset). If the number of valid monthly profiles in a grid cell is less than five (i.e., for the same month in five out of the nine years), then we exclude data in that grid cell; see the dark gray grid cells in Fig. 2c.

Several methodological differences exist between generating our and NASA CALIOP datasets. First, the two datasets have different horizontal resolutions. Also, we sample all valid CALIOP pixels within 1.5° of a grid cell center, whereas the NASA dataset samples all valid pixels within a grid cell. Besides, our CALIOP dataset involves several steps of horizontal interpolation, for purposes of subsequent cloud and NO_2 retrievals, which is not done in the NASA dataset. In addition, we match CALIOP data vertically to the GEOS-Chem vertical resolution, whereas the NASA dataset maintains the original resolution.

Figure 2c shows the spatial distribution of ALH in all seasons based on NASA CALIOP Level-3 all-sky monthly climatology. The horizontal resolution of NASA data is much coarser than ours; and NASA data are largely missing over the southwest with complex terrains. We choose to focus on the comparison over East China (the black box in Fig. 1a). Over East China, the two climatology datasets generally exhibit similar spatial patterns of ALH in all seasons (Fig. 2a, c). The NASA dataset suggests higher ALHs than ours over Eastern China, especially in summer, due mainly to differences in the sampling and regridding processes. Figure 3c further compares the monthly variation of ALH between our (black line with error bars) and NASA (blue filled triangles) datasets averaged over East China. The two datasets are consistent in almost all months, indicating that their regional differences are largely smoothed out by spatial averaging.

References

Acarreta, J. R., De Haan, J. F. and Stammes, P.: Cloud pressure retrieval using the O_2 -O_2 absorption band at 477 nm, J. Geophys. Res., 109(D5), D05204, doi:10.1029/2003JD003915, 2004.

Amiridis, V., Marinou, E., Tsekeri, A., Wandinger, U., Schwarz, A., Giannakaki, E., Mamouri, R., Kokkalis, P., Binietoglou, I., Solomos, S., Herekakis, T., Kazadzis, S., Gerasopoulos, E., Proestakis, E., Kottas, M., Balis, D., Papayannis, A., Kontoes, C., Kourtidis, K., Papagiannopoulos, N., Mona, L., Pappalardo, G., Le Rille, O. and Ansmann, A.: LIVAS: a 3-D multi-wavelength aerosol/cloud database based on

CALIPSO and EARLINET, Atmos. Chem. Phys., 15(13), 7127–7153, doi:10.5194/acp-15-7127-2015, 2015.

Belmonte Rivas, M., Veefkind, P., Boersma, F., Levelt, P., Eskes, H. and Gille, J.: Intercomparison of daytime stratospheric NO_2 satellite retrievals and model simulations, Atmos. Meas. Tech., 7(7), 2203–2225, doi:10.5194/amt-7-2203-2014, 2014.

Boersma, K. F., Eskes, H. J. and Brinksma, E. J.: Error analysis for tropospheric NO_2 retrieval from space, J. Geophys. Res. Atmos., 109(D4), n/a-n/a, doi:10.1029/2003JD003962, 2004.

Boersma, K. F., Eskes, H. J., Veefkind, J. P., Brinksma, E. J., van der A, R. J., Sneep, M., van den Oord, G. H. J., Levelt, P. F., Stammes, P., Gleason, J. F. and Bucsela, E. J.: Near-real time retrieval of tropospheric NO_2 from OMI, Atmos. Chem. Phys., 7(8), 2103–2118, doi:10.5194/acp-7-2103-2007, 2007.

Boersma, K. F., Eskes, H. J., Dirksen, R. J., van der A, R. J., Veefkind, J. P., Stammes, P., Huijnen, V., Kleipool, Q. L., Sneep, M., Claas, J., Leitão, J., Richter, A., Zhou, Y. and Brunner, D.: An improved tropospheric NO_2 column retrieval algorithm for the Ozone Monitoring Instrument, Atmos. Meas. Tech., 4(9), 1905–1928, doi:10.5194/amt-4-1905-2011, 2011.

Boersma, K.F., Eskes, H. J., Richter, A., De Smedt, I., Lorente, A., Beirle, S., van Geffen, J. H. G. M., Zara, M., Peters, E., Van Roozendael, M., Wagner, T., Maasakkers, J. D., van der A, R. J., Nightingale, J., De Rudder, A., Irie, H., and Pinardi, G.: Improving algorithms and uncertainty estimates for satellite NO_2 retrievals: Results from the Quality Assurance for Essential Climate Variables (QA4ECV) project, amt-2018-200, submitted, 2018.

Bucsela, E. J., Celarier, E. A., Wenig, M. O., Gleason, J. F., Veefkind, J. P., Boersma, K. F. and Brinksma, E. J.: Algorithm for NO_2 vertical column retrieval from the ozone monitoring instrument, IEEE Trans. Geosci. Remote Sens., 44(5), 1245–1258, doi:10.1109/TGRS.2005.863715, 2006.

Bucsela, E. J., Krotkov, N. A., Celarier, E. A., Lamsal, L. N., Swartz, W. H., Bhartia, P. K., Boersma, K. F., Veefkind, J. P., Gleason, J. F. and Pickering, K. E.: A new stratospheric and tropospheric NO_2 retrieval algorithm for nadir-viewing satellite instruments: applications to OMI, Atmos. Meas. Tech., 6(10), 2607–2626, doi:10.5194/amt-6-2607-2013, 2013.

Castellanos, P., Boersma, K. F. and van der Werf, G. R.: Satellite observations indicate substantial spatiotemporal variability in biomass burning NO_X emission factors for South America, Atmos. Chem. Phys., 14(8), 3929–3943, doi:10.5194/acp-14-3929-2014, 2014.

Castellanos, P., Boersma, K. F., Torres, O. and de Haan, J. F.: OMI tropospheric NO_2 air mass factors over South America: effects of biomass burning aerosols, Atmos. Meas. Tech., 8(9), 3831–3849, doi:10.5194/amt-8-3831-2015, 2015.

Chazette, P., Raut, J.-C., Dulac, F., Berthier, S., Kim, S.-W., Royer, P., Sanak, J., Loaëc, S. and Grigaut-Desbrosses, H.: Simultaneous observations of lower tropospheric continental aerosols with a ground-based, an airborne, and the spaceborne CALIOP lidar system, J. Geophys. Res., 115(D4), D00H31, doi:10.1029/2009JD012341, 2010.

Chimot, J., Vlemmix, T., Veefkind, J. P., de Haan, J. F. and Levelt, P. F.: Impact of aerosols on the OMI tropospheric NO_2 retrievals over industrialized regions: how accurate is the aerosol correction of cloud-free scenes via a simple cloud model?, Atmos. Meas. Tech., 9(2), 359–382, doi:10.5194/amt-9-359-2016, 2016.

Clémer, K., Van Roozendael, M., Fayt, C., Hendrick, F., Hermans, C., Pinardi, G., Spurr, R., Wang, P. and De Mazière, M.: Multiple wavelength retrieval of tropospheric aerosol optical properties from MAX-DOAS measurements in Beijing, Atmos. Meas. Tech., 3(4), 863–878, doi:10.5194/amt-3-863-2010, 2010.

Cui, Y., Lin, J., Song, C., Liu, M., Yan, Y., Xu, Y. and Huang, B.: Rapid growth in nitrogen dioxide pollution over Western China, 2005–2013, Atmos. Chem. Phys., 16(10), 6207–6221, doi:10.5194/acp-16-6207-2016, 2016.

Dirksen, R. J., Boersma, K. F., Eskes, H. J., Ionov, D. V., Bucsela, E. J., Levelt, P. F. and Kelder, H. M.: Evaluation of stratospheric NO_2 retrieved from the Ozone Monitoring Instrument: Intercomparison, diurnal cycle, and trending, J. Geophys. Res., 116(D8), D08305, doi:10.1029/2010JD014943, 2011.

van Geffen, J. H. G. M., Boersma, K. F., Van Roozendael, M., Hendrick, F., Mahieu, E., De Smedt, I., Sneep, M. and Veefkind, J. P.: Improved spectral fitting of nitrogen dioxide from OMI in the 405–465 nm window, Atmos. Meas. Tech., 8(4), 1685–1699, doi:10.5194/amt-8-1685-2015, 2015.

Gielen, C., Van Roozendael, M., Hendrick, F., Pinardi, G., Vlemmix, T., De Bock, V., De Backer, H., Fayt, C., Hermans, C., Gillotay, D. and Wang, P.: A simple and versatile cloud-screening method for MAX-DOAS retrievals, Atmos. Meas. Tech., 7(10), 3509–3527, doi:10.5194/amt-7-3509-2014, 2014.

Hendrick, F., Muller, J. F., Clemer, K., Wang, P., De Maziere, M., Fayt, C., Gielen, C., Hermans, C., Ma, J. Z., Pinardi, G., Stavrakou, T., Vlemmix, T., and Van Roozendael, M.: Four years of ground-based MAX-DOAS observations of HONO and NO_2 in the Beijing area, Atmospheric Chemistry and Physics, 14, 765-781, 10.5194/acp-14-765-2014, 2014.

Huang, Z., Huang, J., Bi, J., Wang, G., Wang, W., Fu, Q., Li, Z., Tsay, S.-C. and Shi, J.: Dust aerosol vertical structure measurements using three MPL lidars during 2008 China-U.S. joint dust field experiment, J. Geophys. Res. Atmos., 115(D7), n/a-n/a, doi:10.1029/2009JD013273, 2010.

Irie, H., Boersma, K. F., Kanaya, Y., Takashima, H., Pan, X. and Wang, Z. F.: Quantitative bias estimates for tropospheric NO_2 columns retrieved from SCIAMACHY, OMI, and GOME-2 using a common standard for East Asia, Atmos. Meas. Tech., 5(10), 2403–2411, doi:10.5194/amt-5-2403-2012, 2012.

Jethva, H., Torres, O., and Ahn, C.: A ten-year global record of absorbing aerosols above clouds from OMI's near-UV observations, in: Remote Sensing of the Atmosphere, Clouds, and Precipitation Vi, edited by: Im, E., Kumar, R., and Yang, S., Proceedings of SPIE, 2016.

Johnson, M. S., Meskhidze, N. and Praju Kiliyanpilakkil, V.: A global comparison of GEOS-Chem-predicted and remotely-sensed mineral dust aerosol optical depth and extinction profiles, J. Adv. Model. Earth Syst., 4(3), M07001, doi:10.1029/2011MS000109, 2012.

Kacenelenbogen, M., Redemann, J., Vaughan, M. A., Omar, A. H., Russell, P. B., Burton, S., Rogers, R. R., Ferrare, R. A. and Hostetler, C. A.: An evaluation of CALIOP/CALIPSO's aerosol-above-cloud detection and retrieval capability over North America, J. Geophys. Res. Atmos., 119(1), 230–244, doi:10.1002/2013JD020178, 2014.

Kanaya, Y., Irie, H., Takashima, H., Iwabuchi, H., Akimoto, H., Sudo, K., Gu, M., Chong, J., Kim, Y. J., Lee, H., Li, A., Si, F., Xu, J., Xie, P.-H., Liu, W.-Q., Dzhola, A., Postylyakov, O., Ivanov, V., Grechko, E., Terpugova, S. and Panchenko, M.: Long-term MAX-DOAS network observations of NO_2 in Russia and Asia

(MADRAS) during the period 2007-2012: instrumentation, elucidation of climatology, and comparisons with OMI satellite observations and global model simulations, Atmos. Chem. Phys., 14(15), 7909–7927, doi:10.5194/acp-14-7909-2014, 2014.

Kim, S.-W., Heckel, A., Frost, G. J., Richter, A., Gleason, J., Burrows, J. P., McKeen, S., Hsie, E.-Y., Granier, C. and Trainer, M.: NO_2 columns in the western United States observed from space and simulated by a regional chemistry model and their implications for NO_x emissions, J. Geophys. Res., 114(D11), D11301, doi:10.1029/2008JD011343, 2009.

Koffi, B., Schulz, M., Bréon, F.-M., Griesfeller, J., Winker, D., Balkanski, Y., Bauer, S., Berntsen, T., Chin, M., Collins, W. D., Dentener, F., Diehl, T., Easter, R., Ghan, S., Ginoux, P., Gong, S., Horowitz, L. W., Iversen, T., Kirkevåg, A., Koch, D., Krol, M., Myhre, G., Stier, P. and Takemura, T.: Application of the CALIOP layer product to evaluate the vertical distribution of aerosols estimated by global models: AeroCom phase I results, J. Geophys. Res. Atmos., 117(D10), n/a-n/a, doi:10.1029/2011JD016858, 2012.

Leitão, J., Richter, A., Vrekoussis, M., Kokhanovsky, A., Zhang, Q. J., Beekmann, M. and Burrows, J. P.: On the improvement of NO_2 satellite retrievals – aerosol impact on the airmass factors, Atmos. Meas. Tech., 3(2), 475–493, doi:10.5194/amt-3-475-2010, 2010.

Lerot, C., Stavrakou, T., De Smedt, I., Müller, J.-F. and Van Roozendael, M.: Glyoxal vertical columns from GOME-2 backscattered light measurements and comparisons with a global model, Atmos. Chem. Phys., 10(24), 12059–12072, doi:10.5194/acp-10-12059-2010, 2010.

Levy, R. C., Mattoo, S., Munchak, L. A., Remer, L. A., Sayer, A. M., Patadia, F. and Hsu, N. C.: The Collection 6 MODIS aerosol products over land and ocean, Atmos. Meas. Tech., 6(11), 2989–3034, doi:10.5194/amt-6-2989-2013, 2013.

Li, S., Yu, C., Chen, L., Tao, J., Letu, H., Ge, W., Si, Y. and Liu, Y.: Inter-comparison of model-simulated and satellite-retrieved componential aerosol optical depths in China, Atmos. Environ., 141, 320–332, doi:https://doi.org/10.1016/j.atmosenv.2016.06.075, 2016.

Lin, J., Pan, D., Davis, S. J., Zhang, Q., He, K., Wang, C., Streets, D. G., Wuebbles, D. J. and Guan, D.: China's international trade and air pollution in the United States, Proc. Natl. Acad. Sci., 111(5), 1736–1741, doi:10.1073/pnas.1312860111, 2014a.

Lin, J.-T.: Satellite constraint for emissions of nitrogen oxides from anthropogenic, lightning and soil sources over East China on a high-resolution grid, Atmos. Chem. Phys., 12(6), 2881–2898, doi:10.5194/acp-12-2881-2012, 2012.

Lin, J.-T., McElroy, M. B. and Boersma, K. F.: Constraint of anthropogenic NO_X emissions in China from different sectors: a new methodology using multiple satellite retrievals, Atmos. Chem. Phys., 10(1), 63–78, doi:10.5194/acp-10-63-2010, 2010.

Lin, J.-T., Martin, R. V., Boersma, K. F., Sneep, M., Stammes, P., Spurr, R., Wang, P., Van Roozendael, M., Clémer, K. and Irie, H.: Retrieving tropospheric nitrogen dioxide from the Ozone Monitoring Instrument: effects of aerosols, surface reflectance anisotropy, and vertical profile of nitrogen dioxide, Atmos. Chem. Phys., 14(3), 1441–1461, doi:10.5194/acp-14-1441-2014, 2014b.

Lin, J.-T., Liu, M.-Y., Xin, J.-Y., Boersma, K. F., Spurr, R., Martin, R. and Zhang, Q.: Influence of aerosols and surface reflectance on satellite NO_2 retrieval: seasonal and spatial characteristics and implications for NO_x emission constraints, Atmos. Chem. Phys., 15(19), 11217–11241, doi:10.5194/acp-15-11217-2015, 2015.

Lorente, A., Folkert Boersma, K., Yu, H., Dörner, S., Hilboll, A., Richter, A., Liu, M., Lamsal, L. N., Barkley, M., De Smedt, I., Van Roozendael, M., Wang, Y., Wagner, T., Beirle, S., Lin, J.-T., Krotkov, N., Stammes, P., Wang, P., Eskes, H. J. and Krol, M.: Structural uncertainty in air mass factor calculation for NO_2 and HCHO satellite retrievals, Atmos. Meas. Tech., 10(3), 759–782, doi:10.5194/amt-10-759-2017, 2017.

Lucht, W., Schaaf, C. B. and Strahler, A. H.: An algorithm for the retrieval of albedo from space using semiempirical BRDF models, IEEE Trans. Geosci. Remote Sens., 38(2), 977–998, doi:10.1109/36.841980, 2000.

Ma, J. Z., Beirle, S., Jin, J. L., Shaiganfar, R., Yan, P. and Wagner, T.: Tropospheric NO_2 vertical column densities over Beijing: results of the first three years of ground-based MAX-DOAS measurements (2008-2011) and satellite validation, Atmos. Chem. Phys., 13(3), 1547–1567, doi:10.5194/acp-13-1547-2013, 2013.

Ma, X. and Yu, F.: Seasonal variability of aerosol vertical profiles over east US and west Europe: GEOS-Chem/APM simulation and comparison with CALIPSO observations, Atmos. Res., 140–141, 28–37, doi:https://doi.org/10.1016/j.atmosres.2014.01.001, 2014.

Martin, R. V.: An improved retrieval of tropospheric nitrogen dioxide from GOME, J. Geophys. Res., 107(D20), 4437, doi:10.1029/2001JD001027, 2002.

Misra, A., Tripathi, S. N., Kaul, D. S. and Welton, E. J.: Study of MPLNET-Derived Aerosol Climatology over Kanpur, India, and Validation of CALIPSO Level 2 Version 3 Backscatter and Extinction Products, J. Atmos. Ocean. Technol., 29(9), 1285–1294, doi:10.1175/JTECH-D-11-00162.1, 2012.

Miyazaki, K. and Eskes, H.: Constraints on surface NO_X emissions by assimilating satellite observations of multiple species, Geophys. Res. Lett., 40(17), 4745–4750, doi:10.1002/grl.50894, 2013.

Proestakis, E., Amiridis, V., Marinou, E., Georgoulias, A. K., Solomos, S., Kazadzis, S., Chimot, J., Che, H., Alexandri, G., Binietoglou, I., Kourtidis, K. A., de Leeuw, G. and van der A, R. J.: 9-year spatial and temporal evolution of desert dust aerosols over South-East Asia as revealed by CALIOP, Atmos. Chem. Phys. Discuss., 1–35, doi:10.5194/acp-2017-797, 2017.

Richter, A., Begoin, M., Hilboll, A. and Burrows, J. P.: An improved NO_2 retrieval for the GOME-2 satellite instrument, Atmos. Meas. Tech., 4(6), 1147–1159, doi:10.5194/amt-4-1147-2011, 2011.

Marchenko, S., Krotkov, N. A., Lamsal, L. N., Celarier, E. A., Swartz, W. H., and Bucsela, E. J.: Revising the slant column density retrieval of nitrogen dioxide observed by the Ozone Monitoring Instrument, J. Geophys. Res. Atmos., 120(11), 5670–5692, doi:10.1002/2014JD022913, 2015.

Sareen, N., Schwier, A. N., Shapiro, E. L., Mitroo, D. and McNeill, V. F.: Secondary organic material formed by methylglyoxal in aqueous aerosol mimics, Atmos. Chem. Phys., 10(3), 997–1016, doi:10.5194/acp-10-997-2010, 2010.

Sayer, A. M., Munchak, L. A., Hsu, N. C., Levy, R. C., Bettenhausen, C. and Jeong, M.-J.: MODIS Collection 6 aerosol products: Comparison between Aqua's e-Deep Blue, Dark Target, and "merged" data sets, and usage recommendations, J. Geophys. Res. Atmos., 119(24), 13,965-13,989, doi:10.1002/2014JD022453, 2014.

Schenkeveld, V. M. E., Jaross, G., Marchenko, S., Haffner, D., Kleipool, Q. L., Rozemeijer, N. C., Veefkind, J. P., and Levelt, P. F.: In-flight performance of the Ozone Monitoring Instrument, Atmospheric Measurement Techniques, 10, 1957-1986, 10.5194/amt-10-1957-2017, 2017.

Stammes, P., Sneep, M., de Haan, J. F., Veefkind, J. P., Wang, P. and Levelt, P. F.: Effective cloud fractions from the Ozone Monitoring Instrument: Theoretical framework and validation, J. Geophys. Res., 113(D16), D16S38, doi:10.1029/2007JD008820, 2008.

Stavrakou, T., Müller, J.-F., Bauwens, M., De Smedt, I., Lerot, C., Van Roozendael, M., Coheur, P.-F., Clerbaux, C., Boersma, K. F., van der A, R. and Song, Y.: Substantial Underestimation of Post-Harvest Burning Emissions in the North China Plain Revealed by Multi-Species Space Observations, Sci. Rep., 6, 32307, doi:10.1038/srep32307, 2016.

van Donkelaar, A., Martin, R. V., Spurr, R. J. D., Drury, E., Remer, L. A., Levy, R. C., and Wang, J.: Optimal estimation for global ground-level fine particulate matter concentrations, Journal of Geophysical Research-Atmospheres, 118, 5621-5636, 10.1002/jgrd.50479, 2013.

Veefkind, J. P., de Haan, J. F., Sneep, M. and Levelt, P. F.: Improvements to the OMI O_2-O_2 operational cloud algorithm and comparisons with ground-based radar–lidar observations, Atmos. Meas. Tech., 9(12), 6035–6049, doi:10.5194/amt-9-6035-2016, 2016.

Verstraeten, W. W., Neu, J. L., Williams, J. E., Bowman, K. W., Worden, J. R. and Boersma, K. F.: Rapid increases in tropospheric ozone production and export from China, Nat. Geosci., 8, 690 [online] Available from: http://dx.doi.org/10.1038/ngeo2493, 2015.

Wang, J., Jacob, D. J. and Martin, S. T.: Sensitivity of sulfate direct climate forcing to the hysteresis of particle phase transitions, J. Geophys. Res. Atmos., 113(D11), n/a-n/a, doi:10.1029/2007JD009368, 2008a.

Wang, M., Gu, J., Yang, R., Zeng, L. and Wang, S.: Comparison of cloud type and frequency over China from surface, FY-2E, and CloudSat observations, vol. 9259, pp.

925913–925914. [online] Available from: http://dx.doi.org/10.1117/12.2069110, 2014.

Wang, P. and Stammes, P.: Evaluation of SCIAMACHY Oxygen A band cloud heights using Cloudnet measurements, Atmos. Meas. Tech., 7(5), 1331–1350, doi:10.5194/amt-7-1331-2014, 2014.

Wang, P., Stammes, P., van der A, R., Pinardi, G. and van Roozendael, M.: FRESCO+: an improved O_2 A-band cloud retrieval algorithm for tropospheric trace gas retrievals, Atmos. Chem. Phys., 8(21), 6565–6576, doi:10.5194/acp-8-6565-2008, 2008b.

Wang, X., Huang, J., Zhang, R., Chen, B. and Bi, J.: Surface measurements of aerosol properties over northwest China during ARM China 2008 deployment, J. Geophys. Res. Atmos., 115(D7), n/a-n/a, doi:10.1029/2009JD013467, 2010.

Wang, Y., Penning de Vries, M., Xie, P. H., Beirle, S., Dörner, S., Remmers, J., Li, A. and Wagner, T.: Cloud and aerosol classification for 2.5 years of MAX-DOAS observations in Wuxi (China) and comparison to independent data sets, Atmos. Meas. Tech., 8(12), 5133–5156, doi:10.5194/amt-8-5133-2015, 2015.

Wang, Y., Lampel, J., Xie, P., Beirle, S., Li, A., Wu, D. and Wagner, T.: Ground-based MAX-DOAS observations of tropospheric aerosols, NO_2, SO_2 and HCHO in Wuxi, China, from 2011 to 2014, Atmos. Chem. Phys., 17(3), 2189–2215, doi:10.5194/acp-17-2189-2017, 2017a.

Wang, Y., Beirle, S., Lampel, J., Koukouli, M., De Smedt, I., Theys, N., Li, A., Wu, D., Xie, P., Liu, C., Van Roozendael, M., Stavrakou, T., Müller, J.-F. and Wagner, T.: Validation of OMI, GOME-2A and GOME-2B tropospheric NO_2, SO_2 and HCHO products using MAX-DOAS observations from 2011 to 2014 in Wuxi, China:

investigation of the effects of priori profiles and aerosols on the satellite products, Atmos. Chem. Phys., 17(8), 5007–5033, doi:10.5194/acp-17-5007-2017, 2017b.

Winker, D. M., Pelon, J., Coakley, J. A., Ackerman, S. A., Charlson, R. J., Colarco, P. R., Flamant, P., Fu, Q., Hoff, R. M., Kittaka, C., Kubar, T. L., Le Treut, H., Mccormick, M. P., Mégie, G., Poole, L., Powell, K., Trepte, C., Vaughan, M. A. and Wielicki, B. A.: The CALIPSO Mission, Bull. Am. Meteorol. Soc., 91(9), 1211–1230, doi:10.1175/2010BAMS3009.1, 2010.

Winker, D. M., Tackett, J. L., Getzewich, B. J., Liu, Z., Vaughan, M. A. and Rogers, R. R.: The global 3-D distribution of tropospheric aerosols as characterized by CALIOP, Atmos. Chem. Phys., 13(6), 3345–3361, doi:10.5194/acp-13-3345-2013, 2013.

Zara, M., Boersma, K. F., De Smedt, I., Richter, A., Peters, E., Van Geffen, J. H. G. M., Beirle, S., Wagner, T., Van Roozendael, M., Marchenko, S., Lamsal, L. N. and Eskes, H. J.: Improved slant column density retrieval of nitrogen dioxide and formaldehyde for OMI and GOME-2A from QA4ECV: intercomparison, uncertainty characterization, and trends, Atmos. Meas. Tech. Discuss., 1–47, doi:10.5194/amt-2017-453, 2018.

Zhang, Q., Streets, D. G., Carmichael, G. R., He, K. B., Huo, H., Kannari, A., Klimont, Z., Park, I. S., Reddy, S., Fu, J. S., Chen, D., Duan, L., Lei, Y., Wang, L. T. and Yao, Z. L.: Asian emissions in 2006 for the NASA INTEX-B mission, Atmos. Chem. Phys., 9(14), 5131–5153, doi:10.5194/acp-9-5131-2009, 2009.

Zhao, C. and Wang, Y.: Assimilated inversion of NO_X emissions over east Asia using OMI NO_2 column measurements, Geophys. Res. Lett., 36(6), L06805, doi:10.1029/2008GL037123, 2009.

Zhao, H. Y., Zhang, Q., Guan, D. B., Davis, S. J., Liu, Z., Huo, H., Lin, J. T., Liu, W. D. and He, K. B.: Assessment of China's virtual air pollution transport embodied in trade by using a consumption-based emission inventory, Atmos. Chem. Phys., 15(10), 5443–5456, doi:10.5194/acp-15-5443-2015, 2015.

Zhou, Y., Brunner, D., Spurr, R. J. D., Boersma, K. F., Sneep, M., Popp, C. and Buchmann, B.: Accounting for surface reflectance anisotropy in satellite retrievals of tropospheric NO_2, Atmos. Meas. Tech., 3(5), 1185–1203, doi:10.5194/amt-3-1185-2010, 2010.

Zhu, W., Xu, C., Qian, X. and Wei, H.: Statistical analysis of the spatial-temporal distribution of aerosol extinction retrieved by micro-pulse lidar in Kashgar, China, Opt. Express, 21(3), 2531–2537, doi:10.1364/OE.21.002531, 2013.

Table A1. Number of CALIOP observations in a grid cell ($0.667° \times 0.5°$).

	Before filtering				After filtering			
	Mean	Median	Minima	Maximum	Mean	Median	Minima	Maximum
For a month	165	169	0	291	47	39	0	223
For the same month in nine years	1483	1513	192	1921	420	395	0	1548
For all months in nine years	17794	18528	5608	20781	5033	5381	146	12650

Table 1. MAX-DOAS measurement sites and corresponding meteorological stations.

MAX-DOAS site name	Site information	Measurement times	Corresponding meteorological station name	Meteorological station information
Xianghe	116.96°E, 39.75°N, 36 m, suburban	2012/01/01 -2012/12/31	CAPITAL INTERNATIONA	116.89°E, 40.01°N, 35.4 m
IAP	116.38°E, 39.98°N, 92 m, urban	2008/06/22 -2009/04/16	CAPITAL INTERNATIONA	116.89°E, 40.01°N, 35.4 m
Wuxi	120.31°E, 31.57°N, 20 m, urban	2012/01/01 -2012/12/31	HONGQIAO INTL	121.34°E, 31.20°N, 3 m

Table 2. Evaluation of OMI NO_2 products with respect to MAX-DOAS on 27 haze days [1].

	POMINO v1.1	POMINO	DOMINO v2	QA4ECV
Slope	1.07	0.80	1.11	0.58
Intercept (10^{15} molec./cm^2)	-3.58	1.76	-11.79	3.20
R^2	0.76	0.68	0.38	0.34
NMB (%)	4.4	-9.4	-5.0	-26.11

1. The haze days are determined when the ground meteorological station data and MODIS/Aqua corrected reflectance (true color) data both indicate a haze day. Average across the days, AOD = 1.13 (median = 1.10), SSA = 0.90 (0.91), MAX-DOAS NO_2 = 51.92 x 10^{15} molec. cm^{-2}, and CF = 0.06 (0.03).

Table 3. Evaluation of OMI NO_2 products with respect to MAX-DOAS on 36 cloud-free days [1].

	POMINO v1.1	POMINO	DOMINO v2	QA4ECV
Slope	1.30	1.13	0.92	0.79
Intercept	-0.61	0.31	2.32	1.05
R^2	0.55	0.56	0.53	0.63
NMB (%)	29.4	20.8	21.9	-5.83

1. CF=0 in POMINO product. Average across the days, AOD = 0.60 (median = 0.47), SSA = 0.90 (0.91), and MAX-DOAS NO_2 = 26.82 x 10^{15} molec. cm^{-2}.

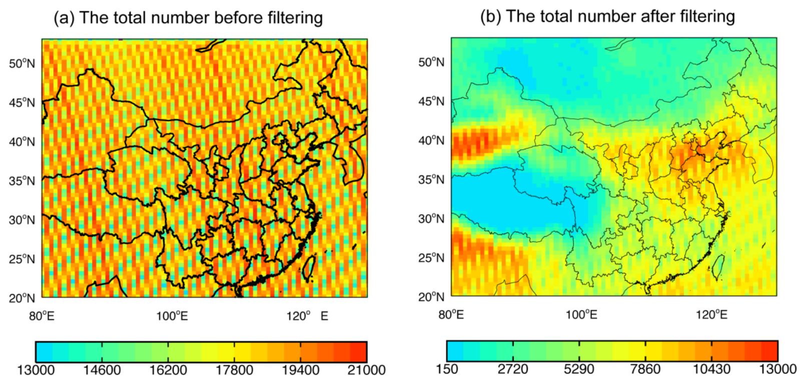

Figure A1. The total number of CALIOP Level-2 aerosol extinction profiles at 532 nm used to derive our climatological (2007–2015) dataset on a 0.667° long. x 0.5° lat. grid (a) before and (b) after filtering.

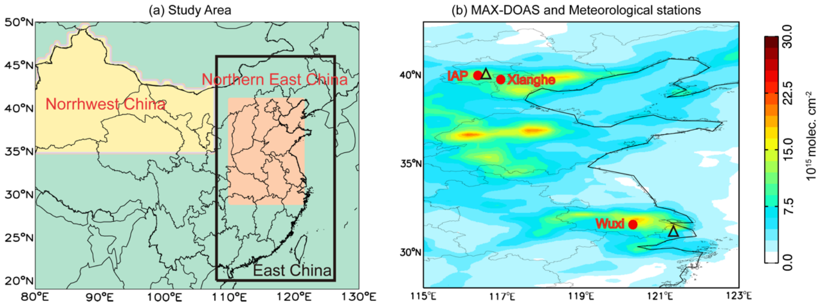

Figure 1. (a) Three study areas: Northern East China, Northwest China, and East China. (b) MAX-DOAS measurement sites (red dots) and corresponding meteorological stations (black triangle) overlaid on POMINO v1.1 NO_2 VCDs in August 2012.

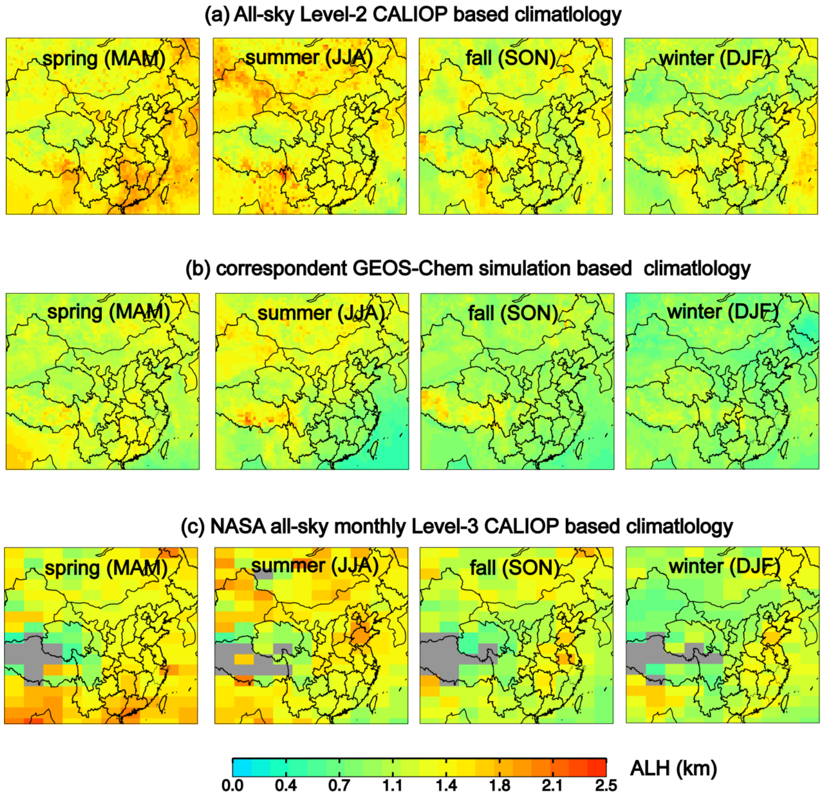

Figure 2. Seasonal spatial patterns of ALH climatology at 532 nm on a 0.667° long. x 0.50 ° lat. grid based on (a) our complied all-sky Level-2 CALIOP data, (b) corresponding GEOS-Chem simulations, and (c) NASA all-sky monthly Level-3 CALIOP dataset.

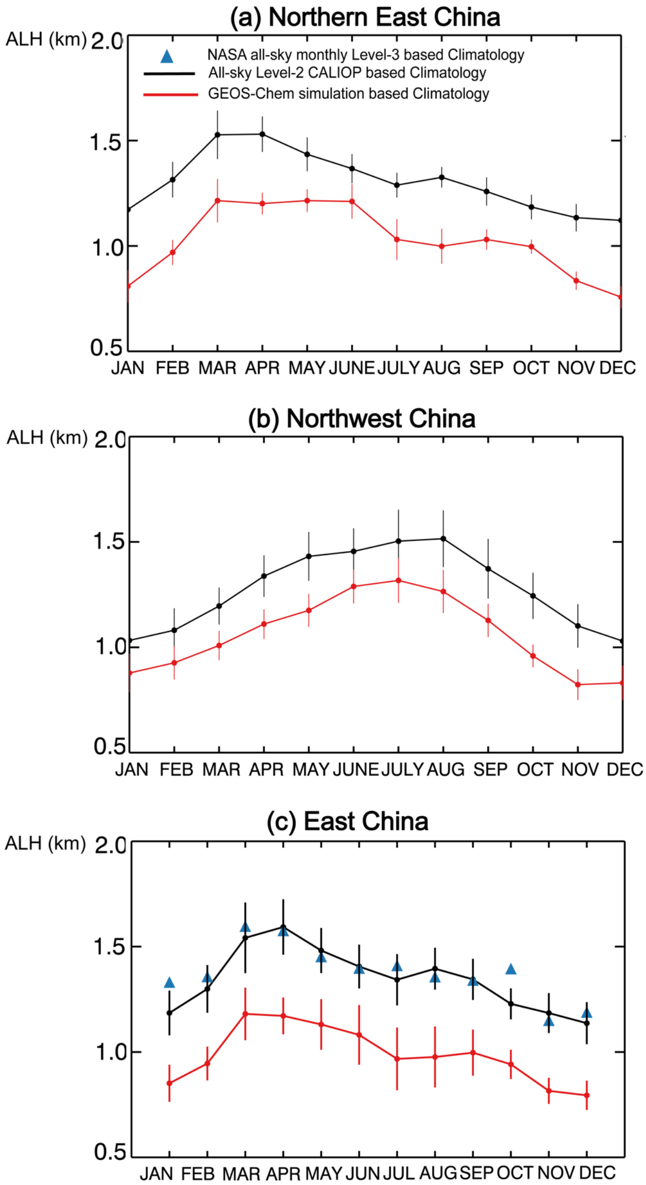

Figure 3. Regional mean ALH monthly climatology over (a) Northern East China, (b) Northwest China, and (c) East China. The error bars stand for 1 standard deviation for spatial variability.

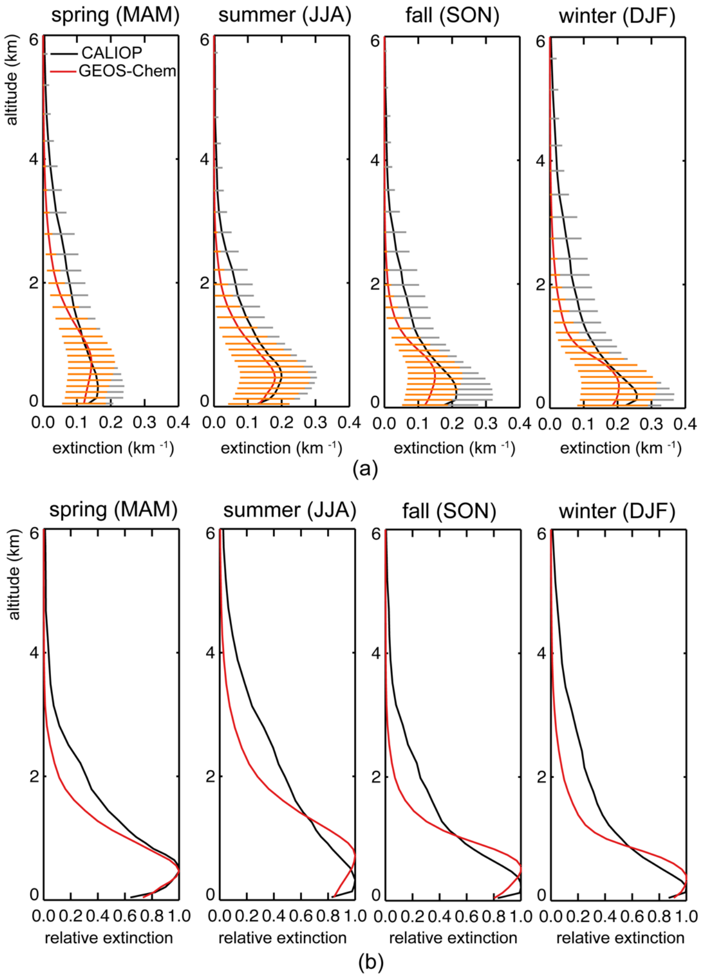

Figure 4. Seasonal climatological aerosol extinction profiles (first row) and corresponding relative extinction profiles (normalized to maximum extinction values, second raw) in spring (MAM), summer (JJA), fall (SON) and winter (DJF) over Northern East China. Model results (in red) are prior to MODIS/Aqua based AOD adjustment. Error bars in (a) represent 1 standard deviation across all grid cells in each season.

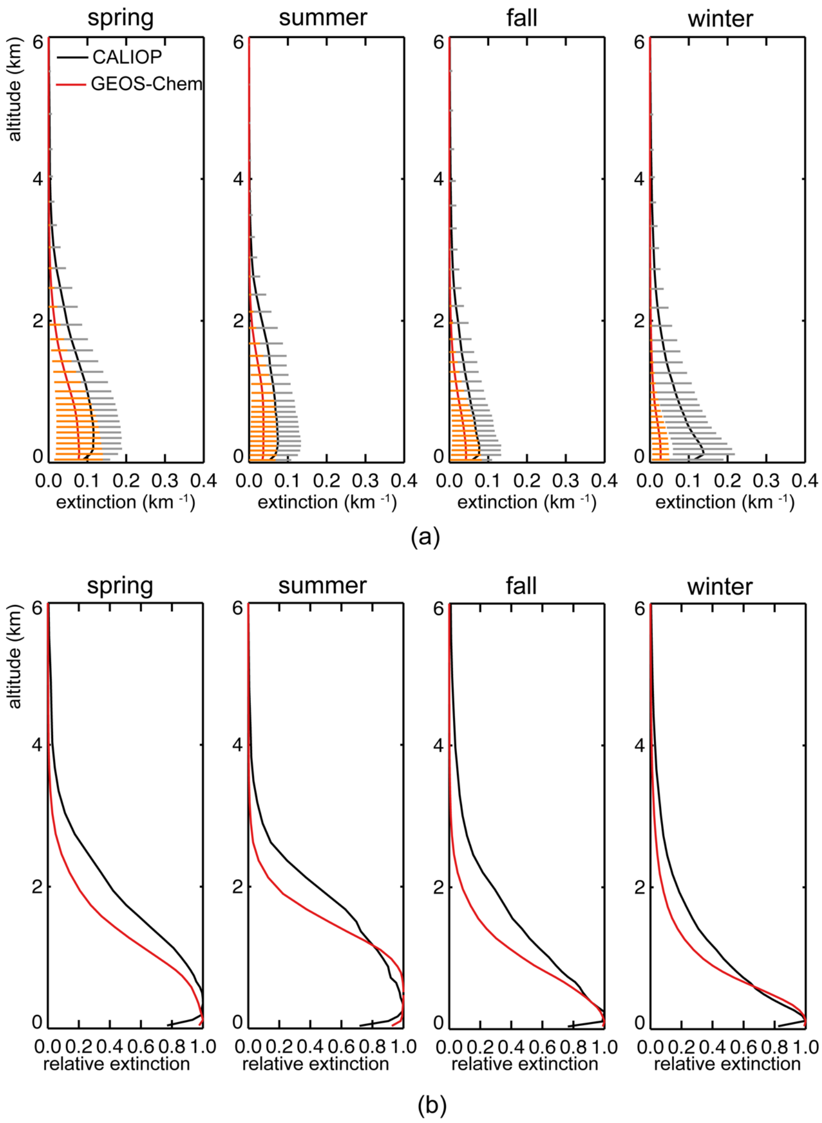

1042 Figure 5. Similar to Fig. 5 but for Northwest China.

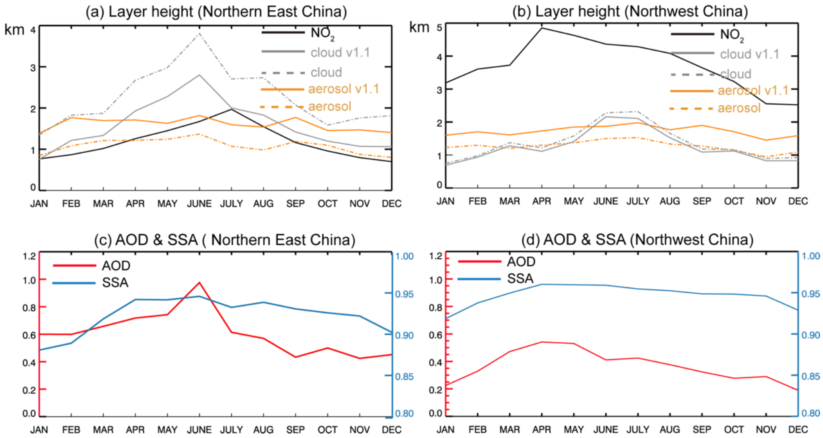

Figure 6. Monthly variations of ALH, CTH and NLH over (a) Northern East China and (b) Northwest China in 2012. Data are averaged across all pixels in each month and region. The grey and orange solid lines denote POMINO v1.1 results, while the corresponding dashed lines denote POMINO. (c–d) Corresponding monthly AOD and SSA.

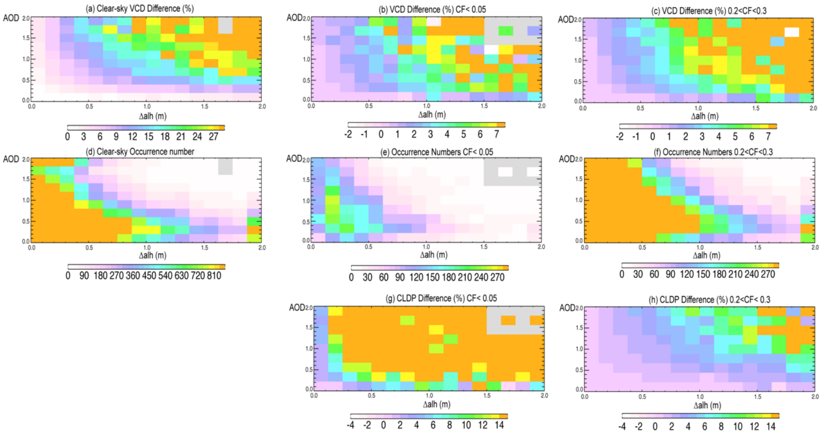

Figure 7. Percentage changes in VCD from POMINO to POMINO v1.1 ([POMINO v1.1 – POMINO] / POMINO) for each bin of ΔALH (bin size = 0.2 km) and AOD (bin size = 0.1) across pixels in 2012 over Northern East China, for (a) cloud-free sky (CF = 0 in POMINO), (b) little-cloudy sky, and (c) modestly cloudy sky. (d-f) The number of occurrences corresponding to (a-c). (g, h) Similar to (b, c) but for the percentage changes in cloud top pressure (CP).

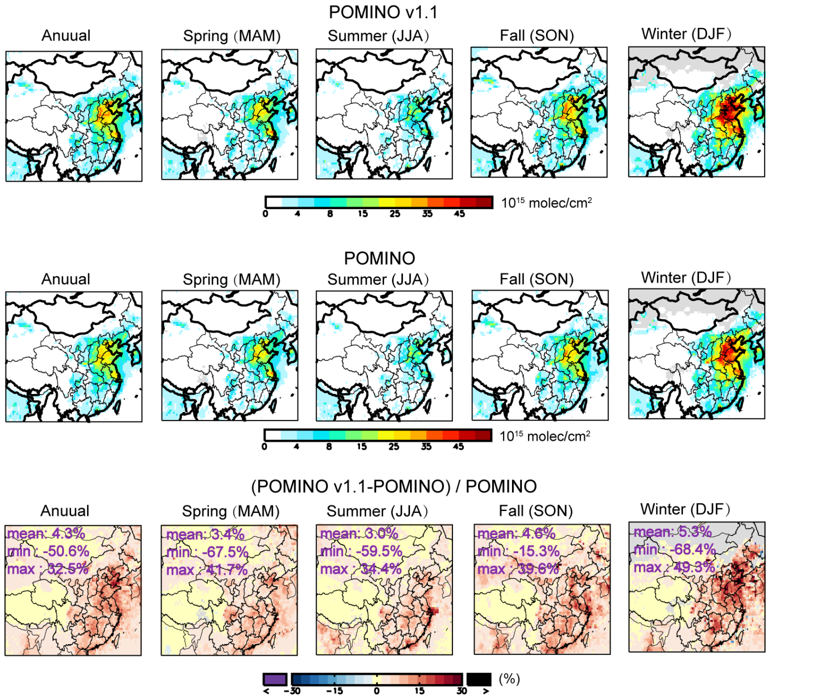

Figure 8. Seasonal spatial distribution of tropospheric NO_2 VCD in 2012 for (a) POMINO v1.1, (b) POMINO, and (c) their relative difference.

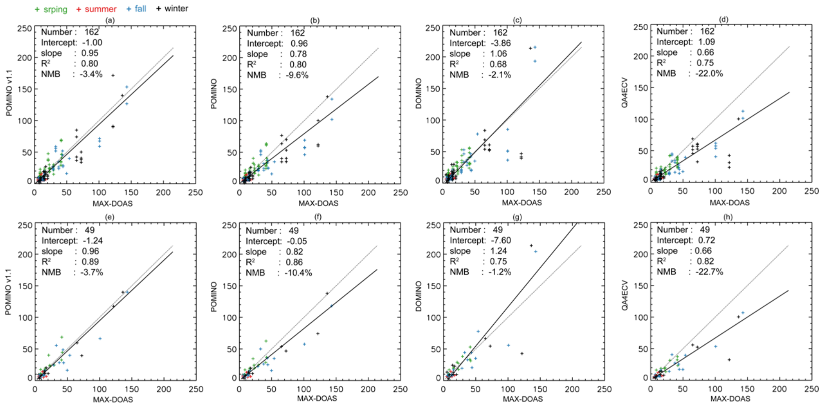

Figure 9. (a–d) Scatterplot for NO_2 VCDs (10^{15} molec. cm^{-2}) between MAX-DOAS and each of the three OMI products. Each "+" corresponds to an OMI pixel, as several pixels may be available in a day. (e–h) Similar to (a–d) but after averaging over all OMI pixels in the same day, such that each "+" represents a day. Also shown are the statistic results from the RMA regression. The black solid line indicates the regression curve and the grey dotted line depict the 1:1 relationship.

10, IAP/CAS, Institute of Atmospheric Physics, Chinese Academy of Sciences, Beijing, China

Correspondence to: Jintai Lin (linjt@pku.edu.cn); K. Folkert Boersma (folkert.boersma@knmi.nl)

Abstract

Satellite retrieval of vertical column densities (VCDs) of tropospheric nitrogen dioxide (NO_2) is critical for NO_x pollution and impact evaluation. For regions with high aerosol loadings, the retrieval accuracy is greatly affected by whether aerosol optical effects are treated implicitly (as additional "effective" clouds) or explicitly, among other factors. Our previous POMINO algorithm explicitly accounts for aerosol effects to improve the retrieval especially in polluted situations over China, by using aerosol information from GEOS-Chem simulations with further monthly constraints by MODIS/Aqua aerosol optical depth (AOD) data. Here we present a major algorithm update, POMINO v1.1, by constructing a monthly climatological data set of aerosol extinction profiles, based on Level-2 CALIOP/CALIPSO data over 2007–2015, to better constrain the modeled aerosol vertical profiles.

We find that GEOS-Chem captures the month-to-month variation of CALIOP aerosol layer height but with a systematic underestimate by about 300–600 m (season and location dependent), due to a too strong negative vertical gradient of extinction above 1 km. Correcting the model aerosol extinction profiles results in small changes in retrieved cloud fraction, increases in cloud top pressure (within 2–6% in most cases), and increases in tropospheric NO_2 VCD by 4–16% over China on a monthly basis in 2012. The improved NO_2 VCDs (in POMINO v1.1) are more consistent with independent ground-based MAX-DOAS observations (R^2 = 0.80, NMB = -3.4%, for 162 pixels in 49 days) than POMINO (R^2 = 0.80, NMB = -9.6%), DOMINO v2 (R^2 =

删除的内容: t

删除的内容: AOD

删除的内容: This study is the kernel updates of our newthe retrieval algorithm, to POMINO v21.1,

删除的内容:

删除的内容: and

0.68, NMB = -2.1%) and QA4ECV (R^2 = 0.75, NMB = -22.0%) are. Especially on haze days, R^2 reaches 0.76 for POMINO v1.1, much higher than that for POMINO (0.68), DOMINO v2 (0.38) and QA4ECV (0.34). Furthermore, the increase in cloud pressure likely reveals a more realistic vertical relationship between cloud and aerosol layers, with aerosols situated above the clouds in certain months instead of always below the clouds. The POMINO v1.1 algorithm is a core step towards our next public release of data product (POMINO v2), and it will also be applied to the recently launched S5P-TropOMI sensor.

1. Introduction

Air pollution is a major environmental problem in China. In particular, China has become the world's largest emitting country of nitrogen oxides (NO_X=NO+NO_2) due to its rapid economic growth, heavy industries, coal-dominated energy sources, and relatively weak emission control (Cui et al., 2016; Lin et al., 2014a; Stavrakou et al., 2016; Zhang et al., 2009). Tropospheric vertical column densities (VCDs) of nitrogen dioxide (NO_2) retrieved from the Ozone Monitoring Instrument (OMI) onboard the Earth Observing System (EOS) Aura satellite have been widely used to monitor and analyze NO_X pollution over China because of its high spatiotemporal coverage (e.g. (Lin et al., 2010; Miyazaki and Eskes, 2013; Verstraeten et al., 2015; Zhao and Wang, 2009). However, NO_2 retrieved from OMI and other space-borne instruments are subject to errors in the conversion process from radiance to VCD, particularly with respect to the calculation of tropospheric air mass factor (AMF) that is used to convert tropospheric slant column density to VCD (e.g. Boersma et al., 2011; Bucsela et al., 2013; Lin et al., 2015; Lorente et al., 2017).

Most current-generation NO_2 algorithms do not explicitly account for the effects of aerosols on NO_2 AMFs and on prerequisite cloud parameter retrievals. These retrievals often adopt an implicit approach wherein cloud algorithms retrieve

带格式的: 上标

删除的内容: 82

删除的内容: 7

删除的内容:

删除的内容: and

删除的内容: This

删除的内容: improvement in ourOur POMINO v1.1 algorithm

删除的内容: ↵

"effective cloud" parameters that include the optical effects of aerosols. This implicit method is based on aerosols exerting an effect on the top-of-atmosphere radiance level, whereas the assumed cloud model does not account for the presence of aerosols in the atmosphere (Stammes et al., 2008; Veefkind et al., 2016; Wang et al., 2008b; Wang and Stammes, 2014). In the absence of clouds, an aerosol optical thickness of 1 is then interpreted as an effective cloud fraction of $\pm$0.10, and the value also depends on the aerosol properties (scattering or absorbing), true surface albedo and geometry angles (Chimot et al., 2016) with an effective cloud pressure closely related to the aerosol layer, at least for aerosols of predominantly scattering nature (e.g. Boersma et al., 2004, 2011, Castellanos et al., 2014, 2015). However, in polluted situations with high aerosol loadings and more absorbing aerosol types, which often occur over China and many other developing regions, the implicit method can result in considerable biases (Castellanos et al., 2014, 2015; Chimot et al., 2016; Kanaya et al., 2014; Lin et al., 2014b).

Lin et al. (2014b, 2015) established the POMINO NO_2 algorithm, which builds on the DOMINO v2 algorithm (for OMI NO_2 slant columns and stratospheric correction), but improves upon it through a more sophisticated AMF calculation over China. In POMINO, the effects of aerosols on cloud retrievals and NO_2 AMFs are explicitly accounted for. In particular, daily information on aerosol optical properties such as aerosol optical depth (AOD), single scattering albedo (SSA), phase function and vertical extinction profiles are taken from nested Asian GEOS-Chem v9-02 simulations. The modeled AOD at 550 nm is further constrained by MODIS/Aqua monthly AOD, with the correction applied to other wavelengths based on modeled aerosol refractive indices (Lin et al., 2014b). However, the POMINO algorithm does not include an observation-based constraint on the vertical profile of aerosols, whose altitude relative to NO_2 has strong and complex influences on NO_2 retrieval (Castellanos et al., 2015; Leitão et al., 2010; Lin et al., 2014b). This study improves

upon the POMINO algorithm by incorporating CALIOP monthly climatology of aerosol vertical extinction profiles to correct for model biases.

The CALIOP lidar, carried on the sun-synchronous CALIPSO satellite, has been acquiring global aerosol extinction profiles since June 2006 (Winker et al., 2010). CALIPSO and Aura are both parts of the National Aeronautics and Space Administration (NASA) A-train constellation of satellites. The overpass time of CALIOP/CALIPSO is only 15 minutes later than OMI/Aura. In spite of issues with the detection limit, radar ratio selection and cloud contamination that cause some biases in CALIOP aerosol extinction vertical profiles (Amiridis et al., 2015; Koffi et al., 2012; Winker et al., 2013), comparisons of aerosol extinction profiles between ground-based lidar and CALIOP show good agreements (Kacenelenbogen et al., 2014; Kim et al., 2009; Misra et al., 2012). However, CALIOP is a nadir-viewing instrument that measures the atmosphere along the satellite ground-track with a narrow field-of-view. This means that the daily geographical coverage of CALIOP is much smaller than that of OMI. Thus previous studies often used monthly/seasonal regional mean CALIOP data to study aerosol vertical distributions or to evaluate model simulations (Chazette et al., 2010; Johnson et al., 2012; Koffi et al., 2012; Ma and Yu, 2014; Sareen et al., 2010).

There exist a few CALIOP Level-3 gridded datasets, such as LIVAS (Amiridis et al. 2015) and NASA official Level-3 monthly dataset (Winker et al., 2013). However, LIVAS is an annual average day-night combined product, not suitable to be applied to OMI NO_2 retrievals (around early afternoon, and in need of a higher temporal resolution than annual). The horizontal resolution (2° long. $\times$ 5° lat.) of NASA official product is much coarser than OMI footprints and the GEOS-Chem model resolution.

删除的内容: are some mature data of

删除的内容:

删除的内容: yearly

删除的内容: but

带格式的: 下标

删除的内容: measurement is only available in the daytime, besides, the temporal resolution (yearly) is not very suitable for daily aerosol extinction profiles usage

删除的内容: s

Here we construct a custom monthly climatology of aerosol vertical extinction profiles based on 9-years (2007–2015) worth of CALIOP Version 3 Level-2 532 nm data. On a climatological basis, we use the CALIOP monthly data to adjust GEOS-Chem profiles in each grid cell for each day of the same month in any year. We then use the corrected GEOS-Chem vertical extinction profiles in the retrievals of cloud parameters and NO_2. Finally, we evaluate our updated POMINO retrieval (hereafter referred to as POMINO v1.1), our previous POMINO product, DOMINO v2 and the newly released Quality Assurance for Essential Climate Variables product (QA4ECV, see Appendix A), using ground-based MAX-DOAS NO_2 column measurements at three urban/suburban sites in East China for the year of 2012 and several months in 2008/2009.

Section 2 describes the construction of CALIOP aerosol extinction vertical profile monthly climatology, the POMINO v1.1 retrieval approach, and the MAX-DOAS data. It also presents the criteria for comparing different NO_2 retrieval products and for selecting coincident OMI and MAX-DOAS data. Section 3 compares our CALIOP climatology with NASA's official Level-3 CALIOP dataset and GEOS-Chem simulation results. Sections 4 and 5 compare POMINO v1.1 to POMINO to analyze the influence of improved aerosol vertical profiles on retrievals of cloud parameters and NO_2 VCDs, respectively. Section 6 evaluates POMINO, POMINO v1.1, DOMNO v2 and QA4ECV NO_2 VCD products using the MAX-DOAS data. Section 7 concludes our study.

2. Data and methods

2.1 CALIOP monthly mean extinction profile climatology

CALIOP is a dual-wavelength polarization lidar measuring attenuated backscatter radiation at 532 and 1064 nm since June 2006. The vertical resolution of aerosol

删除的内容: In order to constrain daily aerosol extinction profiles simulated by GEOS-Chem.However, the major monthly/seasonal CALIOP data are too coarse in spatial resolution (i.e. NASA's official monthly Level-3 CALIOP dataset with spatial resolution 2° long. × 5° lat.) or in temporal resolution (i.e. LIVAS 5-year based 1° × 1° CALIOP dataset).
H

删除的内容: and the existing

删除的内容: and

删除的内容: retrievals

删除的内容:

删除的内容: and

删除的内容: new released Quality Assurance for Essential Cliamte Variables (QA4ECV, see detailed introduction in Appedix B)

删除的内容: s

删除的内容: *Constructing a*

extinction profiles is 30 m below 8.2 km and 60 m up to 20.2 km (Winker et al., 2013), with a total of 399 sampled altitudes. The horizontal resolution of CALIOP scenes is 335 m along the orbital track and is given over a 5 km horizontal resolution in Level-2 data.

As detailed in Appendix B, we use the daily all-sky Version 3 CALIOP Level-2 aerosol profile product at 532 nm from 2007 to 2015 to construct a monthly Level-3 climatological dataset of aerosol extinction profiles over China and nearby regions. This dataset is constructed on the GEOS-Chem model grid (0.667° long. x 0.5° lat.) and vertical resolution (47 layers, with 36 layers or so in the troposphere).

The ratio of climatological monthly CALIOP to monthly GEOS-Chem profiles represents the scaling profile to adjust the daily GEOS-Chem profiles in the same month (see Sect. 2.2).

2.2 POMINO v1.1 retrieval approach

The NO_2 retrieval consists of three steps. First, the total NO_2 slant columns density (SCD) is retrieved using the Differential Optical Absorption Spectroscopy (DOAS) technique (for the 405-465 nm spectral window in the case of OMI). The uncertainty of the SCD is determined by the appropriateness of the fitting technique, the instrument noise, the choice of fitting window, and the orthogonality of the absorbers' cross sections (Bucsela et al., 2006; van Geffen et al., 2015; Lerot et al., 2010; Richter et al., 2011; Zara et al., 2018). The NO_2 SCD in DOMINO v2 has a bias at about 0.5~1.3 × 10^{15} molec. cm^{-2} (Belmonte Rivas et al., 2014; Dirksen et al., 2011; Marchenko et al., 2015; van Geffen et al., 2015; Zara et al., 2018), which can be reduced by improving wavelength calibration and including O_2–O_2 and liquid water absorption in the fitting model (van Geffen et al., 2015). The tropospheric SCD is then obtained by subtracting the stratospheric SCD from the total SCD. The bias in

删除的内容: Here

已下移 [5]: We choose the all-sky product instead of clear-sky data, since previous studies indicate that the climatological aerosol extinction profiles are affected insignificantly by the presence of clouds (Koffi et al. 2012; Winker et al. 2013). As we use this climatological data to adjust GEOS-Chem results, choosing all-sky data improves consistency with the model simulation when doing the daily correction.

已下移 [1]: In brief, only the pixels with Cloud Aerosol Discrimination (CAD) scores between -20 and -100 with extinction Quality Control (QC) flag valued at 0, 1, 18, and 16 are selected. We further discard samples with an extinction uncertainty of 99.9 km^{-1}, which is indicative of unreliable retrieval. We only accept extinction values falling in the range from 0.0 to 1.25, according to CALIOP observation thresholds. Previous studies showed that weakly scattering edges of icy clouds are sometimes misclassified as aerosols (Winker et al. 2013). To eliminate contamination from icy clouds we exclude the aerosol layers above the cloud layer (with layer-top temperature below 0 ℃) when both of them are above 4km (Winker et al. 2013).

已下移 [2]: CALIOP Level-2 data are always presented at the fixed 399 altitudes above sea level. To account for the difference in surface elevation between a CALIOP pixel and the respective model grid cell,

删除的内容: We apply a number of criteria to ensure data quality of each pixel, mainly following Winker et al. (2013) and Amiridis et al. ... [1]

带格式的: 非突出显示

删除的内容:

删除的内容: After the pixel-based screening, we aggregate the CALIOP data at the model grid (0.667° long. x 0.5° lat.) and vertical ... [2]

删除的内容:

已下移 [3]: Figure 1 shows the number of aerosol extinction profiles in each grid cell and 12 x 9 = 108 months that are used to compile the

删除的内容: .

删除的内容: As discussed above, we choose the CALIOP pixels within 1.5° of a grid cell center. We test this choice by examining the ... [3]

已下移 [4]: For each grid cell in each month, we further correct singular values in the vertical profile. In a month, if a grid cell *i* has

批注 [JL1]: Add Zara et al. (2018)

the total SCD is mostly absorbed by this stratospheric separation step, which may not propagate into the tropospheric SCD (van Geffen et al., 2015). The last step converts the tropospheric SCD to VCD by using the tropospheric AMF (VCD = SCD / AMF). The tropospheric AMF is calculated at 438 nm by using look-up tables (in most retrieval algorithms) or online radiative transfer modeling (in POMINO) driven by ancillary parameters, which act as the dominant source of errors in retrieved NO_2 VCD data over polluted areas (Boersma et al., 2007; Lin et al., 2014b, 2015; Lorente et al., 2017).

Our POMINO algorithm focuses on the tropospheric AMF calculation over China and nearby regions, taking the tropospheric SCD (Dirksen et al., 2011) from DOMINO v2 (Boersma et al., 2011). POMINO improves upon the DOMINO v2 algorithm in the treatment of aerosols, surface reflectance, online radiative transfer calculations, spatial resolution of NO_2, temperature and pressure vertical profiles, and consistency between cloud and NO_2 retrievals (Lin et al., 2014b, 2015). In brief, we use the parallelized LIDORT-driven AMFv6 package to derive both cloud parameters and tropospheric NO_2 AMFs for individual OMI pixels online. NO_2 vertical profiles, aerosol optical properties and aerosol vertical profiles are taken from the nested GEOS-Chem model over Asia (0.667 ° long. × 0.5° lat. before May 2013 and 0.3125 ° long. × 0.25 ° lat. afterwards), and pressure and temperature profiles are taken from the GEOS-5 and GEOS-FP assimilated meteorological fields that drive GEOS-Chem simulations. Model aerosols are further adjusted by satellite data (see below). We adjust the pressure profiles based on the difference in elevation between the pixel center and the matching model grid cell (Zhou et al., 2010). We also account for the effects of surface bidirectional reflectance distribution function (BRDF) (Lin et al., 2014b; Zhou et al., 2010) by taking three kernel parameters (isotropic, volumetric and geometric) from the MODIS MCD43C2 data set at 440 nm (Lucht et al., 2000).

删除的内容:

删除的内容: will

删除的内容: at 439 nm

删除的内容: nearly

删除的内容: , improved surface elevation

删除的内容: and other aspects

删除的内容:

删除的内容: without use of look-up tables

删除的内容:

删除的内容:

As a prerequisite to the POMINO NO_2 retrieval, clouds are retrieved through the O_2-O_2 algorithm (Acarreta et al., 2004; Stammes et al., 2008) with O_2-O_2 SCDs from OMCLDO2, and with pressure, temperature, surface reflectance, aerosols and other ancillary information consistent with the NO_2 retrieval. Note that the treatment of cloud scattering (as "effective" Lambertian reflector, as in other NO_2 algorithms) is different from the treatment of aerosol scattering/absorption (vertically resolved based on the Mie scheme).

POMINO uses the temporally and spatially varying aerosol information, including AOD, single scattering albedo (SSA), phase function and vertical profiles from GEOS-Chem simulations. POMINO v1.1 (this work) further uses CALIOP data to constrain the shape of aerosol vertical extinction profile. We run the model at a resolution of 0.3125° long. × 0.25° lat. before May 2013 and 0.667° long. × 0.5° lat. afterwards, as determined by the resolution of the driving meteorological fields. We then regrid the finer resolution model results to 0.667° long. × 0.5° lat., to be consistent with the CALIOP data grid. We then sample the model data at times and locations with valid CALIOP data at 532 nm to establish the model monthly climatology.

For any month in a grid cell, we divide the CALIOP monthly climatology of aerosol extinction profile shape by model climatological profile shape to obtain a unitless scaling profile (Eq. 1), and apply this scaling profile to all days of that month in all years (Eq. 2). Such a climatological adjustment is based on the assumption that systematic model limitations are month-dependent and persist over the years and days (e.g., a too strong vertical gradient, see Sect. 3.3). Although this monthly adjustment means discontinuity on the day-to-day basis (e.g., from the last day of a month to the first day of the next month), such discontinuity does not significantly affect the NO_2 retrieval, based on our sensitivity test.

删除的内容: the

删除的内容: al is done

带格式的: 下标

删除的内容: It should be noticed

删除的内容: s

带格式的: 下标

删除的内容: scattering by clouds and

删除的内容: s in tropospheric AMF calculation are different. The cloud are treated as lambert reflector while Mie scattering scheme is used for aerosols in RTM calculations

删除的内容:

删除的内容:

删除的内容:

删除的内容: 2

删除的内容: 3

带格式的: 下标

删除的内容: significantly

In Eqs. 1 and 2, E^C represents the CALIOP climatological aerosol extinction coefficient, E^G the GEOS-Chem extinction, E^{Gr} the post-scaling model extinction, and R the scaling profile. The subscript *i* denotes a grid cell, *k* a vertical layer, *d* a day, *m* a month, and *y* a year. Note that in Eq. 1, the extinction coefficient at each layer is normalized relative to the maximum value of that profile. This procedure ensures that the scaling is based on the relative shape of the extinction profile and is thus independent of the accuracies of CALIOP and GEOS-Chem AOD. We keep the absolute AOD value of GEOS-Chem unchanged in this step.

删除的内容: Actually, the correction to model simulated aerosol extinction profiles are main restricted by observation. CALIOP observation are only one highly spatialtemporal coverage data we can find.

删除的内容: 2

删除的内容: 3

删除的内容:

删除的内容: 2

$$R_{i,k,m} = \frac{E^C_{i,k,m}/\max(E^C_{i,k,m})}{E^G_{i,k,m}/\max(E^G_{i,k,m})} \quad (1)$$

删除的内容: 2

$$E^{Gr}_{i,k,d,m,y} = E^G_{i,k,d,m,y} \times R_{i,k,m} \quad (2)$$

删除的内容: 3

In POMINO, the GEOS-Chem AOD are further constrained by a MODIS/Aqua Collection 5.1 monthly AOD dataset compiled on the model grid (Lin et al., 2014b, 2015). POMINO v1.1 uses the Collection 5.1 AOD data before May 2013 and Collection 6 data afterwards. For adjustment, model AOD are projected to a 0.667° long. × 0.5° lat. grid and then sampled at times and locations with valid MODIS data (Lin et al., 2015). As shown in Eq. 3, τ^M denotes MODIS AOD, τ^G GEOS-Chem AOD, and τ^{Mr} post-adjustment model AOD. The subscript *i* denotes a grid cell, *d* a day, *m* a month, and *y* a year. This AOD adjustment ensures that in any month, monthly mean GEOS-Chem AOD is the same as MODIS AOD while the modeled day-to-day variability is kept.

删除的内容:

删除的内容: 4

$$\tau^{Gr}_{i,d,m,y} = \frac{\tau^M_{i,m,y}}{\tau^G_{i,m,y}} \times \tau^G_{i,d,m,y} \quad (3)$$

删除的内容: 4

Equations 4–5 show the complex effects of aerosols in calculating the AMF for any pixel. The AMF is the linear sum of tropospheric layer contributions to the slant

删除的内容: 5

删除的内容: 6

column weighted by the vertical subcolumns (Eq. 4). The box AMF, amf_k, describes the sensitivity of NO_2 SCD to layer k, and $x_{a,k}$ represent the subcolumn of layer k from a priori NO_2 profile. The l represent the first integrated layer, which is the layer above the ground for clear sky, or the layer above cloud top for cloudy sky. The t represent the tropopause layer. POMINO assumes the independent pixel approximation (IPA) (Martin et al., 2002; Boersma et al., 2002). This means that the calculated AMF for any pixel consists of a fully cloudy-sky portion (AMF_{clr}) and a fully clear-sky portion (AMF_{cld}), with weights based on the cloud radiance fraction ($\mathrm{CRF} = (1-\mathrm{CF}) \cdot \mathrm{A_{clr}} + \mathrm{CF} \cdot \mathrm{A_{cld}}$, $\mathrm{A_{clr}}$, $\mathrm{A_{cld}}$ are radiance from the clear-sky part and cloudy part of the pixel, respectively.) (Eq. 5). AMF_{cld} is affected by above-cloud aerosols, and AMF_{clr} is affected by aerosols in the entire column. Also, aerosols affect the retrieval of CRF. Thus, the improvement of aerosol vertical profile in POMINO v1.1 affects all the three quantities in Eq. 5 and thus leads to complex impacts on retrieved NO_2 VCD.

$$\mathrm{AMF} = \frac{\sum_l^t amf_k x_{a,k}}{\sum_l^t x_{a,k}} \quad (4)$$

$$\mathrm{AMF} = \mathrm{AMF}_{cld} \cdot \mathrm{CRF} + \mathrm{AMF}_{clr} \cdot (1-\mathrm{CRF}) \quad (5)$$

2.3 OMI pixel selection to evaluate POMINO v1.1, POMINO, DOMINO v2 and QA4ECV

We exclude OMI pixels affected by row anomaly (Schenkeveld et al., 2017) or with high albedo caused by icy/snowy ground. To screen out cloudy scenes, we choose pixels with CRF below 50% (effective cloud fraction is typically below 20%) in POMINO.

The selection of CRF threshold influences the validity of pixels. The "effective" CRF in DOMINO implicitly includes the influence of aerosols. In POMINO, the aerosol

删除的内容: 5

删除的内容: CRF

删除的内容: 6

删除的内容: whole

删除的内容: 6

删除的内容: 5

删除的内容: 6

删除的内容: *and*

contribution is separated from that of the clouds, resulting in a lower CRF than for DOMINO. The CRF differs insignificantly between POMINO and POMINO v1.1, because the same AOD and other non-aerosol ancillary parameters are used in the retrieval process. Using the CRF from POMINO instead of DOMINO or QA4ECV for cloud screening means that the number of "valid" pixels in DOMINO increases by about 25%, particularly because much more pixels with high pollutant (aerosol and NO_2) loadings are now included. This potentially reduces the sampling bias (Lin et al., 2014b, 2015), and the ensemble of pixels now includes scenes with high "aerosol radiative fractions". Further research is needed to fully understand how much these high-aerosol scenes may be subject to the same screening issues as the cloudy scenes. Nevertheless, the limited evidence here and in Lin et al. (2014b, 2015) suggests that including these high-aerosol scenes does not affect the accuracy of NO_2 retrieval.

删除的内容: but

删除的内容: the drawback is that

删除的内容: ing

删除的内容: although

2.4 MAX-DOAS data

We use MAX-DOAS measurements at three suburban or urban sites in East China, including one urban site at the Institute of Atmospheric Physics (IAP) in Beijing (116.38° E, 39.38° N), one suburban site in Xianghe County (116.96° E, 39.75° N) to the south of Beijing, and one urban site in the Wuxi City (120.31° E, 31.57° N) in the Yangzi River delta (YRD). Figure 1 shows the locations of these sites overlaid with POMINO v1.1 NO_2 VCDs in August 2012. Table 1 summarizes the information of MAX-DOAS measurements.

删除的内容: 2

删除的内容: 2

The instruments in IAP and in Xianghe were designed at BIRA-IASB (Clémer et al., 2010). Such an instrument is a dual-channel system composed of two thermally regulated grating spectrometers, covering the ultraviolet (300–390 nm) and visible (400–720 nm) wavelengths. It measures scattered sunlight every 15 minutes at nine elevation angles: 2°, 4°, 6°, 8°, 10°, 12°, 15°, 30°, and 90°. The telescope of the instrument is pointed to the north. The data are analyzed following

Hendrick et al. (2014). The Xianghe suburban site is influenced by pollution from the surrounding major cities like Beijing and Tianjin. At Xianghe, MAX-DOAS data are data are continuously available since early 2011, and data in 2012 are used here for comparison with OMI products. At IAP, MAX-DOAS data are available in 2008 and 2009 (Table 1), thus for comparison purposes we process OMI products to match the MAX-DOAS times.

删除的内容: 2

Located on the roof of an 11-story building, the instrument at Wuxi was developed by Anhui Institute of Optics and Fine Mechanics (AIOFM) (Wang et al., 2015, 2017a). Its telescope is pointed to the north and records at five elevation angles (5°, 10°, 20°, 30° and 90°). Wuxi is a typical urban site affected by heavy NO_x and aerosol pollution. The measurements used here are analyzed in Wang et al. (2017a). Data are available in 2012 for comparison with OMI products.

When comparing the four OMI products against MAX-DOAS observations, temporal and spatial inconsistency in sampling is inevitable. The spatial inconsistency, together with the substantial horizontal inhomogeneity in NO_2, might be more important than the influence of temporal inconsistency (Wang et al., 2017b). The influence of the horizontal inhomogeneity was suggested to be about 10–30% for MAX-DOAS measurements in Beijing (Lin et al., 2014b; Ma et al., 2013) and 10–15% for less polluted locations like Tai'an, Mangshan and Rudong (Irie et al., 2012). Following previous studies (Lin et al., 2014b; Wang et al., 2015, 2017b), we average MAX-DOAS data within 2 h of the OMI overpass time, and we select OMI pixels within 25 km of a MAX-DOAS site whose viewing zenith angle is below 30°. To exclude local pollution events near the MAX-DOAS site (such as the abrupt increase of NO_2 caused by the pass of consequent vehicles during a very short period), the standard deviation of MAX-DOAS data within 2 h should not exceed 20% of their

删除的内容: three

mean value (Lin et al., 2014b). We elect not to spatially average the OMI pixels because they can, to some degree, reflect the spatial variability in NO_2 and aerosols.

We further exclude MAX-DOAS data in cloudy conditions, as clouds can cause large uncertainties in MAX-DOAS and OMI data. To find the actual cloudy days, we use MODIS/Aqua cloud fraction data, MODIS/Aqua Level-3 corrected reflectance (true color) data at the 1^0 x 1^0 resolution, and current weather data observed from the nearest ground meteorological station (indicated by the black triangles in Fig. 1b). Since there is only one meteorological station available near the Beijing area, it is used for both IAP and Xianghe MAX-DOAS sites. We first use MODIS/Aqua corrected reflectance (true color) to distinguish clouds from haze. For cloudy days determined by the reflectance checking, we examine both the MODIS/Aqua cloud fraction data and the meteorological station cloud records, considering that MODIS/Aqua cloud fraction data may be missing or have a too coarse horizontal resolution to accurately interpret the cloud conditions at the MAX-DOAS site. We exclude MAX-DOAS NO_2 data if the MODIS/Aqua cloud fraction is larger than 60% and the meteorological station reports a “BROKEN” (cloud fraction ranges from 5/8 to 7/8) or “OVERCAST” (full cloud cover) sky. For the three MAX-DOAS sites together, this leads to 49 days with valid data out of 64 days with pre-screening data.

We note here that using cloud fraction data from MODIS/Aqua or MAX-DOAS (for Xianghe only, see Gielen et al., 2014) alone to screen cloudy scenes may not be appropriate on heavy-haze days. For example, on 8th January, 2012, MODIS/Aqua cloud fraction is about 70–80% over the North China Plain and MAX-DOAS at Xianghe suggests the presence of “thick clouds”. However, both the meteorological station and MODIS/Aqua corrected reflectance (true color) product suggest that the North China Plain was covered by a thick layer of haze. Consequently, this day was excluded from the analysis.

删除的内容： to some degree

删除的内容: 2

3. Monthly climatology of aerosol extinction profiles from CALIOP and GEOS-Chem

3.1 CALIOP monthly climatology

The aerosol layer height (ALH) is a good indicator to what extent aerosols are mixed vertically (Castellanos et al., 2015). As defined in Eq. A1 in Appendix B, the ALH is the average height of aerosols weighted by vertically resolved aerosol extinction. Figure 2a shows the spatial distribution of our CALIOP ALH climatology in each season. At most places, the ALH reaches a maximum in spring or summer and a minimum in fall or winter. The lowest ALH in fall and winter can be attributed to heavy near-surface pollution and weak vertical transport. The high values in summer are related to strong convective activities. Over the north, the high values in spring are partly associated with Asian dust events, due to high surface winds and dry soil in this season (Huang et al., 2010; Proestakis et al., 2017; Wang et al., 2010), which also affects the oceanic regions via atmospheric transport. The springtime high ALH over the south may be related to the transport of carbonaceous aerosols from Southeast Asian biomass burning (Jethva et al., 2016). Averaged over the domain, the seasonal mean ALHs are 1.48 km, 1.43 km, 1.27km, 1.18 km in spring, summer, fall and winter.

删除的内容: 3

Figure 3a,b further shows the climatological monthly variations of ALH averaged over Northern East China (the anthropogenic source region shown in orange in Fig. 1a) and Northwest China (the dust source region shown in yellow in Fig. 1a). The two regions exhibit distinctive temporal variations. Over Northern East China, the ALH reaches a maximum in April (~1.53 km) and a minimum in December (~1.14 km). Over Northwest China, the ALH peaks in August (~1.59km) because of strongest convection (Zhu et al., 2013), although the springtime ALH is also high.

删除的内容: 4

删除的内容: 2

删除的内容: 2

Figure 4a shows the climatological seasonal regional average vertical profiles of aerosol extinction over Northern East China. Here, the aerosol extinction increases from the ground level to a peak at about 300–600 m (season dependent), above which it decreases gradually. The height of peak extinction is lowest in winter, consistent with a stagnant atmosphere, thin mixing layer, and increased emissions (from residential and industrial sectors). The large error bars (horizontal lines in different layers, standing for 1 standard deviation) indicate strong spatiotemporal variability of aerosol extinction.

Over Northwest China (Fig. 5a), the column total aerosol extinction is much smaller than that over Northern East China (Fig. 4a), due to lower anthropogenic sources and dominant natural dust emissions. Vertically, the decline of extinction from the peak-extinction height to 2 km is also much more gradual than the decline over Northern East China, indicating stronger lifting of surface emitted aerosols. In winter, the column total aerosol extinction is close to the high value in dusty spring, whereas the vertical gradient of extinction is strongest among the seasons. This reflects the high anthropogenic emissions in parts of Northwest China, which have been rapidly increasing in the 2000s due to relatively weak emission control supplemented by growing activities of relocation of polluted industries from the eastern coastal regions (Cui et al., 2016; Zhao et al., 2015).

Overall, the spatial and seasonal variations of CALIOP aerosol vertical profiles are consistent with changes in meteorological conditions, anthropogenic sources, and natural emissions. The data will be used to evaluate and adjust GEOS-Chem simulation results in Sect. 3.2. A comparison of our CALIOP dataset with NASA's official Level-3 data is presented in Appendix C.

3.2 Evaluation of GEOS-Chem aerosol extinction profiles

删除的内容: 5

删除的内容: 6

删除的内容: 5

删除的内容: 3

删除的内容: C

删除的内容: *3.2 Comparison to NASA CALIOP monthly climatology*
We compare our gridded climatological profiles to NASA CALIOP Version 3 Level-3 all-sky monthly profiles at 532 nm (Winker et al. 2013). The NASA Level-3 data has a horizontal resolution of 2° lat. × 5° lon. and a vertical resolution of 60 m (from -0.5 to 12 km above sea level). We combine NASA monthly data over 2007–2015 to construct a monthly climatology for comparison with our own compilation. We only choose aerosol extinction data in the troposphere with error less than 0.15 (the valid range given in the CALIOP dataset). If the number of valid monthly profiles in a grid cell is less than five (i.e., for the same month in five out of the nine years), then we exclude data in that grid cell; see the dark gray grid cells in Fig. 23c.
Several methodological differences exist between generating our and NASA CALIOP datasets. First, the two datasets have different horizontal resolutions. Also, we sample all valid CALIOP pixels within 1.5° of a grid cell center, whereas the NASA dataset samples all valid pixels within a grid cell. Besides, our CALIOP dataset involves several steps of horizontal interpolation, for purposes of subsequent cloud and NO_2 retrievals, which is not done in the NASA dataset. In addition, we match CALIOP data vertically to the GEOS-Chem vertical resolution, whereas the NASA dataset maintains the original resolution.
... [4]

删除的内容: *3*

Figure 2b shows the spatial distribution of seasonal ALHs simulated by GEOS-Chem. The model captures the spatial and seasonal variations of CALIOP ALH (Fig. 2a) to some degree, with an underestimate by about 0.3 km on average. The spatial correlation between CALIOP (Fig. 2a) and GEOS-Chem (Fig. 2b) ALH is 0.37 in spring, 0.57 in summer, 0.40 in fall, and 0.44 in winter. The spatiotemporal consistency and underestimate is also clear from the regional mean monthly ALH data in Fig. 3 – the temporal correlation between GEOS-Chem and CALIOP ALH is 0.90 in Northern East China and 0.97 in Northwest China.

Figures 4a and 5a show the GEOS-Chem simulated 2007–2015 monthly climatological vertical profiles of aerosol extinction coefficient over Northern East China and Northwest China, respectively. Over Northern East China (Fig. 4a), the model (red line) captures the vertical distribution of CALIOP extinction (black line) below the height of 1 km, despite a slight underestimate in the magnitude of extinction and an overestimate in the peak-extinction height. From 1 to 5 km above the ground, the model substantially overestimates the rate of decline in extinction coefficient with increasing altitude. Across the seasons, GEOS-Chem underestimates the magnitude of aerosol extinction by up to 37% (depending on the height). Over Northwest China (Fig. 5a), GEOS-Chem has an underestimate in all seasons, with the largest bias by about 80% in winter likely due to underestimated water-soluble aerosols and dust emissions (Li et al., 2016; Wang et al., 2008a).

Since the POMINO v1.1 algorithm uses MODIS AOD to adjust model AOD, it only uses the CALIOP aerosol extinction profile shape to adjust the modeled shape (Eqs. 1 and 2). Figures 4b and 4b show the vertical shapes of aerosol extinction, averaged across all profiles in each season over Northern East China and Northwest China, respectively. Over Northern East China (Fig. 4b), GEOS-Chem underestimates the CALIOP values above 1 km by 52–71%. This underestimate leads to a lower ALH,

删除的内容: 3
删除的内容: 3
删除的内容: 3
删除的内容: 3
删除的内容: 4
删除的内容: 5
删除的内容: 6
删除的内容: 5
删除的内容: 6
删除的内容: 2
删除的内容: 3
删除的内容: 5
删除的内容: 6
删除的内容: 5

consistent with the finding by van Donkelaar et al. (2013) and Lin et al. (2014b). Over Northwest China (Fig. 5b), the model also underestimates the CALIOP values above 1 km by 50–62%. These results imply the importance of correcting the modeled aerosol vertical shape prior to cloud and NO_2 retrievals.

删除的内容: 6

4. Effects of aerosol vertical profile improvement on cloud retrieval in 2012

Figure 6a, b shows the monthly average ALH and cloud top height (CTH, corresponding to cloud pressure, CP) over Northern East China and Northwest China in 2012. In order to discuss the CTH, only cloudy days are analyzed here, by excluding days with zero cloud fraction (CF = 0, clear-sky cases) in POMINO. Although "clear sky" is used sometimes in the literature to represent low cloud coverage (e.g., CF < 0.2 or CRF < 0.5, Boersma et al., 2011; Chimot et al., 2016), here it strictly means CF = 0 while "cloudy sky" means CF > 0. About 62.7% of days contain non-zero fractions of clouds over Northern East China, and the number is 59.1% for Northwest China. The CF changes from POMINO to POMINO v1.1 (i.e., after aerosol vertical profile adjustment) are negligible (within ±0.5%, not shown) due to the same values of AOD and SSA used in both products. This is because overall CF is mostly driven by the continuum reflectance at 475 nm (mainly determined by AOD and surface reflectance, which remain unchanged), which is independent of aerosol profile but CTH is driven by the O_2-O_2 SCD, which is itself impacted by ALH.

删除的内容: 7

Figure 6a, b shows that over the two regions, the CTH varies notably from one month to another, whereas the ALH is much more stable across the months. Over Northern East China, the ALH increases by 0.52 km from POMINO (orange dashed line) to POMINO v1.1 (orange solid line) due to the CALIOP-based monthly climatological adjustment. The increase in ALH means a stronger "shielding" effect of aerosols on the O_2-O_2 absorbing dimer, which, in turn, results in a reduced CTH by 0.69 km on average. For POMINO over Northern East China (Fig. 6a), the retrieved clouds

删除的内容: 7

删除的内容: 7

usually extend above the aerosol layer, i.e., the CTH (grey dashed line) is much larger than the ALH (orange dashed line). Using the CALIOP climatology in POMINO v1.1 results in the ALH higher than the CTH in fall and winter. The more elevated ALH is consistent with the finding of Jethva et al. (2016) that a significant amount of absorbing aerosols resides above clouds over Northern East China based on 11-year (2004–2015) OMI near-UV observations.

The CTH in Northwest China is much lower than in Northern East China (Fig. 6a versus 7b). This is because the dominant type of actual clouds is (optically thin) cirrus over western China (Wang et al., 2014), which is interpreted by the O_2-O_2 cloud retrieval algorithm as reduced CTH (with cloud base from the ground). The reduction in CTH from POMINO to POMINO v1.1 over Northwest China is also smaller than the reduction over Northern East China, albeit with a similar enhancement in ALH, due to lower aerosol loadings (Fig. 6c versus 6d).

Figure 7g,h presents the relative change in CP from POMINO to POMINO v1.1 as a function of AOD (binned at an interval of 0.1) and changes in ALH from POMINO to POMINO v1.1 (ΔALH, binned every 0.2 km) across all pixels in 2012 over Northern East China. Results are separated for low cloud fraction (CF < 0.05 in POMINO, Fig. 7g) and modest cloud fraction (0.2 < CF < 0.3, Fig. 7h). The median of the CP changes for pixels within each AOD and ΔALH bin is shown. Figure 7e,f presents the corresponding numbers of occurrence under the two cloud conditions.

Figure 7 shows that over Northern East China, the increase in ALH is typically within 0.6 km for the case of CF < 0.05 (Fig. 7e), and the corresponding increase in CP is within 6% (Fig. 7g). In this case, the average CTH (2.95 km in POMINO versus 1.58 km in POMINO v1.1) becomes much lower than the average ALH (1.06 km in POMINO versus 1.98 km in POMINO v1.1). For the case with CF between 0.2 and 0.3, the increase in ALH is within 1.2 km for most scenes (Fig. 7f), which leads to a

删除的内容: 7

删除的内容: 7

删除的内容: 7

删除的内容: 8

删除的内容: 8

删除的内容: 8

删除的内容: 8

删除的内容: 8

删除的内容: 8

删除的内容: 8

删除的内容: 8

CP change of 2% (Fig. 7h), much smaller than the CP change for CF < 0.05 (Fig. 7g). This is partly because the larger the CF is, the smaller a change in CF is required to compensate for the ΔALH in the O_2-O_2 cloud retrieval algorithm. Furthermore, with 0.2 < CF < 0.3, the mean value of CTH is much higher than ALH in both POMINO (2.76 km for CTH versus 1.13km for ALH) and POMINO v1.1 (2.60km for CTH versus 2.09 km for ALH), thus a large portion of clouds are above aerosols so that the change in CP is less sensitive to ΔALH. We find that the summertime data contribute the highest portion (36.5%) to the occurrences for 0.2 < CF < 0.3.

删除的内容: 8

删除的内容: 8

For Northwest China (not shown), the dependence of CP changes to AOD and ΔALH is similar to that for Northern East China. In particular, the CP change is within 10% on average for the case of CF < 0.05 and 1.5% for the case of 0.2 < CF < 0.3.

5. Effects of aerosol vertical profile improvement on NO_2 retrieval in 2012

Figure 7a presents the percentage changes in clear-sky NO_2 VCD from POMINO to POMINO v1.1 as a function of binned AOD and ΔALH over Northern East China. Here, clear-sky pixels are chosen based on CF = 0 in POMINO. In any AOD bin, an increase in ΔALH leads to an enhancement in NO_2. And for any ΔALH, the change in VCD is greater (smaller) when AOD becomes larger (smaller), which indicates that the NO_2 retrieval is more sensitive to ALH in high aerosol loading cases. Clearly, the change in NO_2 is not a linear function of AOD and ΔALH.

删除的内容: 8

For cloudy scenes (Fig. 7b,c, cloud data are based on POMINO), the change in NO_2 VCD is less sensitive to AOD and ΔALH. This is because the existence of clouds limits the optical effect of aerosols on tropospheric NO_2. Figure 6a presents the nitrogen layer height (NLH, defined as the average height of model simulated NO_2 weighted by its volume mixing ratio in each layer) in comparison to the ALH and CLH over Northern East China. The figure shows that the POMINO v1.1 CTH is

删除的内容: 8

删除的内容: 7

higher than the NLH in all months and higher than the ALH in warm months, which means a “shielding” effect on both NO_2 and aerosols.

Over Northwest China (not shown), the changes in clear-sky NO_2 VCD are within 9% for most cases, which are much smaller than over Eastern China (within 18%). This is because the NLH is much higher than the CLH and ALH (Fig. 6b) in absence of surface anthropogenic emissions.

删除的内容: 7

We convert the valid pixels into monthly mean Level-3 values datasets on a 0.25° long. × 0.25° lat. grid. Figure 8a,b compares the seasonal spatial variations of NO_2 VCD in POMINO v1.1 and POMINO in 2012. In both products, NO_2 peaks in winter due to the longest lifetime and highest anthropogenic emissions (Lin, 2012). NO_2 also reaches a maximum over Northern East China as a result of substantial anthropogenic sources. From POMINO to POMINO v1.1, the NO_2 VCD increases by 3.4% (-67.5–41.7%) in spring for the domain average (range), 3.0% (-59.5–34.4%) in summer, 4.6% (-15.3–39.6%) in fall and 5.3% (-68.4–49.3%) in winter. The NO_2 change is highly dependent on the location and season. The increase over Northern East China is largest in winter, wherein the positive value for ΔALH implies that elevated aerosol layers “shield” the NO_2 absorption.

删除的内容: 9

删除的内容: mean

删除的内容: that better

6. Evaluating satellite products using MAX-DOAS data

We use MAX-DOAS data, after cloud screening (Sect. 2.4), to evaluate DOMNO v2, QA4ECV, POMINO and POMINO v1.1. The scatterplots in Fig. 9a-d compare the NO_2 VCDs from 162 OMI pixels on 49 days with their MAX-DOAS counterparts. Different colors differentiate the seasons. The high values of NO_2 VCD (> 30 × 10^{15} molec. cm^{-2}) occur mainly in fall (blue) and winter (black). POMINO v1.1 and POMINO capture the day-to-day variability of MAX-DOAS data, i.e., R^2 = 0.804 and 0.799, respectively. The normalized mean bias (NMB) of POMINO v1.1 relative to

删除的内容: 10a-c

MAX-DOAS data (-3.4%) is smaller than the NMB of POMINO (-9.6%). Also, the reduced major axis (RMA) regression shows that the slope for POMINO v1.1 (0.95) is closer to unity than the slope for POMINO (0.78). When all OMI pixels in a day are averaged (Fig. 9e,f), the correlation across the total of 49 days further increase for both POMINO v1.1 (R^2 = 0.89) and POMINO (R^2 = 0.86), whereas POMINO v1.1 still has a lower NMB (-3.7%) and better slope (0.96) than POMINO (-10.4% and 0.82, respectively). These results suggest that correcting aerosol vertical profiles, at least on a climatology basis, already leads to a significant improved NO_2 retrieval from OMI.

Figure 9 shows that DOMINO v2 is correlated with MAX-DOAS (R^2 = 0.68 in Fig. 9c and 0.75 in Fig. 9g) but not as strong as POMINO and POMINO v1.1 for all days. The discrepancy between DOMINO v2 and MAX-DOAS is particularly large for very high NO_2 values (> 70 × 10^{15} molec. cm^{-2}). The R^2 for QA4ECV (0.75 in Fig. 9d and 0.82 in Fig. 9h) is slightly better than DOMINO, but the NMB is higher (-22.0% and -22.7%) and the slope drops to 0.66. These results are consistent with the finding of Lin et al. (2014b, 2015) that explicitly including aerosol optical effects improves the NO_2 retrieval.

Table 2 further shows the comparison statistics for 27 haze days. The haze days are determined when both the ground meteorological station data and MODIS/Aqua corrected reflectance (true color) data indicate a haze day. The table also lists AOD, SSA, CF and MAX-DOAS NO_2 VCD, as averaged over all haze days. A large amount of absorbing aerosols occurs on these haze days (AOD = 1.13, SSA = 0.90). The average MAX-DOAS NO_2 VCD reaches 51.92 × 10^{15} molec. cm^{-2}. Among the four satellite products, POMINO v1.1 has the highest R^2 (0.76) and the lowest bias (4.4%) with respect to MAX-DOAS, whereas DOMINO v2 and QA4ECV reproduce the variability to a limited extent (R^2 = 0.38 and 0.34, respectively). This is consistent

删除的内容: 11d,e
删除的内容:
批注 [FB3]: Please clarify if this is now for haze days, or all days.
删除的内容: 10c,f
删除的内容: 10
删除的内容: 45
删除的内容: 10
删除的内容: f
删除的内容: well
带格式的: 上标
删除的内容: much
删除的内容: 4
删除的内容: three
删除的内容: s

with the previous finding that the accuracy of DOMINO v2 is reduced for polluted, aerosol-loaded scenes (Boersma et al., 2011; Chimot et al., 2016; Kanaya et al., 2014; Lin et al., 2014b).

Table 3 shows the comparison statistics for 36 cloud-free days (CF = 0 in POMINO and AOD = 0.60 on average). Here, POMINO v1.1, POMINO and DONIMO v2 do not show large differences in R^2 (0.53–0.56) and NMB (20.8–29.4%) with respect to MAX-DOAS. QA4ECV has a higher R^2 (0.63) and a lower NMB (-5.83%), presumably reflecting the improvements in this community best practices approach, at least in mostly cloud-free situations. However, the R^2 values for POMINO and POMINO v1.1 are much smaller than the R^2 values in haze days, whereas the opposite changes are true for DOMINO v2 and QA4ECV. Thus, for this limited set of data, the changes from DOMINO v2 and QA4ECV to POMINO and POMINO v1.1 mainly reflect the improved aerosol treatment in hazy scenes. Further research may use additional MAX-DOAS datasets to evaluate the satellite products more systematically.

7. Conclusions

This paper improves upon our previous POMINO algorithm (Lin et al., 2015) to retrieve the tropospheric NO_2 VCDs from OMI, by compiling a 9-year (2007–2015) CALIOP monthly climatology of aerosol vertical extinction profiles to adjust GEOS-Chem aerosol profiles used in the NO_2 retrieval process. The improved algorithm is referred to as POMINO v1.1. Compared to monthly climatological CALIOP data over China, GEOS-Chem simulations tend to underestimate the aerosol extinction above 1 km, as characterized by an underestimate in ALH by 300–600 m (seasonal and location dependent). Such a bias is corrected in POMINO v1.1 by dividing, for any month and grid cell, the CALIOP monthly climatological profile by

删除的内容: c

带格式的: 段落间距段后: 10 磅, 图案: 清除

删除的内容: 5

删除的内容: the three OMI products

删除的内容: and NMB (20.8–29.4%)

带格式的: 字体: (中文) +中文正文 (宋体), 上标

删除的内容: that in the cloud-free cases the ensemble of algorithms improves the retrieval results

删除的内容: is

删除的内容: ↵

删除的内容: product

the model climatological profile to obtain a scaling profile and then applying the scaling profile to model data in all days of that month in all years.

The aerosol extinction profile correction leads to an insignificant change in CF from POMINO to POMINO v1.1, since the AOD and surface reflectance are unchanged. In contrast, the correction results in a notably increase in CP (i.e., a decrease in CTH), due to lifting of aerosol layers. The CP changes are generally within 6% for scenes with low cloud fraction (CF < 0.05 in POMINO), and within 2% for scenes with modest cloud fraction (0.2 < CF < 0.3 in POMINO).

The NO_2 VCDs increase from POMINO to POMINO v1.1 in most cases due to lifting of aerosol layers that enhances the "shielding" of NO_2 absorption. The NO_2 VCD increases by 3.4% (-67.5–41.7%) in spring for the domain average (range), 3.0% (-59.5–34.4%) in summer, 4.6% (-15.3–39.6%) in fall and 5.3% (-68.4–49.3%) in winter. The NO_2 changes highly season and location dependent, and are most significant for wintertime Northern East China.

Further comparisons with independent MAX-DOAS NO_2 VCD data for 162 OMI pixels in 49 days show good performance of both POMINO v1.1 and POMINO in capturing the day-to-day variation of NO_2 (R^2=0.80, n=162), compared to DOMINO v2 (R^2=0.67) and the new QA4ECV product (R^2=0.75). The NMB is smaller in POMINO v1.1 (-3.4%) than in POMINO (-9.6%), with a slightly better slope (0.804 versus 0.784). On hazy days with high aerosol loadings (AOD = 1.13 on average), POMINO v1.1 has the highest R^2 (0.76) and the lowest bias (4.4%) whereas DOMINO and QA4ECV have difficulty in reproducing the day-to-day variability in MAX-DOAS NO_2 measurements (R^2 = 0.38 and 0.34, respectively). The four products show small differences in R^2 on clear-sky days (CF = 0 in POMINO, AOD = 0.60 on average). Thus the explicit aerosol treatment (in POMINO and POMINO v1.1)

删除的内容: or
删除的内容: has
删除的内容: ,
删除的内容: three
删除的内容: and NMB

and the aerosol vertical profile correction (in POMINO v1.1) improves the NO_2 retrieval especially in hazy cases.

The POMINO v1.1 algorithm is a core step towards our next public release of data product, POMINO v2. This new release will contain a few additional updates, including but not limited to using MODIS Collection 6 Merged 10-km Level-2 AOD data that combine the Dark Target (Levy et al., 2013) and Deep Blue (Sayer et al., 2014) products, as well as MODIS MCD43C2 Collection 6 daily BRDF data. Meanwhile, the POMINO algorithm framework is being applied to the recently launched TropOMI instrument that provides NO_2 information at a much higher spatial resolution (3.5 x 7 km^2). A modified algorithm can also be used to retrieve sulfur dioxide, formaldehyde and other trace gases from TropOMI, for which purposes our algorithm will be available to the community on a collaborative basis. Future research can correct the SSA and NO_2 vertical profile to further improve the retrieval algorithm, and can use more comprehensive independent data to evaluate the resulting satellite products.

Acknowledgements

This research is supported by the National Natural Science Foundation of China (41775115), the 973 program (2014CB441303), the Chinese Scholarship Council, and the EU FP7 QA4ECV project (grant no. 607405).

Appendix A: Introduction to the QA4ECV product

The QA4ECV NO_2 product (http://www.qa4ecv.eu/) builds on a (EU-) consortium best practices approach to retrieve NO_2 from GOME, SCIAMACHY, GOME-2, and OMI. The main contributions are provided by BIRA-IASB, the University of Bremen (IUP), MPIC, KNMI, and Wageningen University. Uncertainties in spectral fitting for NO_2 SCDs and in AMF calculations were evaluated by Zara et al. (2018) and Lorente

- 删除的内容:
- 删除的内容: KFB: I think a sentence on the relatively good performance of QA4ECV in non-hazy days would be useful. Your paper adds value to the literature by being one of the first to do a systematic validation of the QA4ECV product! You have already some good indications when the algorithm does fine, and under which circumstances it is biased. This should be highlighted.
- 删除的内容: (Levy et al., 2013)
- 批注 [JL4]: citation
- 删除的内容: (Sayer et al., 2013)
- 删除的内容: Our POMINO v1.1
- 删除的内容:
- 带格式的
- 带格式的: 标题 1，左，段落间距段后：0 磅，图案：清除
- 删除的内容: **The**
- 删除的内容: **i**
- 带格式的
- 带格式的
- 带格式的: 字体：非加粗
- 删除的内容: EU FP7-project Quality Assurance for Essential ... [5]
- 删除的内容:)
- 删除的内容: is aim at making rapid judgments on validitiy and ... [6]
- 删除的内容: is
- 带格式的: 字体：非加粗
- 带格式的: 下标
- 删除的内容: a kind of
- 删除的内容: essentially an ensemble data sets of satellite products ... [7]
- 删除的内容: and
- 删除的内容: , with a fully traceable quality assurance on all aspects ... [8]
- 带格式的: 下标
- 删除的内容: The u
- 删除的内容: of
- 删除的内容: algorithms
- 删除的内容: the
- 带格式的: 下标
- 删除的内容: ,

et al. (2017), respectively. QA4ECV contains improved SCD NO_2 data (Zara et al., 2018). Lorente et al., (2017) showed that across the above algorithms, there a structural uncertainty by 42% in the NO_2 AMF calculation over polluted areas. By comparing to our POMINO product, Lorente et al. also showed that the choice of aerosol correction may introduce an additional uncertainty by up to 50% for situations with high polluted cases, consistent with Lin et al. (2014b, 2015) and the findings here. For a complete description of the QA4ECV algorithm improvements, and quality assurance, please see Boersma et al. (2018).

Appendix B: Constructing the CALIOP monthly climatology of aerosol extinction vertical profile

Our use the all-sky Level-2 CALIOP data to construct the Level-3 monthly climatology. We choose the all-sky product instead of clear-sky data, since previous studies indicate that the climatological aerosol extinction profiles are affected insignificantly by the presence of clouds (Koffi et al., 2012; Winker et al., 2013). As we use this climatological data to adjust GEOS-Chem results, choosing all-sky data improves consistency with the model simulation when doing the daily correction.

To select valid pixels, we follow the data quality criteria by Winker et al., (2013) and Amiridis et al., (2015). Only the pixels with Cloud Aerosol Discrimination (CAD) scores between -20 and -100 with extinction Quality Control (QC) flag valued at 0, 1, 18, and 16 are selected. We further discard samples with an extinction uncertainty of 99.9 km^{-1}, which is indicative of unreliable retrieval. We only accept extinction values falling in the range from 0.0 to 1.25, according to CALIOP observation thresholds. Previous studies showed that weakly scattering edges of icy clouds are sometimes misclassified as aerosols (Winker et al., 2013). To eliminate contamination from icy clouds we exclude the aerosol layers above the cloud layer (with layer-top temperature below 0 ℃) when both of them are above 4km (Winker et al., 2013).

删除的内容: ,
删除的内容: The improved
删除的内容: NO_2
带格式的: 下标
删除的内容: shows better performance in
删除的内容: but do not altogether eliminated systematic errors in ththee fitting approach
删除的内容: 42%
删除的内容: of
带格式的: 下标
删除的内容: s
删除的内容: aereas
删除的内容: , and
删除的内容: s
删除的内容: average
删除的内容: of
批注 [JL5]: Revise the format of the reference list
带格式的: 荷兰语
删除的内容: ↵
带格式的
删除的内容: **The way to c**
带格式的
带格式的
删除的内容: **mean**
带格式的
带格式的
带格式的
删除的内容: **climatology**
带格式的: 字体: 非加粗
已移动(插入) [5]
删除的内容: The way to select the good quality profile mainly
删除的内容: s
已移动(插入) [1]

After the pixel-based screening, we aggregate the CALIOP data at the model grid (0.667° long. x 0.5° lat.) and vertical resolution (47 layers, with 36 layers or so in the troposphere). For each grid cell, we choose the CALIOP pixels within 1.5° of the grid cell center. CALIOP Level-2 data are always presented at the fixed 399 altitudes above sea level. To account for the difference in surface elevation between a CALIOP pixel and the respective model grid cell, we convert the altitude of the pixel to a height above the ground, by using the surface elevation data provided in CALIOP. We then average horizontally and vertically the profiles of all pixels within one model grid cell and layer. We do the regridding day-by-day for all grid cells to ensure that GEOS-Chem and CALIOP extinction profiles are coincident spatially and temporally. Finally, we compile a monthly climatological dataset by averaging over 2007–2015.

已移动(插入) [2]

Figure A1 shows the number of aerosol extinction profiles in each grid cell and 12 x 9 = 108 months that are used to compile the CALIOP climatology, both before and after data screening. Table A1 presents additional information on monthly and yearly bases. On average, there are 165 and 47 aerosol extinction profiles per month per grid cell before and after screening, respectively. In the final 9-year monthly climatology, each grid cell has about 420 aerosol extinction profiles on average, about 28% of the prior-screening profiles. Figure A1 shows that the number of valid profiles decreases sharply over the Tibet Plateau and at higher latitudes (> 43 ° N) due to complex terrain and icy/snowy ground.

删除的内容:

已移动(插入) [3]

As discussed above, we choose the CALIOP pixels within 1.5° of a grid cell center. We test this choice by examining the aerosol layer height (ALH) produced for that grid cell. The ALH is defined as the extinction-weighted height of aerosols (see Eq. A1, where *n* denotes the number of tropospheric layers, ε_i the aerosol extinction at layer *i*, and H_i the layer center height above the ground). We find that choosing pixels within 1.0° of a grid cell center leads to a nosier horizontal distribution of

ALH, owing to the small footprint of CALIOP. On the other hand, choosing 2.0° leads to a too smooth spatial gradient of ALH with local characteristics of aerosol vertical distributions are largely lost. We thus decide that 1.5° is a good balance between noise and smoothness.

$$ALH = \frac{\sum_{i=1}^{i=n} \varepsilon_i H_i}{\sum_{i=1}^{i=n} \varepsilon_i} \qquad (A1)$$

Certain grid cells do not contain sufficient valid observations for some months of the climatological dataset. We fill in missing monthly values of a grid cell using valid data in the surrounding 5 x 5 = 25 grid cells (within ~ 100 km). If the 25 grid cells do not have enough valid data, we use those in the surrounding 7 x 7 = 49 grid cells (within ~ 150 km). A similar procedure is used by Lin et al. (2014b, 2015) to fill in missing values in the gridded MODIS AOD dataset.

For each grid cell in each month, we further correct singular values in the vertical profile. In a month, if a grid cell *i* has an ALH outside mean±1σ of its surrounding 25 or 49 grid cells, we select *i*'s surrounding grid cell *j* whose ALH is the median of *i*'s surrounding grid cells, and use *j*'s profile to replace *i*'s. Whether 25 or 49 surrounding grid cells are chosen depends on the number of valid pixels shown in Fig. A1b. If the number of valid pixels in *i* is below mean–1σ of all grid cells in the whole domain, which is often the case for Tibetan grid cells, we use *i*'s surrounding 49 grid cells; otherwise we use *i*'s surrounding 25 grid cells.

删除的内容: Certain grid cells do not contain sufficient valid observations for some months of the climatological data set. We fill in missing monthly values of a grid cell using valid data in the surrounding 25 or 49 grid cells.

已移动(插入) [4]

带格式的: 字体: 非加粗

带格式的: 字体: 非加粗

Appendix C. Comparing our and NASA's CALIOP monthly climatology

带格式的: 标题 1

We compare our gridded climatological profiles to NASA CALIOP Version 3 Level-3 all-sky monthly profiles at 532 nm (Winker et al., 2013). The NASA Level-3 data has a horizontal resolution of 2° lat. × 5° lon. and a vertical resolution of 60 m (from -0.5 to 12 km above sea level). We combine NASA monthly data over 2007–

2015 to construct a monthly climatology for comparison with our own compilation. We only choose aerosol extinction data in the troposphere with error less than 0.15 (the valid range given in the CALIOP dataset). If the number of valid monthly profiles in a grid cell is less than five (i.e., for the same month in five out of the nine years), then we exclude data in that grid cell; see the dark gray grid cells in Fig. 2c.

Several methodological differences exist between generating our and NASA CALIOP datasets. First, the two datasets have different horizontal resolutions. Also, we sample all valid CALIOP pixels within 1.5^0 of a grid cell center, whereas the NASA dataset samples all valid pixels within a grid cell. Besides, our CALIOP dataset involves several steps of horizontal interpolation, for purposes of subsequent cloud and NO_2 retrievals, which is not done in the NASA dataset. In addition, we match CALIOP data vertically to the GEOS-Chem vertical resolution, whereas the NASA dataset maintains the original resolution.

Figure 2c shows the spatial distribution of ALH in all seasons based on NASA CALIOP Level-3 all-sky monthly climatology. The horizontal resolution of NASA data is much coarser than ours; and NASA data are largely missing over the southwest with complex terrains. We choose to focus on the comparison over East China (the black box in Fig. 1a). Over East China, the two climatology datasets generally exhibit similar spatial patterns of ALH in all seasons (Fig. 2a, c). The NASA dataset suggests higher ALHs than ours over Eastern China, especially in summer, due mainly to differences in the sampling and regridding processes. Figure 3c further compares the monthly variation of ALH between our (black line with error bars) and NASA (blue filled triangles) datasets averaged over East China. The two datasets are consistent in almost all months, indicating that their regional differences are largely smoothed out by spatial averaging.

References

带格式的：图案：清除

带格式的：字体：非加粗

删除的内容: **Appendix C: The introduction to new version of POMINO product**

In our new relased version, several aspect will be update:

1) Use 9-year CALIOP climatology aerosol extinction profile to adjust GEOS-Chem daily aerosol extinction profiles. This is the main update in our new released version, which will also be applied to the retrieval algorithm of newly laughed TropOMI sensor.

2) MODIS Collection 6 Merged 10-km Level-2 AOD product will be used to replace the MODIS Collection 5 Dark Target (DT) product to adjust model simulation. Previous studies has shown various contextual biases exist in C5 version (Levy et al., 2010; Bréon et al., 2011). The C6 product update**s the widely used DT (Levy et al., 2013) and Deep Blue (DB) product (Sayer et al., 2013). It also relased the merged AOD product to provide a more gap-filled data set based on DT, DB and MODIS-derived climatologies of NDVI (Huete et al., 2011).**

3) MODIS MCD43C2 Collection 6 daily BRDF/Albedo Snow-free Model Parameters Daily L3 Global 0.05Deg data set is used to replace C5 8-day averaged data set to account for the daily BRDF effect of surface. There is improved quality and more retrieval at high latitudes and use current day snow status when retrieval in C6.

带格式的

Acarreta, J. R., De Haan, J. F. and Stammes, P.: Cloud pressure retrieval using the O_2-O_2 absorption band at 477 nm, J. Geophys. Res., 109(D5), D05204, doi:10.1029/2003JD003915, 2004.

Amiridis, V., Marinou, E., Tsekeri, A., Wandinger, U., Schwarz, A., Giannakaki, E., Mamouri, R., Kokkalis, P., Binietoglou, I., Solomos, S., Herekakis, T., Kazadzis, S., Gerasopoulos, E., Proestakis, E., Kottas, M., Balis, D., Papayannis, A., Kontoes, C., Kourtidis, K., Papagiannopoulos, N., Mona, L., Pappalardo, G., Le Rille, O. and Ansmann, A.: LIVAS: a 3-D multi-wavelength aerosol/cloud database based on CALIPSO and EARLINET, Atmos. Chem. Phys., 15(13), 7127–7153, doi:10.5194/acp-15-7127-2015, 2015.

Belmonte Rivas, M., Veefkind, P., Boersma, F., Levelt, P., Eskes, H. and Gille, J.: Intercomparison of daytime stratospheric NO_2 satellite retrievals and model simulations, Atmos. Meas. Tech., 7(7), 2203–2225, doi:10.5194/amt-7-2203-2014, 2014.

Boersma, K. F., Eskes, H. J. and Brinksma, E. J.: Error analysis for tropospheric NO_2 retrieval from space, J. Geophys. Res. Atmos., 109(D4), n/a-n/a, doi:10.1029/2003JD003962, 2004.

Boersma, K. F., Eskes, H. J., Veefkind, J. P., Brinksma, E. J., van der A, R. J., Sneep, M., van den Oord, G. H. J., Levelt, P. F., Stammes, P., Gleason, J. F. and Bucsela, E. J.: Near-real time retrieval of tropospheric NO_2 from OMI, Atmos. Chem. Phys., 7(8), 2103–2118, doi:10.5194/acp-7-2103-2007, 2007.

Boersma, K. F., Eskes, H. J., Dirksen, R. J., van der A, R. J., Veefkind, J. P., Stammes, P., Huijnen, V., Kleipool, Q. L., Sneep, M., Claas, J., Leitão, J., Richter, A., Zhou, Y. and Brunner, D.: An improved tropospheric NO_2 column retrieval algorithm for the

带格式的: 两端对齐

删除的内容: <sub>

删除的内容: </sub&gt

删除的内容: <sub>

删除的内容: </sub&gt

删除的内容: <sub>

删除的内容: </sub&gt

Ozone Monitoring Instrument, Atmos. Meas. Tech., 4(9), 1905–1928, doi:10.5194/amt-4-1905-2011, 2011a.

Boersma, K.F., Eskes, H. J., Richter, A., De Smedt, I., Lorente, A., Beirle, S., van Geffen, J. H. G. M., Zara, M., Peters, E., Van Roozendael, M., Wagner, T., Maasakkers, J. D., van der A, R. J., Nightingale, J., De Rudder, A., Irie, H., and Pinardi, G.: Improving algorithms and uncertainty estimates for satellite NO_2 retrievals: Results from the Quality Assurance for Essential Climate Variables (QA4ECV) project, amt-2018-200, submitted, 2018.

Bucsela, E. J., Celarier, E. A., Wenig, M. O., Gleason, J. F., Veefkind, J. P., Boersma, K. F. and Brinksma, E. J.: Algorithm for NO2 vertical column retrieval from the ozone monitoring instrument, IEEE Trans. Geosci. Remote Sens., 44(5), 1245–1258, doi:10.1109/TGRS.2005.863715, 2006.

Bucsela, E. J., Krotkov, N. A., Celarier, E. A., Lamsal, L. N., Swartz, W. H., Bhartia, P. K., Boersma, K. F., Veefkind, J. P., Gleason, J. F. and Pickering, K. E.: A new stratospheric and tropospheric NO2; retrieval algorithm for nadir-viewing satellite instruments: applications to OMI, Atmos. Meas. Tech., 6(10), 2607–2626, doi:10.5194/amt-6-2607-2013, 2013.

Castellanos, P., Boersma, K. F. and van der Werf, G. R.: Satellite observations indicate substantial spatiotemporal variability in biomass burning NOx; emission factors for South America, Atmos. Chem. Phys., 14(8), 3929–3943, doi:10.5194/acp-14-3929-2014, 2014.

Castellanos, P., Boersma, K. F., Torres, O. and de Haan, J. F.: OMI tropospheric NO2; air mass factors over South America: effects of biomass burning aerosols, Atmos. Meas. Tech., 8(9), 3831–3849, doi:10.5194/amt-8-3831-2015, 2015.

删除的内容: Boersma, K. F., Eskes, H. J., Dirksen, R. J., van der A, R. J., Veefkind, J. P., Stammes, P., Huijnen, V., Kleipool, Q. L., Sneep, M., Claas, J., Leitão, J., Richter, A., Zhou, Y. and Brunner, D.: An improved tropospheric NO₂ column retrieval algorithm for the Ozone Monitoring Instrument, Atmos. Meas. Tech., 4(9), 1905–1928, doi:10.5194/amt-4-1905-2011, 2011b. KFB: cited twice.
Boersma, K. F., Eskes, H. J., Dirksen, R. J., van der A, R. J., Veefkind, J. P., Stammes, P., Huijnen, V., Kleipool, Q. L., Sneep, M., Claas, J., Leitão, J., Richter, A., Zhou, Y. and Brunner, D.: An improved tropospheric NO₂ column retrieval algorithm for the Ozone Monitoring Instrument, Atmos. Meas. Tech., 4(9), 1905–1928, doi:10.5194/amt-4-1905-2011, 2011c. Cited thrice.

删除的内容: /sub

删除的内容: /

删除的内容: <sub>

删除的内容: </sub&gt

删除的内容: <sub>

删除的内容: </sub&gt

删除的内容: <sub>

删除的内容: </sub&gt

Chazette, P., Raut, J.-C., Dulac, F., Berthier, S., Kim, S.-W., Royer, P., Sanak, J., Loaëc, S. and Grigaut-Desbrosses, H.: Simultaneous observations of lower tropospheric continental aerosols with a ground-based, an airborne, and the spaceborne CALIOP lidar system, J. Geophys. Res., 115(D4), D00H31, doi:10.1029/2009JD012341, 2010.

Chimot, J., Vlemmix, T., Veefkind, J. P., de Haan, J. F. and Levelt, P. F.: Impact of aerosols on the OMI tropospheric NO2 retrievals over industrialized regions: how accurate is the aerosol correction of cloud-free scenes via a simple cloud model?, Atmos. Meas. Tech., 9(2), 359–382, doi:10.5194/amt-9-359-2016, 2016.

Clémer, K., Van Roozendael, M., Fayt, C., Hendrick, F., Hermans, C., Pinardi, G., Spurr, R., Wang, P. and De Mazière, M.: Multiple wavelength retrieval of tropospheric aerosol optical properties from MAXDOAS measurements in Beijing, Atmos. Meas. Tech., 3(4), 863–878, doi:10.5194/amt-3-863-2010, 2010.

Cui, Y., Lin, J., Song, C., Liu, M., Yan, Y., Xu, Y. and Huang, B.: Rapid growth in nitrogen dioxide pollution over Western China, 2005–2013, Atmos. Chem. Phys., 16(10), 6207–6221, doi:10.5194/acp-16-6207-2016, 2016.

Dirksen, R. J., Boersma, K. F., Eskes, H. J., Ionov, D. V., Bucsela, E. J., Levelt, P. F. and Kelder, H. M.: Evaluation of stratospheric NO_2 retrieved from the Ozone Monitoring Instrument: Intercomparison, diurnal cycle, and trending, J. Geophys. Res., 116(D8), D08305, doi:10.1029/2010JD014943, 2011.

van Geffen, J. H. G. M., Boersma, K. F., Van Roozendael, M., Hendrick, F., Mahieu, E., De Smedt, I., Sneep, M. and Veefkind, J. P.: Improved spectral fitting of nitrogen dioxide from OMI in the 405–465 nm window, Atmos. Meas. Tech., 8(4), 1685–1699, doi:10.5194/amt-8-1685-2015, 2015.

删除的内容: <sub>

删除的内容: </sub>

Gielen, C., Van Roozendael, M., Hendrick, F., Pinardi, G., Vlemmix, T., De Bock, V., De Backer, H., Fayt, C., Hermans, C., Gillotay, D. and Wang, P.: A simple and versatile cloud-screening method for MAX-DOAS retrievals, Atmos. Meas. Tech., 7(10), 3509–3527, doi:10.5194/amt-7-3509-2014, 2014.

Huang, Z., Huang, J., Bi, J., Wang, G., Wang, W., Fu, Q., Li, Z., Tsay, S.-C. and Shi, J.: Dust aerosol vertical structure measurements using three MPL lidars during 2008 China-U.S. joint dust field experiment, J. Geophys. Res. Atmos., 115(D7), n/a-n/a, doi:10.1029/2009JD013273, 2010.

Irie, H., Boersma, K. F., Kanaya, Y., Takashima, H., Pan, X. and Wang, Z. F.: Quantitative bias estimates for tropospheric NO_2 columns retrieved from SCIAMACHY, OMI, and GOME-2 using a common standard for East Asia, Atmos. Meas. Tech., 5(10), 2403–2411, doi:10.5194/amt-5-2403-2012, 2012.

Johnson, M. S., Meskhidze, N. and Praju Kiliyanpilakkil, V.: A global comparison of GEOS-Chem-predicted and remotely-sensed mineral dust aerosol optical depth and extinction profiles, J. Adv. Model. Earth Syst., 4(3), M07001, doi:10.1029/2011MS000109, 2012.

Kacenelenbogen, M., Redemann, J., Vaughan, M. A., Omar, A. H., Russell, P. B., Burton, S., Rogers, R. R., Ferrare, R. A. and Hostetler, C. A.: An evaluation of CALIOP/CALIPSO's aerosol-above-cloud detection and retrieval capability over North America, J. Geophys. Res. Atmos., 119(1), 230–244, doi:10.1002/2013JD020178, 2014.

Kanaya, Y., Irie, H., Takashima, H., Iwabuchi, H., Akimoto, H., Sudo, K., Gu, M., Chong, J., Kim, Y. J., Lee, H., Li, A., Si, F., Xu, J., Xie, P.-H., Liu, W.-Q., Dzhola, A., Postylyakov, O., Ivanov, V., Grechko, E., Terpugova, S. and Panchenko, M.: Long-term MAX-DOAS network observations of NO_2 in Russia and Asia (MADRAS)

删除的内容: <sub>

删除的内容: </sub&gt

删除的内容: <sub>

删除的内容: </sub>

during the period 2007-2012: instrumentation, elucidation of climatology, and comparisons with OMI satellite observations and global model simulations, Atmos. Chem. Phys., 14(15), 7909–7927, doi:10.5194/acp-14-7909-2014, 2014.

Kim, S.-W., Heckel, A., Frost, G. J., Richter, A., Gleason, J., Burrows, J. P., McKeen, S., Hsie, E.-Y., Granier, C. and Trainer, M.: NO_2 columns in the western United States observed from space and simulated by a regional chemistry model and their implications for NO_x emissions, J. Geophys. Res., 114(D11), D11301, doi:10.1029/2008JD011343, 2009.

Koffi, B., Schulz, M., Bréon, F.-M., Griesfeller, J., Winker, D., Balkanski, Y., Bauer, S., Berntsen, T., Chin, M., Collins, W. D., Dentener, F., Diehl, T., Easter, R., Ghan, S., Ginoux, P., Gong, S., Horowitz, L. W., Iversen, T., Kirkevåg, A., Koch, D., Krol, M., Myhre, G., Stier, P. and Takemura, T.: Application of the CALIOP layer product to evaluate the vertical distribution of aerosols estimated by global models: AeroCom phase I results, J. Geophys. Res. Atmos., 117(D10), n/a-n/a, doi:10.1029/2011JD016858, 2012.

Leitão, J., Richter, A., Vrekoussis, M., Kokhanovsky, A., Zhang, Q. J., Beekmann, M. and Burrows, J. P.: On the improvement of NO2 satellite retrievals – aerosol impact on the airmass factors, Atmos. Meas. Tech., 3(2), 475–493, doi:10.5194/amt-3-475-2010, 2010.

Lerot, C., Stavrakou, T., De Smedt, I., Müller, J.-F. and Van Roozendael, M.: Glyoxal vertical columns from GOME-2 backscattered light measurements and comparisons with a global model, Atmos. Chem. Phys., 10(24), 12059–12072, doi:10.5194/acp-10-12059-2010, 2010.

删除的内容: –

删除的内容: <sub>

删除的内容: </sub>

Levy, R. C., Mattoo, S., Munchak, L. A., Remer, L. A., Sayer, A. M., Patadia, F. and Hsu, N. C.: The Collection 6 MODIS aerosol products over land and ocean, Atmos. Meas. Tech., 6(11), 2989–3034, doi:10.5194/amt-6-2989-2013, 2013.

Li, S., Yu, C., Chen, L., Tao, J., Letu, H., Ge, W., Si, Y. and Liu, Y.: Inter-comparison of model-simulated and satellite-retrieved componential aerosol optical depths in China, Atmos. Environ., 141, 320–332, doi:https://doi.org/10.1016/j.atmosenv.2016.06.075, 2016.

Lin, J., Pan, D., Davis, S. J., Zhang, Q., He, K., Wang, C., Streets, D. G., Wuebbles, D. J. and Guan, D.: China's international trade and air pollution in the United States, Proc. Natl. Acad. Sci., 111(5), 1736–1741, doi:10.1073/pnas.1312860111, 2014a.

Lin, J.-T.: Satellite constraint for emissions of nitrogen oxides from anthropogenic, lightning and soil sources over East China on a high-resolution grid, Atmos. Chem. Phys., 12(6), 2881–2898, doi:10.5194/acp-12-2881-2012, 2012.

Lin, J.-T., McElroy, M. B. and Boersma, K. F.: Constraint of anthropogenic NOx emissions in China from different sectors: a new methodology using multiple satellite retrievals, Atmos. Chem. Phys., 10(1), 63–78, doi:10.5194/acp-10-63-2010, 2010.

Lin, J.-T., Martin, R. V., Boersma, K. F., Sneep, M., Stammes, P., Spurr, R., Wang, P., Van Roozendael, M., Clémer, K. and Irie, H.: Retrieving tropospheric nitrogen dioxide from the Ozone Monitoring Instrument: effects of aerosols, surface reflectance anisotropy, and vertical profile of nitrogen dioxide, Atmos. Chem. Phys., 14(3), 1441–1461, doi:10.5194/acp-14-1441-2014, 2014b.

Lin, J.-T., Liu, M.-Y., Xin, J.-Y., Boersma, K. F., Spurr, R., Martin, R. and Zhang, Q.: Influence of aerosols and surface reflectance on satellite NO_2 retrieval: seasonal and spatial characteristics and implications for NO_x emission constraints, Atmos. Chem. Phys., 15(19), 11217–11241, doi:10.5194/acp-15-11217-2015, 2015.

删除的内容: <sub>

删除的内容: </sub>

Lorente, A., Folkert Boersma, K., Yu, H., Dörner, S., Hilboll, A., Richter, A., Liu, M., Lamsal, L. N., Barkley, M., De Smedt, I., Van Roozendael, M., Wang, Y., Wagner, T., Beirle, S., Lin, J.-T., Krotkov, N., Stammes, P., Wang, P., Eskes, H. J. and Krol, M.: Structural uncertainty in air mass factor calculation for and HCHO satellite retrievals, Atmos. Meas. Tech., 10(3), 759–782, doi:10.5194/amt-10-759-2017, 2017.

删除的内容: NO₂

Lucht, W., Schaaf, C. B. and Strahler, A. H.: An algorithm for the retrieval of albedo from space using semiempirical BRDF models, IEEE Trans. Geosci. Remote Sens., 38(2), 977–998, doi:10.1109/36.841980, 2000.

Ma, J. Z., Beirle, S., Jin, J. L., Shaiganfar, R., Yan, P. and Wagner, T.: Tropospheric NO2 vertical column densities over Beijing: results of the first three years of ground-based MAX-DOAS measurements (2008–2011) and satellite validation, Atmos. Chem. Phys., 13(3), 1547–1567, doi:10.5194/acp-13-1547-2013, 2013.

删除的内容: <sub>

删除的内容: </sub>

Ma, X. and Yu, F.: Seasonal variability of aerosol vertical profiles over east US and west Europe: GEOS-Chem/APM simulation and comparison with CALIPSO observations, Atmos. Res., 140–141, 28–37, doi:https://doi.org/10.1016/j.atmosres.2014.01.001, 2014.

Martin, R. V.: An improved retrieval of tropospheric nitrogen dioxide from GOME, J. Geophys. Res., 107(D20), 4437, doi:10.1029/2001JD001027, 2002.

Misra, A., Tripathi, S. N., Kaul, D. S. and Welton, E. J.: Study of MPLNET-Derived Aerosol Climatology over Kanpur, India, and Validation of CALIPSO Level 2 Version 3 Backscatter and Extinction Products, J. Atmos. Ocean. Technol., 29(9), 1285–1294, doi:10.1175/JTECH-D-11-00162.1, 2012.

Miyazaki, K. and Eskes, H.: Constraints on surface NO_x emissions by assimilating satellite observations of multiple species, Geophys. Res. Lett., 40(17), 4745–4750, doi:10.1002/grl.50894, 2013.

Proestakis, E., Amiridis, V., Marinou, E., Georgoulias, A. K., Solomos, S., Kazadzis, S., Chimot, J., Che, H., Alexandri, G., Binietoglou, I., Kourtidis, K. A., de Leeuw, G. and van der A, R. J.: 9-year spatial and temporal evolution of desert dust aerosols over South-East Asia as revealed by CALIOP, Atmos. Chem. Phys. Discuss., 1–35, doi:10.5194/acp-2017-797, 2017.

Richter, A., Begoin, M., Hilboll, A. and Burrows, J. P.: An improved NO2 retrieval for the GOME-2 satellite instrument, Atmos. Meas. Tech., 4(6), 1147–1159, doi:10.5194/amt-4-1147-2011, 2011.

Sareen, N., Schwier, A. N., Shapiro, E. L., Mitroo, D. and McNeill, V. F.: Secondary organic material formed by methylglyoxal in aqueous aerosol mimics, Atmos. Chem. Phys., 10(3), 997–1016, doi:10.5194/acp-10-997-2010, 2010.

Sayer, A. M., Munchak, L. A., Hsu, N. C., Levy, R. C., Bettenhausen, C. and Jeong, M.-J.: MODIS Collection 6 aerosol products: Comparison between Aqua's e-Deep Blue, Dark Target, and "merged" data sets, and usage recommendations, J. Geophys. Res. Atmos., 119(24), 13,965-13,989, doi:10.1002/2014JD022453, 2014.

Stammes, P., Sneep, M., de Haan, J. F., Veefkind, J. P., Wang, P. and Levelt, P. F.: Effective cloud fractions from the Ozone Monitoring Instrument: Theoretical framework and validation, J. Geophys. Res., 113(D16), D16S38, doi:10.1029/2007JD008820, 2008.

Stavrakou, T., Müller, J.-F., Bauwens, M., De Smedt, I., Lerot, C., Van Roozendael, M., Coheur, P.-F., Clerbaux, C., Boersma, K. F., van der A, R. and Song, Y.: Substantial Underestimation of Post-Harvest Burning Emissions in the North China

删除的内容: x

删除的内容: <sub>

删除的内容: </sub>

Plain Revealed by Multi-Species Space Observations, Sci. Rep., 6, 32307, doi:10.1038/srep32307, 2016.

Veefkind, J. P., de Haan, J. F., Sneep, M. and Levelt, P. F.: Improvements to the OMI O2–O2 operational cloud algorithm and comparisons with ground-based radar–lidar observations, Atmos. Meas. Tech., 9(12), 6035–6049, doi:10.5194/amt-9-6035-2016, 2016.

Verstraeten, W. W., Neu, J. L., Williams, J. E., Bowman, K. W., Worden, J. R. and Boersma, K. F.: Rapid increases in tropospheric ozone production and export from China, Nat. Geosci., 8, 690 [online] Available from: http://dx.doi.org/10.1038/ngeo2493, 2015.

Wang, J., Jacob, D. J. and Martin, S. T.: Sensitivity of sulfate direct climate forcing to the hysteresis of particle phase transitions, J. Geophys. Res. Atmos., 113(D11), n/a-n/a, doi:10.1029/2007JD009368, 2008a.

Wang, M., Gu, J., Yang, R., Zeng, L. and Wang, S.: Comparison of cloud type and frequency over China from surface, FY-2E, and CloudSat observations, vol. 9259, pp. 925913–925914. [online] Available from: http://dx.doi.org/10.1117/12.2069110, 2014.

Wang, P. and Stammes, P.: Evaluation of SCIAMACHY Oxygen A band cloud heights using Cloudnet measurements, Atmos. Meas. Tech., 7(5), 1331–1350, doi:10.5194/amt-7-1331-2014, 2014.

Wang, P., Stammes, P., van der A, R., Pinardi, G. and van Roozendael, M.: FRESCO+: an improved O2 A-band cloud retrieval algorithm for tropospheric trace gas retrievals, Atmos. Chem. Phys., 8(21), 6565–6576, doi:10.5194/acp-8-6565-2008, 2008b.

删除的内容: <sub>

删除的内容: </sub>

删除的内容: <sub>

删除的内容: </sub>

删除的内容: <sub>

删除的内容: </sub>

Wang, X., Huang, J., Zhang, R., Chen, B. and Bi, J.: Surface measurements of aerosol properties over northwest China during ARM China 2008 deployment, J. Geophys. Res. Atmos., 115(D7), n/a-n/a, doi:10.1029/2009JD013467, 2010.

Wang, Y., Penning de Vries, M., Xie, P. H., Beirle, S., Dörner, S., Remmers, J., Li, A. and Wagner, T.: Cloud and aerosol classification for 2.5 years of MAX-DOAS observations in Wuxi (China) and comparison to independent data sets, Atmos. Meas. Tech., 8(12), 5133–5156, doi:10.5194/amt-8-5133-2015, 2015.

Wang, Y., Lampel, J., Xie, P., Beirle, S., Li, A., Wu, D. and Wagner, T.: Ground-based MAX-DOAS observations of tropospheric aerosols, NO2, SO2 and HCHO in Wuxi, China, from 2011 to 2014, Atmos. Chem. Phys., 17(3), 2189–2215, doi:10.5194/acp-17-2189-2017, 2017a.

Wang, Y., Beirle, S., Lampel, J., Koukouli, M., De Smedt, I., Theys, N., Li, A., Wu, D., Xie, P., Liu, C., Van Roozendael, M., Stavrakou, T., Müller, J.-F. and Wagner, T.: Validation of OMI, GOME-2A and GOME-2B tropospheric NO2, SO2 and HCHO products using MAX-DOAS observations from 2011 to 2014 in Wuxi, China: investigation of the effects of priori profiles and aerosols on the satellite products, Atmos. Chem. Phys., 17(8), 5007–5033, doi:10.5194/acp-17-5007-2017, 2017b.

Winker, D. M., Pelon, J., Coakley, J. A., Ackerman, S. A., Charlson, R. J., Colarco, P. R., Flamant, P., Fu, Q., Hoff, R. M., Kittaka, C., Kubar, T. L., Le Treut, H., Mccormick, M. P., Mégie, G., Poole, L., Powell, K., Trepte, C., Vaughan, M. A. and Wielicki, B. A.: The CALIPSO Mission, Bull. Am. Meteorol. Soc., 91(9), 1211–1230, doi:10.1175/2010BAMS3009.1, 2010.

Winker, D. M., Tackett, J. L., Getzewich, B. J., Liu, Z., Vaughan, M. A. and Rogers, R. R.: The global 3-D distribution of tropospheric aerosols as characterized by

删除的内容: <sub>

删除的内容: </sub>

删除的内容: <sub>

删除的内容: </sub>

CALIOP, Atmos. Chem. Phys., 13(6), 3345–3361, doi:10.5194/acp-13-3345-2013, 2013.

Zara, M., Boersma, K. F., De Smedt, I., Richter, A., Peters, E., Van Geffen, J. H. G. M., Beirle, S., Wagner, T., Van Roozendael, M., Marchenko, S., Lamsal, L. N. and Eskes, H. J.: Improved slant column density retrieval of nitrogen dioxide and formaldehyde for OMI and GOME-2A from QA4ECV: intercomparison, uncertainty characterization, and trends, Atmos. Meas. Tech. Discuss., 1–47, doi:10.5194/amt-2017-453, 2018.

Zhang, Q., Streets, D. G., Carmichael, G. R., He, K. B., Huo, H., Kannari, A., Klimont, Z., Park, I. S., Reddy, S., Fu, J. S., Chen, D., Duan, L., Lei, Y., Wang, L. T. and Yao, Z. L.: Asian emissions in 2006 for the NASA INTEX-B mission, Atmos. Chem. Phys., 9(14), 5131–5153, doi:10.5194/acp-9-5131-2009, 2009.

Zhao, C. and Wang, Y.: Assimilated inversion of NO_x emissions over east Asia using OMI NO_2 column measurements, Geophys. Res. Lett., 36(6), L06805, doi:10.1029/2008GL037123, 2009.

Zhao, H. Y., Zhang, Q., Guan, D. B., Davis, S. J., Liu, Z., Huo, H., Lin, J. T., Liu, W. D. and He, K. B.: Assessment of China’s virtual air pollution transport embodied in trade by using a consumption-based emission inventory, Atmos. Chem. Phys., 15(10), 5443–5456, doi:10.5194/acp-15-5443-2015, 2015.

Zhou, Y., Brunner, D., Spurr, R. J. D., Boersma, K. F., Sneep, M., Popp, C. and Buchmann, B.: Accounting for surface reflectance anisotropy in satellite retrievals of tropospheric NO2, Atmos. Meas. Tech., 3(5), 1185–1203, doi:10.5194/amt-3-1185-2010, 2010.

删除的内容:

删除的内容: <sub>

删除的内容: </sub>

Zhu, W., Xu, C., Qian, X. and Wei, H.: Statistical analysis of the spatial-temporal distribution of aerosol extinction retrieved by micro-pulse lidar in Kashgar, China, Opt. Express, 21(3), 2531–2537, doi:10.1364/OE.21.002531, 2013.

Hendrick, F., Muller, J. F., Clemer, K., Wang, P., De Maziere, M., Fayt, C., Gielen, C., Hermans, C., Ma, J. Z., Pinardi, G., Stavrakou, T., Vlemmix, T., and Van Roozendael, M.: Four years of ground-based MAX-DOAS observations of HONO and NO2 in the Beijing area, Atmospheric Chemistry and Physics, 14, 765-781, 10.5194/acp-14-765-2014, 2014.

Jethva, H., Torres, O., and Ahn, C.: A ten-year global record of absorbing aerosols above clouds from OMI's near-UV observations, in: Remote Sensing of the Atmosphere, Clouds, and Precipitation Vi, edited by: Im, E., Kumar, R., and Yang, S., Proceedings of SPIE, 2016.

Schenkeveld, V. M. E., Jaross, G., Marchenko, S., Haffner, D., Kleipool, Q. L., Rozemeijer, N. C., Veefkind, J. P., and Levelt, P. F.: In-flight performance of the Ozone Monitoring Instrument, Atmospheric Measurement Techniques, 10, 1957-1986, 10.5194/amt-10-1957-2017, 2017.

van Donkelaar, A., Martin, R. V., Spurr, R. J. D., Drury, E., Remer, L. A., Levy, R. C., and Wang, J.: Optimal estimation for global ground-level fine particulate matter concentrations, Journal of Geophysical Research-Atmospheres, 118, 5621-5636, 10.1002/jgrd.50479, 2013.

删除的内容: Wang, Y., Lampel, J., Xie, P., Beirle, S., Li, A., Wu, D., and Wagner, T.: Ground-based MAX-DOAS observations of tropospheric aerosols, NO2, SO2 and HCHO in Wuxi, China, from 2011 to 2014, Atmospheric Chemistry and Physics, 17, 2189-2215, 10.5194/acp-17-2189-2017, 2017.

第 7 页: [1] 删除的内容 Jintai Lin 2018/6/21 PM5:19:00

We apply a number of criteria to ensure data quality of each pixel, mainly following Winker et al. (2013) and Amiridis et al. (2015). More detailed inoframtion about criteria to select the Level-2 are referred to Appendix A.

第 7 页: [2] 删除的内容 Jintai Lin 2018/6/21 PM5:20:00

After the pixel-based screening, we aggregate the CALIOP data at the model grid (0.667° long. x 0.5° lat.) and vertical resolution (47 layers, with 36 layers or so in the troposphere). For each grid cell, we choose the CALIOP pixels within 1.5° of the grid cell center. The way to compile gridded CALIOP climatology aerosol extinction profiles is referred to Appendix B. CALIOP Level-2 data are always presented at the fixed 399 altitudes above sea level. To account for the difference in surface elevation between a CALIOP pixel and the respective model grid cell, we convert the altitude of the pixel to a height above the ground, by using the surface elevation data provided in CALIOP. We then average horizontally and vertically the profiles of all pixels within one model grid cell and layer. We do the regridding day-by-day for all grid cells to ensure that GEOS-Chem and CALIOP extinction profiles are coincident spatially and temporally. Finally, we compile a monthly climatological dataset by averaging over 2007–2015.

第 7 页: [3] 删除的内容 Jintai Lin 2018/6/21 PM5:33:00

As discussed above, we choose the CALIOP pixels within 1.5° of a grid cell center. We test this choice by examining the aerosol layer height (ALH) produced for that grid cell. The ALH is defined as the extinction-weighted height of aerosols (see Eq. 1, where n denotes the number of tropospheric layers, ε_i the aerosol extinction at

layer i, and H_i the layer center height above the ground). We find that choosing pixels within 1.0° of a grid cell center leads to a nosier horizontal distribution of ALH, owing to the small footprint of CALIOP. On the other hand, choosing 2.0° leads to a too smooth spatial gradient of ALH with local characteristics of aerosol vertical distributions are largely lost. We thus decide that 1.5° is a good balance between noise and smoothness.

$$\mathrm{ALH} = \frac{\sum_{i=1}^{i=n} \varepsilon_i \mathrm{H}_i}{\sum_{i=1}^{i=n} \varepsilon_i} \qquad (1)$$

Certain grid cells do not contain sufficient valid observations for some months of the climatological dataset. We fill in missing monthly values of a grid cell using valid data in the surrounding 5 x 5 = 25 grid cells (within ~ 100 km). If the 25 grid cells do not have enough valid data (see Appedix B for details next paragraph for details), we use those in the surrounding 7 x 7 = 49 grid cells (within ~ 150 km). A similar procedure is used by Lin et al. (2014b, 2015) to fill in missing values in the gridded MODIS AOD dataset.

第 16 页: [4] 删除的内容	Jintai Lin	2018/6/21 PM5:38:00

3.2 Comparison to NASA CALIOP monthly climatology

We compare our gridded climatological profiles to NASA CALIOP Version 3 Level-3 all-sky monthly profiles at 532 nm (Winker et al. 2013). The NASA Level-3 data has a horizontal resolution of 2° lat. × 5° lon. and a vertical resolution of 60 m (from -0.5 to 12 km above sea level). We combine NASA monthly data over 2007–2015 to construct a monthly climatology for comparison with our own compilation. We only choose aerosol extinction data in the troposphere with error less than 0.15 (the valid range given in the CALIOP dataset). If the number of valid monthly profiles in a grid cell is less than five (i.e., for the same month in five out of the nine years), then we exclude data in that grid cell; see the dark gray grid cells in Fig. 23c.

Several methodological differences exist between generating our and NASA CALIOP datasets. First, the two datasets have different horizontal resolutions. Also, we sample all valid CALIOP pixels within 1.5 ^{0} of a grid cell center, whereas the NASA dataset samples all valid pixels within a grid cell. Besides, our CALIOP dataset involves several steps of horizontal interpolation, for purposes of subsequent cloud and NO_2 retrievals, which is not done in the NASA dataset. In addition, we match CALIOP data vertically to the GEOS-Chem vertical resolution, whereas the NASA dataset maintains the original resolution.

Figure 23c shows the spatial distribution of ALH in all seasons based on NASA CALIOP Level-3 all-sky monthly climatology. The horizontal resolution of NASA data is much coarser than ours; and NASA data are largely missing over the southwest with complex terrains. We choose to focus on the comparison over East China (the black box in Fig. 12a). Over East China, the two climatology datasets generally exhibit similar spatial patterns of ALH in all seasons (Fig. 23a, c). The NASA dataset suggests higher ALHs than ours over Eastern China, especially in summer, due mainly to differences in the sampling and regridding processes. Figure 34c further compares the monthly variation of ALH between our (black line with error bars) and NASA (blue filled triangles) datasets averaged over East China. The two datasets are consistent in almost all months, indicating that their regional differences are largely smoothed out by spatial averaging.

第 25 页: [5] 删除的内容	Jintai Lin	2018/6/21 PM5:44:00

EU FP7-project Quality Assurance for Essential Climate Variables (

第 25 页: [6] 删除的内容	Jintai Lin	2018/6/21 PM5:44:00

is aim at making rapid judgments on validitiy and trustworthiness of Earth Observation data and the derived climate data sets. It

第 25 页: [7] 删除的内容 Folkert Boersma 2018/6/28 AM10:51:00

essentially an ensemble data sets of satellite products provide

第 25 页: [8] 删除的内容 Jintai Lin 2018/6/21 PM5:46:00

, with a fully traceable quality assurance on all aspects of the NO_2, HCHO and carbon monoxide (CO) (Zara et al., 2018)

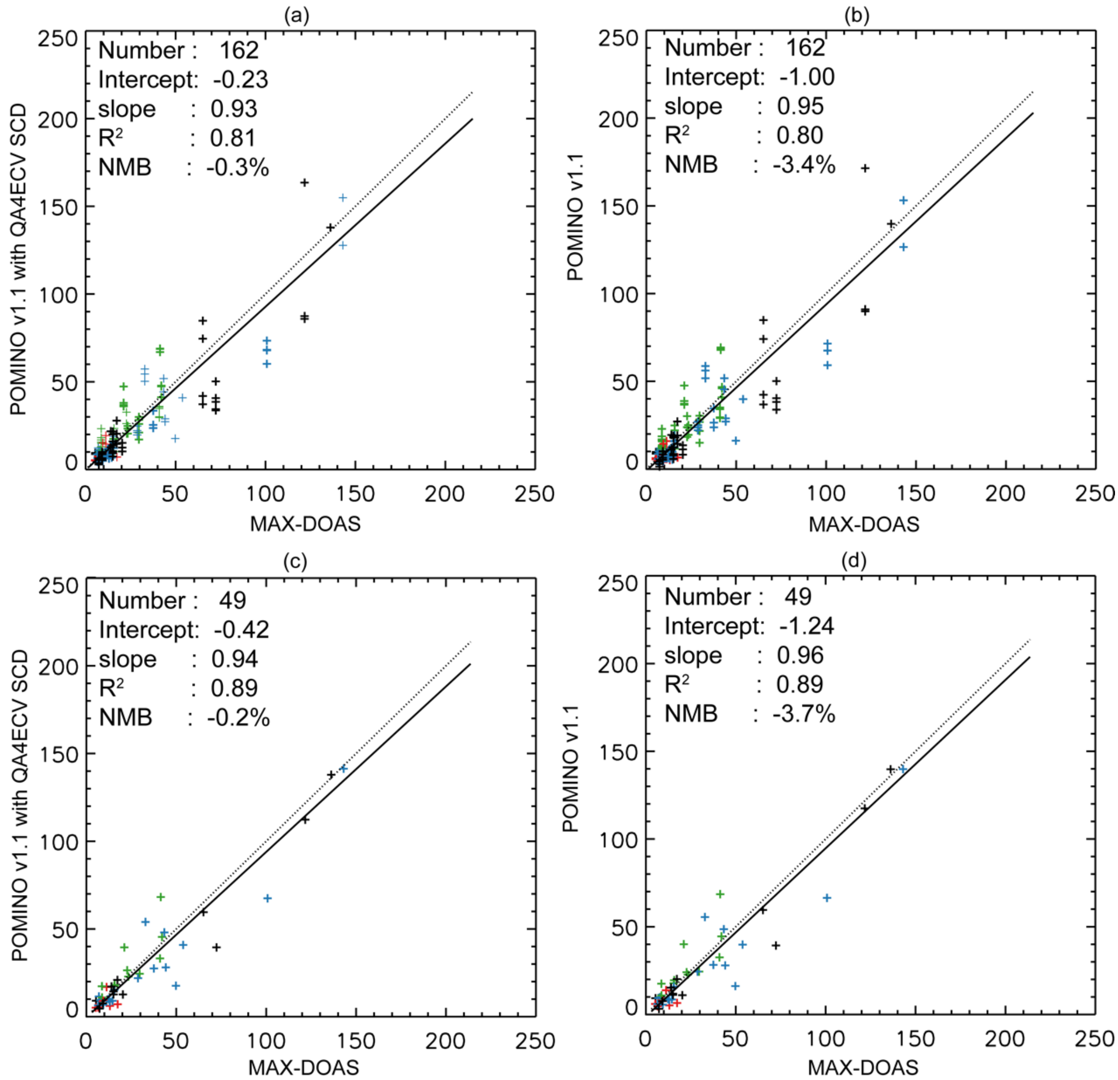

Figure S1. (a-b) Scatter plot for NO_2 VCD (10^{15} molec. cm^{-2}) between MAX-DOAS and POMINO v1.1 data with (a) QA4ECV or (b) DOMINO SCD. Each "+" corresponds to an OMI pixel, as several pixels may be available in a day. (c-d) Similar to (a-b) but after averaging over all OMI pixels in the same day, such that each "+" represents a day.

2) Their explanation for the limited number of MAX-DOAS data is well taken. But, they could still use various statistical methods and maybe other data sources to assess the improvements. Small increase in correlation alone, which may not be statistically significant, cannot be a measure of retrieval improvements (main message of this manuscript). One can raise many questions for results presented in Tables 2 and 3: What explains more than 20% difference between POMINO v1.1 and POMINO?, how is the 30% high bias of v1.1 versus MAX-DOAS an improvement?, what explains a factor of 2 difference in slope between DOMINO and QA4ECV if it is not related to slant column?, why is the comparison so poor for the improved QA4ECV OMI product?, are MAX-DOAS data accurate/reliable?, etc. From Figure 9, the relationship between DOMINO and MAX-DOAS looks much tighter as compared to POMINO and MAX-

DOAS (except for few data points) and POMINO does not show an improvement if MAX-DOAS is the ground truth.

The only difference between POMINO v1.1 and POMINO comes from the different shapes of aerosol vertical profile. Our manuscript, together with several previous studies cited in our manuscript, has clearly shown a systematic error in GEOS-Chem simulated vertical profile. Correcting for this error means an improvement of in the retrieval algorithm from POMINO to POMINO v1.1, regardless of how many MAX-DOAS (or other independent) data are available to demonstrate the algorithm improvement.

In general, the higher NO_2 VCD values in POMINO v1.1 than POMINO are because of the increased shielding effect of aerosols, which leads to smaller NO_2 AMFs. The magnitude of this increase depends on many conditions such as the fraction of clouds. In the revised manuscript, Table 2 shows a 6% increase (NMB of -9.6% versus -3.4%), Table 3 shows a 14% increase (NMB of -9.4% versus 4.4%), and Table 4 shows a 9% increase (NMB of 20.8% versus 29.4%) – these values are specific to their conditions.

Table 3 (Table 4 in our revised manuscript) basically shows that under cloud free conditions (POMINO CF = 0), the aerosol loading is much smaller than under haze days (AOD = 0.60 versus 1.13 in Table 3). In this case, POMINO v1.1, POMINO, and DOMINO v2 have similar bias (20.8%–29.4%) and R^2 (0.53–0.56) against MAX-DOAS NO_2 data, and the performance of QA4ECV is better. QA4ECV is essentially an ensemble of several European retrieval algorithms, all of which treat aerosols as "effective" clouds, thus its better performance (when aerosol loadings are relatively small) is not surprising. In Sect. 6, we have clarified this point that "Here, POMINO v1.1, POMINO and DONIMO v2 do not show large differences in R^2 (0.53–0.56) and NMB (20.8–29.4%) with respect to MAX-DOAS. QA4ECV has a higher R^2 (0.63) and a lower NMB (-5.8%), presumably reflecting the improvements in this (EU-) consortium approach, at least in mostly cloud-free situations. However, the R^2 values for POMINO and POMINO v1.1 are much smaller than the R^2 values in haze days, whereas the opposite changes are true for DOMINO v2 and QA4ECV. Thus, for this limited set of data, the changes from DOMINO v2 and QA4ECV to POMINO and POMINO v1.1 mainly reflect the improved aerosol treatment in hazy scenes."

As for "what explains a factor of 2 difference in slope between DOMINO and QA4ECV if it is not related to slant column?, why is the comparison so poor for the improved QA4ECV OMI product?", both our study and previous studies (van Geffen et al., 2015; Zara et al., 2018) show SCDs contribute insignificantly to the VCD differences. We suspect that the VCD differences come from the fact that QA4ECV is essentially an ensemble of several European retrieval algorithms. However, specific analysis of the difference between DOMINO v2 and QA4ECV is not the main topic of this study.

The reliability of MAX-DOAS data have been analyzed in many papers, including those cited in our paper (Hendrick et al., 2014; Lin et al., 2014b; Wang et al., 2017a).

In our reply to comment 3 of the previous review, we wrote that "We would definitely prefer to have a larger set of MAX-DOAS NO_2 data. Unfortunately, very few high-quality MAX-DOAS measurements are available over China. We have made efforts to get data from multiple sites to enhance the spatial representativeness." Although we have tried very hard to get all data available, the amount of MAX-DOAS data points here do not allow to fully evaluating each satellite product. Based on this limited set of MAX-DOAS data, it is not expected that any product shows superiority in all aspects of comparison with MAX-DOAS – for example, although DOMINO v2 is a relatively older product, it may compare with (this limited set of) MAX-DOAS data better than other products under some special conditions, as pointed out by the reviewer.

Given the limited amount of available MAX-DOAS data, here we test the effect of sampling criteria (i.e., time and distance) on the comparison; the criteria chosen in the main text are described in Line 314-317, and are highlighted in bold in Tables S1 and S2. Table S1 selects OMI pixels within 25 km of MAX-DOAS sites and MAX-DOAS measurements within different hours (1 h, 1.5h, and 2 h) of OMI overpass time. For each product, the comparison results (slope, intercept, R^2, NMB) do not change significantly.

Table S2 selects MAX-DOAS data within 1 h of OMI overpass time and OMI pixels within various distances to MAX-DOAS sites (40 km, 35 km, 30 km, 25 km, and 20 km). For POMINO, POMINO v1.1, and POMINO v1.1 with QA4ECV SCDs, the R^2 value changes slightly when the distance increases from 20 km to 30 km, and starts to decline at longer distances. This reflects that as the distance increases, the satellite data tend to represent regional NO_2, in contrast to the MAX-DOAS data which are "line" measurements. Other statistics (slope, intercept, and NMB) do not change significantly with distance. Similar changes with distance are shown in DOMINO v2 and QA4ECV data.

3) The "Author's Response" does not seem to include a marked-up manuscript version. Therefore, it is not clear if the authors have sufficiently addressed the reviewers' comments and how they are addressed.

We will provide a Microsoft WORD document with changes tracked.

Minor comment:

4) It is difficult to relate the reported contents (numbers) in abstract/conclusions/discussions to tables as the tables provide results for a subset of samples but not for the entire samples. Including statistics of Figure 9 in table would be helpful.

We have added a table (Table 2) to summarize the statistics in Fig. 9, and have changed numbering of other tables accordingly.

Table S1 Evaluation of OMI products against MAX-DOAS under different temporal criteria.

	Slope			Intercept			R^2			NMB (%)		
Hours within OMI overpass time	**1h**	1.5h	2h	**1h**	1.5h	2h	**1h**	1.5h	2h	**1h**	1.5h	2h
Number of pixels	**162**	175	184	**162**	175	184	**162**	175	184	**162**	175	184
POMINO v1.1	**0.95**	0.96	0.97	**-1.00**	-2.24	-2.42	**0.80**	0.77	0.76	**-3.4**	-5.5	-5.5
POMINO	**0.78**	0.80	0.80	**0.96**	-0.04	-0.35	**0.80**	0.78	0.77	**-9.6**	-11.3	-11.3
POMINO v1.1 (with QA4ECV SCD)	**0.93**	0.94	0.94	**0.23**	-1.57	-1.73	**0.81**	0.78	0.76	**-0.3**	-3.1	-2.5
DOMINO v2	**1.06**	1.10	1.10	**-3.86**	-5.08	-5.00	**0.68**	0.68	0.67	**-2.1**	-3.7	-2.2
QA4ECV	**0.66**	0.65	0.67	**1.09**	0.47	0.43	**0.75**	0.72	0.74	**-22.0**	-24.3	-22.7

Table S2 Evaluation of OMI products against MAX-DOAS under different spatial criteria.

Distance from MAX-DOAS site	40km	35km	30km	**25km**	20km	40km	35km	30km	**25km**	20km
Number of pixels	510	383	272	**163**	98	510	383	272	**163**	98
	slope					intercept				
POMINO v1.1	1.03	1.07	0.95	**0.95**	0.98	-4.87	-5.22	-1.67	**-1.00**	-1.57
POMINO	0.80	0.82	0.79	**0.78**	0.71	-0.90	-0.77	0.36	**0.96**	2.12
POMINO v1.1 (with QA4ECV SCD)	1.02	1.05	0.93	**0.93**	0.94	-3.97	-4.37	-0.70	**0.23**	-0.50
DOMINO v2	1.03	1.05	1.05	**1.06**	0.70	-3.91	-4.10	-3.49	**-3.86**	3.37
QA4ECV	0.64	0.64	0.65	**0.66**	0.65	0.15	0.45	0.86	**1.09**	1.34
	R^2					NMB (%)				
POMINO v1.1	0.63	0.64	0.75	**0.80**	0.78	-6.5	-4.9	-4.4	**-3.4**	-5.7
POMINO	0.69	0.71	0.75	**0.80**	0.80	-12.3	-11.0	-10.2	**-9.6**	-12.2
POMINO v1.1 (with QA4ECV SCD)	0.63	0.64	0.75	**0.81**	0.78	-2.1	-0.8	-0.1	**-0.3**	-2.4
DOMINO v2	0.60	0.63	0.66	**0.68**	0.63	1.5	1.2	0.6	**-2.1**	-5.0
QA4ECV	0.64	0.67	0.72	**0.75**	0.68	-22.0	-21.4	-22.0	**-22.0**	-23.4

Improved aerosol correction for OMI tropospheric NO_2 retrieval over East Asia: constraint from CALIOP aerosol vertical profile

Mengyao Liu[1,2], Jintai Lin[1], K. Folkert Boersma[2,3], Gaia Pinardi[4], Yang Wang[5], Julien Chimot[6], Thomas Wagner[5], Pinghua Xie[7,8,9], Henk Eskes[2], Michel Van Roozendael[4], François Hendrick[4], Pucai Wang[10], Ting Wang[10], Yingying Yan[1]

1, Laboratory for Climate and Ocean-Atmosphere Studies, Department of Atmospheric and Oceanic Sciences, School of Physics, Peking University, Beijing, China

2, Royal Netherlands Meteorological Institute, De Bilt, the Netherlands

3, Meteorology and Air Quality department, Wageningen University, Wageningen, the Netherlands

4, Royal Belgian Institute for Space Aeronomy (BIRA-IASB), Brussels, Belgium

5, Max Planck Institute for Chemistry, Mainz, Germany

6, Department of Geoscience and Remote Sensing (GRS), Civil Engineering and Geosciences, TU Delft, the Netherlands

7, Anhui Institute of Optics and Fine Mechanics, Key laboratory of Environmental Optics and Technology, Chinese Academy of Sciences, Hefei, China

8, CAS Center for Excellence in Urban Atmospheric Environment, Institute of Urban Environment, Chinese Academy of Sciences, Xiamen, China

9, School of Environmental Science and Optoelectronic Technology, University of Science and Technology of China, Hefei, China

样式定义: 标题 1: 与下段不同页

样式定义: 标题 2: 段落间距段后: 1 行, 与下段不同页

带格式的: 上标

10, IAP/CAS, Institute of Atmospheric Physics, Chinese Academy of Sciences, Beijing, China

Correspondence to: Jintai Lin (linjt@pku.edu.cn); K. Folkert Boersma (folkert.boersma@knmi.nl)

Abstract

Satellite retrieval of vertical column densities (VCDs) of tropospheric nitrogen dioxide (NO_2) is critical for NO_x pollution and impact evaluation. For regions with high aerosol loadings, the retrieval accuracy is greatly affected by whether aerosol optical effects are treated implicitly (as additional "effective" clouds) or explicitly, among other factors. Our previous POMINO algorithm explicitly accounts for aerosol effects to improve the retrieval especially in polluted situations over China, by using aerosol information from GEOS-Chem simulations with further monthly constraints by MODIS/Aqua aerosol optical depth (AOD) data. Here we present a major algorithm update, POMINO v1.1, by constructing a monthly climatological data set of aerosol extinction profiles, based on Level-2 CALIOP/CALIPSO data over 2007–2015, to better constrain the modeled aerosol vertical profiles.

We find that GEOS-Chem captures the month-to-month variation of CALIOP aerosol layer height but with a systematic underestimate by about 300–600 m (season and location dependent), due to a too strong negative vertical gradient of extinction above 1 km. Correcting the model aerosol extinction profiles results in small changes in retrieved cloud fraction, increases in cloud top pressure (within 2–6% in most cases), and increases in tropospheric NO_2 VCD by 4–16% over China on a monthly basis in 2012. The improved NO_2 VCDs (in POMINO v1.1) are more consistent with independent ground-based MAX-DOAS observations (R^2 = 0.80, NMB = -3.4%, for 162 pixels in 49 days) than POMINO (R^2 = 0.80, NMB = -9.6%), DOMINO v2 (R^2 =

删除的内容: t

删除的内容: AOD

删除的内容: This study is the kernel updates of our newthe retrieval algorithm, to POMINO v21.1,

删除的内容:

删除的内容: and

0.68, NMB = -2.1%) and QA4ECV (R^2 = 0.75, NMB = -22.0%) are. Especially on haze days, R^2 reaches 0.76 for POMINO v1.1, much higher than that for POMINO (0.68), DOMINO v2 (0.38) and QA4ECV (0.34). Furthermore, the increase in cloud pressure likely reveals a more realistic vertical relationship between cloud and aerosol layers, with aerosols situated above the clouds in certain months instead of always below the clouds. The POMINO v1.1 algorithm is a core step towards our next public release of data product (POMINO v2), and it will also be applied to the recently launched S5P-TropOMI sensor.

1. Introduction

Air pollution is a major environmental problem in China. In particular, China has become the world's largest emitting country of nitrogen oxides (NO_X=NO+NO_2) due to its rapid economic growth, heavy industries, coal-dominated energy sources, and relatively weak emission control (Cui et al., 2016; Lin et al., 2014a; Stavrakou et al., 2016; Zhang et al., 2009). Tropospheric vertical column densities (VCDs) of nitrogen dioxide (NO_2) retrieved from the Ozone Monitoring Instrument (OMI) onboard the Earth Observing System (EOS) Aura satellite have been widely used to monitor and analyze NO_X pollution over China because of its high spatiotemporal coverage (e.g. (Lin et al., 2010; Miyazaki and Eskes, 2013; Verstraeten et al., 2015; Zhao and Wang, 2009). However, NO_2 retrieved from OMI and other space-borne instruments are subject to errors in the conversion process from radiance to VCD, particularly with respect to the calculation of tropospheric air mass factor (AMF) that is used to convert tropospheric slant column density to VCD (e.g. Boersma et al., 2011; Bucsela et al., 2013; Lin et al., 2015; Lorente et al., 2017).

Most current-generation NO_2 algorithms do not explicitly account for the effects of aerosols on NO_2 AMFs and on prerequisite cloud parameter retrievals. These retrievals often adopt an implicit approach wherein cloud algorithms retrieve

带格式的: 上标
删除的内容: 82
删除的内容: 7
删除的内容:
删除的内容: and
删除的内容: This
删除的内容: improvement in ourOur POMINO v1.1 algorithm
删除的内容:

"effective cloud" parameters that include the optical effects of aerosols. This implicit method is based on aerosols exerting an effect on the top-of-atmosphere radiance level, whereas the assumed cloud model does not account for the presence of aerosols in the atmosphere (Stammes et al., 2008; Veefkind et al., 2016; Wang et al., 2008b; Wang and Stammes, 2014). In the absence of clouds, an aerosol optical thickness of 1 is then interpreted as an effective cloud fraction of $\pm$0.10, and the value also depends on the aerosol properties (scattering or absorbing), true surface albedo and geometry angles (Chimot et al., 2016) with an effective cloud pressure closely related to the aerosol layer, at least for aerosols of predominantly scattering nature (e.g. Boersma et al., 2004, 2011, Castellanos et al., 2014, 2015). However, in polluted situations with high aerosol loadings and more absorbing aerosol types, which often occur over China and many other developing regions, the implicit method can result in considerable biases (Castellanos et al., 2014, 2015; Chimot et al., 2016; Kanaya et al., 2014; Lin et al., 2014b).

Lin et al. (2014b, 2015) established the POMINO NO_2 algorithm, which builds on the DOMINO v2 algorithm (for OMI NO_2 slant columns and stratospheric correction), but improves upon it through a more sophisticated AMF calculation over China. In POMINO, the effects of aerosols on cloud retrievals and NO_2 AMFs are explicitly accounted for. In particular, daily information on aerosol optical properties such as aerosol optical depth (AOD), single scattering albedo (SSA), phase function and vertical extinction profiles are taken from nested Asian GEOS-Chem v9-02 simulations. The modeled AOD at 550 nm is further constrained by MODIS/Aqua monthly AOD, with the correction applied to other wavelengths based on modeled aerosol refractive indices (Lin et al., 2014b). However, the POMINO algorithm does not include an observation-based constraint on the vertical profile of aerosols, whose altitude relative to NO_2 has strong and complex influences on NO_2 retrieval (Castellanos et al., 2015; Leitão et al., 2010; Lin et al., 2014b). This study improves

upon the POMINO algorithm by incorporating CALIOP monthly climatology of aerosol vertical extinction profiles to correct for model biases.

The CALIOP lidar, carried on the sun-synchronous CALIPSO satellite, has been acquiring global aerosol extinction profiles since June 2006 (Winker et al., 2010). CALIPSO and Aura are both parts of the National Aeronautics and Space Administration (NASA) A-train constellation of satellites. The overpass time of CALIOP/CALIPSO is only 15 minutes later than OMI/Aura. In spite of issues with the detection limit, radar ratio selection and cloud contamination that cause some biases in CALIOP aerosol extinction vertical profiles (Amiridis et al., 2015; Koffi et al., 2012; Winker et al., 2013), comparisons of aerosol extinction profiles between ground-based lidar and CALIOP show good agreements (Kacenelenbogen et al., 2014; Kim et al., 2009; Misra et al., 2012). However, CALIOP is a nadir-viewing instrument that measures the atmosphere along the satellite ground-track with a narrow field-of-view. This means that the daily geographical coverage of CALIOP is much smaller than that of OMI. Thus previous studies often used monthly/seasonal regional mean CALIOP data to study aerosol vertical distributions or to evaluate model simulations (Chazette et al., 2010; Johnson et al., 2012; Koffi et al., 2012; Ma and Yu, 2014; Sareen et al., 2010).

There exist a few CALIOP Level-3 gridded datasets, such as LIVAS (Amiridis et al. 2015) and NASA official Level-3 monthly dataset (Winker et al., 2013). However, LIVAS is an annual average day-night combined product, not suitable to be applied to OMI NO_2 retrievals (around early afternoon, and in need of a higher temporal resolution than annual). The horizontal resolution (2° long. $\times$ 5° lat.) of NASA official product is much coarser than OMI footprints and the GEOS-Chem model resolution.

删除的内容: are some mature data of

删除的内容:

删除的内容: yearly

删除的内容: but

带格式的: 下标

删除的内容: measurement is only available in the daytime, besides, the temporal resolution (yearly) is not very suitable for daily aerosol extinction profiles usage

删除的内容: s

Here we construct a custom monthly climatology of aerosol vertical extinction profiles based on 9-years (2007–2015) worth of CALIOP Version 3 Level-2 532 nm data. On a climatological basis, we use the CALIOP monthly data to adjust GEOS-Chem profiles in each grid cell for each day of the same month in any year. We then use the corrected GEOS-Chem vertical extinction profiles in the retrievals of cloud parameters and NO_2. Finally, we evaluate our updated POMINO retrieval (hereafter referred to as POMINO v1.1), our previous POMINO product, DOMINO v2 and the newly released Quality Assurance for Essential Climate Variables product (QA4ECV, see Appendix A), using ground-based MAX-DOAS NO_2 column measurements at three urban/suburban sites in East China for the year of 2012 and several months in 2008/2009.

Section 2 describes the construction of CALIOP aerosol extinction vertical profile monthly climatology, the POMINO v1.1 retrieval approach, and the MAX-DOAS data. It also presents the criteria for comparing different NO_2 retrieval products and for selecting coincident OMI and MAX-DOAS data. Section 3 compares our CALIOP climatology with NASA's official Level-3 CALIOP dataset and GEOS-Chem simulation results. Sections 4 and 5 compare POMINO v1.1 to POMINO to analyze the influence of improved aerosol vertical profiles on retrievals of cloud parameters and NO_2 VCDs, respectively. Section 6 evaluates POMINO, POMINO v1.1, DOMNO v2 and QA4ECV NO_2 VCD products using the MAX-DOAS data. Section 7 concludes our study.

2. Data and methods

2.1 CALIOP monthly mean extinction profile climatology

CALIOP is a dual-wavelength polarization lidar measuring attenuated backscatter radiation at 532 and 1064 nm since June 2006. The vertical resolution of aerosol

删除的内容: In order to constrain daily aerosol extinction profiles simulated by GEOS-Chem.However, the major monthly/seasonal CALIOP data are too coarse in spatial resolution (i.e. NASA's official monthly Level-3 CALIOP dataset with spatial resolution 2° long. × 5° lat.) or in temporal resolution (i.e. LIVAS 5-year based 1° × 1° CALIOP dataset).
H

删除的内容: and the existing

删除的内容: and

删除的内容: retrievals

删除的内容:

删除的内容: and

删除的内容: new released Quality Assurance for Essential Cliamte Variables (QA4ECV, see detailed introduction in Appedix B)

删除的内容: s

删除的内容: *Constructing a*

extinction profiles is 30 m below 8.2 km and 60 m up to 20.2 km (Winker et al., 2013), with a total of 399 sampled altitudes. The horizontal resolution of CALIOP scenes is 335 m along the orbital track and is given over a 5 km horizontal resolution in Level-2 data.

As detailed in Appendix B, we use the daily all-sky Version 3 CALIOP Level-2 aerosol profile product at 532 nm from 2007 to 2015 to construct a monthly Level-3 climatological dataset of aerosol extinction profiles over China and nearby regions. This dataset is constructed on the GEOS-Chem model grid (0.667° long. x 0.5° lat.) and vertical resolution (47 layers, with 36 layers or so in the troposphere).

The ratio of climatological monthly CALIOP to monthly GEOS-Chem profiles represents the scaling profile to adjust the daily GEOS-Chem profiles in the same month (see Sect. 2.2).

2.2 POMINO v1.1 retrieval approach

The NO_2 retrieval consists of three steps. First, the total NO_2 slant columns density (SCD) is retrieved using the Differential Optical Absorption Spectroscopy (DOAS) technique (for the 405-465 nm spectral window in the case of OMI). The uncertainty of the SCD is determined by the appropriateness of the fitting technique, the instrument noise, the choice of fitting window, and the orthogonality of the absorbers' cross sections (Bucsela et al., 2006; van Geffen et al., 2015; Lerot et al., 2010; Richter et al., 2011; Zara et al., 2018). The NO_2 SCD in DOMINO v2 has a bias at about 0.5~1.3 × 10^{15} molec. cm^{-2} (Belmonte Rivas et al., 2014; Dirksen et al., 2011; Marchenko et al., 2015; van Geffen et al., 2015; Zara et al., 2018), which can be reduced by improving wavelength calibration and including O_2–O_2 and liquid water absorption in the fitting model (van Geffen et al., 2015). The tropospheric SCD is then obtained by subtracting the stratospheric SCD from the total SCD. The bias in

删除的内容: Here

已下移 [5]: We choose the all-sky product instead of clear-sky data, since previous studies indicate that the climatological aerosol extinction profiles are affected insignificantly by the presence of clouds (Koffi et al. 2012; Winker et al. 2013). As we use this climatological data to adjust GEOS-Chem results, choosing all-sky data improves consistency with the model simulation when doing the daily correction.

已下移 [1]: In brief, only the pixels with Cloud Aerosol Discrimination (CAD) scores between -20 and -100 with extinction Quality Control (QC) flag valued at 0, 1, 18, and 16 are selected. We further discard samples with an extinction uncertainty of 99.9 km^{-1}, which is indicative of unreliable retrieval. We only accept extinction values falling in the range from 0.0 to 1.25, according to CALIOP observation thresholds. Previous studies showed that weakly scattering edges of icy clouds are sometimes misclassified as aerosols (Winker et al. 2013). To eliminate contamination from icy clouds we exclude the aerosol layers above the cloud layer (with layer-top temperature below 0 ℃) when both of them are above 4km (Winker et al. 2013).

已下移 [2]: CALIOP Level-2 data are always presented at the fixed 399 altitudes above sea level. To account for the difference in surface elevation between a CALIOP pixel and the respective model grid cell,

删除的内容: We apply a number of criteria to ensure data quality of each pixel, mainly following Winker et al. (2013) and Amiridis et al. ... [1]

带格式的: 非突出显示

删除的内容:

删除的内容: After the pixel-based screening, we aggregate the CALIOP data at the model grid (0.667° long. x 0.5° lat.) and vertical ... [2]

删除的内容:

已下移 [3]: Figure 1 shows the number of aerosol extinction profiles in each grid cell and 12 x 9 = 108 months that are used to compile the

删除的内容: .

删除的内容: As discussed above, we choose the CALIOP pixels within 1.5° of a grid cell center. We test this choice by examining the ... [3]

已下移 [4]: For each grid cell in each month, we further correct singular values in the vertical profile. In a month, if a grid cell *i* has

批注 [JL1]: Add Zara et al. (2018)

the total SCD is mostly absorbed by this stratospheric separation step, which may not propagate into the tropospheric SCD (van Geffen et al., 2015). The last step converts the tropospheric SCD to VCD by using the tropospheric AMF (VCD = SCD / AMF). The tropospheric AMF is calculated at 438 nm by using look-up tables (in most retrieval algorithms) or online radiative transfer modeling (in POMINO) driven by ancillary parameters, which act as the dominant source of errors in retrieved NO_2 VCD data over polluted areas (Boersma et al., 2007; Lin et al., 2014b, 2015; Lorente et al., 2017).

Our POMINO algorithm focuses on the tropospheric AMF calculation over China and nearby regions, taking the tropospheric SCD (Dirksen et al., 2011) from DOMINO v2 (Boersma et al., 2011). POMINO improves upon the DOMINO v2 algorithm in the treatment of aerosols, surface reflectance, online radiative transfer calculations, spatial resolution of NO_2, temperature and pressure vertical profiles, and consistency between cloud and NO_2 retrievals (Lin et al., 2014b, 2015). In brief, we use the parallelized LIDORT-driven AMFv6 package to derive both cloud parameters and tropospheric NO_2 AMFs for individual OMI pixels online. NO_2 vertical profiles, aerosol optical properties and aerosol vertical profiles are taken from the nested GEOS-Chem model over Asia (0.667 ° long. × 0.5° lat. before May 2013 and 0.3125 ° long. × 0.25 ° lat. afterwards), and pressure and temperature profiles are taken from the GEOS-5 and GEOS-FP assimilated meteorological fields that drive GEOS-Chem simulations. Model aerosols are further adjusted by satellite data (see below). We adjust the pressure profiles based on the difference in elevation between the pixel center and the matching model grid cell (Zhou et al., 2010). We also account for the effects of surface bidirectional reflectance distribution function (BRDF) (Lin et al., 2014b; Zhou et al., 2010) by taking three kernel parameters (isotropic, volumetric and geometric) from the MODIS MCD43C2 data set at 440 nm (Lucht et al., 2000).

删除的内容:

删除的内容: will

删除的内容: at 439 nm

删除的内容: nearly

删除的内容: , improved surface elevation

删除的内容: and other aspects

删除的内容:

删除的内容: without use of look-up tables

删除的内容:

删除的内容:

As a prerequisite to the POMINO NO_2 retrieval, clouds are retrieved through the O_2-O_2 algorithm (Acarreta et al., 2004; Stammes et al., 2008) with O_2-O_2 SCDs from OMCLDO2, and with pressure, temperature, surface reflectance, aerosols and other ancillary information consistent with the NO_2 retrieval. Note that the treatment of cloud scattering (as "effective" Lambertian reflector, as in other NO_2 algorithms) is different from the treatment of aerosol scattering/absorption (vertically resolved based on the Mie scheme).

POMINO uses the temporally and spatially varying aerosol information, including AOD, single scattering albedo (SSA), phase function and vertical profiles from GEOS-Chem simulations. POMINO v1.1 (this work) further uses CALIOP data to constrain the shape of aerosol vertical extinction profile. We run the model at a resolution of 0.3125° long. × 0.25° lat. before May 2013 and 0.667° long. × 0.5° lat. afterwards, as determined by the resolution of the driving meteorological fields. We then regrid the finer resolution model results to 0.667° long. × 0.5° lat., to be consistent with the CALIOP data grid. We then sample the model data at times and locations with valid CALIOP data at 532 nm to establish the model monthly climatology.

For any month in a grid cell, we divide the CALIOP monthly climatology of aerosol extinction profile shape by model climatological profile shape to obtain a unitless scaling profile (Eq. 1), and apply this scaling profile to all days of that month in all years (Eq. 2). Such a climatological adjustment is based on the assumption that systematic model limitations are month-dependent and persist over the years and days (e.g., a too strong vertical gradient, see Sect. 3.3). Although this monthly adjustment means discontinuity on the day-to-day basis (e.g., from the last day of a month to the first day of the next month), such discontinuity does not significantly affect the NO_2 retrieval, based on our sensitivity test.

删除的内容: the
删除的内容: al is done
带格式的: 下标
删除的内容: It should be noticed
删除的内容: s
带格式的: 下标
删除的内容: scattering by clouds and
删除的内容: s in tropospheric AMF calculation are different. The cloud are treated as lambert reflector while Mie scattering scheme is used for aerosols in RTM calculations
删除的内容:
删除的内容:
删除的内容:
删除的内容: 2
删除的内容: 3
带格式的: 下标
删除的内容: significantly

In Eqs. 1 and 2, E^{C} represents the CALIOP climatological aerosol extinction coefficient, E^{G} the GEOS-Chem extinction, E^{Gr} the post-scaling model extinction, and R the scaling profile. The subscript *i* denotes a grid cell, *k* a vertical layer, *d* a day, *m* a month, and *y* a year. Note that in Eq. 1, the extinction coefficient at each layer is normalized relative to the maximum value of that profile. This procedure ensures that the scaling is based on the relative shape of the extinction profile and is thus independent of the accuracies of CALIOP and GEOS-Chem AOD. We keep the absolute AOD value of GEOS-Chem unchanged in this step.

$$R_{i,k,m} = \frac{E^{C}_{i,k,m}/\max(E^{C}_{i,k,m})}{E^{G}_{i,k,m}/\max(E^{G}_{i,k,m})} \quad (1)$$

$$E^{Gr}_{i,k,d,m,y} = E^{G}_{i,k,d,m,y} \times R_{i,k,m} \quad (2)$$

In POMINO, the GEOS-Chem AOD are further constrained by a MODIS/Aqua Collection 5.1 monthly AOD dataset compiled on the model grid (Lin et al., 2014b, 2015). POMINO v1.1 uses the Collection 5.1 AOD data before May 2013 and Collection 6 data afterwards. For adjustment, model AOD are projected to a 0.667° long. × 0.5° lat. grid and then sampled at times and locations with valid MODIS data (Lin et al., 2015). As shown in Eq. 3, τ^{M} denotes MODIS AOD, τ^{G} GEOS-Chem AOD, and τ^{Mr} post-adjustment model AOD. The subscript *i* denotes a grid cell, *d* a day, *m* a month, and *y* a year. This AOD adjustment ensures that in any month, monthly mean GEOS-Chem AOD is the same as MODIS AOD while the modeled day-to-day variability is kept.

$$\tau^{Gr}_{i,d,m,y} = \frac{\tau^{M}_{i,m,y}}{\tau^{G}_{i,m,y}} \times \tau^{G}_{i,d,m,y} \quad (3)$$

Equations 4–5 show the complex effects of aerosols in calculating the AMF for any pixel. The AMF is the linear sum of tropospheric layer contributions to the slant

删除的内容: Actually, the correction to model simulated aerosol extinction profiles are main restricted by observation. CALIOP observation are only one highly spatialtemporal coverage data we can find.

删除的内容: 2

删除的内容: 3

删除的内容:

删除的内容: 2

删除的内容: 2

删除的内容: 3

删除的内容:

删除的内容: 4

删除的内容: 4

删除的内容: 5

删除的内容: 6

column weighted by the vertical subcolumns (Eq. 4). The box AMF, amf_k, describes the sensitivity of NO_2 SCD to layer k, and $x_{a,k}$ represent the subcolumn of layer k from a priori NO_2 profile. The l represent the first integrated layer, which is the layer above the ground for clear sky, or the layer above cloud top for cloudy sky. The t represent the tropopause layer. POMINO assumes the independent pixel approximation (IPA) (Martin et al., 2002; Boersma et al., 2002). This means that the calculated AMF for any pixel consists of a fully cloudy-sky portion (AMF_{clr}) and a fully clear-sky portion (AMF_{cld}), with weights based on the cloud radiance fraction ($\mathrm{CRF} = (1 - \mathrm{CF}) \cdot \mathrm{A_{clr}} + \mathrm{CF} \cdot \mathrm{A_{cld}}$, $\mathrm{A_{clr}}$, $\mathrm{A_{cld}}$ are radiance from the clear-sky part and cloudy part of the pixel, respectively.) (Eq. 5). AMF_{cld} is affected by above-cloud aerosols, and AMF_{clr} is affected by aerosols in the entire column. Also, aerosols affect the retrieval of CRF. Thus, the improvement of aerosol vertical profile in POMINO v1.1 affects all the three quantities in Eq. 5 and thus leads to complex impacts on retrieved NO_2 VCD.

$$\mathrm{AMF} = \frac{\sum_l^t amf_k x_{a,k}}{\sum_l^t x_{a,k}} \quad (4)$$

$$\mathrm{AMF} = \mathrm{AMF}_{cld} \cdot \mathrm{CRF} + \mathrm{AMF}_{clr} \cdot (1 - \mathrm{CRF}) \quad (5)$$

2.3 OMI pixel selection to evaluate POMINO v1.1, POMINO, DOMINO v2 and QA4ECV

We exclude OMI pixels affected by row anomaly (Schenkeveld et al., 2017) or with high albedo caused by icy/snowy ground. To screen out cloudy scenes, we choose pixels with CRF below 50% (effective cloud fraction is typically below 20%) in POMINO.

The selection of CRF threshold influences the validity of pixels. The “effective” CRF in DOMINO implicitly includes the influence of aerosols. In POMINO, the aerosol

删除的内容: 5

删除的内容: CRF

删除的内容: 6

删除的内容: whole

删除的内容: 6

删除的内容: 5

删除的内容: 6

删除的内容: *and*

contribution is separated from that of the clouds, resulting in a lower CRF than for DOMINO. The CRF differs insignificantly between POMINO and POMINO v1.1, because the same AOD and other non-aerosol ancillary parameters are used in the retrieval process. Using the CRF from POMINO instead of DOMINO or QA4ECV for cloud screening means that the number of "valid" pixels in DOMINO increases by about 25%, particularly because much more pixels with high pollutant (aerosol and NO_2) loadings are now included. This potentially reduces the sampling bias (Lin et al., 2014b, 2015), and the ensemble of pixels now includes scenes with high "aerosol radiative fractions". Further research is needed to fully understand how much these high-aerosol scenes may be subject to the same screening issues as the cloudy scenes. Nevertheless, the limited evidence here and in Lin et al. (2014b, 2015) suggests that including these high-aerosol scenes does not affect the accuracy of NO_2 retrieval.

删除的内容: but

删除的内容: the drawback is that

删除的内容: ing

删除的内容: although

2.4 MAX-DOAS data

We use MAX-DOAS measurements at three suburban or urban sites in East China, including one urban site at the Institute of Atmospheric Physics (IAP) in Beijing (116.38° E, 39.38 ° N), one suburban site in Xianghe County (116.96° E, 39.75 ° N) to the south of Beijing, and one urban site in the Wuxi City (120.31° E, 31.57 ° N) in the Yangzi River delta (YRD). Figure 1 shows the locations of these sites overlaid with POMINO v1.1 NO_2 VCDs in August 2012. Table 1 summarizes the information of MAX-DOAS measurements.

删除的内容: 2

删除的内容: 2

The instruments in IAP and in Xianghe were designed at BIRA-IASB (Clémer et al., 2010). Such an instrument is a dual-channel system composed of two thermally regulated grating spectrometers, covering the ultraviolet (300–390 nm) and visible (400–720 nm) wavelengths. It measures scattered sunlight every 15 minutes at nine elevation angles: 2° , 4° , 6° , 8° , 10° , 12° , 15° , 30° , and 90° . The telescope of the instrument is pointed to the north. The data are analyzed following

Hendrick et al. (2014). The Xianghe suburban site is influenced by pollution from the surrounding major cities like Beijing and Tianjin. At Xianghe, MAX-DOAS data are data are continuously available since early 2011, and data in 2012 are used here for comparison with OMI products. At IAP, MAX-DOAS data are available in 2008 and 2009 (Table 1), thus for comparison purposes we process OMI products to match the MAX-DOAS times.

删除的内容: 2

Located on the roof of an 11-story building, the instrument at Wuxi was developed by Anhui Institute of Optics and Fine Mechanics (AIOFM) (Wang et al., 2015, 2017a). Its telescope is pointed to the north and records at five elevation angles (5°, 10°, 20°, 30° and 90°). Wuxi is a typical urban site affected by heavy NO_x and aerosol pollution. The measurements used here are analyzed in Wang et al. (2017a). Data are available in 2012 for comparison with OMI products.

When comparing the four OMI products against MAX-DOAS observations, temporal and spatial inconsistency in sampling is inevitable. The spatial inconsistency, together with the substantial horizontal inhomogeneity in NO_2, might be more important than the influence of temporal inconsistency (Wang et al., 2017b). The influence of the horizontal inhomogeneity was suggested to be about 10–30% for MAX-DOAS measurements in Beijing (Lin et al., 2014b; Ma et al., 2013) and 10–15% for less polluted locations like Tai'an, Mangshan and Rudong (Irie et al., 2012). Following previous studies (Lin et al., 2014b; Wang et al., 2015, 2017b), we average MAX-DOAS data within 2 h of the OMI overpass time, and we select OMI pixels within 25 km of a MAX-DOAS site whose viewing zenith angle is below 30°. To exclude local pollution events near the MAX-DOAS site (such as the abrupt increase of NO_2 caused by the pass of consequent vehicles during a very short period), the standard deviation of MAX-DOAS data within 2 h should not exceed 20% of their

删除的内容: three

mean value (Lin et al., 2014b). We elect not to spatially average the OMI pixels because they can, to some degree, reflect the spatial variability in NO_2 and aerosols.

We further exclude MAX-DOAS data in cloudy conditions, as clouds can cause large uncertainties in MAX-DOAS and OMI data. To find the actual cloudy days, we use MODIS/Aqua cloud fraction data, MODIS/Aqua Level-3 corrected reflectance (true color) data at the 1^0 x 1^0 resolution, and current weather data observed from the nearest ground meteorological station (indicated by the black triangles in Fig. 1b). Since there is only one meteorological station available near the Beijing area, it is used for both IAP and Xianghe MAX-DOAS sites. We first use MODIS/Aqua corrected reflectance (true color) to distinguish clouds from haze. For cloudy days determined by the reflectance checking, we examine both the MODIS/Aqua cloud fraction data and the meteorological station cloud records, considering that MODIS/Aqua cloud fraction data may be missing or have a too coarse horizontal resolution to accurately interpret the cloud conditions at the MAX-DOAS site. We exclude MAX-DOAS NO_2 data if the MODIS/Aqua cloud fraction is larger than 60% and the meteorological station reports a “BROKEN” (cloud fraction ranges from 5/8 to 7/8) or “OVERCAST” (full cloud cover) sky. For the three MAX-DOAS sites together, this leads to 49 days with valid data out of 64 days with pre-screening data.

We note here that using cloud fraction data from MODIS/Aqua or MAX-DOAS (for Xianghe only, see Gielen et al., 2014) alone to screen cloudy scenes may not be appropriate on heavy-haze days. For example, on 8th January, 2012, MODIS/Aqua cloud fraction is about 70–80% over the North China Plain and MAX-DOAS at Xianghe suggests the presence of “thick clouds”. However, both the meteorological station and MODIS/Aqua corrected reflectance (true color) product suggest that the North China Plain was covered by a thick layer of haze. Consequently, this day was excluded from the analysis.

删除的内容: to some degree

删除的内容: 2

3. Monthly climatology of aerosol extinction profiles from CALIOP and GEOS-Chem

3.1 CALIOP monthly climatology

The aerosol layer height (ALH) is a good indicator to what extent aerosols are mixed vertically (Castellanos et al., 2015). As defined in Eq. A1 in Appendix B, the ALH is the average height of aerosols weighted by vertically resolved aerosol extinction. Figure 2a shows the spatial distribution of our CALIOP ALH climatology in each season. At most places, the ALH reaches a maximum in spring or summer and a minimum in fall or winter. The lowest ALH in fall and winter can be attributed to heavy near-surface pollution and weak vertical transport. The high values in summer are related to strong convective activities. Over the north, the high values in spring are partly associated with Asian dust events, due to high surface winds and dry soil in this season (Huang et al., 2010; Proestakis et al., 2017; Wang et al., 2010), which also affects the oceanic regions via atmospheric transport. The springtime high ALH over the south may be related to the transport of carbonaceous aerosols from Southeast Asian biomass burning (Jethva et al., 2016). Averaged over the domain, the seasonal mean ALHs are 1.48 km, 1.43 km, 1.27km, 1.18 km in spring, summer, fall and winter.

删除的内容: 3

Figure 3a,b further shows the climatological monthly variations of ALH averaged over Northern East China (the anthropogenic source region shown in orange in Fig. 1a) and Northwest China (the dust source region shown in yellow in Fig. 1a). The two regions exhibit distinctive temporal variations. Over Northern East China, the ALH reaches a maximum in April (~1.53 km) and a minimum in December (~1.14 km). Over Northwest China, the ALH peaks in August (~1.59km) because of strongest convection (Zhu et al., 2013), although the springtime ALH is also high.

删除的内容: 4

删除的内容: 2

删除的内容: 2

Figure 4a shows the climatological seasonal regional average vertical profiles of aerosol extinction over Northern East China. Here, the aerosol extinction increases from the ground level to a peak at about 300–600 m (season dependent), above which it decreases gradually. The height of peak extinction is lowest in winter, consistent with a stagnant atmosphere, thin mixing layer, and increased emissions (from residential and industrial sectors). The large error bars (horizontal lines in different layers, standing for 1 standard deviation) indicate strong spatiotemporal variability of aerosol extinction.

Over Northwest China (Fig. 5a), the column total aerosol extinction is much smaller than that over Northern East China (Fig. 4a), due to lower anthropogenic sources and dominant natural dust emissions. Vertically, the decline of extinction from the peak-extinction height to 2 km is also much more gradual than the decline over Northern East China, indicating stronger lifting of surface emitted aerosols. In winter, the column total aerosol extinction is close to the high value in dusty spring, whereas the vertical gradient of extinction is strongest among the seasons. This reflects the high anthropogenic emissions in parts of Northwest China, which have been rapidly increasing in the 2000s due to relatively weak emission control supplemented by growing activities of relocation of polluted industries from the eastern coastal regions (Cui et al., 2016; Zhao et al., 2015).

Overall, the spatial and seasonal variations of CALIOP aerosol vertical profiles are consistent with changes in meteorological conditions, anthropogenic sources, and natural emissions. The data will be used to evaluate and adjust GEOS-Chem simulation results in Sect. 3.2. A comparison of our CALIOP dataset with NASA's official Level-3 data is presented in Appendix C.

3.2 Evaluation of GEOS-Chem aerosol extinction profiles

删除的内容: 5

删除的内容: 6

删除的内容: 5

删除的内容: 3

删除的内容: C

删除的内容: *3.2 Comparison to NASA CALIOP monthly climatology*

We compare our gridded climatological profiles to NASA CALIOP Version 3 Level-3 all-sky monthly profiles at 532 nm (Winker et al. 2013). The NASA Level-3 data has a horizontal resolution of 2° lat. × 5° lon. and a vertical resolution of 60 m (from -0.5 to 12 km above sea level). We combine NASA monthly data over 2007–2015 to construct a monthly climatology for comparison with our own compilation. We only choose aerosol extinction data in the troposphere with error less than 0.15 (the valid range given in the CALIOP dataset). If the number of valid monthly profiles in a grid cell is less than five (i.e., for the same month in five out of the nine years), then we exclude data in that grid cell; see the dark gray grid cells in Fig. 23c.

Several methodological differences exist between generating our and NASA CALIOP datasets. First, the two datasets have different horizontal resolutions. Also, we sample all valid CALIOP pixels within 1.5° of a grid cell center, whereas the NASA dataset samples all valid pixels within a grid cell. Besides, our CALIOP dataset involves several steps of horizontal interpolation, for purposes of subsequent cloud and NO_2 retrievals, which is not done in the NASA dataset. In addition, we match CALIOP data vertically to the GEOS-Chem vertical resolution, whereas the NASA dataset maintains the original resolution.

... [4]

删除的内容: *3*

Figure 2b shows the spatial distribution of seasonal ALHs simulated by GEOS-Chem. The model captures the spatial and seasonal variations of CALIOP ALH (Fig. 2a) to some degree, with an underestimate by about 0.3 km on average. The spatial correlation between CALIOP (Fig. 2a) and GEOS-Chem (Fig. 2b) ALH is 0.37 in spring, 0.57 in summer, 0.40 in fall, and 0.44 in winter. The spatiotemporal consistency and underestimate is also clear from the regional mean monthly ALH data in Fig. 3 – the temporal correlation between GEOS-Chem and CALIOP ALH is 0.90 in Northern East China and 0.97 in Northwest China.

Figures 4a and 5a show the GEOS-Chem simulated 2007–2015 monthly climatological vertical profiles of aerosol extinction coefficient over Northern East China and Northwest China, respectively. Over Northern East China (Fig. 4a), the model (red line) captures the vertical distribution of CALIOP extinction (black line) below the height of 1 km, despite a slight underestimate in the magnitude of extinction and an overestimate in the peak-extinction height. From 1 to 5 km above the ground, the model substantially overestimates the rate of decline in extinction coefficient with increasing altitude. Across the seasons, GEOS-Chem underestimates the magnitude of aerosol extinction by up to 37% (depending on the height). Over Northwest China (Fig. 5a), GEOS-Chem has an underestimate in all seasons, with the largest bias by about 80% in winter likely due to underestimated water-soluble aerosols and dust emissions (Li et al., 2016; Wang et al., 2008a).

Since the POMINO v1.1 algorithm uses MODIS AOD to adjust model AOD, it only uses the CALIOP aerosol extinction profile shape to adjust the modeled shape (Eqs. 1 and 2). Figures 4b and 4b show the vertical shapes of aerosol extinction, averaged across all profiles in each season over Northern East China and Northwest China, respectively. Over Northern East China (Fig. 4b), GEOS-Chem underestimates the CALIOP values above 1 km by 52–71%. This underestimate leads to a lower ALH,

consistent with the finding by van Donkelaar et al. (2013) and Lin et al. (2014b). Over Northwest China (Fig. 5b), the model also underestimates the CALIOP values above 1 km by 50–62%. These results imply the importance of correcting the modeled aerosol vertical shape prior to cloud and NO_2 retrievals.

4. Effects of aerosol vertical profile improvement on cloud retrieval in 2012

Figure 6a, b shows the monthly average ALH and cloud top height (CTH, corresponding to cloud pressure, CP) over Northern East China and Northwest China in 2012. In order to discuss the CTH, only cloudy days are analyzed here, by excluding days with zero cloud fraction (CF = 0, clear-sky cases) in POMINO. Although "clear sky" is used sometimes in the literature to represent low cloud coverage (e.g., CF < 0.2 or CRF < 0.5, Boersma et al., 2011; Chimot et al., 2016), here it strictly means CF = 0 while "cloudy sky" means CF > 0. About 62.7% of days contain non-zero fractions of clouds over Northern East China, and the number is 59.1% for Northwest China. The CF changes from POMINO to POMINO v1.1 (i.e., after aerosol vertical profile adjustment) are negligible (within ±0.5%, not shown) due to the same values of AOD and SSA used in both products. This is because overall CF is mostly driven by the continuum reflectance at 475 nm (mainly determined by AOD and surface reflectance, which remain unchanged), which is independent of aerosol profile but CTH is driven by the O_2-O_2 SCD, which is itself impacted by ALH.

Figure 6a, b shows that over the two regions, the CTH varies notably from one month to another, whereas the ALH is much more stable across the months. Over Northern East China, the ALH increases by 0.52 km from POMINO (orange dashed line) to POMINO v1.1 (orange solid line) due to the CALIOP-based monthly climatological adjustment. The increase in ALH means a stronger "shielding" effect of aerosols on the O_2-O_2 absorbing dimer, which, in turn, results in a reduced CTH by 0.69 km on average. For POMINO over Northern East China (Fig. 6a), the retrieved clouds

删除的内容: 6

删除的内容: 7

删除的内容: 7

删除的内容: 7

usually extend above the aerosol layer, i.e., the CTH (grey dashed line) is much larger than the ALH (orange dashed line). Using the CALIOP climatology in POMINO v1.1 results in the ALH higher than the CTH in fall and winter. The more elevated ALH is consistent with the finding of Jethva et al. (2016) that a significant amount of absorbing aerosols resides above clouds over Northern East China based on 11-year (2004–2015) OMI near-UV observations.

The CTH in Northwest China is much lower than in Northern East China (Fig. 6a versus 7b). This is because the dominant type of actual clouds is (optically thin) cirrus over western China (Wang et al., 2014), which is interpreted by the O_2-O_2 cloud retrieval algorithm as reduced CTH (with cloud base from the ground). The reduction in CTH from POMINO to POMINO v1.1 over Northwest China is also smaller than the reduction over Northern East China, albeit with a similar enhancement in ALH, due to lower aerosol loadings (Fig. 6c versus 6d).

删除的内容: 7

删除的内容: 7

删除的内容: 7

Figure 7g,h presents the relative change in CP from POMINO to POMINO v1.1 as a function of AOD (binned at an interval of 0.1) and changes in ALH from POMINO to POMINO v1.1 (ΔALH, binned every 0.2 km) across all pixels in 2012 over Northern East China. Results are separated for low cloud fraction (CF < 0.05 in POMINO, Fig. 7g) and modest cloud fraction (0.2 < CF < 0.3, Fig. 7h). The median of the CP changes for pixels within each AOD and ΔALH bin is shown. Figure 7e,f presents the corresponding numbers of occurrence under the two cloud conditions.

删除的内容: 8

删除的内容: 8

删除的内容: 8

删除的内容: 8

Figure 7 shows that over Northern East China, the increase in ALH is typically within 0.6 km for the case of CF < 0.05 (Fig. 7e), and the corresponding increase in CP is within 6% (Fig. 7g). In this case, the average CTH (2.95 km in POMINO versus 1.58 km in POMINO v1.1) becomes much lower than the average ALH (1.06 km in POMINO versus 1.98 km in POMINO v1.1). For the case with CF between 0.2 and 0.3, the increase in ALH is within 1.2 km for most scenes (Fig. 7f), which leads to a

删除的内容: 8

删除的内容: 8

删除的内容: 8

删除的内容: 8

CP change of 2% (Fig. 7h), much smaller than the CP change for CF < 0.05 (Fig. 7g). This is partly because the larger the CF is, the smaller a change in CF is required to compensate for the ΔALH in the O_2-O_2 cloud retrieval algorithm. Furthermore, with 0.2 < CF < 0.3, the mean value of CTH is much higher than ALH in both POMINO (2.76 km for CTH versus 1.13km for ALH) and POMINO v1.1 (2.60km for CTH versus 2.09 km for ALH), thus a large portion of clouds are above aerosols so that the change in CP is less sensitive to ΔALH. We find that the summertime data contribute the highest portion (36.5%) to the occurrences for 0.2 < CF < 0.3.

删除的内容: 8

删除的内容: 8

For Northwest China (not shown), the dependence of CP changes to AOD and ΔALH is similar to that for Northern East China. In particular, the CP change is within 10% on average for the case of CF < 0.05 and 1.5% for the case of 0.2 < CF < 0.3.

5. Effects of aerosol vertical profile improvement on NO_2 retrieval in 2012

Figure 7a presents the percentage changes in clear-sky NO_2 VCD from POMINO to POMINO v1.1 as a function of binned AOD and ΔALH over Northern East China. Here, clear-sky pixels are chosen based on CF = 0 in POMINO. In any AOD bin, an increase in ΔALH leads to an enhancement in NO_2. And for any ΔALH, the change in VCD is greater (smaller) when AOD becomes larger (smaller), which indicates that the NO_2 retrieval is more sensitive to ALH in high aerosol loading cases. Clearly, the change in NO_2 is not a linear function of AOD and ΔALH.

删除的内容: 8

For cloudy scenes (Fig. 7b,c, cloud data are based on POMINO), the change in NO_2 VCD is less sensitive to AOD and ΔALH. This is because the existence of clouds limits the optical effect of aerosols on tropospheric NO_2. Figure 6a presents the nitrogen layer height (NLH, defined as the average height of model simulated NO_2 weighted by its volume mixing ratio in each layer) in comparison to the ALH and CLH over Northern East China. The figure shows that the POMINO v1.1 CTH is

删除的内容: 8

删除的内容: 7

higher than the NLH in all months and higher than the ALH in warm months, which means a "shielding" effect on both NO_2 and aerosols.

Over Northwest China (not shown), the changes in clear-sky NO_2 VCD are within 9% for most cases, which are much smaller than over Eastern China (within 18%). This is because the NLH is much higher than the CLH and ALH (Fig. 6b) in absence of surface anthropogenic emissions.

We convert the valid pixels into monthly mean Level-3 values datasets on a 0.25° long. × 0.25° lat. grid. Figure 8a,b compares the seasonal spatial variations of NO_2 VCD in POMINO v1.1 and POMINO in 2012. In both products, NO_2 peaks in winter due to the longest lifetime and highest anthropogenic emissions (Lin, 2012). NO_2 also reaches a maximum over Northern East China as a result of substantial anthropogenic sources. From POMINO to POMINO v1.1, the NO_2 VCD increases by 3.4% (-67.5–41.7%) in spring for the domain average (range), 3.0% (-59.5–34.4%) in summer, 4.6% (-15.3–39.6%) in fall and 5.3% (-68.4–49.3%) in winter. The NO_2 change is highly dependent on the location and season. The increase over Northern East China is largest in winter, wherein the positive value for ΔALH implies that elevated aerosol layers "shield" the NO_2 absorption.

6. Evaluating satellite products using MAX-DOAS data

We use MAX-DOAS data, after cloud screening (Sect. 2.4), to evaluate DOMNO v2, QA4ECV, POMINO and POMINO v1.1. The scatterplots in Fig. 9a-d compare the NO_2 VCDs from 162 OMI pixels on 49 days with their MAX-DOAS counterparts. Different colors differentiate the seasons. The high values of NO_2 VCD (> 30 × 10^{15} molec. cm^{-2}) occur mainly in fall (blue) and winter (black). POMINO v1.1 and POMINO capture the day-to-day variability of MAX-DOAS data, i.e., R^2 = 0.804 and 0.799, respectively. The normalized mean bias (NMB) of POMINO v1.1 relative to

删除的内容: 7

删除的内容: 9

删除的内容: mean

删除的内容: that better

删除的内容: 10a-c

MAX-DOAS data (-3.4%) is smaller than the NMB of POMINO (-9.6%). Also, the reduced major axis (RMA) regression shows that the slope for POMINO v1.1 (0.95) is closer to unity than the slope for POMINO (0.78). When all OMI pixels in a day are averaged (Fig. 9e,f), the correlation across the total of 49 days further increase for both POMINO v1.1 (R^2 = 0.89) and POMINO (R^2 = 0.86), whereas POMINO v1.1 still has a lower NMB (-3.7%) and better slope (0.96) than POMINO (-10.4% and 0.82, respectively). These results suggest that correcting aerosol vertical profiles at least on a climatology basis, already leads to a significant improved NO_2 retrieval from OMI.

Figure 9 shows that DOMINO v2 is correlated with MAX-DOAS (R^2 = 0.68 in Fig. 9c and 0.75 in Fig. 9g) but not as strong as POMINO and POMINO v1.1 for all days. The discrepancy between DOMINO v2 and MAX-DOAS is particularly large for very high NO_2 values (> 70 × 10^{15} molec. cm^{-2}). The R^2 for QA4ECV (0.75 in Fig. 9d and 0.82 in Fig. 9h) is slightly better than DOMINO, but the NMB is higher (-22.0% and -22.7%) and the slope drops to 0.66. These results are consistent with the finding of Lin et al. (2014b, 2015) that explicitly including aerosol optical effects improves the NO_2 retrieval.

Table 2 further shows the comparison statistics for 27 haze days. The haze days are determined when both the ground meteorological station data and MODIS/Aqua corrected reflectance (true color) data indicate a haze day. The table also lists AOD, SSA, CF and MAX-DOAS NO_2 VCD, as averaged over all haze days. A large amount of absorbing aerosols occurs on these haze days (AOD = 1.13, SSA = 0.90). The average MAX-DOAS NO_2 VCD reaches 51.92 × 10^{15} molec. cm^{-2}. Among the four satellite products, POMINO v1.1 has the highest R^2 (0.76) and the lowest bias (4.4%) with respect to MAX-DOAS, whereas DOMINO v2 and QA4ECV reproduce the variability to a limited extent (R^2 = 0.38 and 0.34, respectively). This is consistent

删除的内容: 11d,e

删除的内容:

批注 [FB3]: Please clarify if this is now for haze days, or all days.

删除的内容: 10c,f

删除的内容: 10

删除的内容: 45

删除的内容: 10

删除的内容: f

删除的内容: well

带格式的: 上标

删除的内容: much

删除的内容: 4

删除的内容: three

删除的内容: s

with the previous finding that the accuracy of DOMINO v2 is reduced for polluted, aerosol-loaded scenes (Boersma et al., 2011; Chimot et al., 2016; Kanaya et al., 2014; Lin et al., 2014b).

Table 3 shows the comparison statistics for 36 cloud-free days (CF = 0 in POMINO and AOD = 0.60 on average). Here, POMINO v1.1, POMINO and DONIMO v2 do not show large differences in R^2 (0.53–0.56) and NMB (20.8–29.4%) with respect to MAX-DOAS. QA4ECV has a higher R^2 (0.63) and a lower NMB (-5.83%), presumably reflecting the improvements in this community best practices approach, at least in mostly cloud-free situations. However, the R^2 values for POMINO and POMINO v1.1 are much smaller than the R^2 values in haze days, whereas the opposite changes are true for DOMINO v2 and QA4ECV. Thus, for this limited set of data, the changes from DOMINO v2 and QA4ECV to POMINO and POMINO v1.1 mainly reflect the improved aerosol treatment in hazy scenes. Further research may use additional MAX-DOAS datasets to evaluate the satellite products more systematically.

7. Conclusions

This paper improves upon our previous POMINO algorithm (Lin et al., 2015) to retrieve the tropospheric NO_2 VCDs from OMI, by compiling a 9-year (2007–2015) CALIOP monthly climatology of aerosol vertical extinction profiles to adjust GEOS-Chem aerosol profiles used in the NO_2 retrieval process. The improved algorithm is referred to as POMINO v1.1. Compared to monthly climatological CALIOP data over China, GEOS-Chem simulations tend to underestimate the aerosol extinction above 1 km, as characterized by an underestimate in ALH by 300–600 m (seasonal and location dependent). Such a bias is corrected in POMINO v1.1 by dividing, for any month and grid cell, the CALIOP monthly climatological profile by

删除的内容: c

带格式的: 段落间距段后: 10 磅, 图案: 清除

删除的内容: 5

删除的内容: the three OMI products

删除的内容: and NMB (20.8–29.4%)

带格式的: 字体: (中文) +中文正文 (宋体), 上标

删除的内容: that in the cloud-free cases the ensemble of algorithms improves the retrieval results

删除的内容: is

删除的内容: ↵

删除的内容: product

the model climatological profile to obtain a scaling profile and then applying the scaling profile to model data in all days of that month in all years.

The aerosol extinction profile correction leads to an insignificant change in CF from POMINO to POMINO v1.1, since the AOD and surface reflectance are unchanged. In contrast, the correction results in a notably increase in CP (i.e., a decrease in CTH), due to lifting of aerosol layers. The CP changes are generally within 6% for scenes with low cloud fraction (CF < 0.05 in POMINO), and within 2% for scenes with modest cloud fraction (0.2 < CF < 0.3 in POMINO).

The NO_2 VCDs increase from POMINO to POMINO v1.1 in most cases due to lifting of aerosol layers that enhances the "shielding" of NO_2 absorption. The NO_2 VCD increases by 3.4% (-67.5–41.7%) in spring for the domain average (range), 3.0% (-59.5–34.4%) in summer, 4.6% (-15.3–39.6%) in fall and 5.3% (-68.4–49.3%) in winter. The NO_2 changes highly season and location dependent, and are most significant for wintertime Northern East China.

Further comparisons with independent MAX-DOAS NO_2 VCD data for 162 OMI pixels in 49 days show good performance of both POMINO v1.1 and POMINO in capturing the day-to-day variation of NO_2 (R^2=0.80, n=162), compared to DOMINO v2 (R^2=0.67) and the new QA4ECV product (R^2=0.75). The NMB is smaller in POMINO v1.1 (-3.4%) than in POMINO (-9.6%), with a slightly better slope (0.804 versus 0.784). On hazy days with high aerosol loadings (AOD = 1.13 on average), POMINO v1.1 has the highest R^2 (0.76) and the lowest bias (4.4%) whereas DOMINO and QA4ECV have difficulty in reproducing the day-to-day variability in MAX-DOAS NO_2 measurements (R^2 = 0.38 and 0.34, respectively). The four products show small differences in R^2 on clear-sky days (CF = 0 in POMINO, AOD = 0.60 on average). Thus the explicit aerosol treatment (in POMINO and POMINO v1.1)

删除的内容: or

删除的内容: has

删除的内容: ,

删除的内容: three

删除的内容: and NMB

and the aerosol vertical profile correction (in POMINO v1.1) improves the NO_2 retrieval especially in hazy cases.

The POMINO v1.1 algorithm is a core step towards our next public release of data product, POMINO v2. This new release will contain a few additional updates, including but not limited to using MODIS Collection 6 Merged 10-km Level-2 AOD data that combine the Dark Target (Levy et al., 2013) and Deep Blue (Sayer et al., 2014) products, as well as MODIS MCD43C2 Collection 6 daily BRDF data. Meanwhile, the POMINO algorithm framework is being applied to the recently launched TropOMI instrument that provides NO_2 information at a much higher spatial resolution (3.5 x 7 km^2). A modified algorithm can also be used to retrieve sulfur dioxide, formaldehyde and other trace gases from TropOMI, for which purposes our algorithm will be available to the community on a collaborative basis. Future research can correct the SSA and NO_2 vertical profile to further improve the retrieval algorithm, and can use more comprehensive independent data to evaluate the resulting satellite products.

Acknowledgements

This research is supported by the National Natural Science Foundation of China (41775115), the 973 program (2014CB441303), the Chinese Scholarship Council, and the EU FP7 QA4ECV project (grant no. 607405).

Appendix A: Introduction to the QA4ECV product

The QA4ECV NO_2 product (http://www.qa4ecv.eu/) builds on a (EU-) consortium best practices approach to retrieve NO_2 from GOME, SCIAMACHY, GOME-2, and OMI. The main contributions are provided by BIRA-IASB, the University of Bremen (IUP), MPIC, KNMI, and Wageningen University. Uncertainties in spectral fitting for NO_2 SCDs and in AMF calculations were evaluated by Zara et al. (2018) and Lorente

删除的内容:

删除的内容: KFB: I think a sentence on the relatively good performance of QA4ECV in non-hazy days would be useful. Your paper adds value to the literature by being one of the first to do a systematic validation of the QA4ECV product! You have already some good indications when the algorithm does fine, and under which circumstances it is biased. This should be highlighted.

删除的内容: (Levy et al., 2013)

批注 [JL4]: citation

删除的内容: (Sayer et al., 2013)

删除的内容: Our POMINO v1.1

删除的内容:

带格式的

带格式的: 标题 1, 左, 段落间距段后: 0 磅, 图案: 清除

删除的内容: The

删除的内容: i

带格式的

带格式的

带格式的: 字体: 非加粗

删除的内容: EU FP7-project Quality Assurance for Essential ... [5]

删除的内容:)

删除的内容: is aim at making rapid judgments on validitiy and ... [6]

删除的内容: is

带格式的: 字体: 非加粗

带格式的: 下标

删除的内容: a kind of

删除的内容: essentially an ensemble data sets of satellite products ... [7]

删除的内容: and

删除的内容: , with a fully traceable quality assurance on all aspects ... [8]

带格式的: 下标

删除的内容: The u

删除的内容: of

删除的内容: algorithms

删除的内容: the

带格式的: 下标

删除的内容: ,

et al. (2017), respectively. QA4ECV contains improved SCD NO_2 data (Zara et al., 2018). Lorente et al., (2017) showed that across the above algorithms, there a structural uncertainty by 42% in the NO_2 AMF calculation over polluted areas. By comparing to our POMINO product, Lorente et al. also showed that the choice of aerosol correction may introduce an additional uncertainty by up to 50% for situations with high polluted cases, consistent with Lin et al. (2014b, 2015) and the findings here. For a complete description of the QA4ECV algorithm improvements, and quality assurance, please see Boersma et al. (2018).

Appendix B: Constructing the CALIOP monthly climatology of aerosol extinction vertical profile

Our use the all-sky Level-2 CALIOP data to construct the Level-3 monthly climatology. We choose the all-sky product instead of clear-sky data, since previous studies indicate that the climatological aerosol extinction profiles are affected insignificantly by the presence of clouds (Koffi et al., 2012; Winker et al., 2013). As we use this climatological data to adjust GEOS-Chem results, choosing all-sky data improves consistency with the model simulation when doing the daily correction.

To select valid pixels, we follow the data quality criteria by Winker et al., (2013) and Amiridis et al., (2015). Only the pixels with Cloud Aerosol Discrimination (CAD) scores between -20 and -100 with extinction Quality Control (QC) flag valued at 0, 1, 18, and 16 are selected. We further discard samples with an extinction uncertainty of 99.9 km^{-1}, which is indicative of unreliable retrieval. We only accept extinction values falling in the range from 0.0 to 1.25, according to CALIOP observation thresholds. Previous studies showed that weakly scattering edges of icy clouds are sometimes misclassified as aerosols (Winker et al., 2013). To eliminate contamination from icy clouds we exclude the aerosol layers above the cloud layer (with layer-top temperature below 0 ℃) when both of them are above 4km (Winker et al., 2013).

删除的内容: ,
删除的内容: The improved
删除的内容: NO_2
带格式的: 下标
删除的内容: shows better performance in
删除的内容: but do not altogether eliminated systematic errors in ththee fitting approach
删除的内容: 42%
删除的内容: of
带格式的: 下标
删除的内容: s
删除的内容: aereas
删除的内容: , and
删除的内容: s
删除的内容: average
删除的内容: of
批注 [JL5]: Revise the format of the reference list
带格式的: 荷兰语
删除的内容: ↵ ↵
带格式的
删除的内容: **The way to c**
带格式的
带格式的
删除的内容: **mean**
带格式的
带格式的
带格式的
删除的内容: **climatology**
带格式的: 字体: 非加粗
已移动(插入) [5]
删除的内容: The way to select the good quality profile mainly
删除的内容: s
已移动(插入) [1]

After the pixel-based screening, we aggregate the CALIOP data at the model grid (0.667° long. x 0.5° lat.) and vertical resolution (47 layers, with 36 layers or so in the troposphere). For each grid cell, we choose the CALIOP pixels within 1.5° of the grid cell center. CALIOP Level-2 data are always presented at the fixed 399 altitudes above sea level. To account for the difference in surface elevation between a CALIOP pixel and the respective model grid cell, we convert the altitude of the pixel to a height above the ground, by using the surface elevation data provided in CALIOP. We then average horizontally and vertically the profiles of all pixels within one model grid cell and layer. We do the regridding day-by-day for all grid cells to ensure that GEOS-Chem and CALIOP extinction profiles are coincident spatially and temporally. Finally, we compile a monthly climatological dataset by averaging over 2007–2015.

已移动(插入) [2]

Figure A1 shows the number of aerosol extinction profiles in each grid cell and 12 x 9 = 108 months that are used to compile the CALIOP climatology, both before and after data screening. Table A1 presents additional information on monthly and yearly bases. On average, there are 165 and 47 aerosol extinction profiles per month per grid cell before and after screening, respectively. In the final 9-year monthly climatology, each grid cell has about 420 aerosol extinction profiles on average, about 28% of the prior-screening profiles. Figure A1 shows that the number of valid profiles decreases sharply over the Tibet Plateau and at higher latitudes (> 43 ° N) due to complex terrain and icy/snowy ground.

删除的内容:

已移动(插入) [3]

As discussed above, we choose the CALIOP pixels within 1.5° of a grid cell center. We test this choice by examining the aerosol layer height (ALH) produced for that grid cell. The ALH is defined as the extinction-weighted height of aerosols (see Eq. A1, where *n* denotes the number of tropospheric layers, ε_i the aerosol extinction at layer *i*, and H_i the layer center height above the ground). We find that choosing pixels within 1.0° of a grid cell center leads to a nosier horizontal distribution of

ALH, owing to the small footprint of CALIOP. On the other hand, choosing 2.0° leads to a too smooth spatial gradient of ALH with local characteristics of aerosol vertical distributions are largely lost. We thus decide that 1.5° is a good balance between noise and smoothness.

$$\mathrm{ALH} = \frac{\sum_{i=1}^{i=n} \varepsilon_i \mathrm{H}_i}{\sum_{i=1}^{i=n} \varepsilon_i} \qquad \text{(A1)}$$

Certain grid cells do not contain sufficient valid observations for some months of the climatological dataset. We fill in missing monthly values of a grid cell using valid data in the surrounding 5 x 5 = 25 grid cells (within ~ 100 km). If the 25 grid cells do not have enough valid data, we use those in the surrounding 7 x 7 = 49 grid cells (within ~ 150 km). A similar procedure is used by Lin et al. (2014b, 2015) to fill in missing values in the gridded MODIS AOD dataset.

For each grid cell in each month, we further correct singular values in the vertical profile. In a month, if a grid cell *i* has an ALH outside mean±1σ of its surrounding 25 or 49 grid cells, we select *i*'s surrounding grid cell *j* whose ALH is the median of *i*'s surrounding grid cells, and use *j*'s profile to replace *i*'s. Whether 25 or 49 surrounding grid cells are chosen depends on the number of valid pixels shown in Fig. A1b. If the number of valid pixels in *i* is below mean–1σ of all grid cells in the whole domain, which is often the case for Tibetan grid cells, we use *i*'s surrounding 49 grid cells; otherwise we use *i*'s surrounding 25 grid cells.

Appendix C. Comparing our and NASA's CALIOP monthly climatology

We compare our gridded climatological profiles to NASA CALIOP Version 3 Level-3 all-sky monthly profiles at 532 nm (Winker et al., 2013). The NASA Level-3 data has a horizontal resolution of 2° lat. × 5° lon. and a vertical resolution of 60 m (from -0.5 to 12 km above sea level). We combine NASA monthly data over 2007–

删除的内容: Certain grid cells do not contain sufficient valid observations for some months of the climatological data set. We fill in missing monthly values of a grid cell using valid data in the surrounding 25 or 49 grid cells.

已移动(插入) [4]

带格式的: 字体: 非加粗

带格式的: 字体: 非加粗

带格式的: 标题 1

2015 to construct a monthly climatology for comparison with our own compilation. We only choose aerosol extinction data in the troposphere with error less than 0.15 (the valid range given in the CALIOP dataset). If the number of valid monthly profiles in a grid cell is less than five (i.e., for the same month in five out of the nine years), then we exclude data in that grid cell; see the dark gray grid cells in Fig. 2c.

Several methodological differences exist between generating our and NASA CALIOP datasets. First, the two datasets have different horizontal resolutions. Also, we sample all valid CALIOP pixels within 1.5^0 of a grid cell center, whereas the NASA dataset samples all valid pixels within a grid cell. Besides, our CALIOP dataset involves several steps of horizontal interpolation, for purposes of subsequent cloud and NO_2 retrievals, which is not done in the NASA dataset. In addition, we match CALIOP data vertically to the GEOS-Chem vertical resolution, whereas the NASA dataset maintains the original resolution.

Figure 2c shows the spatial distribution of ALH in all seasons based on NASA CALIOP Level-3 all-sky monthly climatology. The horizontal resolution of NASA data is much coarser than ours; and NASA data are largely missing over the southwest with complex terrains. We choose to focus on the comparison over East China (the black box in Fig. 1a). Over East China, the two climatology datasets generally exhibit similar spatial patterns of ALH in all seasons (Fig. 2a, c). The NASA dataset suggests higher ALHs than ours over Eastern China, especially in summer, due mainly to differences in the sampling and regridding processes. Figure 3c further compares the monthly variation of ALH between our (black line with error bars) and NASA (blue filled triangles) datasets averaged over East China. The two datasets are consistent in almost all months, indicating that their regional differences are largely smoothed out by spatial averaging.

References

带格式的：图案：清除

带格式的：字体：非加粗

删除的内容：**Appendix C: The introduction to new version of POMINO product**

In our new relased version, several aspect will be update:

1) Use 9-year CALIOP climatology aerosol extinction profile to adjust GEOS-Chem daily aerosol extinction profiles. This is the main update in our new released version, which will also be applied to the retrieval algorithm of newly laughed TropOMI sensor.

2) MODIS Collection 6 Merged 10-km Level-2 AOD product will be used to replace the MODIS Collection 5 Dark Target (DT) product to adjust model simulation. Previous studies has shown various contextual biases exist in C5 version (Levy et al., 2010; Bréon et al., 2011). The C6 product update**s the widely used DT (Levy et al., 2013) and Deep Blue (DB) product (Sayer et al., 2013). It also relased the merged AOD product to provide a more gap-filled data set based on DT, DB and MODIS-derived climatologies of NDVI (Huete et al., 2011).**

3) MODIS MCD43C2 Collection 6 daily BRDF/Albedo Snow-free Model Parameters Daily L3 Global 0.05Deg data set is used to replace C5 8-day averaged data set to account for the daily BRDF effect of surface. There is improved quality and more retrieval at high latitudes and use current day snow status when retrieval in C6.

带格式的

Acarreta, J. R., De Haan, J. F. and Stammes, P.: Cloud pressure retrieval using the O_2-O_2 absorption band at 477 nm, J. Geophys. Res., 109(D5), D05204, doi:10.1029/2003JD003915, 2004.

Amiridis, V., Marinou, E., Tsekeri, A., Wandinger, U., Schwarz, A., Giannakaki, E., Mamouri, R., Kokkalis, P., Binietoglou, I., Solomos, S., Herekakis, T., Kazadzis, S., Gerasopoulos, E., Proestakis, E., Kottas, M., Balis, D., Papayannis, A., Kontoes, C., Kourtidis, K., Papagiannopoulos, N., Mona, L., Pappalardo, G., Le Rille, O. and Ansmann, A.: LIVAS: a 3-D multi-wavelength aerosol/cloud database based on CALIPSO and EARLINET, Atmos. Chem. Phys., 15(13), 7127–7153, doi:10.5194/acp-15-7127-2015, 2015.

Belmonte Rivas, M., Veefkind, P., Boersma, F., Levelt, P., Eskes, H. and Gille, J.: Intercomparison of daytime stratospheric NO2; satellite retrievals and model simulations, Atmos. Meas. Tech., 7(7), 2203–2225, doi:10.5194/amt-7-2203-2014, 2014.

Boersma, K. F., Eskes, H. J. and Brinksma, E. J.: Error analysis for tropospheric NO_2 retrieval from space, J. Geophys. Res. Atmos., 109(D4), n/a-n/a, doi:10.1029/2003JD003962, 2004.

Boersma, K. F., Eskes, H. J., Veefkind, J. P., Brinksma, E. J., van der A, R. J., Sneep, M., van den Oord, G. H. J., Levelt, P. F., Stammes, P., Gleason, J. F. and Bucsela, E. J.: Near-real time retrieval of tropospheric NO2; from OMI, Atmos. Chem. Phys., 7(8), 2103–2118, doi:10.5194/acp-7-2103-2007, 2007.

Boersma, K. F., Eskes, H. J., Dirksen, R. J., van der A, R. J., Veefkind, J. P., Stammes, P., Huijnen, V., Kleipool, Q. L., Sneep, M., Claas, J., Leitão, J., Richter, A., Zhou, Y. and Brunner, D.: An improved tropospheric NO2; column retrieval algorithm for the

带格式的：两端对齐

删除的内容: <sub>

删除的内容: </sub&gt

删除的内容: <sub>

删除的内容: </sub&gt

删除的内容: <sub>

删除的内容: </sub&gt

Ozone Monitoring Instrument, Atmos. Meas. Tech., 4(9), 1905–1928, doi:10.5194/amt-4-1905-2011, 2011a.

Boersma, K.F., Eskes, H. J., Richter, A., De Smedt, I., Lorente, A., Beirle, S., van Geffen, J. H. G. M., Zara, M., Peters, E., Van Roozendael, M., Wagner, T., Maasakkers, J. D., van der A, R. J., Nightingale, J., De Rudder, A., Irie, H., and Pinardi, G.: Improving algorithms and uncertainty estimates for satellite NO_2 retrievals: Results from the Quality Assurance for Essential Climate Variables (QA4ECV) project, amt-2018-200, submitted, 2018.

Bucsela, E. J., Celarier, E. A., Wenig, M. O., Gleason, J. F., Veefkind, J. P., Boersma, K. F. and Brinksma, E. J.: Algorithm for NO2 vertical column retrieval from the ozone monitoring instrument, IEEE Trans. Geosci. Remote Sens., 44(5), 1245–1258, doi:10.1109/TGRS.2005.863715, 2006.

Bucsela, E. J., Krotkov, N. A., Celarier, E. A., Lamsal, L. N., Swartz, W. H., Bhartia, P. K., Boersma, K. F., Veefkind, J. P., Gleason, J. F. and Pickering, K. E.: A new stratospheric and tropospheric NO2; retrieval algorithm for nadir-viewing satellite instruments: applications to OMI, Atmos. Meas. Tech., 6(10), 2607–2626, doi:10.5194/amt-6-2607-2013, 2013.

Castellanos, P., Boersma, K. F. and van der Werf, G. R.: Satellite observations indicate substantial spatiotemporal variability in biomass burning NOx; emission factors for South America, Atmos. Chem. Phys., 14(8), 3929–3943, doi:10.5194/acp-14-3929-2014, 2014.

Castellanos, P., Boersma, K. F., Torres, O. and de Haan, J. F.: OMI tropospheric NO2; air mass factors over South America: effects of biomass burning aerosols, Atmos. Meas. Tech., 8(9), 3831–3849, doi:10.5194/amt-8-3831-2015, 2015.

删除的内容: Boersma, K. F., Eskes, H. J., Dirksen, R. J., van der A, R. J., Veefkind, J. P., Stammes, P., Huijnen, V., Kleipool, Q. L., Sneep, M., Claas, J., Leitão, J., Richter, A., Zhou, Y. and Brunner, D.: An improved tropospheric NO₂ column retrieval algorithm for the Ozone Monitoring Instrument, Atmos. Meas. Tech., 4(9), 1905–1928, doi:10.5194/amt-4-1905-2011, 2011b. KFB: cited twice.

Boersma, K. F., Eskes, H. J., Dirksen, R. J., van der A, R. J., Veefkind, J. P., Stammes, P., Huijnen, V., Kleipool, Q. L., Sneep, M., Claas, J., Leitão, J., Richter, A., Zhou, Y. and Brunner, D.: An improved tropospheric NO₂ column retrieval algorithm for the Ozone Monitoring Instrument, Atmos. Meas. Tech., 4(9), 1905–1928, doi:10.5194/amt-4-1905-2011, 2011c. Cited thrice.

删除的内容: /sub

删除的内容: /

删除的内容: <sub>

删除的内容: </sub&gt

删除的内容: <sub>

删除的内容: </sub&gt

删除的内容: <sub>

删除的内容: </sub&gt

Chazette, P., Raut, J.-C., Dulac, F., Berthier, S., Kim, S.-W., Royer, P., Sanak, J., Loaëc, S. and Grigaut-Desbrosses, H.: Simultaneous observations of lower tropospheric continental aerosols with a ground-based, an airborne, and the spaceborne CALIOP lidar system, J. Geophys. Res., 115(D4), D00H31, doi:10.1029/2009JD012341, 2010.

Chimot, J., Vlemmix, T., Veefkind, J. P., de Haan, J. F. and Levelt, P. F.: Impact of aerosols on the OMI tropospheric NO2 retrievals over industrialized regions: how accurate is the aerosol correction of cloud-free scenes via a simple cloud model?, Atmos. Meas. Tech., 9(2), 359–382, doi:10.5194/amt-9-359-2016, 2016.

Clémer, K., Van Roozendael, M., Fayt, C., Hendrick, F., Hermans, C., Pinardi, G., Spurr, R., Wang, P. and De Mazière, M.: Multiple wavelength retrieval of tropospheric aerosol optical properties from MAXDOAS measurements in Beijing, Atmos. Meas. Tech., 3(4), 863–878, doi:10.5194/amt-3-863-2010, 2010.

Cui, Y., Lin, J., Song, C., Liu, M., Yan, Y., Xu, Y. and Huang, B.: Rapid growth in nitrogen dioxide pollution over Western China, 2005–2013, Atmos. Chem. Phys., 16(10), 6207–6221, doi:10.5194/acp-16-6207-2016, 2016.

Dirksen, R. J., Boersma, K. F., Eskes, H. J., Ionov, D. V., Bucsela, E. J., Levelt, P. F. and Kelder, H. M.: Evaluation of stratospheric NO_2 retrieved from the Ozone Monitoring Instrument: Intercomparison, diurnal cycle, and trending, J. Geophys. Res., 116(D8), D08305, doi:10.1029/2010JD014943, 2011.

van Geffen, J. H. G. M., Boersma, K. F., Van Roozendael, M., Hendrick, F., Mahieu, E., De Smedt, I., Sneep, M. and Veefkind, J. P.: Improved spectral fitting of nitrogen dioxide from OMI in the 405–465 nm window, Atmos. Meas. Tech., 8(4), 1685–1699, doi:10.5194/amt-8-1685-2015, 2015.

删除的内容: <sub>

删除的内容: </sub>

Gielen, C., Van Roozendael, M., Hendrick, F., Pinardi, G., Vlemmix, T., De Bock, V., De Backer, H., Fayt, C., Hermans, C., Gillotay, D. and Wang, P.: A simple and versatile cloud-screening method for MAX-DOAS retrievals, Atmos. Meas. Tech., 7(10), 3509–3527, doi:10.5194/amt-7-3509-2014, 2014.

Huang, Z., Huang, J., Bi, J., Wang, G., Wang, W., Fu, Q., Li, Z., Tsay, S.-C. and Shi, J.: Dust aerosol vertical structure measurements using three MPL lidars during 2008 China-U.S. joint dust field experiment, J. Geophys. Res. Atmos., 115(D7), n/a-n/a, doi:10.1029/2009JD013273, 2010.

Irie, H., Boersma, K. F., Kanaya, Y., Takashima, H., Pan, X. and Wang, Z. F.: Quantitative bias estimates for tropospheric NO_2 columns retrieved from SCIAMACHY, OMI, and GOME-2 using a common standard for East Asia, Atmos. Meas. Tech., 5(10), 2403–2411, doi:10.5194/amt-5-2403-2012, 2012.

Johnson, M. S., Meskhidze, N. and Praju Kiliyanpilakkil, V.: A global comparison of GEOS-Chem-predicted and remotely-sensed mineral dust aerosol optical depth and extinction profiles, J. Adv. Model. Earth Syst., 4(3), M07001, doi:10.1029/2011MS000109, 2012.

Kacenelenbogen, M., Redemann, J., Vaughan, M. A., Omar, A. H., Russell, P. B., Burton, S., Rogers, R. R., Ferrare, R. A. and Hostetler, C. A.: An evaluation of CALIOP/CALIPSO's aerosol-above-cloud detection and retrieval capability over North America, J. Geophys. Res. Atmos., 119(1), 230–244, doi:10.1002/2013JD020178, 2014.

Kanaya, Y., Irie, H., Takashima, H., Iwabuchi, H., Akimoto, H., Sudo, K., Gu, M., Chong, J., Kim, Y. J., Lee, H., Li, A., Si, F., Xu, J., Xie, P.-H., Liu, W.-Q., Dzhola, A., Postylyakov, O., Ivanov, V., Grechko, E., Terpugova, S. and Panchenko, M.: Long-term MAX-DOAS network observations of NO_2 in Russia and Asia (MADRAS)

删除的内容: <sub>

删除的内容: </sub&gt

删除的内容: <sub>

删除的内容: </sub>

during the period 2007 2012: instrumentation, elucidation of climatology, and comparisons with OMI satellite observations and global model simulations, Atmos. Chem. Phys., 14(15), 7909–7927, doi:10.5194/acp-14-7909-2014, 2014.

Kim, S.-W., Heckel, A., Frost, G. J., Richter, A., Gleason, J., Burrows, J. P., McKeen, S., Hsie, E.-Y., Granier, C. and Trainer, M.: NO_2 columns in the western United States observed from space and simulated by a regional chemistry model and their implications for NO_x emissions, J. Geophys. Res., 114(D11), D11301, doi:10.1029/2008JD011343, 2009.

Koffi, B., Schulz, M., Bréon, F.-M., Griesfeller, J., Winker, D., Balkanski, Y., Bauer, S., Berntsen, T., Chin, M., Collins, W. D., Dentener, F., Diehl, T., Easter, R., Ghan, S., Ginoux, P., Gong, S., Horowitz, L. W., Iversen, T., Kirkevåg, A., Koch, D., Krol, M., Myhre, G., Stier, P. and Takemura, T.: Application of the CALIOP layer product to evaluate the vertical distribution of aerosols estimated by global models: AeroCom phase I results, J. Geophys. Res. Atmos., 117(D10), n/a-n/a, doi:10.1029/2011JD016858, 2012.

Leitão, J., Richter, A., Vrekoussis, M., Kokhanovsky, A., Zhang, Q. J., Beekmann, M. and Burrows, J. P.: On the improvement of NO2 satellite retrievals – aerosol impact on the airmass factors, Atmos. Meas. Tech., 3(2), 475–493, doi:10.5194/amt-3-475-2010, 2010.

Lerot, C., Stavrakou, T., De Smedt, I., Müller, J.-F. and Van Roozendael, M.: Glyoxal vertical columns from GOME-2 backscattered light measurements and comparisons with a global model, Atmos. Chem. Phys., 10(24), 12059–12072, doi:10.5194/acp-10-12059-2010, 2010.

删除的内容: –

删除的内容: <sub>

删除的内容: </sub>

Levy, R. C., Mattoo, S., Munchak, L. A., Remer, L. A., Sayer, A. M., Patadia, F. and Hsu, N. C.: The Collection 6 MODIS aerosol products over land and ocean, Atmos. Meas. Tech., 6(11), 2989–3034, doi:10.5194/amt-6-2989-2013, 2013.

Li, S., Yu, C., Chen, L., Tao, J., Letu, H., Ge, W., Si, Y. and Liu, Y.: Inter-comparison of model-simulated and satellite-retrieved componential aerosol optical depths in China, Atmos. Environ., 141, 320–332, doi:https://doi.org/10.1016/j.atmosenv.2016.06.075, 2016.

Lin, J., Pan, D., Davis, S. J., Zhang, Q., He, K., Wang, C., Streets, D. G., Wuebbles, D. J. and Guan, D.: China's international trade and air pollution in the United States, Proc. Natl. Acad. Sci., 111(5), 1736–1741, doi:10.1073/pnas.1312860111, 2014a.

Lin, J.-T.: Satellite constraint for emissions of nitrogen oxides from anthropogenic, lightning and soil sources over East China on a high-resolution grid, Atmos. Chem. Phys., 12(6), 2881–2898, doi:10.5194/acp-12-2881-2012, 2012.

Lin, J.-T., McElroy, M. B. and Boersma, K. F.: Constraint of anthropogenic NOx emissions in China from different sectors: a new methodology using multiple satellite retrievals, Atmos. Chem. Phys., 10(1), 63–78, doi:10.5194/acp-10-63-2010, 2010.

Lin, J.-T., Martin, R. V., Boersma, K. F., Sneep, M., Stammes, P., Spurr, R., Wang, P., Van Roozendael, M., Clémer, K. and Irie, H.: Retrieving tropospheric nitrogen dioxide from the Ozone Monitoring Instrument: effects of aerosols, surface reflectance anisotropy, and vertical profile of nitrogen dioxide, Atmos. Chem. Phys., 14(3), 1441–1461, doi:10.5194/acp-14-1441-2014, 2014b.

Lin, J.-T., Liu, M.-Y., Xin, J.-Y., Boersma, K. F., Spurr, R., Martin, R. and Zhang, Q.: Influence of aerosols and surface reflectance on satellite NO_2 retrieval: seasonal and spatial characteristics and implications for NO_x emission constraints, Atmos. Chem. Phys., 15(19), 11217–11241, doi:10.5194/acp-15-11217-2015, 2015.

删除的内容: <sub>

删除的内容: </sub>

Lorente, A., Folkert Boersma, K., Yu, H., Dörner, S., Hilboll, A., Richter, A., Liu, M., Lamsal, L. N., Barkley, M., De Smedt, I., Van Roozendael, M., Wang, Y., Wagner, T., Beirle, S., Lin, J.-T., Krotkov, N., Stammes, P., Wang, P., Eskes, H. J. and Krol, M.: Structural uncertainty in air mass factor calculation for and HCHO satellite retrievals, Atmos. Meas. Tech., 10(3), 759–782, doi:10.5194/amt-10-759-2017, 2017.

删除的内容: NO₂

Lucht, W., Schaaf, C. B. and Strahler, A. H.: An algorithm for the retrieval of albedo from space using semiempirical BRDF models, IEEE Trans. Geosci. Remote Sens., 38(2), 977–998, doi:10.1109/36.841980, 2000.

Ma, J. Z., Beirle, S., Jin, J. L., Shaiganfar, R., Yan, P. and Wagner, T.: Tropospheric NO2 vertical column densities over Beijing: results of the first three years of ground-based MAX-DOAS measurements (2008–2011) and satellite validation, Atmos. Chem. Phys., 13(3), 1547–1567, doi:10.5194/acp-13-1547-2013, 2013.

删除的内容: <sub>

删除的内容: </sub>

Ma, X. and Yu, F.: Seasonal variability of aerosol vertical profiles over east US and west Europe: GEOS-Chem/APM simulation and comparison with CALIPSO observations, Atmos. Res., 140–141, 28–37, doi:https://doi.org/10.1016/j.atmosres.2014.01.001, 2014.

Martin, R. V.: An improved retrieval of tropospheric nitrogen dioxide from GOME, J. Geophys. Res., 107(D20), 4437, doi:10.1029/2001JD001027, 2002.

Misra, A., Tripathi, S. N., Kaul, D. S. and Welton, E. J.: Study of MPLNET-Derived Aerosol Climatology over Kanpur, India, and Validation of CALIPSO Level 2 Version 3 Backscatter and Extinction Products, J. Atmos. Ocean. Technol., 29(9), 1285–1294, doi:10.1175/JTECH-D-11-00162.1, 2012.

Miyazaki, K. and Eskes, H.: Constraints on surface NO_x emissions by assimilating satellite observations of multiple species, Geophys. Res. Lett., 40(17), 4745–4750, doi:10.1002/grl.50894, 2013.

Proestakis, E., Amiridis, V., Marinou, E., Georgoulias, A. K., Solomos, S., Kazadzis, S., Chimot, J., Che, H., Alexandri, G., Binietoglou, I., Kourtidis, K. A., de Leeuw, G. and van der A, R. J.: 9-year spatial and temporal evolution of desert dust aerosols over South-East Asia as revealed by CALIOP, Atmos. Chem. Phys. Discuss., 1–35, doi:10.5194/acp-2017-797, 2017.

Richter, A., Begoin, M., Hilboll, A. and Burrows, J. P.: An improved NO2 retrieval for the GOME-2 satellite instrument, Atmos. Meas. Tech., 4(6), 1147–1159, doi:10.5194/amt-4-1147-2011, 2011.

Sareen, N., Schwier, A. N., Shapiro, E. L., Mitroo, D. and McNeill, V. F.: Secondary organic material formed by methylglyoxal in aqueous aerosol mimics, Atmos. Chem. Phys., 10(3), 997–1016, doi:10.5194/acp-10-997-2010, 2010.

Sayer, A. M., Munchak, L. A., Hsu, N. C., Levy, R. C., Bettenhausen, C. and Jeong, M.-J.: MODIS Collection 6 aerosol products: Comparison between Aqua's e-Deep Blue, Dark Target, and "merged" data sets, and usage recommendations, J. Geophys. Res. Atmos., 119(24), 13,965-13,989, doi:10.1002/2014JD022453, 2014.

Stammes, P., Sneep, M., de Haan, J. F., Veefkind, J. P., Wang, P. and Levelt, P. F.: Effective cloud fractions from the Ozone Monitoring Instrument: Theoretical framework and validation, J. Geophys. Res., 113(D16), D16S38, doi:10.1029/2007JD008820, 2008.

Stavrakou, T., Müller, J.-F., Bauwens, M., De Smedt, I., Lerot, C., Van Roozendael, M., Coheur, P.-F., Clerbaux, C., Boersma, K. F., van der A, R. and Song, Y.: Substantial Underestimation of Post-Harvest Burning Emissions in the North China

删除的内容: x

删除的内容: <sub>

删除的内容: </sub>

Plain Revealed by Multi-Species Space Observations, Sci. Rep., 6, 32307, doi:10.1038/srep32307, 2016.

Veefkind, J. P., de Haan, J. F., Sneep, M. and Levelt, P. F.: Improvements to the OMI O2–O2 operational cloud algorithm and comparisons with ground-based radar–lidar observations, Atmos. Meas. Tech., 9(12), 6035–6049, doi:10.5194/amt-9-6035-2016, 2016.

Verstraeten, W. W., Neu, J. L., Williams, J. E., Bowman, K. W., Worden, J. R. and Boersma, K. F.: Rapid increases in tropospheric ozone production and export from China, Nat. Geosci., 8, 690 [online] Available from: http://dx.doi.org/10.1038/ngeo2493, 2015.

Wang, J., Jacob, D. J. and Martin, S. T.: Sensitivity of sulfate direct climate forcing to the hysteresis of particle phase transitions, J. Geophys. Res. Atmos., 113(D11), n/a-n/a, doi:10.1029/2007JD009368, 2008a.

Wang, M., Gu, J., Yang, R., Zeng, L. and Wang, S.: Comparison of cloud type and frequency over China from surface, FY-2E, and CloudSat observations, vol. 9259, pp. 925913–925914. [online] Available from: http://dx.doi.org/10.1117/12.2069110, 2014.

Wang, P. and Stammes, P.: Evaluation of SCIAMACHY Oxygen A band cloud heights using Cloudnet measurements, Atmos. Meas. Tech., 7(5), 1331–1350, doi:10.5194/amt-7-1331-2014, 2014.

Wang, P., Stammes, P., van der A, R., Pinardi, G. and van Roozendael, M.: FRESCO+: an improved O2 A-band cloud retrieval algorithm for tropospheric trace gas retrievals, Atmos. Chem. Phys., 8(21), 6565–6576, doi:10.5194/acp-8-6565-2008, 2008b.

删除的内容: <sub>

删除的内容: </sub>

删除的内容: <sub>

删除的内容: </sub>

删除的内容: <sub>

删除的内容: </sub>

Wang, X., Huang, J., Zhang, R., Chen, B. and Bi, J.: Surface measurements of aerosol properties over northwest China during ARM China 2008 deployment, J. Geophys. Res. Atmos., 115(D7), n/a-n/a, doi:10.1029/2009JD013467, 2010.

Wang, Y., Penning de Vries, M., Xie, P. H., Beirle, S., Dörner, S., Remmers, J., Li, A. and Wagner, T.: Cloud and aerosol classification for 2.5 years of MAX-DOAS observations in Wuxi (China) and comparison to independent data sets, Atmos. Meas. Tech., 8(12), 5133–5156, doi:10.5194/amt-8-5133-2015, 2015.

Wang, Y., Lampel, J., Xie, P., Beirle, S., Li, A., Wu, D. and Wagner, T.: Ground-based MAX-DOAS observations of tropospheric aerosols, NO2, SO2 and HCHO in Wuxi, China, from 2011 to 2014, Atmos. Chem. Phys., 17(3), 2189–2215, doi:10.5194/acp-17-2189-2017, 2017a.

Wang, Y., Beirle, S., Lampel, J., Koukouli, M., De Smedt, I., Theys, N., Li, A., Wu, D., Xie, P., Liu, C., Van Roozendael, M., Stavrakou, T., Müller, J.-F. and Wagner, T.: Validation of OMI, GOME-2A and GOME-2B tropospheric NO2, SO2 and HCHO products using MAX-DOAS observations from 2011 to 2014 in Wuxi, China: investigation of the effects of priori profiles and aerosols on the satellite products, Atmos. Chem. Phys., 17(8), 5007–5033, doi:10.5194/acp-17-5007-2017, 2017b.

Winker, D. M., Pelon, J., Coakley, J. A., Ackerman, S. A., Charlson, R. J., Colarco, P. R., Flamant, P., Fu, Q., Hoff, R. M., Kittaka, C., Kubar, T. L., Le Treut, H., Mccormick, M. P., Mégie, G., Poole, L., Powell, K., Trepte, C., Vaughan, M. A. and Wielicki, B. A.: The CALIPSO Mission, Bull. Am. Meteorol. Soc., 91(9), 1211–1230, doi:10.1175/2010BAMS3009.1, 2010.

Winker, D. M., Tackett, J. L., Getzewich, B. J., Liu, Z., Vaughan, M. A. and Rogers, R. R.: The global 3-D distribution of tropospheric aerosols as characterized by

删除的内容: <sub>

删除的内容: </sub>

删除的内容: <sub>

删除的内容: </sub>

CALIOP, Atmos. Chem. Phys., 13(6), 3345–3361, doi:10.5194/acp-13-3345-2013, 2013.

Zara, M., Boersma, K. F., De Smedt, I., Richter, A., Peters, E., Van Geffen, J. H. G. M., Beirle, S., Wagner, T., Van Roozendael, M., Marchenko, S., Lamsal, L. N. and Eskes, H. J.: Improved slant column density retrieval of nitrogen dioxide and formaldehyde for OMI and GOME-2A from QA4ECV: intercomparison, uncertainty characterization, and trends, Atmos. Meas. Tech. Discuss., 1–47, doi:10.5194/amt-2017-453, 2018.

Zhang, Q., Streets, D. G., Carmichael, G. R., He, K. B., Huo, H., Kannari, A., Klimont, Z., Park, I. S., Reddy, S., Fu, J. S., Chen, D., Duan, L., Lei, Y., Wang, L. T. and Yao, Z. L.: Asian emissions in 2006 for the NASA INTEX-B mission, Atmos. Chem. Phys., 9(14), 5131–5153, doi:10.5194/acp-9-5131-2009, 2009.

Zhao, C. and Wang, Y.: Assimilated inversion of NO_x emissions over east Asia using OMI NO_2 column measurements, Geophys. Res. Lett., 36(6), L06805, doi:10.1029/2008GL037123, 2009.

Zhao, H. Y., Zhang, Q., Guan, D. B., Davis, S. J., Liu, Z., Huo, H., Lin, J. T., Liu, W. D. and He, K. B.: Assessment of China's virtual air pollution transport embodied in trade by using a consumption-based emission inventory, Atmos. Chem. Phys., 15(10), 5443–5456, doi:10.5194/acp-15-5443-2015, 2015.

Zhou, Y., Brunner, D., Spurr, R. J. D., Boersma, K. F., Sneep, M., Popp, C. and Buchmann, B.: Accounting for surface reflectance anisotropy in satellite retrievals of tropospheric NO2, Atmos. Meas. Tech., 3(5), 1185–1203, doi:10.5194/amt-3-1185-2010, 2010.

删除的内容:

删除的内容: <sub>

删除的内容: </sub>

Zhu, W., Xu, C., Qian, X. and Wei, H.: Statistical analysis of the spatial-temporal distribution of aerosol extinction retrieved by micro-pulse lidar in Kashgar, China, Opt. Express, 21(3), 2531–2537, doi:10.1364/OE.21.002531, 2013.

Hendrick, F., Muller, J. F., Clemer, K., Wang, P., De Maziere, M., Fayt, C., Gielen, C., Hermans, C., Ma, J. Z., Pinardi, G., Stavrakou, T., Vlemmix, T., and Van Roozendael, M.: Four years of ground-based MAX-DOAS observations of HONO and NO2 in the Beijing area, Atmospheric Chemistry and Physics, 14, 765-781, 10.5194/acp-14-765-2014, 2014.

Jethva, H., Torres, O., and Ahn, C.: A ten-year global record of absorbing aerosols above clouds from OMI's near-UV observations, in: Remote Sensing of the Atmosphere, Clouds, and Precipitation Vi, edited by: Im, E., Kumar, R., and Yang, S., Proceedings of SPIE, 2016.

Schenkeveld, V. M. E., Jaross, G., Marchenko, S., Haffner, D., Kleipool, Q. L., Rozemeijer, N. C., Veefkind, J. P., and Levelt, P. F.: In-flight performance of the Ozone Monitoring Instrument, Atmospheric Measurement Techniques, 10, 1957-1986, 10.5194/amt-10-1957-2017, 2017.

van Donkelaar, A., Martin, R. V., Spurr, R. J. D., Drury, E., Remer, L. A., Levy, R. C., and Wang, J.: Optimal estimation for global ground-level fine particulate matter concentrations, Journal of Geophysical Research-Atmospheres, 118, 5621-5636, 10.1002/jgrd.50479, 2013.

删除的内容: Wang, Y., Lampel, J., Xie, P., Beirle, S., Li, A., Wu, D., and Wagner, T.: Ground-based MAX-DOAS observations of tropospheric aerosols, NO2, SO2 and HCHO in Wuxi, China, from 2011 to 2014, Atmospheric Chemistry and Physics, 17, 2189-2215, 10.5194/acp-17-2189-2017, 2017.

第 7 页: [1] 删除的内容 Jintai Lin 2018/6/21 PM5:19:00

We apply a number of criteria to ensure data quality of each pixel, mainly following Winker et al. (2013) and Amiridis et al. (2015). More detailed inoframtion about criteria to select the Level-2 are referred to Appendix A.

第 7 页: [2] 删除的内容 Jintai Lin 2018/6/21 PM5:20:00

After the pixel-based screening, we aggregate the CALIOP data at the model grid (0.667° long. x 0.5° lat.) and vertical resolution (47 layers, with 36 layers or so in the troposphere). For each grid cell, we choose the CALIOP pixels within 1.5° of the grid cell center. The way to compile gridded CALIOP climatology aerosol extinction profiles is referred to Appendix B. CALIOP Level-2 data are always presented at the fixed 399 altitudes above sea level. To account for the difference in surface elevation between a CALIOP pixel and the respective model grid cell, we convert the altitude of the pixel to a height above the ground, by using the surface elevation data provided in CALIOP. We then average horizontally and vertically the profiles of all pixels within one model grid cell and layer. We do the regridding day-by-day for all grid cells to ensure that GEOS-Chem and CALIOP extinction profiles are coincident spatially and temporally. Finally, we compile a monthly climatological dataset by averaging over 2007–2015.

第 7 页: [3] 删除的内容 Jintai Lin 2018/6/21 PM5:33:00

As discussed above, we choose the CALIOP pixels within 1.5° of a grid cell center. We test this choice by examining the aerosol layer height (ALH) produced for that grid cell. The ALH is defined as the extinction-weighted height of aerosols (see Eq. 1, where n denotes the number of tropospheric layers, ε_i the aerosol extinction at

layer i, and H_i the layer center height above the ground). We find that choosing pixels within 1.0° of a grid cell center leads to a nosier horizontal distribution of ALH, owing to the small footprint of CALIOP. On the other hand, choosing 2.0° leads to a too smooth spatial gradient of ALH with local characteristics of aerosol vertical distributions are largely lost. We thus decide that 1.5° is a good balance between noise and smoothness.

$$\mathrm{ALH} = \frac{\sum_{i=1}^{i=n} \varepsilon_i \mathrm{H}_i}{\sum_{i=1}^{i=n} \varepsilon_i} \qquad (1)$$

Certain grid cells do not contain sufficient valid observations for some months of the climatological dataset. We fill in missing monthly values of a grid cell using valid data in the surrounding 5 x 5 = 25 grid cells (within ~ 100 km). If the 25 grid cells do not have enough valid data (see Appedix B for details next paragraph for details), we use those in the surrounding 7 x 7 = 49 grid cells (within ~ 150 km). A similar procedure is used by Lin et al. (2014b, 2015) to fill in missing values in the gridded MODIS AOD dataset.

第 16 页: [4] 删除的内容 Jintai Lin 2018/6/21 PM5:38:00

3.2 Comparison to NASA CALIOP monthly climatology

We compare our gridded climatological profiles to NASA CALIOP Version 3 Level-3 all-sky monthly profiles at 532 nm (Winker et al. 2013). The NASA Level-3 data has a horizontal resolution of 2° lat. × 5° lon. and a vertical resolution of 60 m (from -0.5 to 12 km above sea level). We combine NASA monthly data over 2007–2015 to construct a monthly climatology for comparison with our own compilation. We only choose aerosol extinction data in the troposphere with error less than 0.15 (the valid range given in the CALIOP dataset). If the number of valid monthly profiles in a grid cell is less than five (i.e., for the same month in five out of the nine years), then we exclude data in that grid cell; see the dark gray grid cells in Fig. 23c.

Several methodological differences exist between generating our and NASA CALIOP datasets. First, the two datasets have different horizontal resolutions. Also, we sample all valid CALIOP pixels within 1.5 ^{0} of a grid cell center, whereas the NASA dataset samples all valid pixels within a grid cell. Besides, our CALIOP dataset involves several steps of horizontal interpolation, for purposes of subsequent cloud and NO_2 retrievals, which is not done in the NASA dataset. In addition, we match CALIOP data vertically to the GEOS-Chem vertical resolution, whereas the NASA dataset maintains the original resolution.

Figure 23c shows the spatial distribution of ALH in all seasons based on NASA CALIOP Level-3 all-sky monthly climatology. The horizontal resolution of NASA data is much coarser than ours; and NASA data are largely missing over the southwest with complex terrains. We choose to focus on the comparison over East China (the black box in Fig. 12a). Over East China, the two climatology datasets generally exhibit similar spatial patterns of ALH in all seasons (Fig. 23a, c). The NASA dataset suggests higher ALHs than ours over Eastern China, especially in summer, due mainly to differences in the sampling and regridding processes. Figure 34c further compares the monthly variation of ALH between our (black line with error bars) and NASA (blue filled triangles) datasets averaged over East China. The two datasets are consistent in almost all months, indicating that their regional differences are largely smoothed out by spatial averaging.

第 25 页: [5] 删除的内容	Jintai Lin	2018/6/21 PM5:44:00

EU FP7-project Quality Assurance for Essential Climate Variables (

第 25 页: [6] 删除的内容	Jintai Lin	2018/6/21 PM5:44:00

is aim at making rapid judgments on validitiy and trustworthiness of Earth Observation data and the derived climate data sets. It

第 25 页: [7] 删除的内容　　Folkert Boersma　　2018/6/28 AM10:51:00

essentially an ensemble data sets of satellite products provide

第 25 页: [8] 删除的内容　　Jintai Lin　　2018/6/21 PM5:46:00

, with a fully traceable quality assurance on all aspects of the NO_2, HCHO and carbon monoxide (CO) (Zara et al., 2018)

that using the same version of MODIS AOD data would be better. However, the difference in C5.1 and C6 is relatively small (C6 is smaller by 13.7% averaged over East China in 2012), compared to the difference between GEOS-Chem and C5.1 or between CEOS-Chem and C6. Our one-year test by using C5.1 versus C6 AOD (to correct model AOD) leads to 3.8% decrease in the retrieved NO_2 averaged over East China in 2012.

As suggested by the second reviewer, we have included the newest QA4ECV NO2 product in the revised manuscript. Figure 9, Table 2 and Table 3 have been updated accordingly. QA4ECV is biased low in cases with high aerosol loading, but its R^2 with respect to MAX-DOAS is better than DOMINO v2. This additional comparison further strengthens the importance of aerosol correction in NO_2 retrieval over East Asia. Despite its various limitations discussed here, POMINO v1.1 is closer to MAX-DOAS than QA4ECV is, especially in hazy days, highlighting the capability of POMINO v1.1.

Given these above discussions, we have decided to not release POMINO v1.1 to users. Rather, we will eventually release POMINO v2, which will include MODIS C6 merged AOD and MCD43C2 C6 daily BRDF. The POMINO v1.1 will be used as an intermediate (and the most important) step between POMINO and POMINO v2. And this paper documents how improvement in aerosol vertical distribution affects the POMINO NO_2 product, such that all other factors are consistent between POMINO and POMINO v1.1. We have clarified this point in the revised abstract and conclusion.

2. To justify the improvement in the retrieved product, authors have used a small set of MAX-DOAS measurements. Improvements are justified based on improved correlation coefficient with the POMINO product. It appears from Figure 10 that the enhanced correlation might, in fact, be driven by changes in ~6 data points only with very large (>100 x 10^15 molec cm-2) values. In many instances (for columns < 100 x 10^15 molec cm2), the agreement between OMI and MAX-DOAS appears to be better for DOMINO. Author should use different means of validation, larger set of validation datasets, and various statistical methods to assess the products.

The high values represent very polluted cases that our algorithm intends to capture. Excluding these polluted cases would lead to a substantial sampling bias over polluted regions. We have made the distinction between hazy cases and less hazy situations. The latter are more representative for retrievals over the US and Europe. In those cases, QA4ECV may perform better and POMINO is more likely to be biased high (Table 3).

We would definitely prefer to have a larger set of MAX-DOAS NO_2 data. Unfortunately, very few high-quality MAX-DOAS measurements are available over China. We have made efforts to get data from multiple sites to enhance the spatial representativeness. Our criteria to select MAX-DOAS data and OMI data mainly follow Wang et al., (2017b) and Lin et al., (2014), who have already discussed the influence from various statistical methods.

We have included a statement in the end of Sect. 6 that “Further research may use additional MAX-DOAS datasets to evaluate the satellite products more systematically.”

3. The whole discussion about processing (filtering, regridding) and comparison of CALIPSO data is distracting and unnecessary. These could be completely removed, shortened, or moved to the Appendix/Supplementary section. Also, data processing is largely subjective. Why not use more mature data assimilation technique instead?

We have revised the manuscript accordingly. The discussion on the treatment of CALIOP data has been moved to Appendix B.

Data assimilation is subject to the very limited availability of CALIOP data. It is also computationally prohibitive for our application here (multiple years over a large domain on a high-resolution grid).

Specific comments

1. Page 9, line 225: This statement may not be true. Please, replace “will not” to “may not”.

Changed.

2. Page 9, line 227-231: Please be more specific on AMF calculation. What wavelength range is used for AMF for POMINO/DOMINO? I assume this is more important than the difference between online and look-up table approach.

Changed. The wavelength is 438 nm in both DOMINO and POMINO. The dependence of AMF on the wavelength is weak (actually 0.25%/nm, Boersma et al. (2018)). Other details of AMF calculations can be found in Lin et al. (2014b, 2015).

3. Page 9, line 228: This paper is all about POMINO and DOMINO. Please, say “DOMINO” instead of “in most retrieval algorithms”.

As far as we know, most algorithms use look-up tables, including but not limited to NASA’s SP product, DOMINO, and others participating the QA4ECV project.

4. Page 10, line 237: What are those “Other aspects”? Please, list them.

Changed.

5. Page 10, lines 237-239: This statement is likely misleading as look-up table may have been used in certain aspect of your calculation. Please, remove "without use of look-up tables".

Changed.

6. Page 10, lines 239-244, 257-259: See my general comment. The same product cannot use simulated fields from two different models. The retrievals should be based on single model.

See response to general comment.

7. Page 13, lines 314-316: How does the se of CALIPSO constraints affect cloud pressure, cloud fraction, and radiative cloud fraction? Please include relevant results and discussions.

The detailed results can be found in Sect. 4.

8. Page 13, lines 321-325: Please, clarify this statement.

Clarified.

9. Page 14, line 360: What is the justification of 2-hour averaging of MAX-DOAS? Why do you expect instantaneous OMI measurements compare well with MAX-DOAS averaged over 2-hours? Is this exercise described in the following sentences motivated to show only good results?

As already clarified in manuscript, we used the criteria based on several previous studies (Lin et al., 2014; Wang et al., 2015, 2017b). These previous papers have already discussed the most appropriate criteria to balance data coverage, passing time, spatial domain around the pixel center, etc.

10. Page 15, lines 366-367: "to some degree" is redundant.

Changed.

11. Page 15, lines 374-375: Why is this necessary? How do cloud and haze differ for their impact on measurement sensitivity of OMI?

As emphasized in the manuscript, we wanted to separate the hazy days from cloudy days. Some days are cloud-free but hazy (with heavy NO2 pollution as well). These days were filtered out in DOMINO and QA4ECV through the criteria on cloud radiance fraction. By comparison, our algorithm was able to retain these days and avoid sampling bias (by missing polluted days) while preserving the overall accuracy of NO2 product.

As explained in the manuscript, neither the OMI cloud product nor the MODIS cloud product is able to provide the true cloud fraction, so we used the meteorological monitoring stations and the MODIS RGB product to manually check whether a day is cloudy or hazy.

12. Page 16, line 395: Please, add citations for this statement.

Changed.

13. Page 17, line 418: How does the emission strength affect the height of peak extinction?

The effect of emission strength on aerosol vertical profiles is season and location dependent. For the case here (Figure 4), emissions over Eastern China are higher in winter, in which season the atmosphere is more stagnant vertically. This means that more aerosols are concentrated near the surface, thus decreasing the height of peak extinction.

14. Page 19, lines 470-472: The spatial correlations suggest that GEOS-Chem performs very poorly in simulating aerosol fields. Why do you still use GEOS-Chem? Could not you just use CALIPSO-based aerosol information?

GEOS-Chem provides daily and spatially resolved information, which is what is needed by the satellite retrieval. CALIOP, in contrast, has poor temporal and spatial coverage, preventing fully CALIOP-based aerosol profile information to be used to retrieve the NO_2 product. The spatial correlation between GEOS-Chem and CALIOP is not as good as their temporal correlation. We thus used CALIOP for monthly climatological corrections, while retaining the GEOS-Chem simulated day-to-day variability.

Anonymous Referee #2

The paper "Improved aerosol correction for OMI tropospheric NO2 retrieval over East Asia: constraint from CALIOP aerosol vertical profile" by Liu et al. describes an improved OMI tropospheric NO2 retrieval for East China using CALIOP aerosol vertical profile information. This study updates the POMINO retrieval algorithm described in Lin et al., 2014 and 2015. Comparisons have been made between the NO2 satellite data and ground-based MAX-DOAS measurements at three sites in East-China.

The topic of the manuscript is within the scope of AMT and it is of interest to the scientific community. It can be recommended for publication, if the authors make an effort to address the comments listed below, and improve the manuscript accordingly.

Specific comments:

Section 2.2

P9-10 The improved POMINO NO2 algorithm for China builds on the Dutch OMI NO2 v2 algorithm from 2011. The DOMINO v2 algorithm is now about 7 years old, and the authors shortly discuss some recent improvements in the satellite retrieval (e.g. improvements in the slant column retrieval). Please include the recently released "Dutch/European" OMI NO2 product provided in the framework of the QA4ECV project (v1.1) in this discussion as well (e.g. including the latest developments in the STS and the trop. AMF algorithms).

Thank you for this valuable suggestion. We have now included an evaluation of QA4ECV in the revised manuscript. Figure 9, Table 2 and Table 3 have been updated accordingly. QA4ECV is still bias low in highly polluted cases, although its R^2 with respect to MAX-DOAS is better than DOMINO v2. This additional comparison further strengthens the importance of aerosol correction in NO_2 retrieval over East Asia. POMINO v1.1 is closer to MAX-DOAS than QA4ECV is, especially in hazy days, highlighting the capability of POMINO v1.1.

P11 The authors mention that the climatological adjustments in the aerosol information is based on the assumption that systematic model limitations are month-dependent and persist over the years and days. On the other hand, the daily variations in the aerosol extinction profile are coming from the model only (Eq. 3). How good are the daily variations in the aerosol parameters modeled by GEOS-Chem?

The extent to which model aerosol information can be corrected depends on the availability of aerosol observations. MODIS and especially CALIOP suffer from low coverage on the day-to-day scale, preventing their direct use in satellite NO2 retrieval product and in daily correction of model aerosols.

Previous studies have shown that GEOS-Chem is able to simulate day-to-day variation of AOD from AERONET (Li et al., 2013, 2015) and satellite (Johnson et al., 2012), surface $PM_{2.5}$ (Liu et al., 2018), and aerosol vertical profile (Ford and Heald, 2012).

P11 From Eq. (2) and (3), I would expect a "jump" in the aerosol extinction profile from the last day of the month to the first day of the next month (because of the change in R). Is this 'jump' also noticeable in the trop. AMF and VCD?

Here we test this "jump" issue over Northern East China. For every first day in each month of year 2012, we use the monthly correction from the last month (ie. For 1st, Feb, we will use the ratio of January to adjust aerosol extinction profile of GEOS-Chem on this day). Figure R1 shows the test results. In particular, the difference in NO_2 VCD between this sensitivity test and our actual retrieval is below 3.8% for most cases. Besides, the distribution of VCD difference seems to be random. Thus the "jump" issue does not influence our results systematically.

We have added in the revised Sect. 2.2 that "Although this monthly adjustment means discontinuity on the day-to-day basis (e.g., from the last day of a month to the first day of the next month), such discontinuity does not affect the NO_2 retrieval significantly, based on our sensitivity test."

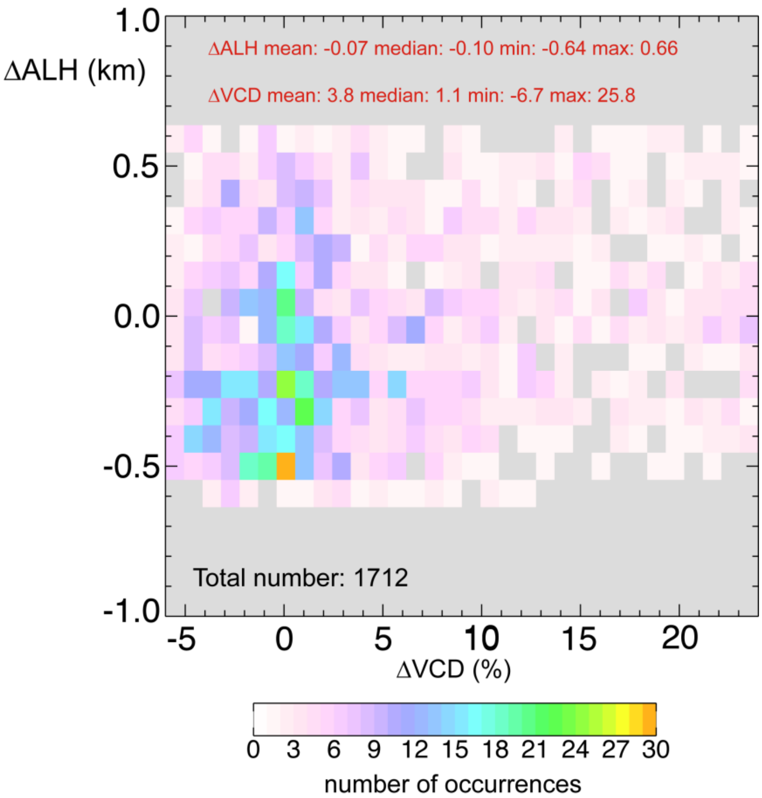

Figure R1. Percentage change in retrieved NO_2 VCD when using the CALIOP aerosol extinction profile in a formal month (POMINO_change) to adjust modeled profile on the first day of each month ([POMINO_change-POMINO v1.1]/[POMINO v1.1]), for each bin of ΔALH (bin size = 0.1 km) and ΔVCD (bin size = 1%) across pixels in 2012 over Northern East China. Here we only choose the pixels with WCLD < 0.5, surface albedo < 0.3 and SZA < 70°.

P12 How large is the effect of neglecting polarization in the RTM (LIDORT) on the trop. AMF calculation?

The impact of polarization is small, affecting stratospheric retrievals by 0.1% and reducing tropospheric AMF by < 0.5% (Boersma et al., 2011). According on Lorente et al., (2017), top-of-atmosphere reflectance simulated by four RTMs (DAK with polarization, McArtim, SCIATRAN and VLIDORT with polarization) agree within 1.5%.

Section 3.1

Fig.3 For some specific areas there seem to be large differences between the two CALIOP ALH datasets, e.g. for Shandong in summer. Is this only caused by the differences in resolution/sampling/regridding, or are there other factors?

The large difference over Shandong is persistent across the seasons. It is mainly caused by resolution/sampling/regridding process. Our climatological dataset uses the same criteria as the NASA Level-3 product does, but we aim at compiling a climatology to adjust GEOS-Chem outputs in a temporally and spatially consistent manner.

Section 4

A difficult/confusing concept of the POMINO NO2 algorithm is that for the trop. AMF, (thin) clouds are treated as reflecting boundaries in the RTM calculations (using effective cloud parameters retrieved from the O2-O2 band), while Mie parameters are used in the RTM for the layers with aerosols. It is clear that the aerosols are included in the POMINO O2-O2 cloud retrieval, but the different treatment of scattering by clouds and aerosols in the trop. AMF calculation could be addressed in more detail.

As in all other cloud products used for NO_2 retrieval, we treat clouds as “effective” Lambertian reflector with a fixed albedo (80%). Assuming Mie scattering for clouds implies an explicit treatment of vertical cloud structure, cloud droplet sizes, etc., which is actually a new direction we could explore for NO_2 retrieval.

We have added a statement in the revised Sect. 2.2: “Note that the treatment of cloud scattering (as “effective” Lambertian reflector, as in other NO_2 algorithms) is different from the treatment of aerosol scattering/absorption (vertically resolved based on the Mie scheme).”

Section 6

The evaluating of the improved OMI NO2 product with MAX-DOAS data is an important part of this study. However, the number of measurements/points in Fig. 10 seems low (e.g. compared to other satellite validation studies using the BIRA-IASB MAXDOAS data at these sites). Can the number of points be increased, e.g. by increasing the time period, relaxing the cloud screening, collocation criteria etc? Then the statistics can be improved and also time series could be added.

We would definitely prefer to have a larger set of MAX-DOAS NO_2 data. Unfortunately, very few high-quality MAX-DOAS measurements are available over China. We have made efforts to get data from multiple sites to enhance the spatial representativeness. Our criteria to select MAX-DOAS data and OMI data mainly follow Wang et al., (2017b) and Lin et al., (2014b), who have already discussed the influence from various statistical methods.

We have included a statement in the end of Sect. 6 that "Further research may use additional MAX-DOAS datasets to evaluate the satellite products more systematically."

In addition to the comparisons in Fig. 10, the MAXDOAS retrieved NO2 profiles could also be exploited with the Averaging Kernel (AK) of the OMI NO2 columns. Comparisons of the satellite NO2 columns with these "smoothed" MAXDOAS NO2 columns could provide useful additional information (e.g. to isolate the impact of the satellite a priori NO2 profile).

We only have the vertical profiles at Xianghe, with lack of spatial representativeness. Our previous study (Lin et al., 2014b) shows that using the MAX-DOAS vertical profiles have a minor impact on the retrieved NO_2.

References:

Ford, B. and Heald, C. L.: An A-train and model perspective on the vertical distribution of aerosols and CO in the Northern Hemisphere, J. Geophys. Res. Atmos., 117(D6), n/a-n/a, doi:10.1029/2011JD016977, 2012.

Johnson, M. S., Meskhidze, N. and Praju Kiliyanpilakkil, V.: A global comparison of GEOS-Chem-predicted and remotely-sensed mineral dust aerosol optical depth and extinction profiles, J. Adv. Model. Earth Syst., 4(3), M07001, doi:10.1029/2011MS000109, 2012.

Li, S., Garay, M. J., Chen, L., Rees, E. and Liu, Y.: Comparison of GEOS-Chem aerosol optical depth with AERONET and MISR data over the contiguous United States, , 118(April), 228–241, doi:10.1002/jgrd.50867, 2013.

Li, S., Chen, L., Fan, M., Tao, J., Wang, Z., Yu, C., Si, Y., Letu, H. and Liu, Y.: Estimation of GEOS-Chem and GOCART Simulated Aerosol Profiles Using CALIPSO Observations over the Contiguous United States, , (2008), 3256–3265, doi:10.4209/aaqr.2015.03.0173, 2015.

Liu, M., Lin, J., Wang, Y., Sun, Y., Zheng, B., Shao, J., Chen, L., Zheng, Y., Chen, J., Fu, M., Yan, Y., Zhang, Q. and Wu, Z.: Spatiotemporal variability of NO_2 and $PM_{2.5}$ over Eastern China: observational and model analyses with a novel statistical method, Atmos. Chem. Phys. Discuss., 2018, 1–34, doi:10.5194/acp-2017-1180, 2018.

Improved aerosol correction for OMI tropospheric NO_2 retrieval over East Asia: constraint from CALIOP aerosol vertical profile

Mengyao Liu[1,2], Jintai Lin[1], K. Folkert Boersma[2,3], Gaia Pinardi[4], Yang Wang[5], Julien Chimot[6], Thomas Wagner[5], Pinghua Xie[7,8,9], Henk Eskes[2], Michel Van Roozendael[4], François Hendrick[4], Pucai Wang[10], Ting Wang[10], Yingying Yan[1], Lulu Chen[1], Ruijing Ni[1]

1, Laboratory for Climate and Ocean-Atmosphere Studies, Department of Atmospheric and Oceanic Sciences, School of Physics, Peking University, Beijing, China

2, Royal Netherlands Meteorological Institute, De Bilt, the Netherlands

3, Meteorology and Air Quality department, Wageningen University, Wageningen, the Netherlands

4, Royal Belgian Institute for Space Aeronomy (BIRA-IASB), Brussels, Belgium

5, Max Planck Institute for Chemistry, Mainz, Germany

6, Department of Geoscience and Remote Sensing (GRS), Civil Engineering and Geosciences, TU Delft, the Netherlands

7, Anhui Institute of Optics and Fine Mechanics, Key laboratory of Environmental Optics and Technology, Chinese Academy of Sciences, Hefei, China

8, CAS Center for Excellence in Urban Atmospheric Environment, Institute of Urban Environment, Chinese Academy of Sciences, Xiamen, China

9, School of Environmental Science and Optoelectronic Technology, University of Science and Technology of China, Hefei, China

批注 [Microsof1]: Add new co-authors

10, IAP/CAS, Institute of Atmospheric Physics, Chinese Academy of Sciences, Beijing, China

Correspondence to: Jintai Lin (linjt@pku.edu.cn); K. Folkert Boersma (folkert.boersma@knmi.nl)

Abstract

Satellite retrieval of vertical column densities (VCDs) of tropospheric nitrogen dioxide (NO_2) is critical for NO_x pollution and impact evaluation. For regions with high aerosol loadings, the retrieval accuracy is greatly affected by whether aerosol optical effects are treated implicitly (as additional "effective" clouds) or explicitly, among other factors. Our previous POMINO algorithm explicitly accounts for aerosol effects to improve the retrieval especially in polluted situations over China, by using aerosol information from GEOS-Chem simulations with further monthly constraints by MODIS/Aqua aerosol optical depth (AOD) data. Here we present a major algorithm update, POMINO v1.1, by constructing a monthly climatological data set of aerosol extinction profiles, based on Level-2 CALIOP/CALIPSO data over 2007–2015, to better constrain the modeled aerosol vertical profiles.

We find that GEOS-Chem captures the month-to-month variation of CALIOP aerosol layer height but with a systematic underestimate by about 300–600 m (season and location dependent), due to a too strong negative vertical gradient of extinction above 1 km. Correcting the model aerosol extinction profiles results in small changes in retrieved cloud fraction, increases in cloud top pressure (within 2–6% in most cases), and increases in tropospheric NO_2 VCD by 4–16% over China on a monthly basis in 2012. The improved NO_2 VCDs (in POMINO v1.1) are more consistent with independent ground-based MAX-DOAS observations (R^2 = 0.80, NMB = -3.4%, for 162 pixels in 49 days) than POMINO (R^2 = 0.80, NMB = -9.6%), DOMINO v2 (R^2 =

0.68, NMB = -2.1%) and QA4ECV (R^2 = 0.75, NMB = -22.0%) are. Especially on haze days, R^2 reaches 0.76 for POMINO v1.1, much higher than that for POMINO (0.68), DOMINO v2 (0.38) and QA4ECV (0.34). Furthermore, the increase in cloud pressure likely reveals a more realistic vertical relationship between cloud and aerosol layers, with aerosols situated above the clouds in certain months instead of always below the clouds. The POMINO v1.1 algorithm is a core step towards our next public release of data product (POMINO v2), and it will also be applied to the recently launched S5P-TropOMI sensor.

批注 [Microsof2]: Add QA4ECV results.

批注 [Microsof3]: Clarify POMINO v1.1 won't be our new released product.

1. Introduction

Air pollution is a major environmental problem in China. In particular, China has become the world's largest emitting country of nitrogen oxides (NO_X=NO+NO_2) due to its rapid economic growth, heavy industries, coal-dominated energy sources, and relatively weak emission control (Cui et al., 2016; Lin et al., 2014a; Stavrakou et al., 2016; Zhang et al., 2009). Tropospheric vertical column densities (VCDs) of nitrogen dioxide (NO_2) retrieved from the Ozone Monitoring Instrument (OMI) onboard the Earth Observing System (EOS) Aura satellite have been widely used to monitor and analyze NO_X pollution over China because of its high spatiotemporal coverage (e.g. (Lin et al., 2010; Miyazaki and Eskes, 2013; Verstraeten et al., 2015; Zhao and Wang, 2009). However, NO_2 retrieved from OMI and other space-borne instruments are subject to errors in the conversion process from radiance to VCD, particularly with respect to the calculation of tropospheric air mass factor (AMF) that is used to convert tropospheric slant column density to VCD (e.g. Boersma et al., 2011; Bucsela et al., 2013; Lin et al., 2015; Lorente et al., 2017).

Most current-generation NO_2 algorithms do not explicitly account for the effects of aerosols on NO_2 AMFs and on prerequisite cloud parameter retrievals. These retrievals often adopt an implicit approach wherein cloud algorithms retrieve "effective cloud" parameters that include the optical effects of aerosols. This implicit method is based on aerosols exerting an effect on the top-of-atmosphere radiance level, whereas the assumed cloud model does not account for the presence of aerosols in the atmosphere (Stammes et al., 2008; Veefkind et al., 2016; Wang et al., 2008b; Wang and Stammes, 2014). In the absence of clouds, an aerosol optical thickness of 1 is then interpreted as an effective cloud fraction of ± 0.10, and the value also depends on the aerosol properties (scattering or absorbing), true surface albedo and geometry angles (Chimot et al., 2016) with an effective cloud pressure closely related to the aerosol layer, at least for aerosols of predominantly scattering nature (e.g. Boersma et al., 2004, 2011, Castellanos et al., 2014, 2015). However, in polluted situations with high aerosol loadings and more absorbing aerosol types, which often occur over China and many other developing regions, the implicit method can result in considerable biases (Castellanos et al., 2014, 2015; Chimot et al., 2016; Kanaya et al., 2014; Lin et al., 2014b).

Lin et al. (2014b, 2015) established the POMINO NO_2 algorithm, which builds on the DOMINO v2 algorithm (for OMI NO_2 slant columns and stratospheric correction), but improves upon it through a more sophisticated AMF calculation over China. In POMINO, the effects of aerosols on cloud retrievals and NO_2 AMFs are explicitly accounted for. In particular, daily information on aerosol optical properties such as aerosol optical depth (AOD), single scattering albedo (SSA), phase function and vertical extinction profiles are taken from nested Asian GEOS-Chem v9-02 simulations. The modeled AOD at 550 nm is further constrained by MODIS/Aqua monthly AOD, with the correction applied to other wavelengths based on modeled aerosol refractive indices (Lin et al., 2014b). However, the POMINO algorithm does not include an observation-based constraint on the vertical profile of aerosols, whose altitude relative to NO_2 has strong and complex influences on NO_2 retrieval (Castellanos et al., 2015; Leitão et al., 2010; Lin et al., 2014b). This study improves upon the POMINO algorithm by incorporating CALIOP monthly climatology of aerosol vertical extinction profiles to correct for model biases.

The CALIOP lidar, carried on the sun-synchronous CALIPSO satellite, has been acquiring global aerosol extinction profiles since June 2006 (Winker et al., 2010). CALIPSO and Aura are both parts of the National Aeronautics and Space Administration (NASA) A-train constellation of satellites. The overpass time of CALIOP/CALIPSO is only 15 minutes later than OMI/Aura. In spite of issues with the detection limit, radar ratio selection and cloud contamination that cause some biases in CALIOP aerosol extinction vertical profiles (Amiridis et al., 2015; Koffi et al., 2012; Winker et al., 2013), comparisons of aerosol extinction profiles between ground-based lidar and CALIOP show good agreements (Kacenelenbogen et al., 2014; Kim et al., 2009; Misra et al., 2012). However, CALIOP is a nadir-viewing instrument that measures the atmosphere along the satellite ground-track with a narrow field-of-view. This means that the daily geographical coverage of CALIOP is much smaller than that of OMI. Thus previous studies often used monthly/seasonal regional mean CALIOP data to study aerosol vertical distributions or to evaluate model simulations (Chazette et al., 2010; Johnson et al., 2012; Koffi et al., 2012; Ma and Yu, 2014; Sareen et al., 2010).

There exist a few CALIOP Level-3 gridded datasets, such as LIVAS (Amiridis et al. 2015) and NASA official Level-3 monthly dataset (Winker et al., 2013). However, LIVAS is an annual average day-night combined product, not suitable to be applied to OMI NO_2 retrievals (around early afternoon, and in need of a higher temporal resolution than annual). The horizontal resolution (2° long. × 5° lat.) of NASA official product is much coarser than OMI footprints and the GEOS-Chem model resolution.

批注 **[Microsof4]:** Clarify our statements

Here we construct a custom monthly climatology of aerosol vertical extinction profiles based on 9-years (2007–2015) worth of CALIOP Version 3 Level-2 532 nm data. On a climatological basis, we use the CALIOP monthly data to adjust GEOS-Chem profiles in each grid cell for each day of the same month in any year. We then use the corrected GEOS-Chem vertical extinction profiles in the retrievals of cloud parameters and NO_2. Finally, we evaluate our updated POMINO retrieval (hereafter referred to as POMINO v1.1), our previous POMINO product, DOMINO v2 and the newly released Quality Assurance for Essential Climate Variables product (QA4ECV, see Appendix A), using ground-based MAX-DOAS NO_2 column measurements at three urban/suburban sites in East China for the year of 2012 and several months in 2008/2009.

Section 2 describes the construction of CALIOP aerosol extinction vertical profile monthly climatology, the POMINO v1.1 retrieval approach, and the MAX-DOAS data. It also presents the criteria for comparing different NO_2 retrieval products and for selecting coincident OMI and MAX-DOAS data. Section 3 compares our CALIOP climatology with NASA's official Level-3 CALIOP dataset and GEOS-Chem simulation results. Sections 4 and 5 compare POMINO v1.1 to POMINO to analyze the influence of improved aerosol vertical profiles on retrievals of cloud parameters and NO_2 VCDs, respectively. Section 6 evaluates POMINO, POMINO v1.1, DOMNO v2 and QA4ECV NO_2 VCD products using the MAX-DOAS data. Section 7 concludes our study.

2. Data and methods

2.1 CALIOP monthly mean extinction profile climatology

CALIOP is a dual-wavelength polarization lidar measuring attenuated backscatter radiation at 532 and 1064 nm since June 2006. The vertical resolution of aerosol extinction profiles is 30 m below 8.2 km and 60 m up to 20.2 km (Winker et al., 2013), with a total of 399 sampled altitudes. The horizontal resolution of CALIOP scenes is

335 m along the orbital track and is given over a 5 km horizontal resolution in Level-2 data.

As detailed in Appendix B, we use the daily all-sky Version 3 CALIOP Level-2 aerosol profile product at 532 nm from 2007 to 2015 to construct a monthly Level-3 climatological dataset of aerosol extinction profiles over China and nearby regions. This dataset is constructed on the GEOS-Chem model grid (0.667° long. x 0.5° lat.) and vertical resolution (47 layers, with 36 layers or so in the troposphere). The ratio of climatological monthly CALIOP to monthly GEOS-Chem profiles represents the scaling profile to adjust the daily GEOS-Chem profiles in the same month (see Sect. 2.2)

2.2 POMINO v1.1 retrieval approach

The NO_2 retrieval consists of three steps. First, the total NO_2 slant columns density (SCD) is retrieved using the Differential Optical Absorption Spectroscopy (DOAS) technique (for the 405-465 nm spectral window in the case of OMI). The uncertainty of the SCD is determined by the appropriateness of the fitting technique, the instrument noise, the choice of fitting window, and the orthogonality of the absorbers' cross sections (Bucsela et al., 2006; van Geffen et al., 2015; Lerot et al., 2010; Richter et al., 2011; Zara et al., 2018). The NO_2 SCD in DOMINO v2 has a bias at about $0.5\sim1.3 \times 10^{15}$ molec. cm^{-2} (Belmonte Rivas et al., 2014; Dirksen et al., 2011; van Geffen et al., 2015; Marchenko et al., 2015; Zara et al., 2018), which can be reduced by improving wavelength calibration and including O_2-O_2 and liquid water absorption in the fitting model (van Geffen et al., 2015; Zara et al., 2018). The tropospheric SCD is then obtained by subtracting the stratospheric SCD from the total SCD. The bias in the total SCD is mostly absorbed by this stratospheric separation step, which may not propagate into the tropospheric SCD (van Geffen et al., 2015). The last step converts the tropospheric SCD to VCD by using the tropospheric AMF (VCD = SCD / AMF). The tropospheric AMF is calculated at 438 nm by using look-up tables (in most retrieval algorithms) or online radiative transfer modeling (in POMINO) driven by ancillary parameters, which act as the dominant source of errors in retrieved NO_2 VCD data over polluted areas (Boersma et al., 2007; Lin et al., 2014b, 2015; Lorente et al., 2017).

Our POMINO algorithm focuses on the tropospheric AMF calculation over China and nearby regions, taking the tropospheric SCD (Dirksen et al., 2011) from DOMINO v2 (Boersma et al., 2011). POMINO improves upon the DOMINO v2 algorithm in the treatment of aerosols, surface reflectance, online radiative transfer calculations, spatial resolution of NO_2, temperature and pressure vertical profiles, and consistency between cloud and NO_2 retrievals (Lin et al., 2014b, 2015). In brief, we use the parallelized LIDORT-driven AMFv6 package to derive both cloud parameters and tropospheric NO_2 AMFs for individual OMI pixels online. NO_2 vertical profiles, aerosol optical properties and aerosol vertical profiles are taken from the nested GEOS-Chem model over Asia (0.667 ° long.×0.5° lat. before May 2013 and 0.3125 ° long.×0.25 ° lat. afterwards), and pressure and temperature profiles are taken from the GEOS-5 and GEOS-FP assimilated meteorological fields that drive GEOS-Chem simulations. Model aerosols are further adjusted by satellite data (see below). We adjust the pressure profiles based on the difference in elevation between the pixel center and the matching model grid cell (Zhou et al., 2010). We also account for the effects of surface bidirectional reflectance distribution function (BRDF) (Lin et al., 2014b; Zhou et al., 2010) by taking three kernel parameters (isotropic, volumetric and geometric) from the MODIS MCD43C2 data set at 440 nm (Lucht et al., 2000).

As a prerequisite to the POMINO NO_2 retrieval, clouds are retrieved through the O_2-O_2 algorithm (Acarreta et al., 2004; Stammes et al., 2008) with O_2-O_2 SCDs from OMCLDO2, and with pressure, temperature, surface reflectance, aerosols and other ancillary information consistent with the NO_2 retrieval. Note that the treatment of cloud scattering (as “effective” Lambertian reflector, as in other NO_2 algorithms) is different from the treatment of aerosol scattering/absorption (vertically resolved based on the Mie scheme).

批注 **[Microsof5]:** Add specific explanations.

POMINO uses the temporally and spatially varying aerosol information, including AOD, single scattering albedo (SSA), phase function and vertical profiles from GEOS-Chem simulations. POMINO v1.1 (this work) further uses CALIOP data to constrain the shape of aerosol vertical extinction profile. We run the model at a resolution of 0.3125° long.×0.25° lat. before May 2013 and 0.667° long.×0.5° lat. afterwards, as determined by the resolution of the driving meteorological fields. We then regrid the finer resolution model results to 0.667° long.×0.5° lat., to be consistent with the CALIOP data grid. We then sample the model data at times and locations with valid CALIOP data at 532 nm to establish the model monthly climatology.

For any month in a grid cell, we divide the CALIOP monthly climatology of aerosol extinction profile shape by model climatological profile shape to obtain a unitless scaling profile (Eq. 1), and apply this scaling profile to all days of that month in all years (Eq. 2). Such a climatological adjustment is based on the assumption that systematic model limitations are month-dependent and persist over the years and days (e.g., a too strong vertical gradient, see Sect. 3.3). Although this monthly adjustment means discontinuity on the day-to-day basis (e.g., from the last day of a month to the first day of the next month), such discontinuity does not significantly affect the NO_2 retrieval, based on our sensitivity test.

In Eqs. 1 and 2, E^{C} represents the CALIOP climatological aerosol extinction coefficient, E^{G} the GEOS-Chem extinction, E^{Gr} the post-scaling model extinction, and R the scaling profile. The subscript *i* denotes a grid cell, *k* a vertical layer, *d* a day, *m* a month, and *y* a year. Note that in Eq. 1, the extinction coefficient at each layer is normalized relative to the maximum value of that profile. This procedure ensures that the scaling is based on the relative shape of the extinction profile and is thus independent of the accuracies of CALIOP and GEOS-Chem AOD. We keep the absolute AOD value of GEOS-Chem unchanged in this step.

$$R_{i,k,m} = \frac{E^{C}_{i,k,m}/\max(E^{C}_{i,k,m})}{E^{G}_{i,k,m}/max(E^{G}_{i,k,m})} \quad (1)$$

$$E^{Gr}_{i,k,d,m,y} = E^{G}_{i,k,d,m,y} \times R_{i,k,m} \quad (2)$$

In POMINO, the GEOS-Chem AOD are further constrained by a MODIS/Aqua Collection 5.1 monthly AOD dataset compiled on the model grid (Lin et al., 2014b, 2015). POMINO v1.1 uses the Collection 5.1 AOD data before May 2013 and Collection 6 data afterwards. For adjustment, model AOD are projected to a 0.667° long.×0.5° lat. grid and then sampled at times and locations with valid MODIS data (Lin et al., 2015). As shown in Eq. 3, τ^{M} denotes MODIS AOD, τ^{G} GEOS-Chem AOD, and τ^{Mr} post-adjustment model AOD. The subscript *i* denotes a grid cell, *d* a day, *m* a month, and *y* a year. This AOD adjustment ensures that in any month, monthly mean GEOS-Chem AOD is the same as MODIS AOD while the modeled day-to-day variability is kept.

$$\tau^{Gr}_{i,d,m,y} = \frac{\tau^{M}_{i,m,y}}{\tau^{G}_{i,m,y}} \times \tau^{G}_{i,d,m,y} \quad (3)$$

Equations 4–5 show the complex effects of aerosols in calculating the AMF for any pixel. The AMF is the linear sum of tropospheric layer contributions to the slant column weighted by the vertical sub columns (Eq. 4). The box AMF, amf_k, describes the sensitivity of NO_2 SCD to layer k, and $x_{a,k}$ represent the subcolumn of layer k from a priori NO_2 profile. The l represent the first integrated layer, which is the layer above the ground for clear sky, or the layer above cloud top for cloudy sky. The t represent the tropopause layer. POMINO assumes the independent pixel approximation (IPA)

(Martin et al., 2002; Boersma et al., 2002). This means that the calculated AMF for any pixel consists of a fully cloudy-sky portion (AMF_{clr}) and a fully clear-sky portion (AMF_{cld}), with weights based on the cloud radiance fraction (CRF = $(1-\mathrm{CF})\cdot \mathrm{A_{clr}} + \mathrm{CF}\cdot \mathrm{A_{cld}}$, where $\mathrm{A_{clr}}$, $\mathrm{A_{cld}}$ are radiance from the clear-sky part and fully cloudy part of the pixel, respectively.) (Eq. 5). AMF_{cld} is affected by above-cloud aerosols, and AMF_{clr} is affected by aerosols in the entire column. Also, aerosols affect the retrieval of CRF. Thus, the improvement of aerosol vertical profile in POMINO v1.1 affects all the three quantities in Eq. 5 and thus leads to complex impacts on retrieved NO_2 VCD.

$$\mathrm{AMF} = \frac{\sum_l^t amf_k x_{a,k}}{\sum_l^t x_{a,k}} \quad (4)$$

$$\mathrm{AMF} = \mathrm{AMF}_{cld}\cdot \mathrm{CRF} + \mathrm{AMF}_{clr}\cdot(1-\mathrm{CRF}) \quad (5)$$

2.3 OMI pixel selection to evaluate POMINO v1.1, POMINO, DOMINO v2 and QA4ECV

We exclude OMI pixels affected by row anomaly (Schenkeveld et al., 2017) or with high albedo caused by icy/snowy ground. To screen out cloudy scenes, we choose pixels with CRF below 50% (effective cloud fraction is typically below 20%) in POMINO.

The selection of CRF threshold influences the validity of pixels. The “effective” CRF in DOMINO implicitly includes the influence of aerosols. In POMINO, the aerosol contribution is separated from that of the clouds, resulting in a lower CRF than for DOMINO. The CRF differs insignificantly between POMINO and POMINO v1.1, because the same AOD and other non-aerosol ancillary parameters are used in the retrieval process. Using the CRF from POMINO instead of DOMINO or QA4ECV for cloud screening means that the number of “valid” pixels in DOMINO increases by about 25%, particularly because much more pixels with high pollutant (aerosol and NO_2)

批注 **[Microsof6]:** Add explanation for CRF.

loadings are now included. This potentially reduces the sampling bias (Lin et al., 2014b, 2015), and the ensemble of pixels now includes scenes with high “aerosol radiative fractions”. Further research is needed to fully understand how much these high-aerosol scenes may be subject to the same screening issues as the cloudy scenes. Nevertheless, the limited evidence here and in Lin et al. (2014b, 2015) suggests that including these high-aerosol scenes does not affect the accuracy of NO_2 retrieval.

2.4 MAX-DOAS data

We use MAX-DOAS measurements at three suburban or urban sites in East China, including one urban site at the Institute of Atmospheric Physics (IAP) in Beijing (116.38° E, 39.38 ° N), one suburban site in Xianghe County (116.96° E, 39.75 ° N) to the south of Beijing, and one urban site in the Wuxi City (120.31° E, 31.57 ° N) in the Yangzi River delta (YRD). Figure 1 shows the locations of these sites overlaid with POMINO v1.1 NO_2 VCDs in August 2012. Table 1 summarizes the information of MAX-DOAS measurements.

The instruments in IAP and in Xianghe were designed at BIRA-IASB (Clémer et al., 2010). Such an instrument is a dual-channel system composed of two thermally regulated grating spectrometers, covering the ultraviolet (300–390 nm) and visible (400–720 nm) wavelengths. It measures scattered sunlight every 15 minutes at nine elevation angles: 2°, 4°, 6°, 8°, 10°, 12°, 15°, 30°, and 90°. The telescope of the instrument is pointed to the north. The data are analyzed following Hendrick et al. (2014). The Xianghe suburban site is influenced by pollution from the surrounding major cities like Beijing and Tianjin. At Xianghe, MAX-DOAS data are data are continuously available since early 2011, and data in 2012 are used here for comparison with OMI products. At IAP, MAX-DOAS data are available in 2008 and 2009 (Table 1), thus for comparison purposes we process OMI products to match the MAX-DOAS times.

Located on the roof of an 11-story building, the instrument at Wuxi was developed by Anhui Institute of Optics and Fine Mechanics (AIOFM) (Wang et al., 2015, 2017a). Its telescope is pointed to the north and records at five elevation angles (5°, 10°, 20°, 30° and 90°). Wuxi is a typical urban site affected by heavy NO_x and aerosol pollution. The measurements used here are analyzed in Wang et al. (2017a). Data are available in 2012 for comparison with OMI products.

When comparing the four OMI products against MAX-DOAS observations, temporal and spatial inconsistency in sampling is inevitable. The spatial inconsistency, together with the substantial horizontal inhomogeneity in NO_2, might be more important than the influence of temporal inconsistency (Wang et al., 2017b). The influence of the horizontal inhomogeneity was suggested to be about 10–30% for MAX-DOAS measurements in Beijing (Lin et al., 2014b; Ma et al., 2013) and 10–15% for less polluted locations like Tai'an, Mangshan and Rudong (Irie et al., 2012). Following previous studies (Lin et al., 2014b; Wang et al., 2015, 2017b), we average MAX-DOAS data within 2 h of the OMI overpass time, and we select OMI pixels within 25 km of a MAX-DOAS site whose viewing zenith angle is below 30°. To exclude local pollution events near the MAX-DOAS site (such as the abrupt increase of NO_2 caused by the pass of consequent vehicles during a very short period), the standard deviation of MAX-DOAS data within 2 h should not exceed 20% of their mean value (Lin et al., 2014b). We elect not to spatially average the OMI pixels because they can, to some degree, reflect the spatial variability in NO_2 and aerosols.

We further exclude MAX-DOAS data in cloudy conditions, as clouds can cause large uncertainties in MAX-DOAS and OMI data. To find the actual cloudy days, we use MODIS/Aqua cloud fraction data, MODIS/Aqua Level-3 corrected reflectance (true color) data at the $1° \times 1°$ resolution, and current weather data observed from the nearest ground meteorological station (indicated by the black triangles in Fig. 1b).

Since there is only one meteorological station available near the Beijing area, it is used for both IAP and Xianghe MAX-DOAS sites. We first use MODIS/Aqua corrected reflectance (true color) to distinguish clouds from haze. For cloudy days determined by the reflectance checking, we examine both the MODIS/Aqua cloud fraction data and the meteorological station cloud records, considering that MODIS/Aqua cloud fraction data may be missing or have a too coarse horizontal resolution to accurately interpret the cloud conditions at the MAX-DOAS site. We exclude MAX-DOAS NO_2 data if the MODIS/Aqua cloud fraction is larger than 60% and the meteorological station reports a "BROKEN" (cloud fraction ranges from 5/8 to 7/8) or "OVERCAST" (full cloud cover) sky. For the three MAX-DOAS sites together, this leads to 49 days with valid data out of 64 days with pre-screening data.

We note here that using cloud fraction data from MODIS/Aqua or MAX-DOAS (for Xianghe only, see Gielen et al., 2014) alone to screen cloudy scenes may not be appropriate on heavy-haze days. For example, on 8th January, 2012, MODIS/Aqua cloud fraction is about 70–80% over the North China Plain and MAX-DOAS at Xianghe suggests the presence of "thick clouds". However, both the meteorological station and MODIS/Aqua corrected reflectance (true color) product suggest that the North China Plain was covered by a thick layer of haze. Consequently, this day was excluded from the analysis.

3. Monthly climatology of aerosol extinction profiles from CALIOP and GEOS-Chem

3.1 CALIOP monthly climatology

The aerosol layer height (ALH) is a good indicator to what extent aerosols are mixed vertically (Castellanos et al., 2015). As defined in Eq. A1 in Appendix B, the ALH is the average height of aerosols weighted by vertically resolved aerosol extinction. Figure

2a shows the spatial distribution of our CALIOP ALH climatology in each season. At most places, the ALH reaches a maximum in spring or summer and a minimum in fall or winter. The lowest ALH in fall and winter can be attributed to heavy near-surface pollution and weak vertical transport. The high values in summer are related to strong convective activities. Over the north, the high values in spring are partly associated with Asian dust events, due to high surface winds and dry soil in this season (Huang et al., 2010; Proestakis et al., 2017; Wang et al., 2010), which also affects the oceanic regions via atmospheric transport. The springtime high ALH over the south may be related to the transport of carbonaceous aerosols from Southeast Asian biomass burning (Jethva et al., 2016). Averaged over the domain, the seasonal mean ALHs are 1.48 km, 1.43 km, 1.27km, 1.18 km in spring, summer, fall and winter.

Figure 3a,b further shows the climatological monthly variations of ALH averaged over Northern East China (the anthropogenic source region shown in orange in Fig. 1a) and Northwest China (the dust source region shown in yellow in Fig. 1a). The two regions exhibit distinctive temporal variations. Over Northern East China, the ALH reaches a maximum in April (~1.53 km) and a minimum in December (~1.14 km). Over Northwest China, the ALH peaks in August (~1.59km) because of strongest convection (Zhu et al., 2013), although the springtime ALH is also high.

Figure 4a shows the climatological seasonal regional average vertical profiles of aerosol extinction over Northern East China. Here, the aerosol extinction increases from the ground level to a peak at about 300–600 m (season dependent), above which it decreases gradually. The height of peak extinction is lowest in winter, consistent with a stagnant atmosphere, thin mixing layer, and increased emissions (from residential and industrial sectors). The large error bars (horizontal lines in different layers, standing for 1 standard deviation) indicate strong spatiotemporal variability of aerosol extinction.

Over Northwest China (Fig. 5a), the column total aerosol extinction is much smaller than that over Northern East China (Fig. 4a), due to lower anthropogenic sources and dominant natural dust emissions. Vertically, the decline of extinction from the peak-extinction height to 2 km is also much more gradual than the decline over Northern East China, indicating stronger lifting of surface emitted aerosols. In winter, the column total aerosol extinction is close to the high value in dusty spring, whereas the vertical gradient of extinction is strongest among the seasons. This reflects the high anthropogenic emissions in parts of Northwest China, which have been rapidly increasing in the 2000s due to relatively weak emission control supplemented by growing activities of relocation of polluted industries from the eastern coastal regions (Cui et al., 2016; Zhao et al., 2015).

Overall, the spatial and seasonal variations of CALIOP aerosol vertical profiles are consistent with changes in meteorological conditions, anthropogenic sources, and natural emissions. The data will be used to evaluate and adjust GEOS-Chem simulation results in Sect. 3.2. A comparison of our CALIOP dataset with NASA's official Level-3 data is presented in Appendix C.

3.2 Evaluation of GEOS-Chem aerosol extinction profiles

Figure 2b shows the spatial distribution of seasonal ALHs simulated by GEOS-Chem. The model captures the spatial and seasonal variations of CALIOP ALH (Fig. 2a) to some degree, with an underestimate by about 0.3 km on average. The spatial correlation between CALIOP (Fig. 2a) and GEOS-Chem (Fig. 2b) ALH is 0.37 in spring, 0.57 in summer, 0.40 in fall, and 0.44 in winter. The spatiotemporal consistency and underestimate is also clear from the regional mean monthly ALH data in Fig. 3 – the temporal correlation between GEOS-Chem and CALIOP ALH is 0.90 in Northern East China and 0.97 in Northwest China.

Figures 4a and 5a show the GEOS-Chem simulated 2007–2015 monthly climatological vertical profiles of aerosol extinction coefficient over Northern East China and Northwest China, respectively. Over Northern East China (Fig. 4a), the model (red line) captures the vertical distribution of CALIOP extinction (black line) below the height of 1 km, despite a slight underestimate in the magnitude of extinction and an overestimate in the peak-extinction height. From 1 to 5 km above the ground, the model substantially overestimates the rate of decline in extinction coefficient with increasing altitude. Across the seasons, GEOS-Chem underestimates the magnitude of aerosol extinction by up to 37% (depending on the height). Over Northwest China (Fig. 5a), GEOS-Chem has an underestimate in all seasons, with the largest bias by about 80% in winter likely due to underestimated water-soluble aerosols and dust emissions (Li et al., 2016; Wang et al., 2008a).

Since the POMINO v1.1 algorithm uses MODIS AOD to adjust model AOD, it only uses the CALIOP aerosol extinction profile shape to adjust the modeled shape (Eqs. 1 and 2). Figures 4b and 4b show the vertical shapes of aerosol extinction, averaged across all profiles in each season over Northern East China and Northwest China, respectively. Over Northern East China (Fig. 4b), GEOS-Chem underestimates the CALIOP values above 1 km by 52–71%. This underestimate leads to a lower ALH, consistent with the finding by van Donkelaar et al. (2013) and Lin et al. (2014b). Over Northwest China (Fig. 5b), the model also underestimates the CALIOP values above 1 km by 50–62%. These results imply the importance of correcting the modeled aerosol vertical shape prior to cloud and NO_2 retrievals.

4. Effects of aerosol vertical profile improvement on cloud retrieval in 2012

Figure 6a, b shows the monthly average ALH and cloud top height (CTH, corresponding to cloud pressure, CP) over Northern East China and Northwest China in 2012. In order to discuss the CTH, only cloudy days are analyzed here, by excluding days with zero cloud fraction (CF = 0, clear-sky cases) in POMINO. Although "clear sky" is used sometimes in the literature to represent low cloud coverage (e.g., CF < 0.2 or CRF < 0.5, Boersma et al., 2011; Chimot et al., 2016), here it strictly means CF = 0 while "cloudy sky" means CF > 0. About 62.7% of days contain non-zero fractions of clouds over Northern East China, and the number is 59.1% for Northwest China. The CF changes from POMINO to POMINO v1.1 (i.e., after aerosol vertical profile adjustment) are negligible (within ±0.5%, not shown) due to the same values of AOD and SSA used in both products. This is because overall CF is mostly driven by the continuum reflectance at 475 nm (mainly determined by AOD and surface reflectance, which remain unchanged), which is independent of aerosol profile but CTH is driven by the O_2-O_2 SCD, which is itself impacted by ALH.

Figure 6a, b shows that over the two regions, the CTH varies notably from one month to another, whereas the ALH is much more stable across the months. Over Northern East China, the ALH increases by 0.52 km from POMINO (orange dashed line) to POMINO v1.1 (orange solid line) due to the CALIOP-based monthly climatological adjustment. The increase in ALH means a stronger "shielding" effect of aerosols on the O_2-O_2 absorbing dimer, which, in turn, results in a reduced CTH by 0.69 km on average. For POMINO over Northern East China (Fig. 6a), the retrieved clouds usually extend above the aerosol layer, i.e., the CTH (grey dashed line) is much larger than the ALH (orange dashed line). Using the CALIOP climatology in POMINO v1.1 results in the ALH higher than the CTH in fall and winter. The more elevated ALH is consistent with the finding of Jethva et al. (2016) that a significant amount of absorbing aerosols resides above clouds over Northern East China based on 11-year (2004–2015) OMI near-UV observations.

The CTH in Northwest China is much lower than in Northern East China (Fig. 6a versus 7b). This is because the dominant type of actual clouds is (optically thin) cirrus over western China (Wang et al., 2014), which is interpreted by the O_2-O_2 cloud retrieval algorithm as reduced CTH (with cloud base from the ground). The reduction in CTH from POMINO to POMINO v1.1 over Northwest China is also smaller than the reduction over Northern East China, albeit with a similar enhancement in ALH, due to lower aerosol loadings (Fig. 6c versus 6d).

Figure 7g,h presents the relative change in CP from POMINO to POMINO v1.1 as a function of AOD (binned at an interval of 0.1) and changes in ALH from POMINO to POMINO v1.1 (ΔALH, binned every 0.2 km) across all pixels in 2012 over Northern East China. Results are separated for low cloud fraction (CF < 0.05 in POMINO, Fig. 7g) and modest cloud fraction (0.2 < CF < 0.3, Fig. 7h). The median of the CP changes for pixels within each AOD and ΔALH bin is shown. Figure 7e,f presents the corresponding numbers of occurrence under the two cloud conditions.

Figure 7 shows that over Northern East China, the increase in ALH is typically within 0.6 km for the case of CF < 0.05 (Fig. 7e), and the corresponding increase in CP is within 6% (Fig. 7g). In this case, the average CTH (2.95 km in POMINO versus 1.58 km in POMINO v1.1) becomes much lower than the average ALH (1.06 km in POMINO versus 1.98 km in POMINO v1.1). For the case with CF between 0.2 and 0.3, the increase in ALH is within 1.2 km for most scenes (Fig. 7f), which leads to a CP change of 2% (Fig. 7h), much smaller than the CP change for CF < 0.05 (Fig. 7g). This is partly because the larger the CF is, the smaller a change in CF is required to compensate for the ΔALH in the O_2-O_2 cloud retrieval algorithm. Furthermore, with 0.2 < CF < 0.3, the mean value of CTH is much higher than ALH in both POMINO (2.76 km for CTH versus 1.13km for ALH) and POMINO v1.1 (2.60km for CTH versus 2.09 km for ALH), thus a large portion of clouds are above aerosols so that the change in CP is less sensitive to ΔALH. We find that the summertime data contribute the highest portion (36.5%) to the occurrences for 0.2 < CF < 0.3.

For Northwest China (not shown), the dependence of CP changes to AOD and ΔALH is similar to that for Northern East China. In particular, the CP change is within 10% on average for the case of CF < 0.05 and 1.5% for the case of 0.2 < CF < 0.3.

5. Effects of aerosol vertical profile improvement on NO_2 retrieval in 2012

Figure 7a presents the percentage changes in clear-sky NO_2 VCD from POMINO to POMINO v1.1 as a function of binned AOD and ΔALH over Northern East China. Here, clear-sky pixels are chosen based on CF = 0 in POMINO. In any AOD bin, an increase in ΔALH leads to an enhancement in NO_2. And for any ΔALH, the change in VCD is greater (smaller) when AOD becomes larger (smaller), which indicates that the NO_2 retrieval is more sensitive to ALH in high aerosol loading cases. Clearly, the change in NO_2 is not a linear function of AOD and ΔALH.

For cloudy scenes (Fig. 7b,c, cloud data are based on POMINO), the change in NO_2 VCD is less sensitive to AOD and ΔALH. This is because the existence of clouds limits the optical effect of aerosols on tropospheric NO_2. Figure 6a presents the nitrogen layer height (NLH, defined as the average height of model simulated NO_2 weighted by its volume mixing ratio in each layer) in comparison to the ALH and CLH over Northern East China. The figure shows that the POMINO v1.1 CTH is higher than the NLH in all months and higher than the ALH in warm months, which means a “shielding” effect on both NO_2 and aerosols.

Over Northwest China (not shown), the changes in clear-sky NO_2 VCD are within 9% for most cases, which are much smaller than over Eastern China (within 18%). This is because the NLH is much higher than the CLH and ALH (Fig. 6b) in absence of surface anthropogenic emissions.

We convert the valid pixels into monthly mean Level-3 values datasets on a 0.25° long. × 0.25° lat. grid. Figure 8a,b compares the seasonal spatial variations of NO_2 VCD in POMINO v1.1 and POMINO in 2012. In both products, NO_2 peaks in winter due to the longest lifetime and highest anthropogenic emissions (Lin, 2012). NO_2 also reaches a maximum over Northern East China as a result of substantial anthropogenic sources. From POMINO to POMINO v1.1, the NO_2 VCD increases by 3.4% (-67.5–41.7%) in spring for the domain average (range), 3.0% (-59.5–34.4%) in summer, 4.6% (-15.3–39.6%) in fall and 5.3% (-68.4–49.3%) in winter. The NO_2 change is highly dependent on the location and season. The increase over Northern East China is largest in winter, wherein the positive value for ΔALH implies that elevated aerosol layers "shield" the NO_2 absorption.

6. Evaluating satellite products using MAX-DOAS data

We use MAX-DOAS data, after cloud screening (Sect. 2.4), to evaluate DOMNO v2, QA4ECV, POMINO and POMINO v1.1. The scatterplots in Fig. 9a-d compare the NO_2 VCDs from 162 OMI pixels on 49 days with their MAX-DOAS counterparts. Different colors differentiate the seasons. The high values of NO_2 VCD (> 30 × 10^{15} molec. cm^{-2}) occur mainly in fall (blue) and winter (black). POMINO v1.1 and POMINO capture the day-to-day variability of MAX-DOAS data, i.e., R^2 = 0.804 and 0.799, respectively. The normalized mean bias (NMB) of POMINO v1.1 relative to MAX-DOAS data (-3.4%) is smaller than the NMB of POMINO (-9.6%). Also, the reduced major axis (RMA) regression shows that the slope for POMINO v1.1 (0.95) is closer to unity than the slope for POMINO (0.78). When all OMI pixels in a day are averaged (Fig. 9e,f), the correlation across the total of 49 days further increase for both POMINO v1.1 (R^2 = 0.89) and POMINO (R^2 = 0.86), whereas POMINO v1.1 still has a lower NMB (-3.7%) and better slope (0.96) than POMINO (-10.4% and 0.82, respectively). These results suggest that correcting aerosol vertical profiles, at least on a climatology basis, already leads to a significant improved NO_2 retrieval from OMI.

Figure 9 shows that DOMINO v2 is correlated with MAX-DOAS ($R^2 = 0.68$ in Fig. 9c and 0.75 in Fig. 9g) but not as strong as POMINO and POMINO v1.1 for all days. The discrepancy between DOMINO v2 and MAX-DOAS is particularly large for very high NO_2 values (> 70 × 10^{15} molec. cm^{-2}). The R^2 for QA4ECV (0.75 in Fig. 9d and 0.82 in Fig. 9h) is slightly better than DOMINO, but the NMB is higher (-22.0% and -22.7%) and the slope drops to 0.66. These results are consistent with the finding of Lin et al. (2014b, 2015) that explicitly including aerosol optical effects improves the NO_2 retrieval.

Table 2 further shows the comparison statistics for 27 haze days. The haze days are determined when both the ground meteorological station data and MODIS/Aqua corrected reflectance (true color) data indicate a haze day. The table also lists AOD, SSA, CF and MAX-DOAS NO_2 VCD, as averaged over all haze days. A large amount of absorbing aerosols occurs on these haze days (AOD = 1.13, SSA = 0.90). The average MAX-DOAS NO_2 VCD reaches 51.92 × 10^{15} molec. cm^{-2}. Among the four satellite products, POMINO v1.1 has the highest R^2 (0.76) and the lowest bias (4.4%) with respect to MAX-DOAS, whereas DOMINO v2 and QA4ECV reproduce the variability to a limited extent (R^2 = 0.38 and 0.34, respectively). This is consistent with the previous finding that the accuracy of DOMINO v2 is reduced for polluted, aerosol-loaded scenes (Boersma et al., 2011; Chimot et al., 2016; Kanaya et al., 2014; Lin et al., 2014b).

Table 3 shows the comparison statistics for 36 cloud-free days (CF = 0 in POMINO, and AOD = 0.60 on average). Here, POMINO v1.1, POMINO and DONIMO v2 do not show large differences in R^2 (0.53–0.56) and NMB (20.8–29.4%) with respect to MAX-DOAS. QA4ECV has a higher R^2 (0.63) and a lower NMB (-5.83%), presumably

批注 **[Microsof7]:** Add discussion about QA4ECV product.

reflecting the improvements in this (EU-) consortium approach, at least in mostly cloud-free situations. However, the R^2 values for POMINO and POMINO v1.1 are much smaller than the R^2 values in haze days, whereas the opposite changes are true for DOMINO v2 and QA4ECV. Thus, for this limited set of data, the changes from DOMINO v2 and QA4ECV to POMINO and POMINO v1.1 mainly reflect the improved aerosol treatment in hazy scenes. Further research may use additional MAX-DOAS datasets to evaluate the satellite products more systematically.

7. Conclusions

This paper improves upon our previous POMINO algorithm (Lin et al., 2015) to retrieve the tropospheric NO_2 VCDs from OMI, by compiling a 9-year (2007–2015) CALIOP monthly climatology of aerosol vertical extinction profiles to adjust GEOS-Chem aerosol profiles used in the NO_2 retrieval process. The improved algorithm is referred to as POMINO v1.1. Compared to monthly climatological CALIOP data over China, GEOS-Chem simulations tend to underestimate the aerosol extinction above 1 km, as characterized by an underestimate in ALH by 300–600 m (seasonal and location dependent). Such a bias is corrected in POMINO v1.1 by dividing, for any month and grid cell, the CALIOP monthly climatological profile by the model climatological profile to obtain a scaling profile and then applying the scaling profile to model data in all days of that month in all years.

The aerosol extinction profile correction leads to an insignificant change in CF from POMINO to POMINO v1.1, since the AOD and surface reflectance are unchanged. In contrast, the correction results in a notably increase in CP (i.e., a decrease in CTH), due to lifting of aerosol layers. The CP changes are generally within 6% for scenes with low cloud fraction ($CF < 0.05$ in POMINO), and within 2% for scenes with modest cloud fraction ($0.2 < CF < 0.3$ in POMINO).

The NO_2 VCDs increase from POMINO to POMINO v1.1 in most cases due to lifting of aerosol layers that enhances the "shielding" of NO_2 absorption. The NO_2 VCD increases by 3.4% (-67.5–41.7%) in spring for the domain average (range), 3.0% (-59.5–34.4%) in summer, 4.6% (-15.3–39.6%) in fall and 5.3% (-68.4–49.3%) in winter. The NO_2 changes highly season and location dependent, and are most significant for wintertime Northern East China.

Further comparisons with independent MAX-DOAS NO_2 VCD data for 162 OMI pixels in 49 days show good performance of both POMINO v1.1 and POMINO in capturing the day-to-day variation of NO_2 (R^2=0.80, n=162), compared to DOMINO v2 (R^2=0.67) and the new QA4ECV product (R^2=0.75). The NMB is smaller in POMINO v1.1 (-3.4%) than in POMINO (-9.6%), with a slightly better slope (0.804 versus 0.784). On hazy days with high aerosol loadings (AOD = 1.13 on average), POMINO v1.1 has the highest R^2 (0.76) and the lowest bias (4.4%) whereas DOMINO and QA4ECV have difficulty in reproducing the day-to-day variability in MAX-DOAS NO_2 measurements (R^2 = 0.38 and 0.34, respectively). The four products show small differences in R^2 on clear-sky days (CF = 0 in POMINO, AOD = 0.60 on average), among which QA4ECV shows a highest R^2 (0.63) and lowest NMB (-5.83%), presumably reflecting the improvements in less polluted place such as Europe and the US. Thus the explicit aerosol treatment (in POMINO and POMINO v1.1) and the aerosol vertical profile correction (in POMINO v1.1) improves the NO_2 retrieval especially in hazy cases.

The POMINO v1.1 algorithm is a core step towards our next public release of data product, POMINO v2. This new release will contain a few additional updates, including but not limited to using MODIS Collection 6 Merged 10-km Level-2 AOD data that combine the Dark Target (Levy et al., 2013) and Deep Blue (Sayer et al., 2014) products, as well as MODIS MCD43C2 Collection 6 daily BRDF data. Meanwhile, the POMINO

批注 [Microsof8]: Clarify POMINO v1.1 won't be our released version.

algorithm framework is being applied to the recently launched TropOMI instrument that provides NO_2 information at a much higher spatial resolution (3.5 x 7 km^2). A modified algorithm can also be used to retrieve sulfur dioxide, formaldehyde and other trace gases from TropOMI, for which purposes our algorithm will be available to the community on a collaborative basis. Future research can correct the SSA and NO_2 vertical profile to further improve the retrieval algorithm, and can use more comprehensive independent data to evaluate the resulting satellite products.

Acknowledgements

This research is supported by the National Natural Science Foundation of China (41775115), the 973 program (2014CB441303), the Chinese Scholarship Council, and the EU FP7 QA4ECV project (grant no. 607405).

Appendix A: Introduction to the QA4ECV product

The QA4ECV NO_2 product (http://www.qa4ecv.eu/) builds on a (EU-) consortium approach to retrieve NO_2 from GOME, SCIAMACHY, GOME-2, and OMI. The main contributions are provided by BIRA-IASB, the University of Bremen (IUP), MPIC, KNMI, and Wageningen University. Uncertainties in spectral fitting for NO_2 SCDs and in AMF calculations were evaluated by Zara et al. (2018) and Lorente et al. (2017), respectively. QA4ECV contains improved SCD NO_2 data (Zara et al., 2018). Lorente et al., (2017) showed that across the above algorithms, there a structural uncertainty by 42% in the NO_2 AMF calculation over polluted areas. By comparing to our POMINO product, Lorente et al. also showed that the choice of aerosol correction may introduce an additional uncertainty by up to 50% for situations with high polluted cases, consistent with Lin et al. (2014b, 2015) and the findings here. For a complete description of the QA4ECV algorithm improvements, and quality assurance, please see Boersma et al. (2018).

Appendix B: Constructing the CALIOP monthly climatology of aerosol extinction vertical profile

Our use the all-sky Level-2 CALIOP data to construct the Level-3 monthly climatology. We choose the all-sky product instead of clear-sky data, since previous studies indicate that the climatological aerosol extinction profiles are affected insignificantly by the presence of clouds (Koffi et al., 2012; Winker et al., 2013). As we use this climatological data to adjust GEOS-Chem results, choosing all-sky data improves consistency with the model simulation when doing the daily correction.

To select valid pixels, we follow the data quality criteria by Winker et al., (2013) and Amiridis et al., (2015). Only the pixels with Cloud Aerosol Discrimination (CAD) scores between -20 and -100 with extinction Quality Control (QC) flag valued at 0, 1, 18, and 16 are selected. We further discard samples with an extinction uncertainty of 99.9 km^{-1}, which is indicative of unreliable retrieval. We only accept extinction values falling in the range from 0.0 to 1.25, according to CALIOP observation thresholds. Previous studies showed that weakly scattering edges of icy clouds are sometimes misclassified as aerosols (Winker et al., 2013). To eliminate contamination from icy clouds we exclude the aerosol layers above the cloud layer (with layer-top temperature below 0 ℃) when both of them are above 4km (Winker et al., 2013).

After the pixel-based screening, we aggregate the CALIOP data at the model grid (0.667° long. x 0.5° lat.) and vertical resolution (47 layers, with 36 layers or so in the troposphere). For each grid cell, we choose the CALIOP pixels within 1.5° of the grid cell center. CALIOP Level-2 data are always presented at the fixed 399 altitudes above sea level. To account for the difference in surface elevation between a CALIOP pixel and the respective model grid cell, we convert the altitude of the pixel to a height above the ground, by using the surface elevation data provided in CALIOP. We then average horizontally and vertically the profiles of all pixels within one model grid cell and layer.

We do the regridding day-by-day for all grid cells to ensure that GEOS-Chem and CALIOP extinction profiles are coincident spatially and temporally. Finally, we compile a monthly climatological dataset by averaging over 2007–2015.

Figure A1 shows the number of aerosol extinction profiles in each grid cell and 12 x 9 = 108 months that are used to compile the CALIOP climatology, both before and after data screening. Table A1 presents additional information on monthly and yearly bases. On average, there are 165 and 47 aerosol extinction profiles per month per grid cell before and after screening, respectively. In the final 9-year monthly climatology, each grid cell has about 420 aerosol extinction profiles on average, about 28% of the prior-screening profiles. Figure A1 shows that the number of valid profiles decreases sharply over the Tibet Plateau and at higher latitudes (> 43 ° N) due to complex terrain and icy/snowy ground.

As discussed above, we choose the CALIOP pixels within 1.5° of a grid cell center. We test this choice by examining the aerosol layer height (ALH) produced for that grid cell. The ALH is defined as the extinction-weighted height of aerosols (see Eq. A1, where *n* denotes the number of tropospheric layers, ε_i the aerosol extinction at layer i, and H_i the layer center height above the ground). We find that choosing pixels within 1.0° of a grid cell center leads to a nosier horizontal distribution of ALH, owing to the small footprint of CALIOP. On the other hand, choosing 2.0° leads to a too smooth spatial gradient of ALH with local characteristics of aerosol vertical distributions are largely lost. We thus decide that 1.5 ° is a good balance between noise and smoothness.

$$\mathrm{ALH} = \frac{\sum_{i=1}^{i=n} \varepsilon_i \mathrm{H}_i}{\sum_{i=1}^{i=n} \varepsilon_i} \qquad \text{(A1)}$$

Certain grid cells do not contain sufficient valid observations for some months of the climatological dataset. We fill in missing monthly values of a grid cell using valid data in the surrounding 5 x 5 = 25 grid cells (within ~ 100 km). If the 25 grid cells do not have enough valid data, we use those in the surrounding 7 x 7 = 49 grid cells (within ~ 150 km). A similar procedure is used by Lin et al. (2014b, 2015) to fill in missing values in the gridded MODIS AOD dataset.

For each grid cell in each month, we further correct singular values in the vertical profile. In a month, if a grid cell *i* has an ALH outside mean $\pm 1\sigma$ of its surrounding 25 or 49 grid cells, we select *i*'s surrounding grid cell *j* whose ALH is the median of *i*'s surrounding grid cells, and use *j*'s profile to replace *i*'s. Whether 25 or 49 surrounding grid cells are chosen depends on the number of valid pixels shown in Fig. A1b. If the number of valid pixels in *i* is below mean–1 σ of all grid cells in the whole domain, which is often the case for Tibetan grid cells, we use *i*'s surrounding 49 grid cells; otherwise we use *i*'s surrounding 25 grid cells.

Appendix C. Comparing our and NASA's CALIOP monthly climatology

We compare our gridded climatological profiles to NASA CALIOP Version 3 Level-3 all-sky monthly profiles at 532 nm (Winker et al., 2013). The NASA Level-3 data has a horizontal resolution of 2° lat. × 5° lon. and a vertical resolution of 60 m (from -0.5 to 12 km above sea level). We combine NASA monthly data over 2007–2015 to construct a monthly climatology for comparison with our own compilation. We only choose aerosol extinction data in the troposphere with error less than 0.15 (the valid range given in the CALIOP dataset). If the number of valid monthly profiles in a grid cell is less than five (i.e., for the same month in five out of the nine years), then we exclude data in that grid cell; see the dark gray grid cells in Fig. 2c.

Several methodological differences exist between generating our and NASA CALIOP datasets. First, the two datasets have different horizontal resolutions. Also, we sample all valid CALIOP pixels within 1.5° of a grid cell center, whereas the NASA dataset samples all valid pixels within a grid cell. Besides, our CALIOP dataset involves several steps of horizontal interpolation, for purposes of subsequent cloud and NO_2 retrievals, which is not done in the NASA dataset. In addition, we match CALIOP data vertically to the GEOS-Chem vertical resolution, whereas the NASA dataset maintains the original resolution.

Figure 2c shows the spatial distribution of ALH in all seasons based on NASA CALIOP Level-3 all-sky monthly climatology. The horizontal resolution of NASA data is much coarser than ours; and NASA data are largely missing over the southwest with complex terrains. We choose to focus on the comparison over East China (the black box in Fig. 1a). Over East China, the two climatology datasets generally exhibit similar spatial patterns of ALH in all seasons (Fig. 2a, c). The NASA dataset suggests higher ALHs than ours over Eastern China, especially in summer, due mainly to differences in the sampling and regridding processes. Figure 3c further compares the monthly variation of ALH between our (black line with error bars) and NASA (blue filled triangles) datasets averaged over East China. The two datasets are consistent in almost all months, indicating that their regional differences are largely smoothed out by spatial averaging.

References

Acarreta, J. R., De Haan, J. F. and Stammes, P.: Cloud pressure retrieval using the O_2-O_2 absorption band at 477 nm, J. Geophys. Res., 109(D5), D05204, doi:10.1029/2003JD003915, 2004.

Amiridis, V., Marinou, E., Tsekeri, A., Wandinger, U., Schwarz, A., Giannakaki, E., Mamouri, R., Kokkalis, P., Binietoglou, I., Solomos, S., Herekakis, T., Kazadzis, S., Gerasopoulos, E., Proestakis, E., Kottas, M., Balis, D., Papayannis, A., Kontoes, C., Kourtidis, K., Papagiannopoulos, N., Mona, L., Pappalardo, G., Le Rille, O. and Ansmann, A.: LIVAS: a 3-D multi-wavelength aerosol/cloud database based on

CALIPSO and EARLINET, Atmos. Chem. Phys., 15(13), 7127–7153, doi:10.5194/acp-15-7127-2015, 2015.

Belmonte Rivas, M., Veefkind, P., Boersma, F., Levelt, P., Eskes, H. and Gille, J.: Intercomparison of daytime stratospheric NO_2 satellite retrievals and model simulations, Atmos. Meas. Tech., 7(7), 2203–2225, doi:10.5194/amt-7-2203-2014, 2014.

Boersma, K. F., Eskes, H. J. and Brinksma, E. J.: Error analysis for tropospheric NO_2 retrieval from space, J. Geophys. Res. Atmos., 109(D4), n/a-n/a, doi:10.1029/2003JD003962, 2004.

Boersma, K. F., Eskes, H. J., Veefkind, J. P., Brinksma, E. J., van der A, R. J., Sneep, M., van den Oord, G. H. J., Levelt, P. F., Stammes, P., Gleason, J. F. and Bucsela, E. J.: Near-real time retrieval of tropospheric NO_2 from OMI, Atmos. Chem. Phys., 7(8), 2103–2118, doi:10.5194/acp-7-2103-2007, 2007.

Boersma, K. F., Eskes, H. J., Dirksen, R. J., van der A, R. J., Veefkind, J. P., Stammes, P., Huijnen, V., Kleipool, Q. L., Sneep, M., Claas, J., Leitão, J., Richter, A., Zhou, Y. and Brunner, D.: An improved tropospheric NO_2 column retrieval algorithm for the Ozone Monitoring Instrument, Atmos. Meas. Tech., 4(9), 1905–1928, doi:10.5194/amt-4-1905-2011, 2011.

Boersma, K.F., Eskes, H. J., Richter, A., De Smedt, I., Lorente, A., Beirle, S., van Geffen, J. H. G. M., Zara, M., Peters, E., Van Roozendael, M., Wagner, T., Maasakkers, J. D., van der A, R. J., Nightingale, J., De Rudder, A., Irie, H., and Pinardi, G.: Improving algorithms and uncertainty estimates for satellite NO_2 retrievals: Results from the Quality Assurance for Essential Climate Variables (QA4ECV) project, amt-2018-200, submitted, 2018.

Bucsela, E. J., Celarier, E. A., Wenig, M. O., Gleason, J. F., Veefkind, J. P., Boersma, K. F. and Brinksma, E. J.: Algorithm for NO_2 vertical column retrieval from the ozone monitoring instrument, IEEE Trans. Geosci. Remote Sens., 44(5), 1245–1258, doi:10.1109/TGRS.2005.863715, 2006.

Bucsela, E. J., Krotkov, N. A., Celarier, E. A., Lamsal, L. N., Swartz, W. H., Bhartia, P. K., Boersma, K. F., Veefkind, J. P., Gleason, J. F. and Pickering, K. E.: A new stratospheric and tropospheric NO_2 retrieval algorithm for nadir-viewing satellite instruments: applications to OMI, Atmos. Meas. Tech., 6(10), 2607–2626, doi:10.5194/amt-6-2607-2013, 2013.

Castellanos, P., Boersma, K. F. and van der Werf, G. R.: Satellite observations indicate substantial spatiotemporal variability in biomass burning NO_X emission factors for South America, Atmos. Chem. Phys., 14(8), 3929–3943, doi:10.5194/acp-14-3929-2014, 2014.

Castellanos, P., Boersma, K. F., Torres, O. and de Haan, J. F.: OMI tropospheric NO_2 air mass factors over South America: effects of biomass burning aerosols, Atmos. Meas. Tech., 8(9), 3831–3849, doi:10.5194/amt-8-3831-2015, 2015.

Chazette, P., Raut, J.-C., Dulac, F., Berthier, S., Kim, S.-W., Royer, P., Sanak, J., Loaëc, S. and Grigaut-Desbrosses, H.: Simultaneous observations of lower tropospheric continental aerosols with a ground-based, an airborne, and the spaceborne CALIOP lidar system, J. Geophys. Res., 115(D4), D00H31, doi:10.1029/2009JD012341, 2010.

Chimot, J., Vlemmix, T., Veefkind, J. P., de Haan, J. F. and Levelt, P. F.: Impact of aerosols on the OMI tropospheric NO_2 retrievals over industrialized regions: how accurate is the aerosol correction of cloud-free scenes via a simple cloud model?, Atmos. Meas. Tech., 9(2), 359–382, doi:10.5194/amt-9-359-2016, 2016.

Clémer, K., Van Roozendael, M., Fayt, C., Hendrick, F., Hermans, C., Pinardi, G., Spurr, R., Wang, P. and De Mazière, M.: Multiple wavelength retrieval of tropospheric aerosol optical properties from MAX-DOAS measurements in Beijing, Atmos. Meas. Tech., 3(4), 863–878, doi:10.5194/amt-3-863-2010, 2010.

Cui, Y., Lin, J., Song, C., Liu, M., Yan, Y., Xu, Y. and Huang, B.: Rapid growth in nitrogen dioxide pollution over Western China, 2005–2013, Atmos. Chem. Phys., 16(10), 6207–6221, doi:10.5194/acp-16-6207-2016, 2016.

Dirksen, R. J., Boersma, K. F., Eskes, H. J., Ionov, D. V., Bucsela, E. J., Levelt, P. F. and Kelder, H. M.: Evaluation of stratospheric NO_2 retrieved from the Ozone Monitoring Instrument: Intercomparison, diurnal cycle, and trending, J. Geophys. Res., 116(D8), D08305, doi:10.1029/2010JD014943, 2011.

van Geffen, J. H. G. M., Boersma, K. F., Van Roozendael, M., Hendrick, F., Mahieu, E., De Smedt, I., Sneep, M. and Veefkind, J. P.: Improved spectral fitting of nitrogen dioxide from OMI in the 405–465 nm window, Atmos. Meas. Tech., 8(4), 1685–1699, doi:10.5194/amt-8-1685-2015, 2015.

Gielen, C., Van Roozendael, M., Hendrick, F., Pinardi, G., Vlemmix, T., De Bock, V., De Backer, H., Fayt, C., Hermans, C., Gillotay, D. and Wang, P.: A simple and versatile cloud-screening method for MAX-DOAS retrievals, Atmos. Meas. Tech., 7(10), 3509–3527, doi:10.5194/amt-7-3509-2014, 2014.

Hendrick, F., Muller, J. F., Clemer, K., Wang, P., De Maziere, M., Fayt, C., Gielen, C., Hermans, C., Ma, J. Z., Pinardi, G., Stavrakou, T., Vlemmix, T., and Van Roozendael, M.: Four years of ground-based MAX-DOAS observations of HONO and NO_2 in the Beijing area, Atmospheric Chemistry and Physics, 14, 765-781, 10.5194/acp-14-765-2014, 2014.

Huang, Z., Huang, J., Bi, J., Wang, G., Wang, W., Fu, Q., Li, Z., Tsay, S.-C. and Shi, J.: Dust aerosol vertical structure measurements using three MPL lidars during 2008 China-U.S. joint dust field experiment, J. Geophys. Res. Atmos., 115(D7), n/a-n/a, doi:10.1029/2009JD013273, 2010.

Irie, H., Boersma, K. F., Kanaya, Y., Takashima, H., Pan, X. and Wang, Z. F.: Quantitative bias estimates for tropospheric NO_2 columns retrieved from SCIAMACHY, OMI, and GOME-2 using a common standard for East Asia, Atmos. Meas. Tech., 5(10), 2403–2411, doi:10.5194/amt-5-2403-2012, 2012.

Jethva, H., Torres, O., and Ahn, C.: A ten-year global record of absorbing aerosols above clouds from OMI's near-UV observations, in: Remote Sensing of the Atmosphere, Clouds, and Precipitation Vi, edited by: Im, E., Kumar, R., and Yang, S., Proceedings of SPIE, 2016.

Johnson, M. S., Meskhidze, N. and Praju Kiliyanpilakkil, V.: A global comparison of GEOS-Chem-predicted and remotely-sensed mineral dust aerosol optical depth and extinction profiles, J. Adv. Model. Earth Syst., 4(3), M07001, doi:10.1029/2011MS000109, 2012.

Kacenelenbogen, M., Redemann, J., Vaughan, M. A., Omar, A. H., Russell, P. B., Burton, S., Rogers, R. R., Ferrare, R. A. and Hostetler, C. A.: An evaluation of CALIOP/CALIPSO's aerosol-above-cloud detection and retrieval capability over North America, J. Geophys. Res. Atmos., 119(1), 230–244, doi:10.1002/2013JD020178, 2014.

Kanaya, Y., Irie, H., Takashima, H., Iwabuchi, H., Akimoto, H., Sudo, K., Gu, M., Chong, J., Kim, Y. J., Lee, H., Li, A., Si, F., Xu, J., Xie, P.-H., Liu, W.-Q., Dzhola, A., Postylyakov, O., Ivanov, V., Grechko, E., Terpugova, S. and Panchenko, M.: Long-term MAX-DOAS network observations of NO_2 in Russia and Asia

(MADRAS) during the period 2007-2012: instrumentation, elucidation of climatology, and comparisons with OMI satellite observations and global model simulations, Atmos. Chem. Phys., 14(15), 7909–7927, doi:10.5194/acp-14-7909-2014, 2014.

Kim, S.-W., Heckel, A., Frost, G. J., Richter, A., Gleason, J., Burrows, J. P., McKeen, S., Hsie, E.-Y., Granier, C. and Trainer, M.: NO_2 columns in the western United States observed from space and simulated by a regional chemistry model and their implications for NO_x emissions, J. Geophys. Res., 114(D11), D11301, doi:10.1029/2008JD011343, 2009.

Koffi, B., Schulz, M., Bréon, F.-M., Griesfeller, J., Winker, D., Balkanski, Y., Bauer, S., Berntsen, T., Chin, M., Collins, W. D., Dentener, F., Diehl, T., Easter, R., Ghan, S., Ginoux, P., Gong, S., Horowitz, L. W., Iversen, T., Kirkevåg, A., Koch, D., Krol, M., Myhre, G., Stier, P. and Takemura, T.: Application of the CALIOP layer product to evaluate the vertical distribution of aerosols estimated by global models: AeroCom phase I results, J. Geophys. Res. Atmos., 117(D10), n/a-n/a, doi:10.1029/2011JD016858, 2012.

Leitão, J., Richter, A., Vrekoussis, M., Kokhanovsky, A., Zhang, Q. J., Beekmann, M. and Burrows, J. P.: On the improvement of NO_2 satellite retrievals – aerosol impact on the airmass factors, Atmos. Meas. Tech., 3(2), 475–493, doi:10.5194/amt-3-475-2010, 2010.

Lerot, C., Stavrakou, T., De Smedt, I., Müller, J.-F. and Van Roozendael, M.: Glyoxal vertical columns from GOME-2 backscattered light measurements and comparisons with a global model, Atmos. Chem. Phys., 10(24), 12059–12072, doi:10.5194/acp-10-12059-2010, 2010.

Levy, R. C., Mattoo, S., Munchak, L. A., Remer, L. A., Sayer, A. M., Patadia, F. and Hsu, N. C.: The Collection 6 MODIS aerosol products over land and ocean, Atmos. Meas. Tech., 6(11), 2989–3034, doi:10.5194/amt-6-2989-2013, 2013.

Li, S., Yu, C., Chen, L., Tao, J., Letu, H., Ge, W., Si, Y. and Liu, Y.: Inter-comparison of model-simulated and satellite-retrieved componential aerosol optical depths in China, Atmos. Environ., 141, 320–332, doi:https://doi.org/10.1016/j.atmosenv.2016.06.075, 2016.

Lin, J., Pan, D., Davis, S. J., Zhang, Q., He, K., Wang, C., Streets, D. G., Wuebbles, D. J. and Guan, D.: China's international trade and air pollution in the United States, Proc. Natl. Acad. Sci., 111(5), 1736–1741, doi:10.1073/pnas.1312860111, 2014a.

Lin, J.-T.: Satellite constraint for emissions of nitrogen oxides from anthropogenic, lightning and soil sources over East China on a high-resolution grid, Atmos. Chem. Phys., 12(6), 2881–2898, doi:10.5194/acp-12-2881-2012, 2012.

Lin, J.-T., McElroy, M. B. and Boersma, K. F.: Constraint of anthropogenic NO_X emissions in China from different sectors: a new methodology using multiple satellite retrievals, Atmos. Chem. Phys., 10(1), 63–78, doi:10.5194/acp-10-63-2010, 2010.

Lin, J.-T., Martin, R. V., Boersma, K. F., Sneep, M., Stammes, P., Spurr, R., Wang, P., Van Roozendael, M., Clémer, K. and Irie, H.: Retrieving tropospheric nitrogen dioxide from the Ozone Monitoring Instrument: effects of aerosols, surface reflectance anisotropy, and vertical profile of nitrogen dioxide, Atmos. Chem. Phys., 14(3), 1441–1461, doi:10.5194/acp-14-1441-2014, 2014b.

Lin, J.-T., Liu, M.-Y., Xin, J.-Y., Boersma, K. F., Spurr, R., Martin, R. and Zhang, Q.: Influence of aerosols and surface reflectance on satellite NO_2 retrieval: seasonal and spatial characteristics and implications for NO_x emission constraints, Atmos. Chem. Phys., 15(19), 11217–11241, doi:10.5194/acp-15-11217-2015, 2015.

Lorente, A., Folkert Boersma, K., Yu, H., Dörner, S., Hilboll, A., Richter, A., Liu, M., Lamsal, L. N., Barkley, M., De Smedt, I., Van Roozendael, M., Wang, Y., Wagner, T., Beirle, S., Lin, J.-T., Krotkov, N., Stammes, P., Wang, P., Eskes, H. J. and Krol, M.: Structural uncertainty in air mass factor calculation for NO_2 and HCHO satellite retrievals, Atmos. Meas. Tech., 10(3), 759–782, doi:10.5194/amt-10-759-2017, 2017.

Lucht, W., Schaaf, C. B. and Strahler, A. H.: An algorithm for the retrieval of albedo from space using semiempirical BRDF models, IEEE Trans. Geosci. Remote Sens., 38(2), 977–998, doi:10.1109/36.841980, 2000.

Ma, J. Z., Beirle, S., Jin, J. L., Shaiganfar, R., Yan, P. and Wagner, T.: Tropospheric NO_2 vertical column densities over Beijing: results of the first three years of ground-based MAX-DOAS measurements (2008-2011) and satellite validation, Atmos. Chem. Phys., 13(3), 1547–1567, doi:10.5194/acp-13-1547-2013, 2013.

Ma, X. and Yu, F.: Seasonal variability of aerosol vertical profiles over east US and west Europe: GEOS-Chem/APM simulation and comparison with CALIPSO observations, Atmos. Res., 140–141, 28–37, doi:https://doi.org/10.1016/j.atmosres.2014.01.001, 2014.

Martin, R. V.: An improved retrieval of tropospheric nitrogen dioxide from GOME, J. Geophys. Res., 107(D20), 4437, doi:10.1029/2001JD001027, 2002.

Misra, A., Tripathi, S. N., Kaul, D. S. and Welton, E. J.: Study of MPLNET-Derived Aerosol Climatology over Kanpur, India, and Validation of CALIPSO Level 2 Version 3 Backscatter and Extinction Products, J. Atmos. Ocean. Technol., 29(9), 1285–1294, doi:10.1175/JTECH-D-11-00162.1, 2012.

Miyazaki, K. and Eskes, H.: Constraints on surface NO_X emissions by assimilating satellite observations of multiple species, Geophys. Res. Lett., 40(17), 4745–4750, doi:10.1002/grl.50894, 2013.

Proestakis, E., Amiridis, V., Marinou, E., Georgoulias, A. K., Solomos, S., Kazadzis, S., Chimot, J., Che, H., Alexandri, G., Binietoglou, I., Kourtidis, K. A., de Leeuw, G. and van der A, R. J.: 9-year spatial and temporal evolution of desert dust aerosols over South-East Asia as revealed by CALIOP, Atmos. Chem. Phys. Discuss., 1–35, doi:10.5194/acp-2017-797, 2017.

Richter, A., Begoin, M., Hilboll, A. and Burrows, J. P.: An improved NO_2 retrieval for the GOME-2 satellite instrument, Atmos. Meas. Tech., 4(6), 1147–1159, doi:10.5194/amt-4-1147-2011, 2011.

Marchenko, S., Krotkov, N. A., Lamsal, L. N., Celarier, E. A., Swartz, W. H., and Bucsela, E. J.: Revising the slant column density retrieval of nitrogen dioxide observed by the Ozone Monitoring Instrument, J. Geophys. Res. Atmos., 120(11), 5670–5692, doi:10.1002/2014JD022913, 2015.

Sareen, N., Schwier, A. N., Shapiro, E. L., Mitroo, D. and McNeill, V. F.: Secondary organic material formed by methylglyoxal in aqueous aerosol mimics, Atmos. Chem. Phys., 10(3), 997–1016, doi:10.5194/acp-10-997-2010, 2010.

Sayer, A. M., Munchak, L. A., Hsu, N. C., Levy, R. C., Bettenhausen, C. and Jeong, M.-J.: MODIS Collection 6 aerosol products: Comparison between Aqua's e-Deep Blue, Dark Target, and "merged" data sets, and usage recommendations, J. Geophys. Res. Atmos., 119(24), 13,965-13,989, doi:10.1002/2014JD022453, 2014.

Schenkeveld, V. M. E., Jaross, G., Marchenko, S., Haffner, D., Kleipool, Q. L., Rozemeijer, N. C., Veefkind, J. P., and Levelt, P. F.: In-flight performance of the Ozone Monitoring Instrument, Atmospheric Measurement Techniques, 10, 1957-1986, 10.5194/amt-10-1957-2017, 2017.

Stammes, P., Sneep, M., de Haan, J. F., Veefkind, J. P., Wang, P. and Levelt, P. F.: Effective cloud fractions from the Ozone Monitoring Instrument: Theoretical framework and validation, J. Geophys. Res., 113(D16), D16S38, doi:10.1029/2007JD008820, 2008.

Stavrakou, T., Müller, J.-F., Bauwens, M., De Smedt, I., Lerot, C., Van Roozendael, M., Coheur, P.-F., Clerbaux, C., Boersma, K. F., van der A, R. and Song, Y.: Substantial Underestimation of Post-Harvest Burning Emissions in the North China Plain Revealed by Multi-Species Space Observations, Sci. Rep., 6, 32307, doi:10.1038/srep32307, 2016.

van Donkelaar, A., Martin, R. V., Spurr, R. J. D., Drury, E., Remer, L. A., Levy, R. C., and Wang, J.: Optimal estimation for global ground-level fine particulate matter concentrations, Journal of Geophysical Research-Atmospheres, 118, 5621-5636, 10.1002/jgrd.50479, 2013.

Veefkind, J. P., de Haan, J. F., Sneep, M. and Levelt, P. F.: Improvements to the OMI O_2-O_2 operational cloud algorithm and comparisons with ground-based radar–lidar observations, Atmos. Meas. Tech., 9(12), 6035–6049, doi:10.5194/amt-9-6035-2016, 2016.

Verstraeten, W. W., Neu, J. L., Williams, J. E., Bowman, K. W., Worden, J. R. and Boersma, K. F.: Rapid increases in tropospheric ozone production and export from China, Nat. Geosci., 8, 690 [online] Available from: http://dx.doi.org/10.1038/ngeo2493, 2015.

Wang, J., Jacob, D. J. and Martin, S. T.: Sensitivity of sulfate direct climate forcing to the hysteresis of particle phase transitions, J. Geophys. Res. Atmos., 113(D11), n/a-n/a, doi:10.1029/2007JD009368, 2008a.

Wang, M., Gu, J., Yang, R., Zeng, L. and Wang, S.: Comparison of cloud type and frequency over China from surface, FY-2E, and CloudSat observations, vol. 9259, pp.

925913–925914. [online] Available from: http://dx.doi.org/10.1117/12.2069110, 2014.

Wang, P. and Stammes, P.: Evaluation of SCIAMACHY Oxygen A band cloud heights using Cloudnet measurements, Atmos. Meas. Tech., 7(5), 1331–1350, doi:10.5194/amt-7-1331-2014, 2014.

Wang, P., Stammes, P., van der A, R., Pinardi, G. and van Roozendael, M.: FRESCO+: an improved O_2 A-band cloud retrieval algorithm for tropospheric trace gas retrievals, Atmos. Chem. Phys., 8(21), 6565–6576, doi:10.5194/acp-8-6565-2008, 2008b.

Wang, X., Huang, J., Zhang, R., Chen, B. and Bi, J.: Surface measurements of aerosol properties over northwest China during ARM China 2008 deployment, J. Geophys. Res. Atmos., 115(D7), n/a-n/a, doi:10.1029/2009JD013467, 2010.

Wang, Y., Penning de Vries, M., Xie, P. H., Beirle, S., Dörner, S., Remmers, J., Li, A. and Wagner, T.: Cloud and aerosol classification for 2.5 years of MAX-DOAS observations in Wuxi (China) and comparison to independent data sets, Atmos. Meas. Tech., 8(12), 5133–5156, doi:10.5194/amt-8-5133-2015, 2015.

Wang, Y., Lampel, J., Xie, P., Beirle, S., Li, A., Wu, D. and Wagner, T.: Ground-based MAX-DOAS observations of tropospheric aerosols, NO_2, SO_2 and HCHO in Wuxi, China, from 2011 to 2014, Atmos. Chem. Phys., 17(3), 2189–2215, doi:10.5194/acp-17-2189-2017, 2017a.

Wang, Y., Beirle, S., Lampel, J., Koukouli, M., De Smedt, I., Theys, N., Li, A., Wu, D., Xie, P., Liu, C., Van Roozendael, M., Stavrakou, T., Müller, J.-F. and Wagner, T.: Validation of OMI, GOME-2A and GOME-2B tropospheric NO_2, SO_2 and HCHO products using MAX-DOAS observations from 2011 to 2014 in Wuxi, China:

investigation of the effects of priori profiles and aerosols on the satellite products, Atmos. Chem. Phys., 17(8), 5007–5033, doi:10.5194/acp-17-5007-2017, 2017b.

Winker, D. M., Pelon, J., Coakley, J. A., Ackerman, S. A., Charlson, R. J., Colarco, P. R., Flamant, P., Fu, Q., Hoff, R. M., Kittaka, C., Kubar, T. L., Le Treut, H., Mccormick, M. P., Mégie, G., Poole, L., Powell, K., Trepte, C., Vaughan, M. A. and Wielicki, B. A.: The CALIPSO Mission, Bull. Am. Meteorol. Soc., 91(9), 1211–1230, doi:10.1175/2010BAMS3009.1, 2010.

Winker, D. M., Tackett, J. L., Getzewich, B. J., Liu, Z., Vaughan, M. A. and Rogers, R. R.: The global 3-D distribution of tropospheric aerosols as characterized by CALIOP, Atmos. Chem. Phys., 13(6), 3345–3361, doi:10.5194/acp-13-3345-2013, 2013.

Zara, M., Boersma, K. F., De Smedt, I., Richter, A., Peters, E., Van Geffen, J. H. G. M., Beirle, S., Wagner, T., Van Roozendael, M., Marchenko, S., Lamsal, L. N. and Eskes, H. J.: Improved slant column density retrieval of nitrogen dioxide and formaldehyde for OMI and GOME-2A from QA4ECV: intercomparison, uncertainty characterization, and trends, Atmos. Meas. Tech. Discuss., 1–47, doi:10.5194/amt-2017-453, 2018.

Zhang, Q., Streets, D. G., Carmichael, G. R., He, K. B., Huo, H., Kannari, A., Klimont, Z., Park, I. S., Reddy, S., Fu, J. S., Chen, D., Duan, L., Lei, Y., Wang, L. T. and Yao, Z. L.: Asian emissions in 2006 for the NASA INTEX-B mission, Atmos. Chem. Phys., 9(14), 5131–5153, doi:10.5194/acp-9-5131-2009, 2009.

Zhao, C. and Wang, Y.: Assimilated inversion of NO_X emissions over east Asia using OMI NO_2 column measurements, Geophys. Res. Lett., 36(6), L06805, doi:10.1029/2008GL037123, 2009.

Zhao, H. Y., Zhang, Q., Guan, D. B., Davis, S. J., Liu, Z., Huo, H., Lin, J. T., Liu, W. D. and He, K. B.: Assessment of China's virtual air pollution transport embodied in trade by using a consumption-based emission inventory, Atmos. Chem. Phys., 15(10), 5443–5456, doi:10.5194/acp-15-5443-2015, 2015.

Zhou, Y., Brunner, D., Spurr, R. J. D., Boersma, K. F., Sneep, M., Popp, C. and Buchmann, B.: Accounting for surface reflectance anisotropy in satellite retrievals of tropospheric NO_2, Atmos. Meas. Tech., 3(5), 1185–1203, doi:10.5194/amt-3-1185-2010, 2010.

Zhu, W., Xu, C., Qian, X. and Wei, H.: Statistical analysis of the spatial-temporal distribution of aerosol extinction retrieved by micro-pulse lidar in Kashgar, China, Opt. Express, 21(3), 2531–2537, doi:10.1364/OE.21.002531, 2013.

Table A1. Number of CALIOP observations in a grid cell (0.667°× 0.5°).

	Before filtering				After filtering			
	Mean	Median	Minima	Maximum	Mean	Median	Minima	Maximum
For a month	165	169	0	291	47	39	0	223
For the same month in nine years	1483	1513	192	1921	420	395	0	1548
For all months in nine years	17794	18528	5608	20781	5033	5381	146	12650

Table 1. MAX-DOAS measurement sites and corresponding meteorological stations.

MAX-DOAS site name	Site information	Measurement times	Corresponding meteorological station name	Meteorological station information
Xianghe	116.96°E, 39.75°N, 36 m, suburban	2012/01/01 -2012/12/31	CAPITAL INTERNATIONA	116.89°E, 40.01°N, 35.4 m
IAP	116.38°E, 39.98°N, 92 m, urban	2008/06/22 -2009/04/16	CAPITAL INTERNATIONA	116.89°E, 40.01°N, 35.4 m
Wuxi	120.31°E, 31.57°N, 20 m, urban	2012/01/01 -2012/12/31	HONGQIAO INTL	121.34°E, 31.20°N, 3 m

Table 2. Evaluation of OMI NO_2 products with respect to MAX-DOAS on 27 haze days [1].

	POMINO v1.1	POMINO	DOMINO v2	QA4ECV
Slope	1.07	0.80	1.11	0.58
Intercept (10^{15} molec./cm^2)	-3.58	1.76	-11.79	3.20
R^2	0.76	0.68	0.38	0.34
NMB (%)	4.4	-9.4	-5.0	-26.11

1. The haze days are determined when the ground meteorological station data and MODIS/Aqua corrected reflectance (true color) data both indicate a haze day. Average across the days, AOD = 1.13 (median = 1.10), SSA = 0.90 (0.91), MAX-DOAS NO_2 = 51.92 x 10^{15} molec. cm^{-2}, and CF = 0.06 (0.03).

Table 3. Evaluation of OMI NO_2 products with respect to MAX-DOAS on 36 cloud-free days [1].

	POMINO v1.1	POMINO	DOMINO v2	QA4ECV
Slope	1.30	1.13	0.92	0.79
Intercept	-0.61	0.31	2.32	1.05
R^2	0.55	0.56	0.53	0.63
NMB (%)	29.4	20.8	21.9	-5.83

1. CF=0 in POMINO product. Average across the days, AOD = 0.60 (median = 0.47), SSA = 0.90 (0.91), and MAX-DOAS NO_2 = 26.82 x 10^{15} molec. cm^{-2}.

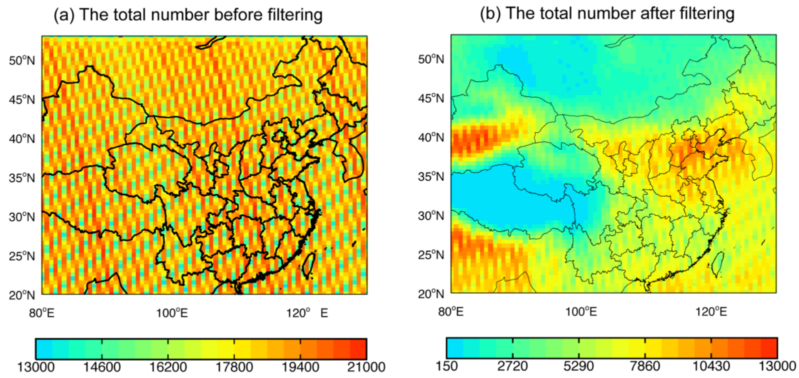

Figure A1. The total number of CALIOP Level-2 aerosol extinction profiles at 532 nm used to derive our climatological (2007–2015) dataset on a 0.667° long. x 0.5° lat. grid (a) before and (b) after filtering.

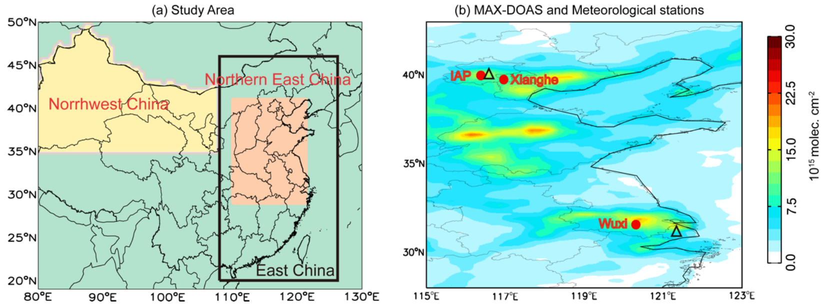

Figure 1. (a) Three study areas: Northern East China, Northwest China, and East China. (b) MAX-DOAS measurement sites (red dots) and corresponding meteorological stations (black triangle) overlaid on POMINO v1.1 NO_2 VCDs in August 2012.

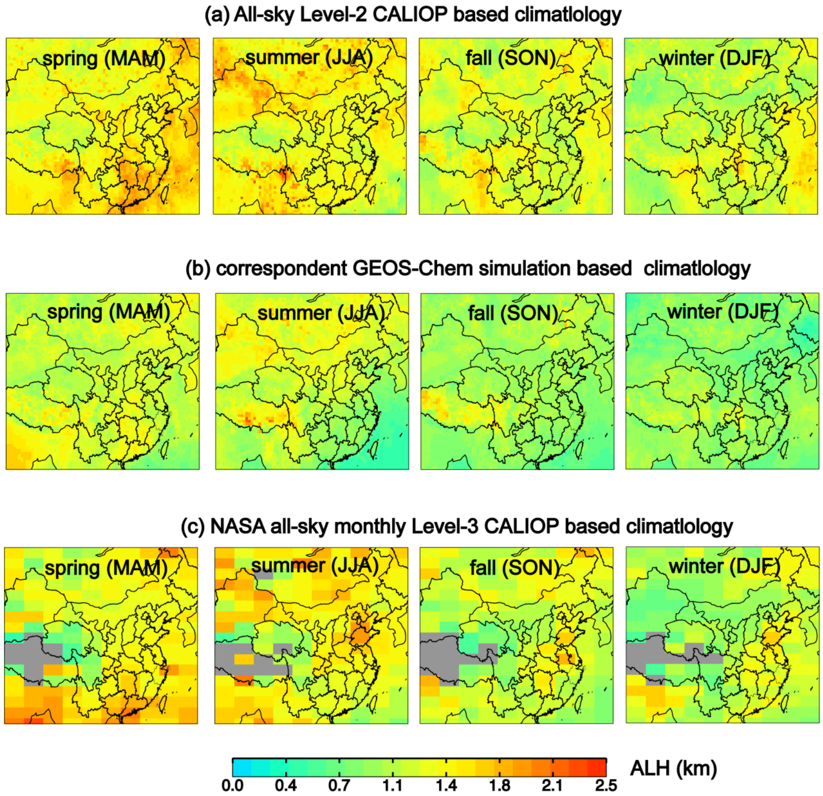

Figure 2. Seasonal spatial patterns of ALH climatology at 532 nm on a 0.667° long. x 0.50 ° lat. grid based on (a) our complied all-sky Level-2 CALIOP data, (b) corresponding GEOS-Chem simulations, and (c) NASA all-sky monthly Level-3 CALIOP dataset.

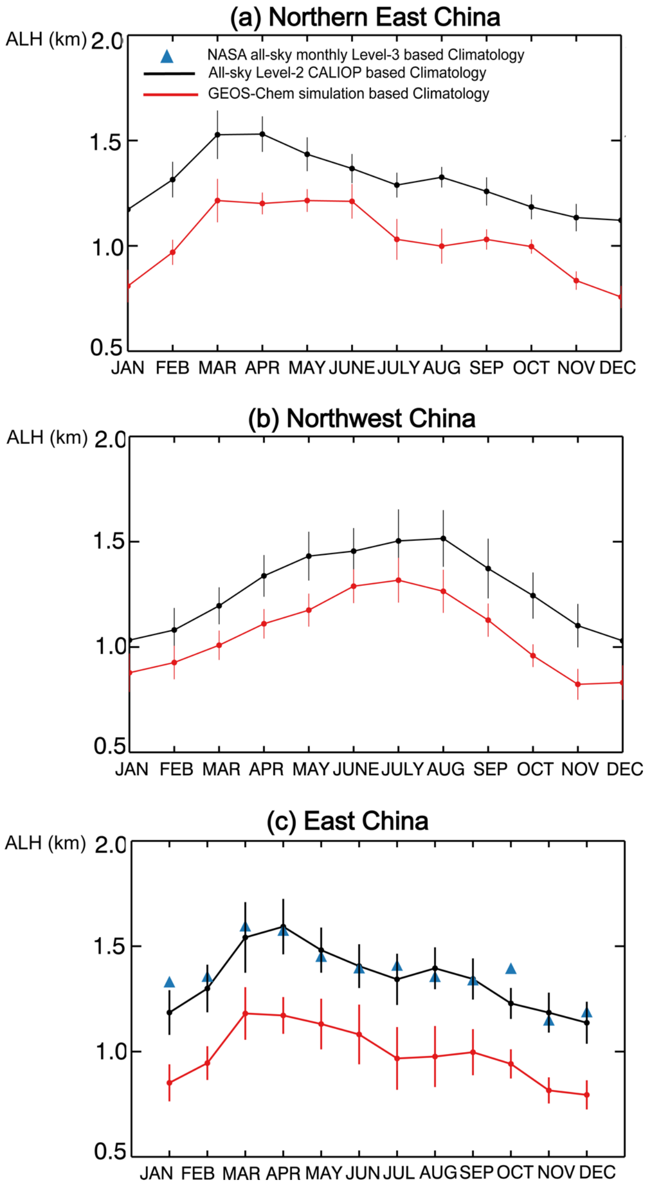

Figure 3. Regional mean ALH monthly climatology over (a) Northern East China, (b) Northwest China, and (c) East China. The error bars stand for 1 standard deviation for spatial variability.

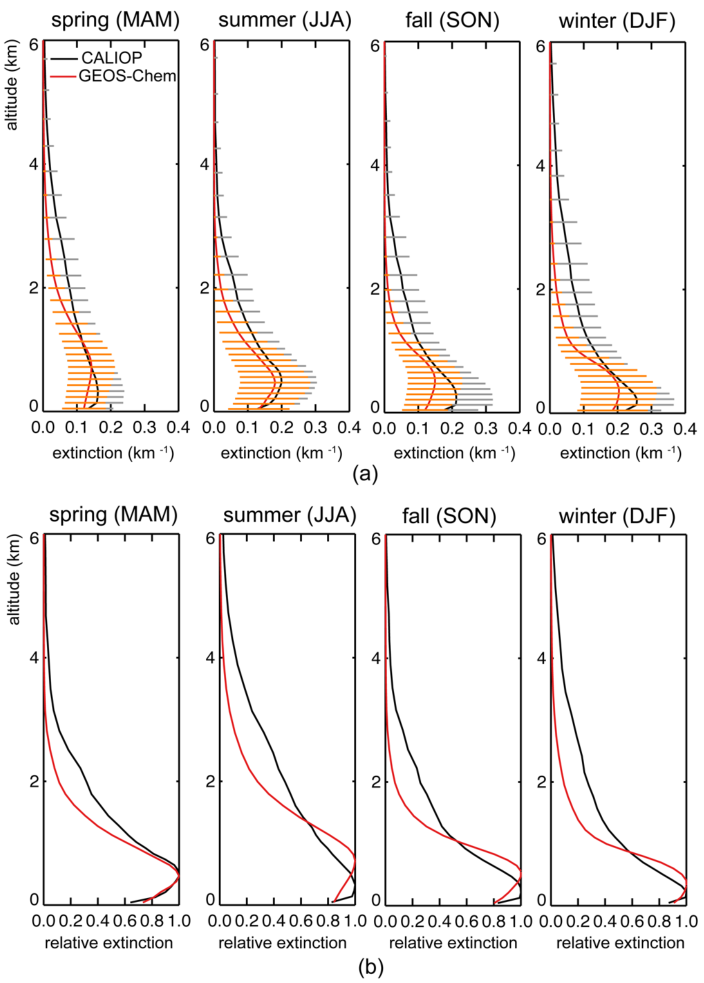

Figure 4. Seasonal climatological aerosol extinction profiles (first row) and corresponding relative extinction profiles (normalized to maximum extinction values, second raw) in spring (MAM), summer (JJA), fall (SON) and winter (DJF) over Northern East China. Model results (in red) are prior to MODIS/Aqua based AOD adjustment. Error bars in (a) represent 1 standard deviation across all grid cells in each season.

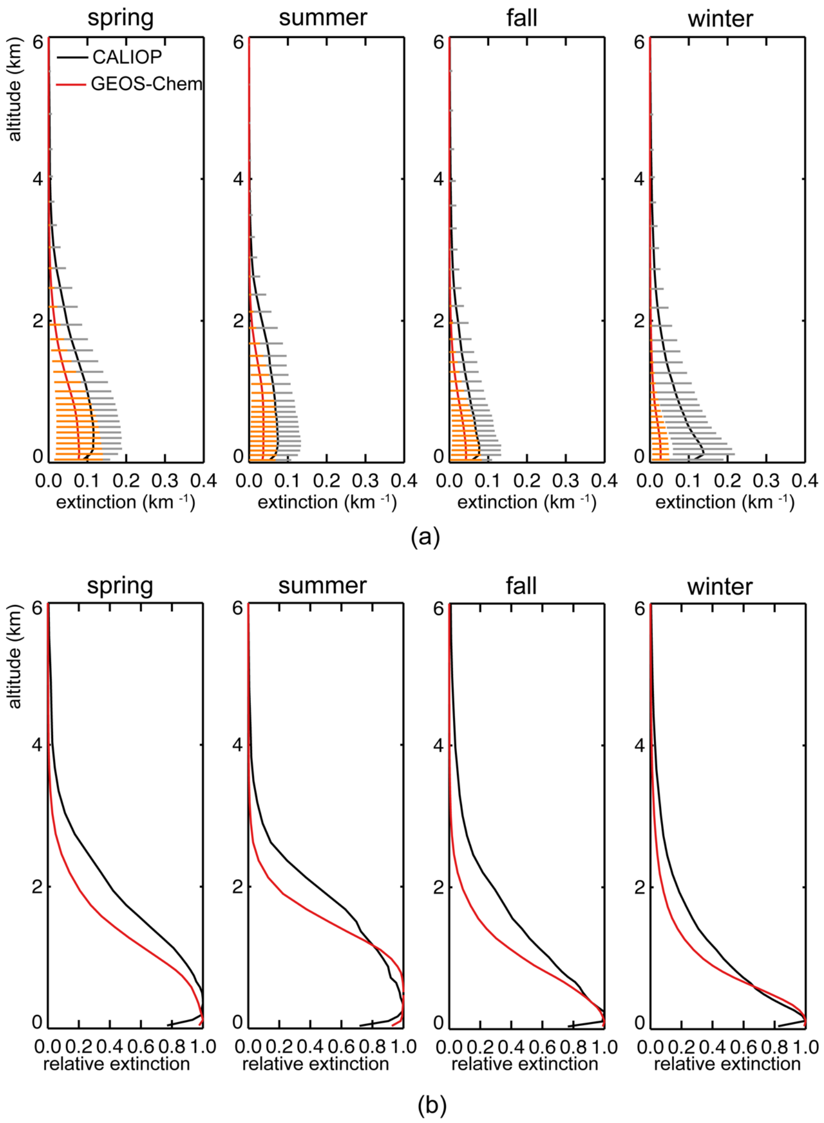

1042 Figure 5. Similar to Fig. 5 but for Northwest China.

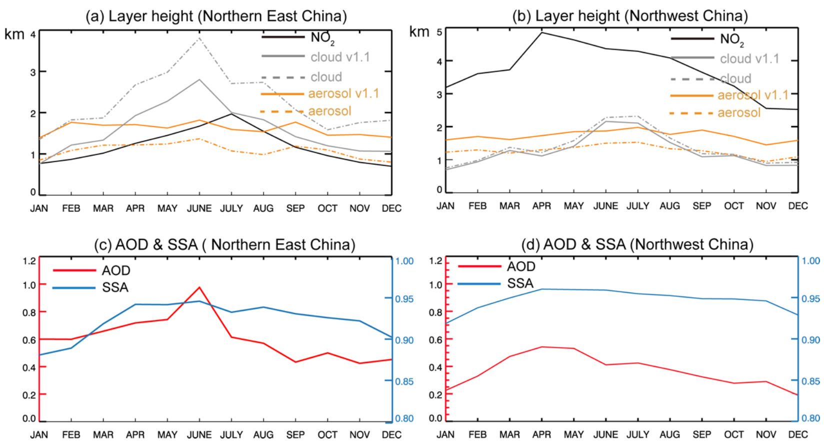

Figure 6. Monthly variations of ALH, CTH and NLH over (a) Northern East China and (b) Northwest China in 2012. Data are averaged across all pixels in each month and region. The grey and orange solid lines denote POMINO v1.1 results, while the corresponding dashed lines denote POMINO. (c–d) Corresponding monthly AOD and SSA.

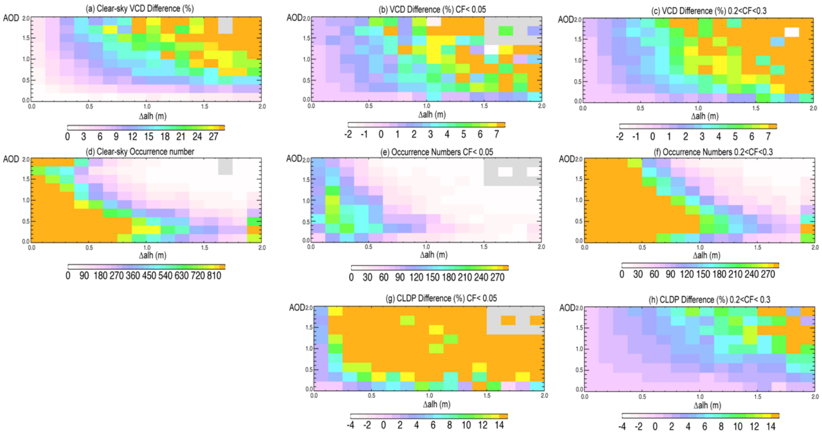

Figure 7. Percentage changes in VCD from POMINO to POMINO v1.1 ([POMINO v1.1 – POMINO] / POMINO) for each bin of ΔALH (bin size = 0.2 km) and AOD (bin size = 0.1) across pixels in 2012 over Northern East China, for (a) cloud-free sky (CF = 0 in POMINO), (b) little-cloudy sky, and (c) modestly cloudy sky. (d-f) The number of occurrences corresponding to (a-c). (g, h) Similar to (b, c) but for the percentage changes in cloud top pressure (CP).

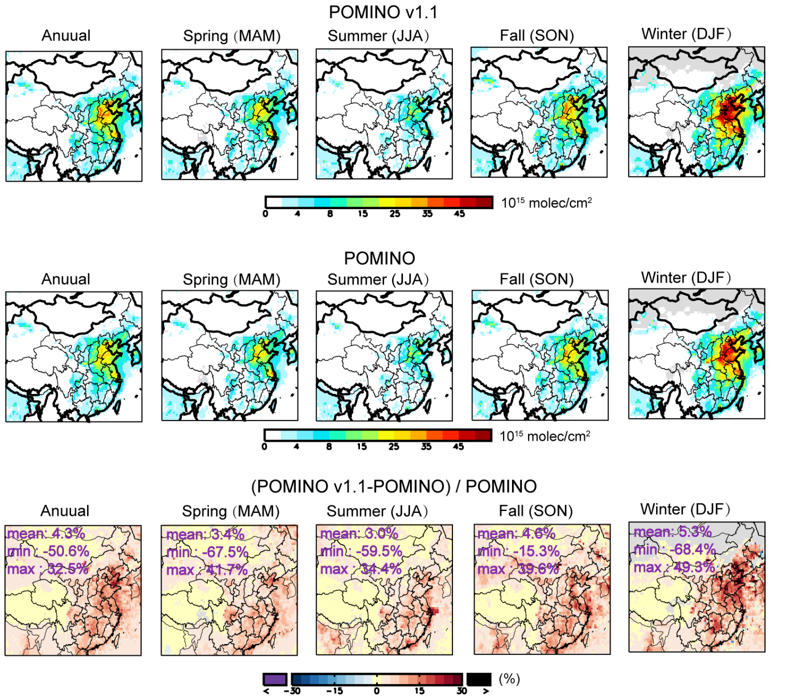

Figure 8. Seasonal spatial distribution of tropospheric NO_2 VCD in 2012 for (a) POMINO v1.1, (b) POMINO, and (c) their relative difference.

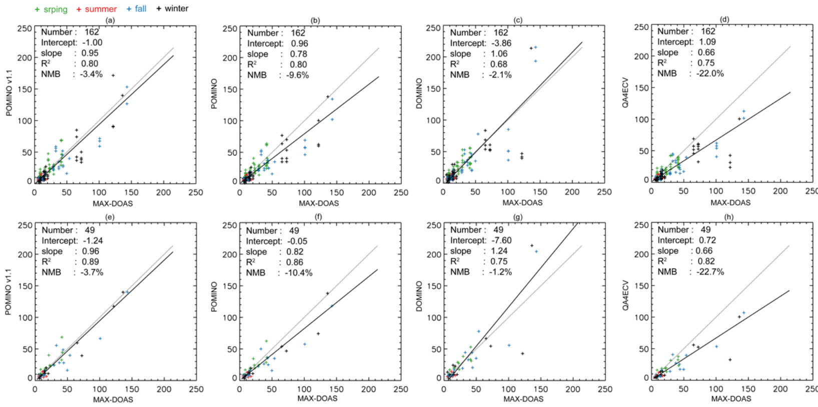

Figure 9. (a–d) Scatterplot for NO_2 VCDs (10^{15} molec. cm^{-2}) between MAX-DOAS and each of the three OMI products. Each "+" corresponds to an OMI pixel, as several pixels may be available in a day. (e–h) Similar to (a–d) but after averaging over all OMI pixels in the same day, such that each "+" represents a day. Also shown are the statistic results from the RMA regression. The black solid line indicates the regression curve and the grey dotted line depict the 1:1 relationship.